Unlocking the doors of transcription:

Key transcriptional regulators in calcium and magnesium reabsorption

Andreas Kompatscher

Unlocking the doors of transcription:

Key transcriptional regulators in calcium and magnesium reabsorption

Andreas Kompatscher

The research presented in this thesis was performed at the department of Physiology, Radboud Institute for Molecular Life Sciences, Radboud university medical center, The Netherlands and financially supported by grant from the Netherlands Organization for Scientific Research, grant NWO VICI 016.130.668 and the EURenOmics project from the European Union seventh Framework Programme (FP7/2007–2013, agreement no. 305608). The publication of this thesis was financially supported by the Dutch Kidney Foundation.

ISBN
978-94-028-1109-4

Design/lay-out
Promotie In Zicht, Arnhem

Print
Ipskamp Printing, Enschede

Unlocking the doors of transcription:

Key transcriptional regulators in calcium and magnesium reabsorption

Proefschrift

ter verkrijging van de graad van doctor
aan de Radboud Universiteit Nijmegen
op het gezag van de Rector Magnificus prof. dr. J.H.J.M. van Krieken,
volgens besluit van het college van decanen
in het openbaar te verdedigen op woensdag 12 september 2018
om 16.30 uur precies

door

Andreas Kompatscher
geboren op 9 februari 1988
te Bolzano, Italië

Promotoren
Prof. dr. J.G.J. Hoenderop
Prof. dr. R.J.M. Bindels

Copromotor
Dr. J.H.F. de Baaij

Manuscriptcommissie
Prof. dr. A. Cambi
Prof. dr. G.J.M. Pruijn
Dr. A.M. van Eerde (UMC Utrecht)

Table of contents

1 Introduction to the role of transcriptional regulation in renal electrolyte disorders

Magnesium and calcium transport in the kidney

Magnesium (Mg^{2+}) and calcium (Ca^{2+}) are essential ions for life. Careful maintenance of the levels of these ions in the body is paramount for proper functioning and survival. Adequate Mg^{2+} and Ca^{2+} homeostasis in the body is maintained by the uptake of these ions by the intestines, resorption in bone and excretion by the kidneys.[1] The focus of this thesis will be on the kidney, which is essential for the careful management of ion concentrations in the blood.[2] A kidney consists of approximately 1 million nephrons, which are the functional units that facilitate (ion) reabsorption (Figure 1). Every nephron consists of a glomerular filter and tubule, where metabolic waste products, ions and water are pushed into the luminal space of the tubule, leaving proteins and other large molecules behind in the bloodstream. The kidney is responsible for the recovery of 95-99% of the filtered Mg^{2+} and Ca^{2+} ions.[1] The nephron is divided into several segments, each with unique properties for the reabsorption of ions and water. The segments most important for the uptake of Mg^{2+} and Ca^{2+} are the proximal tubule (PT), thick ascending limb of Henle's loop (TAL), distal convoluted tubule (DCT) and connecting tubule (CNT) (Figure 1).

Proximal Tubule

In the first segment called the PT, 60-70% of the filtered Ca^{2+} is reabsorbed.[3] The Na^+-driven water uptake taking place in the proximal tubule causes an increase in the luminal concentration of Ca^{2+}, subsequently driving passive diffusion through tight junctions between epithelial cells (Figure 1) and ending in the renal interstitium.[4] Only 10-25% of Mg^{2+} is reabsorbed in the proximal tubule via the same pathway.[5, 6]

Thick ascending limb of Henle's loop

By combined action of the paracellular and transcellular transport process, the TAL is responsible for uptake of large amounts of Ca^{2+} (20-25%) and Mg^{2+} (50-70%).[3, 7] Paracellular transport means that ions are transported between cells, whereas transcellular transport takes ions through cells. The TAL is divided into two distinct segments, namely the medullary TAL (mTAL) and cortical TAL (cTAL). The mTAL is mostly responsible for the paracellular uptake of Na^+ without the reabsorption of water.[8] The decreased concentration of Na^+ at the luminal side of the mTAL is hypothesized to facilitate the back leak of Na^+ in the following segment the cTAL.[9] A strong lumen-positive voltage (+10mV) facilitates passive paracellular transport, which is promoted by the activity of the Na^+-K^+-$2Cl^-$ co-transporter (NKCC2) and the extrusion of K^+ via the K^+-channel ROMK at the apical membrane (Figure 2).[3, 10] Divalent cation reabsorption is mainly executed in the cTAL, which largely depends on tight junction permeability.[11] Tight junctions in the TAL are occupied by a modular array of claudin proteins, an extensive gene family consisting of 24 members. The claudins

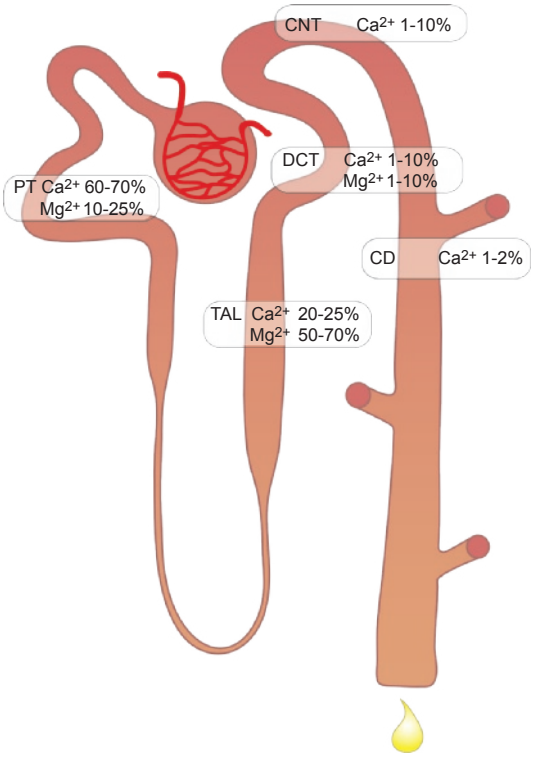

Figure 1 | Ca^{2+} and Mg^{2+} reabsorption along the nephron

Along the nephron 95-99% of Ca^{2+} and Mg^{2+} is reabsorbed. Bulk uptake of 60-70% of Ca^{2+} takes place along the whole proximal tubule (PT), whereas only 10-25% of Mg^{2+} is taken up in the late proximal tubule. In the thick ascending limb of Henle's loop (TAL) 50-70% of Mg^{2+} is taken up by paracellular transport through the tight junctions between the TAL cells. A large part of the remaining Ca^{2+} 20-25% is taken up in the TAL as well. In the distal convoluted tubule (DCT) the remaining 10% of Mg^{2+} is taken up. No Mg^{2+} is taken up past this segment. The late DCT and connecting tubule (CNT) are responsible for another 5-10% of Ca^{2+} transport. Any remaining Ca^{2+} that requires to be reabsorbed (1-2%) is taken up in the collecting duct (CD). The remaining Ca^{2+} and Mg^{2+} are excreted via the urine.

specific for the TAL are Claudin3, 10, 11, 14, 16, & 19. Depending on the configuration of claudins in the tight junction, the barrier is more permeable for cations versus anions and even changes the permeability for divalent versus monovalent cations.[12] The tight junction in the cTAL consists of Claudin3, 16 & 19 and is highly selective for the paracellular uptake of Mg^{2+} and Ca^{2+}, whereas the tight junctions in the mTAL

mostly consist of Claudin10b and are highly selective for Na^+ (Figure 2).[8] Recent studies show that increased plasma Mg^{2+} and Ca^{2+} lead to changes in the configuration of the cTAL tight junctions by the addition of Claudin14 into the junction.[13, 14] This shifts the preference of the tight junction from divalent cations, like Mg^{2+} and Ca^{2+}, to monovalent ions like Na^+, restricting Mg^{2+} and Ca^{2+} uptake into the bloodstream. This change in tight junction permeability is regulated by the calcium-sensing receptor (CaSR) (Figure 2).[14, 15]

The distal convoluted tubule

The DCT is the last segment of the nephron that absorbs Mg^{2+}.[16] Contrary to upstream segments, the DCT actively reabsorbs Mg^{2+} via the apical Mg^{2+} ion channel transient receptor potential cation channel subfamily M, member 6 (TRPM6).[17] Unlike Ca^{2+}, there is no sufficient chemical gradient for Mg^{2+} to cross the plasma membrane, since luminal concentrations hover around 0.2-0.7 mM and intracellular concentrations vary between 0.5-1.0 mM. Therefore, Mg^{2+} reabsorption via TRPM6 relies on a negative membrane potential (-5mV).[1] The maintenance of this negative membrane potential is highly reliant on K^+ extrusion via either the Kv1.1 or ROMK channel and uptake of Na^+ via the thiazide-sensitive Na-Cl-cotransporter (NCC) (Figure 3).[18-20] The mechanism behind Mg^{2+} extrusion from the basolateral side of the DCT is still unknown. Several proteins are suggested to transport Mg^{2+} across the basolateral membrane. Recent studies implicate solute carrier family 41 member 1 (SLC41A1), which has been previously identified as a Na^+-driven Mg^{2+} extruder.[21] Others identified solute carrier family 41 member 3 (SLC41A3) as the potential basolateral Mg^{2+} extruder, since it was significantly increased in the DCTs of mice that were fed a low Mg^{2+}-diet and loss of SLC41A3 in zebrafish resulted in renal Mg^{2+} wasting.[22, 23] However, it is still unclear whether SLC41A1 or SLC41A3 are expressed at the basolateral side of the DCT and how they function on the physiological level. Although the exact means of Mg^{2+} transport here are unknown, a negative membrane potential is essential to provide Mg^{2+} with an electrochemical driving force to cross the basolateral membrane. This membrane potential is maintained by the continuous recycling of K^+, which is extruded by the Kir4.1/Kir5.1 inward rectifying K^+ channel and taken up and exchanged for Na^+ by the basolateral Na^+-K^+-adenosine triphosphatase (Na^+-K^+-ATPase) (Figure 3).[24-26] This ensures that Mg^{2+} can be efficiently extruded across the basolateral membrane.

The connecting tubule

The final fraction of Ca^{2+} is reabsorbed actively in the late DCT and CNT (Figure 1) via the epithelial Ca^{2+} channel transient receptor potential vanilloid 5 (TRPV5) and extruded by the Na^+-Ca^{2+} exchanger (NCX1) and the plasma membrane Ca^{2+}-ATPase (PMCA1b).[3, 27] The remaining Mg^{2+} and Ca^{2+} (1-2%) is excreted by the kidney.[28]

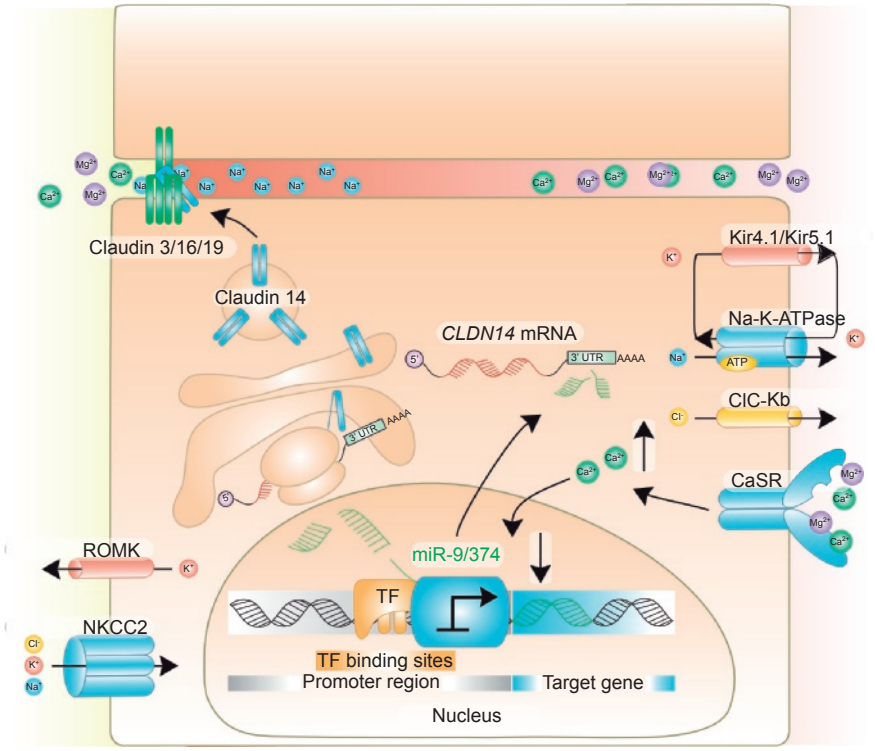

Figure 2 | Mechanisms of Ca^{2+} and Mg^{2+} transport in the TAL

The Claudin3/16/19 tight junction complex facilitates the reabsorption of Ca^{2+} and Mg^{2+} from the pro-urine. The Na^{+}-K^{+}-$2Cl^{-}$ cotransporter and the K^{+}-channel ROMK maintain a positive membrane potential, which promotes the paracelllular transport of Ca^{2+} and Mg^{2+} in the tight junctions. An abundance of Ca^{2+} and Mg^{2+} at the basolateral side of the cell will activate the G protein-coupled Ca^{2+}-sensing receptor (CaSR) by the binding of Ca^{2+} and Mg^{2+} to the receptor. Activation of the CaSR will increase intracellular Ca^{2+} concentrations, which then acts as a signaling molecule, and causes downregulation of microRNAs (miRNA) Mir-9 and Mir-374b expression levels in the nucleus. Downregulation of these miRNAs will increase the production of Claudin14 protein, which in turn will be incorporated into the Claudin3/16/19 complex. Inclusion of the Claudin14 protein in the tight junction complex shifts the ion permeability towards monovalent cations like Na^{+} instead of divalent cations, decreasing the reabsorption of Ca^{2+} and Mg^{2+} in the TAL.

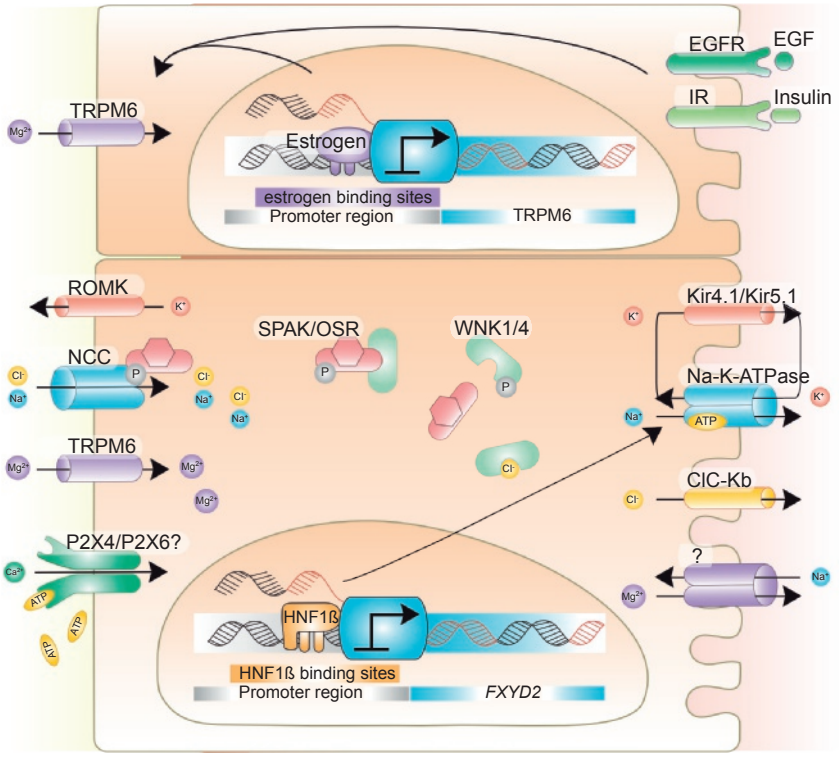

Figure 3 | Mechanisms of Ca^{2+} and Mg^{2+} transport in the DCT

In the DCT, TRPM6 facilitates Mg^{2+} uptake from the pro-urine. This is dependent on the voltage gated back leak of K^+ via the ROMK K^+-channel and the uptake of Na^+ and Cl^- via the Na^+-Cl^- cotransporter (NCC). At the basolateral membrane an as of yet unknown Mg^{2+} transporter extrudes Mg^{2+} outside the cell. This process is highly reliant on a positive Na^+ gradient, which is maintained by the Na^+-K^+-ATPase. Na^+-K^+-ATPase activity is in turn dependent on the continuous recycling of K^+ via the Kir4.1/Kir5.1 potassium channel. This process in turn also facilitates the extrusion of Cl^- via the Chloride channel protein Kb (ClC-Kb). Transcription factor HNF1β is a known transcriptional regulator of the FXYD domain containing ion transport regulator 2 (*FXYD2)* gene, which encodes for the γ-subunit of the Na^+-K^+-ATPase. Activation of the epidermal growth factor receptor (EGFR) and insulin receptor (IR) by their respective signaling molecules results in an intracellular signaling cascade, which results in increased TRPM6 membrane expression. Additionally, estrogens stimulate TRPM6 mRNA expression.

Mg^{2+} and Ca^{2+} electrolyte disorders in the thick ascending limb of Henle's loop

Over the decades, various gene mutations have been described that resulted in disturbed Mg^{2+} and Ca^{2+} reabsorption in the TAL. In this segment, the most common genetic disturbances of ion reabsorption will be described.

Bartter syndrome

The most common electrolyte disorder is Bartter syndrome, which is characterized by hypokalemic alkalosis, elevated renin and aldosterone levels, and low blood pressure.[29] Bartter syndrome is caused by a mutation in either solute carrier family 12 member 1 (*SLC12A1)* encoding for NKCC2 (Bartter syndrome type 1; OMIM: 601678), ATP-sensitive inward rectifier potassium channel 1 (*KCNJ1)* (Bartter syndrome, type 2; OMIM: 600359) encoding for ROMK, Chloride channel protein ClC-Kb (*ClC-Kb)* (Bartter syndrome, type 3; OMIM: 602023), *Barttin* (Bartter syndrome, type 4; OMIM: 606412) and the *CaSR* (Bartter syndrome, type 5; OMIM: 601199).[30-33] Bartter's syndrome type 5 is accompanied with hypocalcemia, hypercalciuria and hypomagnesemia due to activating mutations in the CaSR. Increased activation of the CASR is known to inhibit the activity of the ROMK channel in rats, which explains the Bartter's syndrome symptoms observed in these CaSR patients.[34]

Autosomal dominant hypocalcemia and familial hypocalciuric hypercalcemia

Mutations in the CaSR can be activating or inactivating, depending on the nature of the mutation, which leads to opposing phenotypes.[35, 36] Heterozygous gain-of-function mutations cause autosomal dominant hypocalcemia (ADH: OMIM 601198). These patients suffer from renal Mg^{2+} wasting, hypomagnesemia, renal Ca^{2+} wasting and hypocalcemia often combined with hypoparathyroidism.[37] In around 50% of the cases the resulting hypocalcemia and hypomagnesemia is mild and asymptomatic, the other 50% experiences paresthesias, carpopedal spasm, and seizures. 10% of patients also develop nephrocalcinosis, fully mimicking the FHHNC type 1 phenotype at the renal level. In 35% of patients, additional ectopic and basal ganglia calcifications have been found.[38] Loss-of-function mutations in the CaSR cause familial hypocalciuric hypercalcemia (FHH: OMIM 145980), which results in the hyperabsorption of Ca^{2+} and Mg^{2+} and subsequent low levels in the urine. Additional nephrolithiasis and peptic ulcers are relatively uncommon. Since most patients are asymptotic, the disorder is considered mostly benign.[39]

Familial hypomagnesemia with hypocalcuria and nephrocalcinosis type 1 & 2

Several mutations directly disturb the tight junctions in the TAL. Mutations in *Claudin16* (*CLDN16)* are known to cause familial hypomagnesemia with hypocalcuria and nephrocalcinosis Type I (FHHNC type 1; OMIM: 248250).[40] Patients with mutations in *CLDN16* suffer from renal Mg^{2+} wasting, hypomagnesemia, renal Ca^{2+} wasting, nephrocalcinosis and renal failure. Other segments like the DCT and CNT cannot compensate for the loss of Mg^{2+} and Ca^{2+} reabsorption in the TAL. Treatment with Mg^{2+} supplementation is not able to restore Mg^{2+} levels or alleviating other symptoms in patients.[41] Several dozen mutations in *CLDN16* have been described and all are characterized by a recessive mode of inheritance.[42] Similarly, mutations in *CLDN19* are also known to cause familial hypomagnesemia with hypocalcuria and nephrocalcinosis (FHHNC type 2; OMIM: 248250). These patients suffer from a severe hypomagnesemia combined with hypercalciuria and nephrocalcinosis. Additionally, patients develop ocular defects as claudin19 is expressed in the retina.[43] Furthermore, FHHNC type 2 patients seem to be more prone to developing chronic kidney disease (CKD) and develop this disease earlier in life than FHHNC type 1 patients.[42] As with FHHNC type 1, oral Mg^{2+} supplementation or use of thiazide diuretics does not significantly improve serum Mg^{2+} levels.[42] As described earlier Claudin16 and Claudin19 are the main components for the Mg^{2+} and Ca^{2+} selective tight junction pore. Mutations in either *CLDN16* or *CLDN19* cause a reduction in the tight junction selectivity for Ca^{2+} and Mg^{2+}, decreasing the influx of Mg^{2+} and Ca^{2+} through the tight junction pore.[9] Depending on the nature of the mutation misfolding of the claudin protein can also occur relegating it to the endoplasmatic reticulum (ER), which changes the claudin configuration in the tight junctions in the TAL.[44, 45]

Mg^{2+} and Ca^{2+} electrolyte disorders in the distal convoluted tubule

Disturbed Mg^{2+} reabsorption in the DCT typically leads to renal Mg^{2+} wasting and subsequent hypomagnesemia, since the DCT is the final point for Mg^{2+} reabsorption in the renal tubule. Several genetic disorders that cause Mg^{2+} disorders are due to defects in the DCT.

Mutations in the epithelial Mg^{2+} channel TRPM6

Autosomal-recessive mutations in Mg^{2+} channel TRPM6 are known to cause severe hypomagnesemia (0.1-0.3 mmol/L) and secondary hypocalcemia (HSH, OMIM: 602014), resulting in severe muscular and neurological complications including seizures and mental retardation.[46, 47] Since TRPM6 is expressed in both the intestines

and kidney defects result in reduced intestinal reabsorption and renal Mg^{2+} wasting, explaining the severity of the phenotype.[17] Mg^{2+} supplementation does improve serum Mg^{2+} levels, but in general do not recover to normal levels.[48] In mice, knocking out *Trpm6* results in early neonatal lethality, however heterozygous *Trpm6* knockout (KO) mice already display decreased Mg^{2+} reabsorption and wasting.[49]

Mutations in regulators of TRPM6 result in hypomagnesemia and renal Mg^{2+} wasting

An important stimulator of TRPM6 function is the epidermal growth factor (EGF) hormone. A mutation in *EGF* was reported to cause isolated autosomal recessive hypomagnesemia (IRH, OMIM: 611718).[50] The patients suffered from epileptic seizures and psychomotor retardation. Plasma renin activity, plasma aldosterone, and parathyroid hormone concentrations were normal. The patient mutation leads to impaired basolateral sorting of EGF, which hampers to induce the signaling cascade required for TRPM6 activation.[51, 52] Injecting wildtype mice with EGF receptor (EGFR) inhibitor erlotinib does indeed cause a small but significant decrease in serum Mg^{2+} levels.[53] Furthermore, colorectal cancer patients that were treated with EGFR antagonist cetuximab develop hypomagnesemia. It is therefore no suprise that a patient with a mutation in the EGFR also developed hypomagnesemia.[54] This provides additional evidence that EGF is an important signaling hormone for maintaining Mg^{2+} homeostasis.[51]

Gitelman syndrome

Defects in solute carrier family 12 member 3 (*SLC12A3)* encoding for NCC cause Gitelman syndrome (OMIM: 263800), a disorder characterized by Dr. Gitelman in 1966.[55] Patients present with hypomagnesemia, hypokalemia, hypocalciuria and metabolic alkalosis, which is in some occasions associated with mild hypotension. Patients are generally treated with Mg^{2+} supplementation.[56] In some cases this resulted in restored K^+ levels showing that the hypokalemia is likely secondary to the hypomagnesemia.[57] NCC KO mice confirm this hypothesis, since they are hypomagnesemic but present with normal K^+ levels under basal conditions.[58] Interestingly, NCC KO mice have significantly reduced TRPM6 expression levels, which would explain the observed hypomagnesemia.[59] However, it is as of yet unclear why a loss in NCC function results in decreased TRPM6 expression. Although it has been suggested that atrophy of the DCT segment could in part explain this phenomenon.[60]

SeSAME-EAST syndrome

Mutations in ATP-sensitive inward rectifier potassium channel 10 (*KCNJ10)* encoding for the Kir4.1 inward rectifying K^+ channel lead to Seizures, Sensorineural deafness, Ataxia, Mental retardation and Electrolyte imbalance or Epilepsy, Ataxia, Sensorineural

deafness, Tubulopathy (SeSAME-EAST, OMIM: 612780).[26, 61, 62] Patients have marked electrolyte abnormalities reminiscent of Gitelman syndrome, including severe hypomagnesemia, hypokalemia and metabolic alkalosis. In some patients' high renin, aldosterone levels, salt craving and polyuria were observed. K^+ channel subunit Kir4.1 together with the ATP-sensitive inward rectifier potassium channel 16 (*KCNJ16)* encoding for the Kir5.1 K^+-channel subunit are responsible for maintaining the basolateral membrane potential in the DCT (Figure 3). Any defects in Kir4.1 functioning lead to decreased K^+ availability, which decreases Na^+-K^+-ATPase activity. It is hypothesized that decreased activity of the Na^+-K^+-ATPase will depolarize the basolateral membrane potential. In turn this will hamper the extrusion of Cl^- by the CIC-Kb channel. A rise in intracellular Cl^- inhibits NCC activity, which in turn is required for Mg^{2+} reabsorption by TRPM6. Indeed, kidney-specific Kir4.1 KO mice showed decreased NCC activity and expression. These mice exhibited hypochloremic metabolic alkalosis with hypokalemia and urinary Na^+, K^+ and Mg^{2+} wasting.[63] No TRPM6 activity or expression levels were measured to assess the direct effect of *Kcnj10* loss on TRPM6 functioning. To compensate for the loss of Na^+ in the DCT by decreased NCC functioning, epithelial Na^+-channel (ENaC) activity in the CNT and CD is increased at the expense of increased K^+ extrusion via ROMK. Therefore, SeSAME-EAST patients suffer from both hypomagnesemia and hypokalemia. Treatment usually involves Mg^{2+} and K^+ supplementation in combination with aldosterone antagonists or ENaC inhibitors.[24] Additionally Kir4.1 patients suffer from severe seizures, cerebellar ataxia and hearing loss, due to the loss of Kir4.1 functioning in neurons and glial cells.[64]

Na^+-K^+-ATPase y-subunit

Direct disturbances in Na^+-K^+-ATPase functioning in the DCT can be attributed to missense mutations in the *FXYD* domain containing ion transport regulator 2 (*FXYD2*) encoding for the y-subunit of the Na^+-K^+-ATPase. The c.121G>A mutation in *FXYD2* results in a p.Gly41Arg missense mutation, which causes misrouting of the y-subunit to the membrane, decreasing the activity of the Na^+-K^+-ATPase.[65, 66] Curiously, this did not result in a SeSAME-EAST-like phenotype. Patients diagnosed with dominant isolated hypomagnesemia (IDH, OMIM: 154020) suffer from a severe renal Mg^{2+} wasting and hypomagnesemia (0.4 mmol/L) lacking any other electrolyte disturbances except for a slight loss of Ca^{2+} in the urine. The exact role of the y-subunit remains unclear. It is hypothesized to stabilize the alpha and beta-subunit of the Na^+-K^+-ATPase at the membrane. Other reports show that the y-subunit might function as an inward rectifier channel on its own.[67] Although, this seems unlikely, since there is no evidence for the existence of such a channel *in vivo*.

Autosomal Dominant Tubulointersitial Kidney Disease (HNF1β)

Deletions or mutations in hepatocyte nuclear factor 1 homeobox β (*HNF1β*), encoding for the transcription factor HNF1β, cause autosomal dominant tubulo-interstitial kidney disease (ADTKD-HNF1β, OMIM: 137920). HNF1β is a transcription factor important for regulating gene expression in kidney development.[68] Patients suffer from a heterogeneous phenotype, which is characterized by renal cysts and maturity onset diabetes of the young (MODY).[69-74] Around 50% of the patients are affected by a whole-gene deletion at the 17q12 position in the genome, which contains around ~10 genes including *HNF1β*. The remaining cases consist of point mutations along the entire coding sequence.[69, 75] An extensive meta-analysis of *HNF1β* patients with point mutations or whole-gene deletions demonstrated that there were no phenotypical differences with regard to the kidney or MODY defects.[76] However, 40% of 17q12 patients exhibited a neurodevelopmental disorder compared to the intragenic mutations, which is possibly caused by one of the other genes missing in these patients.[77] *HNF1β* patients are also known to present with a wide variety of renal and extra-renal symptoms like, genital tract malformation (CAKUT),[78, 79] abnormal liver function,[80] pancreatic hypoplasia,[81] hyperparathyroidism and electrolyte disturbances.[69, 82, 83] *De novo* mutations in the *HNF1β* gene are encountered in 30-50% of new cases, which might explain the high phenotypical heterogeneity observed in patients.[84] The electrolyte disorder is characterized by a hypomagnesemia, hypokalemia, hypocalcuria and metabolic alkalosis mimicking both Gitelman and SeSAME-EAST syndrome. Renal cysts are reported in ~70% of patients, MODY in ~50% and hypomagnesemia in ~45%.[69]

Hyperphenylalaninemia, BH4-deficient, D

Patients with mutations in pterin-4a-carbinolamine dehydratase/dimerization factor (*PCBD1*) were diagnosed with hypomagnesemia, renal Mg^{2+} loss and in two cases MODY (Hyperphenylalaninemia, BH4-deficient, D; OMIM: 126090).[85] This was attributed to the fact that PCBD1 is a crucial binding factor and coactivator of HNF1α and HNF1β, which explains the commonalities between ADTKD-HNF1β and the *PCBD1* patient phenotypes.[86, 87]

Kenny-Caffey syndrome type 2 (FAM111a)

Although ubiquitously expressed throughout the body, mutations in FAM111a gives rise to a rather specific disease phenotype. Patients suffer from a severe short stature, gracile bones, severe bouts of hypocalcemia, low levels of parathyroid hormone (PTH) and hypomagnesemia.[88-91] The most commonly found mutation c.1706G>A (p.Arg569His) results in a milder phenotype known as Kenny-Caffey syndrome type 2 (KCS, OMIM: 244460), whereas mutations and deletions at or surrounding the c.1026_1028delTTC (p.Ser342del) develop osteocraniostenosis (OCS, OMIM:

602361).[88, 92] The difference between both syndromes is mainly severity. Whereas KCS patients can survive well into adulthood, OCS patients usually do not survive beyond the neonatal period. KCS type 2 patients are often treated with Ca^{2+} and vitamin D supplementation, although this often does not sufficiently correct Ca^{2+}, Mg^{2+} and PTH deficiencies.[92] Mg^{2+} supplementation tends to correct the Ca^{2+} and PTH deficiency much more effectively.[88] This has led to the hypothesis that the Mg^{2+} deficiency could be the primary defect in KCS type 2. However, little is known about FAM111as' function. Over the years FAM111a has been mainly implicated as an inhibitor of SV40 and adenovirus replication.[93] Recently FAM111a was identified as a binding partner of the proliferating cell nuclear antigen (PCNA).[94] PCNA is a key docking protein involved in the mitotic replication process, where it recruits other proteins involved in the replication process. It is hypothesized that FAM111a facilitates this docking process by binding PCNA and stabilizing it on both DNA strands.[94] It remains however unclear how an electrolyte disorder with such specific symptoms as Kenney-Caffey syndrome type 2 is caused by a general defect in DNA replication. As of yet there are no FAM111a KO models to study the pathophysiology of Kenney-Caffey syndrome type 2.

Regulatory mechanisms of ion transport

Paracrine regulation

The rate-limiting factor for a kidney cell to transport Ca^{2+} or Mg^{2+} across the plasma membrane is determined by the amount of Ca^{2+} or Mg^{2+} ions that can enter through a single channel or transporter and the amount of channels or transporters that are located at the membrane at any given moment (Figure 4, #1). There are several cellular processes at various levels that regulate either the activity or abundance of ion channels. Post-translational modification of ion channels and transporter like phosphorylation or glycosylation can dramatically alter transport dynamics at the cell-surface (Figure 4, #6).[95, 96] A fast regulatory mechanism is the insertion and retrieval of channels from the cell surface, which enables a rapid cellular response to fast ion fluxes. Upon retrieval, channels can either be degraded or re-enter into the plasma membrane (Figure 4, #4,5). In the DCT, EGF facilitates such a response by quickly recruiting TRPM6 to the apical membrane by initiating an intracellular signaling cascade.[51] Another crucial regulator is insulin, which can directly affect TRPM6 activity through cyclin-dependent kinase 5 (cdk5)-dependent phosphorylation of the channel (Figure 3).[95] An important signaling molecule for regulating Ca^{2+} and Mg^{2+} transport is adenosine triphosphate (ATP). ATP acts as an autocrine and paracrine signalling molecule modulating ion transport processes in the kidney and intestine.[97, 98] High amounts of ATP (25-100 µmol/L) are released in response to

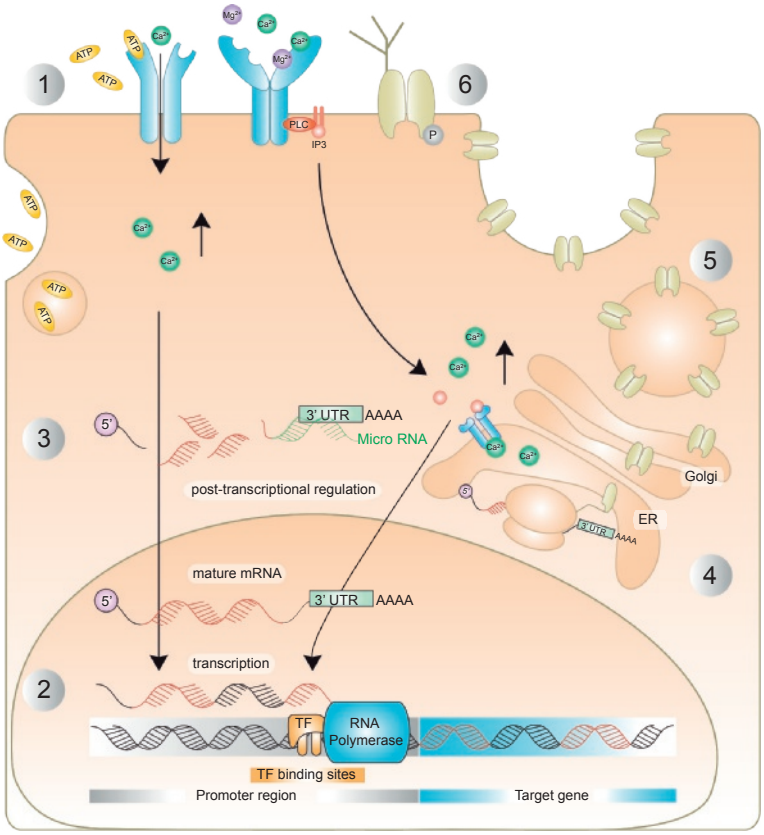

Figure 4 | Regulatory mechanisms involved in the expression of ion channels at the plasma membrane.

1) Autocrine release of adenosine triphosphate (ATP) stimulates purinergic channels to increase Ca^{2+} uptake into the cell. Binding of Ca^{2+} and Mg^{2+} activates a G protein-coupled protein receptor, which initiates an intracellular pathway that results in the release of intracellular Ca^{2+} from the endoplasmatic reticulum (ER). 2) The increase in intracellular Ca^{2+} changes transcription factor (TF) binding to specific sites in the promoter. 3) Post-transcriptional modifications like miRNA binding to the 3'-UTR reduces mRNA levels and facilitates gene silencing. 4) Translation. 5) Post-translation; Vesicular insertion and retrieval. 6) Post-translational modification; Phosphorylation and glycosylation.

various stimuli like flow and neuronal activation.[99] Extracellular ATP activates purinergic receptors, like P2X and P2Y receptors, to facilitate or inhibit the non-selective influx of cations (Figure 4, #1).[97] For example, extracellular ATP release is known to inhibit ENaC mediated Na^+ uptake in the collecting duct.[100] In the DCT, P2X4 and P2X6 are the most abundant purinergic receptors and recently it has been shown that P2X4 inhibits TRPM6 mediated Mg^{2+} uptake.[101] However more research is needed to elucidate how purinergic signaling is influencing TRPM6 activity.

Mg^{2+} and Ca^{2+} sensing

The CaSR is a G-protein coupled receptor (GCPR) expressed on the basolateral side of the TAL.[102] Both Ca^{2+} and Mg^{2+} can bind and activate the receptor to regulate reabsorption of Ca^{2+} and Mg^{2+}.[103] Although, a five-fold higher concentration of Mg^{2+} then Ca^{2+} is needed to elicit the same CaSR-mediated intracellular Ca^{2+} response. Investigations in microperfused rat cTAL, show that acute inhibition of the CaSR increases the permeability to Ca^{2+} of the paracellular pathway instead of altering NaCl reabsorption or change the transepithelial potential difference.[104] CaSR stimulation activates a transcriptional pathway to decrease the transcript levels of two microRNAs (miRNA), Mir-9 and Mir-374.[13, 15, 105] MiRNAs are single-stranded, non-coding RNAs of 19-25 nucleotides. MiRNAs can bind the 3'-untranslated region (3'-UTR) of messenger RNAs (mRNA) and result in the degradation of the targeted mRNA. In this way miRNAs control the amount of mRNA that is translated into protein (Figure 4, #3).[106] Mir-9 and Mir-374 are known to target the 3'-UTR of *CLDN14*. Activation of the CaSR decreases the amount of available Mir-9 and Mir-374. In turn, this facilitates *CLDN14* mRNA translation into protein and targeting to the tight junction decreasing Mg^{2+} and Ca^{2+} reabsorption in the TAL (Figure 2).[13] In case of an activating CaSR mutation, the CaSR signaling pathway is overactive resulting in an increase in claudin14 in the mTAL tight junctions, which hampers the uptake of Ca^{2+} and Mg^{2+}. Injecting wild-type mice with CaSR agonist cinacalcet did indeed increase Claudin14 expression and a subsequent decrease in Ca^{2+} and Mg^{2+} uptake. In contrast, injections with CaSR antagonist NPS-2143 resulted in the opposite effect.[15] Taken together, this data adequately explains what occurs in patients that suffer from activating (ADH) or inactivating (FHH) CaSR mutations.

Transcriptional regulation

Transcriptional regulation is responsible for the long-term control of ion channel abundance at the cell surface. Activation of GCPRs, Ca^{2+}-channels, or the diffusion of lipophillic hormones into the intracellular compartment can initiate signaling cascades that stimulate various transcription factors.[15, 107-110] Transcription factors bind to the responsive elements within proximal promoters of target genes and modulate the recruitment of the transcriptional machinery needed to start transcription at the

transcription start site (TSS) (Figure 4, #2). Downstream, upstream or intronic enhancer and silencer sites regulate gene transcription by providing binding elements/sequences for regulatory proteins that affect promoter activity. These sequence motifs are specific to an enhancer-transcription factor and often highly conserved between species. Additionally, the level of chromatin packing can significantly alter the levels of transcription. The last layer of regulation appears at the post-transcriptional level, splicing, 5'-methyl capping, polyadenylation and cleavage initiated by small RNAs are determining whether mature RNA is degraded or translated in ribosomes. MiRNAs silence target mRNAs through translational repression affecting the rate of protein synthesis and eventually the number of ion channels available at the plasma membrane (Figure 4, #4,5,6). Along the nephron, a pattern of segment-specific and more ubiquitous transcription factors has been identified.[111] However, the transcriptional targets of these transcription factors remain elusive and therefore also their effect on electrolyte reabsorption. It has been shown that Mg^{2+} depletion increases human *CLDN16* promoter activity and the addition of Mg^{2+} decreased its activity in transfected human embryonic kidney (HEK293) cells.[112] Although as of yet, no Mg^{2+} responsive element was identified that affects the promoter activity of *CLDN16*. Similar experiments found that the addition of 1,25-dihydroxyvitamin D_3 ($1,25(OH)_2D_3$) inhibits *CLDN16* promoter activity in HEK293.[113] Adding transiently transfected CaSR significantly increased the inhibitory effect, which was explained as a compensatory mechanism for $1,25(OH)_2VitD_3$-mediated intestinal uptake. Although, experiments in mice show that activation of the CaSR regulates expression of *CLDN14* via a nuclear factor of activated T-cells (NFAT)-mediated pathway. In contrast, the expression levels of Claudin16 and Claudin19 were unaffected.[15] In DCT, the transcriptional regulation of Mg^{2+} and Ca^{2+} transport has been studied in a limited capacity. A KO mouse model of potassium channel subunit Kir4.1 demonstrated a decrease in NCC expression levels in the DCT.[63] Furthermore, it is known that TRPM6 expression levels are modulated by estrogen in wild-type mice.[50] EGF-induced modulation of TRMP6 mRNA levels was identified to be mediated via an ERK/AP-1-dependent pathway. As mutations in the binding sites of AP-1 in the promoter sequence of *TRPM6* abolished the EGF-induced increase in *TRPM6* mRNA levels.[109] It is however in general unclear, which transcriptional elements are involved and what their exact transcriptional targets are in the DCT (Figure 3).

Transcriptional regulation by HNF1β: a master regulator of Mg^{2+} transport

An important player in the transcriptional regulation of Mg^{2+} transport is HNF1β. HNF1β is part of the homeodomain-containing transcription factors. It binds to DNA through a typical POU-region and an atypical POU homeodomain (POU_H), which

ChIP-seq (BOX1)

In general, transcription factors have thousands of bindings sites in the genome. All of which can potentially contribute to the transcription of target genes. The classic binding site for a transcription factor is located in the proximal promoter directly upstream of the TSS.[121] *In silico* analysis can reveal predicted binding sites that match with a motif specific for a transcription factor in the target promoter. However, numerous downsides are that only one target promoter is analyzed and predicted binding sites *in silico* are not necessarily real *in vitro*. Additionally, potential binding sites upstream or downstream of that promoter can be missed. Therefore, chromatin immunoprecipitation and sequencing (ChIP-seq) has been developed for genome-wide assessment of all protein-DNA interactions for a single transcription factor or histone modification.[122] Nuclei are extracted from the cell or tissue sample and all chromatin is crosslinked, ensuring that all DNA-bound proteins remain fixed. The crosslinked chromatin is than sheared into smaller fragments; around the 200-600 base pair (bp) range, either by sonication or through an enzymatic process. Now a highly specific antibody against the transcription factor or histone modification of interest is used to immunoprecipitate the protein-DNA complex from the chromatin sample. After decrosslinking, these samples are sequenced using a next generation sequencing platform. Between 100-400 million reads are generated in a single run of which ~60-80% can be aligned uniquely to the genome. The resulting dataset consists of a genome-wide map of all binding sites of the transcription factor specific to the used cell or tissue type. There are however certain downsides to ChIP-seq that have to be considered. For example, antibody quality is very important to generate specific and low-noise data. If such a ChIP-grade antibody is not available then ChIP-seq can either result in low quality data or could be no option at all. Furthermore, sample quantity can be a limiting factor. The average ChIP-seq experiment requires ~10^6-10^7 cells and between 10-100ng of DNA. Although advances in ChIP protocols and sequencing techniques means that nowadays ChIP-seq experiments can be performed with as little as ~10^4-10^5 cells.[121, 123] It is, therefore, possible to perform ChIP-seq on rare cell populations or valuable tissues.

specifically recognize the consensus sequence 5'-RGTTAATNATTAAC-3' (R: purine, N: unspecified nucleotide;). HNF1β forms homodimers or heterodimers with the related HNF1α through its dimerization domain and requires dimerization factor pterin-4-alpha-carbinolamine dehydratase (PCBD1) to facilitate this dimerization.[85, 86] HNF1β is

RNA-seq (BOX2)

In general, mRNA levels in various cell and tissue types are assessed by real-time quantitative PCR (RT-qPCR). Although this method is extremely sensitive and precise, it comes with a large drawback. As it is only feasible to investigate the transcriptional levels of a relatively small sample of target genes and that these targets have to be determined a priori based on previous knowledge. To investigate the effect of a treatment on a specific cell and tissue type it is often preferable to proceed with an unbiased approach and assess the complete transcriptional profile. This is possible with RNA-sequencing, which is a next generation sequencing method that allows for the genome-wide assessement of the complete transcriptome in a given sample. RNA-seq sets out to determine all species of transcript, including mRNAs, non-coding RNAs and small RNAs. In addition, it provides information on the transcriptional structure of genes, in terms of their 5' and 3' ends, start sites, splicing patterns and other post-transcriptional modifications. Furthemore, RNA-seq allows for the quantification of changing expression levels of each transcript over time and under various conditions. In general, RNA is isolated from a cell or tissue type of interest and then converted to a library of cDNA fragments with adaptors on one or both ends, which are used as an identifiying tag for the library. This RNA-seq library is then often amplified (depending on the sequencing platform) and sequenced in a high-throughput manner to obtain short sequences from one end (single-end sequencing) or both ends (pair-end sequencing). The sequenced reads tend to be between 30-400 bp in length depending on the sequencing platform. After sequencing, the reads are aligned to either a reference genome or reference transcripts to provide a genome-wide map for transcription that contains the information on both expression levels and transcriptional structure.[124] RNA-seq has a couple of distinct advantages over micro-array based techniques. For example, RNA-seq is not limited to the detection of sequences that correspond to known genomic transcripts allowing for transcriptome analysis in non-model organisms. Furthermore, RNA-seq is incredibly sensitive allowing for the reveal of transcript boundaries at single base resolution. Additionally, short reads give information on the connectivity between two exons, whereas longer reads can span multiple exons, which allows for more complex transcriptome analysis. This combined with the low background signal of RNA-seq, as reads can be unambigously mapped to unique regions in the genome and no upper limit for quantification, whereas micro-arrays lose sensitivity for low and highly expressed genes. It makes RNA-seq the first sequencing-based technique to provide complete coverage of the transcriptome in a high-throughput and quantitative manner. There are some

disadvantages to RNA-seq that should be considered. Library construction requires fragmentation of the RNA, which introduces certain biases that favor the transcript body compared to the transcript ends. Additionally, most RNA-seq platforms require an amplification step during library preparation and this can introduce a bias towards highly available sequences, skewing quantification results.[124] However this can be easily checked by RT-qPCR. Despite these small drawbacks, RNA-seq has enabled the generation of a complete picture of the transcriptome and its organization in different cell types and species.

a key transcription factor in embryogenesis, as it is involved in the development of tubular structures in the kidney, liver, pancreas and the genital tract.[114] In the adult kidney, HNF1β is expressed throughout the epithelial cells of the nephron. Known targets of HNF1β are *PKHD1*, *UMOD, KIF12* and *PKD2*, which are all cystic disease genes.[115-118] *PKHD1, KIF12* and *PKD2* are ubiquitously expressed in the epithelial cells of the nephron. Uromodulin *(*UMOD*)* is highly expressed in TAL, although lower expression levels have been reported in DCT. It is unknown whether the DCT expression has any functional relevance. Loss of HNF1β decreases the expression of all three proteins, which induce proliferation of renal epithelial cells causing cyst formation during nephrogenesis. *FXYD2a* is a transcriptional target of HNF1β that has been hypothesized to contribute to hypomagnesemia and hypokalemia observed in ADTKD-HNF1β.[25] However, HNF1β only regulates the ya-subunit of the Na^+-K^+-ATPase, which is not expressed in the DCT.[119, 120] It is therefore unlikely that the loss of HNF1β has an effect on Na^+-K^+-ATPase activity via this pathway. It can, therefore, not be excluded that HNF1β additionally regulates other DCT genes, contributing to the electrolyte disturbances observed in ADTKD-HNF1β. It has also been shown that mutations in PCBD1 decreased the promoter activity of *Fxyd2* when co-expressed with HNF1β. Furthermore, wildtype mice that were fed a low Mg^{2+} diet displayed significant upregulation of *Pcbd1* expression in the DCT.[22] These findings confirm that PCBD1 is an important factor in regulating Mg^{2+} reabsorption together with HNF1β. Although it is unclear, which downstream targets of HNF1β are affected.

Outline of this thesis

The aim of this thesis was to increase our understanding of the transcriptional regulation of Mg^{2+} and Ca^{2+} transporters in the kidney. Although much is known about the biochemical and molecular basis of Mg^{2+} and Ca^{2+} transport pathways and its regulatory networks, there is little knowledge on how Mg^{2+} and Ca^{2+} reabsorption

is regulated at the transcriptional level. **Chapter 2** provides a genome-wide assessment of all binding sites of transcription factor HNF1β in the DCT. The potassium channel subunit Kir5.1 was identified as a target of HNF1β. Luciferase assays, siRNA knockdown expriments, and a HNF1β renal knockout mouse was used to confirm the regulation of Kir5.1 by HNF1β. These results contribute to a increased understanding of the transcriptional regulation behind Mg^{2+} handling in the DCT. In **chapter 3** the CaSR was identified as a novel target gene of HNF1β in the TAL. Additional luciferase assays and siRNA knockdown experiments were performed to confirm the transcriptional regulation of HNF1β on the CaSR. This study revealed HNF1β as a novel transcriptional activator of Mg^{2+} and Ca^{2+} transport in the TAL. **Chapter 4** investigates the function of nuclear protein FAM111a in renal Mg^{2+} transport. Both RNA-sequencing and GFP-pulldown experiments were used to identify transcriptional targets and binding partners. These findings contribute to a better understanding of the renal electrolyte phenotype in FAM111a patients and could lead to potential new treatments for Kenney-Caffey syndrome type 2 patients. In **chapter 5** P2x6 KO mouse were characterized to investigate its potential renal electrolyte phenotype by performing metabolic cage experiments and subsequent screening of magnesiotropic genes with real-time quantitative-PCR (RT-qPCR). In **chapter 6** the findings of this thesis are summarized and further discussed by placing them in the context of current knowledge on the transcriptional regulation behind Ca^{2+} and Mg^{2+} transport in the TAL and DCT.

References

1. de Baaij JH, Hoenderop JG, Bindels RJ. Magnesium in man: implications for health and disease. *Physiological reviews* 2015; **95:** 1-46.
2. Bindels RJ. 2009 Homer W. Smith Award: Minerals in motion: from new ion transporters to new concepts. *J Am Soc Nephrol* 2010; **21:** 1263-1269.
3. Hoenderop JG, Nilius B, Bindels RJ. Calcium absorption across epithelia. *Physiological reviews* 2005; **85:** 373-422.
4. Friedman PA. Mechanisms of renal calcium transport. *Exp Nephrol* 2000; **8:** 343-350.
5. Le Grimellec C. Micropuncture study along the proximal convoluted tubule. Electrolyte reabsorption in first convolutions. *Pflugers Archiv : European journal of physiology* 1975; **354:** 133-150.
6. Quamme GA. Recent developments in intestinal magnesium absorption. *Curr Opin Gastroenterol* 2008; **24:** 230-235.
7. Shareghi GR, Agus ZS. Magnesium transport in the cortical thick ascending limb of Henle's loop of the rabbit. *The Journal of clinical investigation* 1982; **69:** 759-769.
8. Bleich M, Wulfmeyer VC, Himmerkus N*, et al.* Heterogeneity of tight junctions in the thick ascending limb. *Ann N Y Acad Sci* 2017.
9. Shan Q, Himmerkus N, Hou J*, et al.* Insights into driving forces and paracellular permeability from claudin-16 knockdown mouse. *Ann N Y Acad Sci* 2009; **1165:** 148-151.
10. Greger R, Velazquez H. The cortical thick ascending limb and early distal convoluted tubule in the urinary concentrating mechanism. *Kidney Int* 1987; **31:** 590-596.
11. Greger R. Cation selectivity of the isolated perfused cortical thick ascending limb of Henle's loop of rabbit kidney. *Pflugers Arch* 1981; **390:** 30-37.
12. Gunzel D, Yu AS. Claudins and the modulation of tight junction permeability. *Physiol Rev* 2013; **93:** 525-569.
13. Gong Y, Renigunta V, Himmerkus N*, et al.* Claudin-14 regulates renal Ca(+)(+) transport in response to CaSR signalling via a novel microRNA pathway. *EMBO J* 2012; **31:** 1999-2012.
14. Dimke H, Desai P, Borovac J*, et al.* Activation of the Ca(2+)-sensing receptor increases renal claudin-14 expression and urinary Ca(2+) excretion. *American journal of physiology Renal physiology* 2013; **304:** F761-769.
15. Gong Y, Hou J. Claudin-14 underlies Ca(+)(+)-sensing receptor-mediated Ca(+)(+) metabolism via NFAT-microRNA-based mechanisms. *Journal of the American Society of Nephrology : JASN* 2014; **25:** 745-760.
16. Brunette MG, Vigneault N, Carriere S. Micropuncture study of magnesium transport along the nephron in the young rat. *Am J Physiol* 1974; **227:** 891-896.
17. Voets T, Nilius B, Hoefs S*, et al.* TRPM6 forms the Mg2+ influx channel involved in intestinal and renal Mg2+ absorption. *The Journal of biological chemistry* 2004; **279:** 19-25.
18. Glaudemans B, van der Wijst J, Scola RH*, et al.* A missense mutation in the Kv1.1 voltage-gated potassium channel-encoding gene KCNA1 is linked to human autosomal dominant hypomagnesemia. *The Journal of clinical investigation* 2009; **119:** 936-942.
19. Yang L, Frindt G, Palmer LG. Magnesium modulates ROMK channel-mediated potassium secretion. *Journal of the American Society of Nephrology : JASN* 2010; **21:** 2109-2116.
20. Xi Q, Hoenderop JG, Bindels RJ. Regulation of magnesium reabsorption in DCT. *Pflugers Arch* 2009; **458:** 89-98.
21. Kolisek M, Nestler A, Vormann J*, et al.* Human gene SLC41A1 encodes for the Na+/Mg(2)+ exchanger. *American journal of physiology Cell physiology* 2012; **302:** C318-326.
22. de Baaij JH, Groot Koerkamp MJ, Lavrijsen M*, et al.* Elucidation of the distal convoluted tubule transcriptome identifies new candidate genes involved in renal Mg(2+) handling. *American journal of physiology Renal physiology* 2013; **305:** F1563-1573.
23. de Baaij JH, Arjona FJ, van den Brand M*, et al.* Identification of SLC41A3 as a novel player in magnesium homeostasis. *Sci Rep* 2016; **6:** 28565.

24. Bandulik S, Schmidt K, Bockenhauer D*, et al.* The salt-wasting phenotype of EAST syndrome, a disease with multifaceted symptoms linked to the KCNJ10 K+ channel. *Pflugers Archiv : European journal of physiology* 2011; **461:** 423-435.
25. Ferre S, Veenstra GJ, Bouwmeester R*, et al.* HNF-1B specifically regulates the transcription of the gammaa-subunit of the Na+/K+-ATPase. *Biochemical and biophysical research communications* 2011; **404:** 284-290.
26. Bockenhauer D, Feather S, Stanescu HC*, et al.* Epilepsy, ataxia, sensorineural deafness, tubulopathy, and KCNJ10 mutations. *N Engl J Med* 2009; **360:** 1960-1970.
27. Hoenderop JG, van der Kemp AW, Hartog A*, et al.* Molecular identification of the apical Ca2+ channel in 1, 25-dihydroxyvitamin D3-responsive epithelia. *The Journal of biological chemistry* 1999; **274:** 8375-8378.
28. Friedman PA, Gesek FA. Cellular calcium transport in renal epithelia: measurement, mechanisms, and regulation. *Physiological reviews* 1995; **75:** 429-471.
29. Bartter FC, Pronove P, Gill JR, Jr.*, et al.* Hyperplasia of the juxtaglomerular complex with hyperaldosteronism and hypokalemic alkalosis. A new syndrome. *Am J Med* 1962; **33:** 811-828.
30. Birkenhager R, Otto E, Schurmann MJ*, et al.* Mutation of BSND causes Bartter syndrome with sensorineural deafness and kidney failure. *Nature genetics* 2001; **29:** 310-314.
31. Simon DB, Bindra RS, Mansfield TA*, et al.* Mutations in the chloride channel gene, CLCNKB, cause Bartter's syndrome type III. *Nature genetics* 1997; **17:** 171-178.
32. Simon DB, Karet FE, Hamdan JM*, et al.* Bartter's syndrome, hypokalaemic alkalosis with hypercalciuria, is caused by mutations in the Na-K-2Cl cotransporter NKCC2. *Nature genetics* 1996; **13:** 183-188.
33. Simon DB, Karet FE, Rodriguez-Soriano J*, et al.* Genetic heterogeneity of Bartter's syndrome revealed by mutations in the K+ channel, ROMK. *Nature genetics* 1996; **14:** 152-156.
34. Brown EM, MacLeod RJ. Extracellular calcium sensing and extracellular calcium signaling. *Physiol Rev* 2001; **81:** 239-297.
35. Bai M, Quinn S, Trivedi S*, et al.* Expression and characterization of inactivating and activating mutations in the human Ca2+o-sensing receptor. *The Journal of biological chemistry* 1996; **271:** 19537-19545.
36. Hannan FM, Nesbit MA, Zhang C*, et al.* Identification of 70 calcium-sensing receptor mutations in hyper- and hypo-calcaemic patients: evidence for clustering of extracellular domain mutations at calcium-binding sites. *Hum Mol Genet* 2012; **21:** 2768-2778.
37. Thakker RV. Genetic developments in hypoparathyroidism. *Lancet* 2001; **357:** 974-976.
38. Nesbit MA, Hannan FM, Howles SA*, et al.* Mutations affecting G-protein subunit alpha11 in hypercalcemia and hypocalcemia. *N Engl J Med* 2013; **368:** 2476-2486.
39. Hannan FM, Nesbit MA, Turner JJ*, et al.* Comparison of human chromosome 19q13 and syntenic region on mouse chromosome 7 reveals absence, in man, of 11.6 Mb containing four mouse calcium-sensing receptor-related sequences: relevance to familial benign hypocalciuric hypercalcaemia type 3. *European journal of human genetics : EJHG* 2010; **18:** 442-447.
40. Simon DB, Lu Y, Choate KA*, et al.* Paracellin-1, a renal tight junction protein required for paracellular Mg2+ resorption. *Science* 1999; **285:** 103-106.
41. Wolf MT, Dotsch J, Konrad M*, et al.* Follow-up of five patients with FHHNC due to mutations in the Paracellin-1 gene. *Pediatric nephrology* 2002; **17:** 602-608.
42. Godron A, Harambat J, Boccio V*, et al.* Familial hypomagnesemia with hypercalciuria and nephrocalcinosis: phenotype-genotype correlation and outcome in 32 patients with CLDN16 or CLDN19 mutations. *Clinical journal of the American Society of Nephrology : CJASN* 2012; **7:** 801-809.
43. Konrad M, Schaller A, Seelow D*, et al.* Mutations in the tight-junction gene claudin 19 (CLDN19) are associated with renal magnesium wasting, renal failure, and severe ocular involvement. *Am J Hum Genet* 2006; **79:** 949-957.
44. Hou J, Renigunta A, Konrad M*, et al.* Claudin-16 and claudin-19 interact and form a cation-selective tight junction complex. *J Clin Invest* 2008; **118:** 619-628.
45. Hou J, Renigunta A, Gomes AS*, et al.* Claudin-16 and claudin-19 interaction is required for their assembly into tight junctions and for renal reabsorption of magnesium. *Proc Natl Acad Sci U S A* 2009; **106:** 15350-15355.

46. Schlingmann KP, Weber S, Peters M*, et al.* Hypomagnesemia with secondary hypocalcemia is caused by mutations in TRPM6, a new member of the TRPM gene family. *Nature genetics* 2002; **31:** 166-170.
47. Walder RY, Landau D, Meyer P*, et al.* Mutation of TRPM6 causes familial hypomagnesemia with secondary hypocalcemia. *Nature genetics* 2002; **31:** 171-174.
48. Lainez S, Schlingmann KP, van der Wijst J*, et al.* New TRPM6 missense mutations linked to hypomagnesemia with secondary hypocalcemia. *European journal of human genetics : EJHG* 2014; **22:** 497-504.
49. Woudenberg-Vrenken TE, Sukinta A, van der Kemp AW*, et al.* Transient receptor potential melastatin 6 knockout mice are lethal whereas heterozygous deletion results in mild hypomagnesemia. *Nephron Physiol* 2011; **117:** p11-19.
50. Groenestege WM, Hoenderop JG, van den Heuvel L*, et al.* The epithelial Mg2+ channel transient receptor potential melastatin 6 is regulated by dietary Mg2+ content and estrogens. *Journal of the American Society of Nephrology : JASN* 2006; **17:** 1035-1043.
51. Groenestege WM, Thebault S, van der Wijst J*, et al.* Impaired basolateral sorting of pro-EGF causes isolated recessive renal hypomagnesemia. *The Journal of clinical investigation* 2007; **117:** 2260-2267.
52. Thebault S, Alexander RT, Tiel Groenestege WM*, et al.* EGF increases TRPM6 activity and surface expression. *Journal of the American Society of Nephrology : JASN* 2009; **20:** 78-85.
53. Dimke H, van der Wijst J, Alexander TR*, et al.* Effects of the EGFR Inhibitor Erlotinib on Magnesium Handling. *Journal of the American Society of Nephrology : JASN* 2010; **21:** 1309-1316.
54. Campbell P, Morton PE, Takeichi T*, et al.* Epithelial inflammation resulting from an inherited loss-of-function mutation in EGFR. *J Invest Dermatol* 2014; **134:** 2570-2578.
55. Gitelman HJ, Graham JB, Welt LG. A new familial disorder characterized by hypokalemia and hypomagnesemia. *Trans Assoc Am Physicians* 1966; **79:** 221-235.
56. Knoers NV, Levtchenko EN. Gitelman syndrome. *Orphanet J Rare Dis* 2008; **3:** 22.
57. Gullner HG, Gill JR, Jr., Bartter FC. Correction of hypokalemia by magnesium repletion in familial hypokalemic alkalosis with tubulopathy. *Am J Med* 1981; **71:** 578-582.
58. Schultheis PJ, Lorenz JN, Meneton P*, et al.* Phenotype resembling Gitelman's syndrome in mice lacking the apical Na+-Cl- cotransporter of the distal convoluted tubule. *The Journal of biological chemistry* 1998; **273:** 29150-29155.
59. Nijenhuis T, Vallon V, van der Kemp AW*, et al.* Enhanced passive Ca2+ reabsorption and reduced Mg2+ channel abundance explains thiazide-induced hypocalciuria and hypomagnesemia. *The Journal of clinical investigation* 2005; **115:** 1651-1658.
60. Loffing J, Vallon V, Loffing-Cueni D*, et al.* Altered renal distal tubule structure and renal Na(+) and Ca(2+) handling in a mouse model for Gitelman's syndrome. *Journal of the American Society of Nephrology : JASN* 2004; **15:** 2276-2288.
61. Reichold M, Zdebik AA, Lieberer E*, et al.* KCNJ10 gene mutations causing EAST syndrome (epilepsy, ataxia, sensorineural deafness, and tubulopathy) disrupt channel function. *Proceedings of the National Academy of Sciences of the United States of America* 2010; **107:** 14490-14495.
62. Scholl UI, Choi M, Liu T*, et al.* Seizures, sensorineural deafness, ataxia, mental retardation, and electrolyte imbalance (SeSAME syndrome) caused by mutations in KCNJ10. *Proceedings of the National Academy of Sciences of the United States of America* 2009; **106:** 5842-5847.
63. Cuevas CA, Su XT, Wang MX*, et al.* Potassium Sensing by Renal Distal Tubules Requires Kir4.1. *Journal of the American Society of Nephrology : JASN* 2017.
64. Cross JH, Arora R, Heckemann RA*, et al.* Neurological features of epilepsy, ataxia, sensorineural deafness, tubulopathy syndrome. *Dev Med Child Neurol* 2013; **55:** 846-856.
65. Meij IC, Koenderink JB, van Bokhoven H*, et al.* Dominant isolated renal magnesium loss is caused by misrouting of the Na(+),K(+)-ATPase gamma-subunit. *Nature genetics* 2000; **26:** 265-266.
66. de Baaij JH, Dorresteijn EM, Hennekam EA*, et al.* Recurrent FXYD2 p.Gly41Arg mutation in patients with isolated dominant hypomagnesaemia. *Nephrology, dialysis, transplantation : official publication of the European Dialysis and Transplant Association - European Renal Association* 2015.
67. Sha Q, Pearson W, Burcea LC*, et al.* Human FXYD2 G41R mutation responsible for renal hypomagnesemia behaves as an inward-rectifying cation channel. *American journal of physiology Renal physiology* 2008; **295:** F91-99.

68. Lote CJ, Thewles A, Wood JA*, et al.* The hypomagnesaemic action of FK506: urinary excretion of magnesium and calcium and the role of parathyroid hormone. *Clin Sci (Lond)* 2000; **99:** 285-292.
69. Adalat S, Woolf AS, Johnstone KA*, et al.* HNF1B mutations associate with hypomagnesemia and renal magnesium wasting. *Journal of the American Society of Nephrology : JASN* 2009; **20:** 1123-1131.
70. Chen YZ, Gao Q, Zhao XZ*, et al.* Systematic review of TCF2 anomalies in renal cysts and diabetes syndrome/maturity onset diabetes of the young type 5. *Chinese medical journal* 2010; **123:** 3326-3333.
71. Horikawa Y, Iwasaki N, Hara M*, et al.* Mutation in hepatocyte nuclear factor-1 beta gene (TCF2) associated with MODY. *Nature genetics* 1997; **17:** 384-385.
72. Bingham C, Bulman MP, Ellard S*, et al.* Mutations in the hepatocyte nuclear factor-1beta gene are associated with familial hypoplastic glomerulocystic kidney disease. *American journal of human genetics* 2001; **68:** 219-224.
73. Bingham C, Ellard S, van't Hoff WG*, et al.* Atypical familial juvenile hyperuricemic nephropathy associated with a hepatocyte nuclear factor-1beta gene mutation. *Kidney international* 2003; **63:** 1645-1651.
74. Verhave JC, Bech AP, Wetzels JF*, et al.* Hepatocyte Nuclear Factor 1beta-Associated Kidney Disease: More than Renal Cysts and Diabetes. *Journal of the American Society of Nephrology : JASN* 2015.
75. Clissold RL, Hamilton AJ, Hattersley AT*, et al.* HNF1B-associated renal and extra-renal disease-an expanding clinical spectrum. *Nature reviews Nephrology* 2015; **11:** 102-112.
76. Edghill EL, Bingham C, Slingerland AS*, et al.* Hepatocyte nuclear factor-1 beta mutations cause neonatal diabetes and intrauterine growth retardation: support for a critical role of HNF-1beta in human pancreatic development. *Diabetic medicine : a journal of the British Diabetic Association* 2006; **23:** 1301-1306.
77. Clissold RL, Shaw-Smith C, Turnpenny P*, et al.* Chromosome 17q12 microdeletions but not intragenic HNF1B mutations link developmental kidney disease and psychiatric disorder. *Kidney international* 2016; **90:** 203-211.
78. Lindner TH, Njolstad PR, Horikawa Y*, et al.* A novel syndrome of diabetes mellitus, renal dysfunction and genital malformation associated with a partial deletion of the pseudo-POU domain of hepatocyte nuclear factor-1beta. *Human molecular genetics* 1999; **8:** 2001-2008.
79. Bingham C, Ellard S, Cole TR*, et al.* Solitary functioning kidney and diverse genital tract malformations associated with hepatocyte nuclear factor-1beta mutations. *Kidney international* 2002; **61:** 1243-1251.
80. Iwasaki N, Ogata M, Tomonaga O*, et al.* Liver and kidney function in Japanese patients with maturity-onset diabetes of the young. *Diabetes care* 1998; **21:** 2144-2148.
81. Haldorsen IS, Vesterhus M, Raeder H*, et al.* Lack of pancreatic body and tail in HNF1B mutation carriers. *Diabetic medicine : a journal of the British Diabetic Association* 2008; **25:** 782-787.
82. van der Made CI, Hoorn EJ, de la Faille R*, et al.* Hypomagnesemia as First Clinical Manifestation of ADTKD-HNF1B: A Case Series and Literature Review. *American journal of nephrology* 2015; **42:** 85-90.
83. Ferre S, Bongers EM, Sonneveld R*, et al.* Early development of hyperparathyroidism due to loss of PTH transcriptional repression in patients with HNF1beta mutations? *The Journal of clinical endocrinology and metabolism* 2013; **98:** 4089-4096.
84. Faguer S, Decramer S, Chassaing N*, et al.* Diagnosis, management, and prognosis of HNF1B nephropathy in adulthood. *Kidney international* 2011; **80:** 768-776.
85. Ferre S, de Baaij JH, Ferreira P*, et al.* Mutations in PCBD1 cause hypomagnesemia and renal magnesium wasting. *Journal of the American Society of Nephrology : JASN* 2014; **25:** 574-586.
86. Mendel DB, Khavari PA, Conley PB*, et al.* Characterization of a cofactor that regulates dimerization of a mammalian homeodomain protein. *Science* 1991; **254:** 1762-1767.
87. Rose RB, Bayle JH, Endrizzi JA*, et al.* Structural basis of dimerization, coactivator recognition and MODY3 mutations in HNF-1alpha. *Nat Struct Biol* 2000; **7:** 744-748.
88. Unger S, Gorna MW, Le Bechec A*, et al.* FAM111A mutations result in hypoparathyroidism and impaired skeletal development. *Am J Hum Genet* 2013; **92:** 990-995.
89. Bergada I, Schiffrin A, Abu Srair H*, et al.* Kenny syndrome: description of additional abnormalities and molecular studies. *Hum Genet* 1988; **80:** 39-42.
90. Fanconi S, Fischer JA, Wieland P*, et al.* Kenny syndrome: evidence for idiopathic hypoparathyroidism in two patients and for abnormal parathyroid hormone in one. *J Pediatr* 1986; **109:** 469-475.

91. Nikkel SM, Ahmed A, Smith A*, et al.* Mother-to-daughter transmission of Kenny-Caffey syndrome associated with the recurrent, dominant FAM111A mutation p.Arg569His. *Clin Genet* 2014; **86:** 394-395.
92. Isojima T, Doi K, Mitsui J*, et al.* A recurrent de novo FAM111A mutation causes Kenny-Caffey syndrome type 2. *J Bone Miner Res* 2014; **29:** 992-998.
93. Fine DA, Rozenblatt-Rosen O, Padi M*, et al.* Identification of FAM111A as an SV40 host range restriction and adenovirus helper factor. *PLoS Pathog* 2012; **8:** e1002949.
94. Alabert C, Bukowski-Wills JC, Lee SB*, et al.* Nascent chromatin capture proteomics determines chromatin dynamics during DNA replication and identifies unknown fork components. *Nat Cell Biol* 2014; **16:** 281-293.
95. Nair AV, Hocher B, Verkaart S*, et al.* Loss of insulin-induced activation of TRPM6 magnesium channels results in impaired glucose tolerance during pregnancy. *Proceedings of the National Academy of Sciences of the United States of America* 2012; **109:** 11324-11329.
96. Leunissen EH, Blanchard MG, Sheedfar F*, et al.* Urinary beta-galactosidase stimulates Ca2+ transport by stabilizing TRPV5 at the plasma membrane. *Glycobiology* 2016; **26:** 472-481.
97. Leipziger J. Luminal nucleotides are tonic inhibitors of renal tubular transport. *Current opinion in nephrology and hypertension* 2011; **20:** 518-522.
98. Novak I. Purinergic signalling in epithelial ion transport: regulation of secretion and absorption. *Acta Physiol (Oxf)* 2011; **202:** 501-522.
99. Cooke HJ, Wunderlich J, Christofi FL. "The force be with you": ATP in gut mechanosensory transduction. *News Physiol Sci* 2003; **18:** 43-49.
100. Wildman SS, Marks J, Turner CM*, et al.* Sodium-dependent regulation of renal amiloride-sensitive currents by apical P2 receptors. *Journal of the American Society of Nephrology : JASN* 2008; **19:** 731-742.
101. de Baaij JH, Blanchard MG, Lavrijsen M*, et al.* P2X4 receptor regulation of transient receptor potential melastatin type 6 (TRPM6) Mg2+ channels. *Pflugers Archiv : European journal of physiology* 2014; **466:** 1941-1952.
102. Riccardi D, Brown EM. Physiology and pathophysiology of the calcium-sensing receptor in the kidney. *Am J Physiol Renal Physiol* 2010; **298:** F485-499.
103. Riccardi D, Park J, Lee WS*, et al.* Cloning and functional expression of a rat kidney extracellular calcium/polyvalent cation-sensing receptor. *Proc Natl Acad Sci U S A* 1995; **92:** 131-135.
104. Loupy A, Ramakrishnan SK, Wootla B*, et al.* PTH-independent regulation of blood calcium concentration by the calcium-sensing receptor. *The Journal of clinical investigation* 2012; **122:** 3355-3367.
105. Toka HR. New functional aspects of the extracellular calcium-sensing receptor. *Current opinion in nephrology and hypertension* 2014; **23:** 352-360.
106. Tian T, Wang J, Zhou X. A review: microRNA detection methods. *Org Biomol Chem* 2015; **13:** 2226-2238.
107. Nijenhuis T, Sloan AJ, Hoenderop JG*, et al.* Angiotensin II contributes to podocyte injury by increasing TRPC6 expression via an NFAT-mediated positive feedback signaling pathway. *Am J Pathol* 2011; **179:** 1719-1732.
108. Hoenderop JG, Dardenne O, Van Abel M*, et al.* Modulation of renal Ca2+ transport protein genes by dietary Ca2+ and 1,25-dihydroxyvitamin D3 in 25-hydroxyvitamin D3-1alpha-hydroxylase knockout mice. *FASEB J* 2002; **16:** 1398-1406.
109. Ikari A, Sanada A, Okude C*, et al.* Up-regulation of TRPM6 transcriptional activity by AP-1 in renal epithelial cells. *J Cell Physiol* 2010; **222:** 481-487.
110. van Abel M, Hoenderop JG, van der Kemp AW*, et al.* Coordinated control of renal Ca(2+) transport proteins by parathyroid hormone. *Kidney international* 2005; **68:** 1708-1721.
111. Lee JW, Chou CL, Knepper MA. Deep Sequencing in Microdissected Renal Tubules Identifies Nephron Segment-Specific Transcriptomes. *Journal of the American Society of Nephrology : JASN* 2015; **26:** 2669-2677.
112. Efrati E, Hirsch A, Kladnitsky O*, et al.* Transcriptional regulation of the claudin-16 gene by Mg2+ availability. *Cell Physiol Biochem* 2010; **25:** 705-714.
113. Kladnitsky O, Rozenfeld J, Azulay-Debby H*, et al.* The claudin-16 channel gene is transcriptionally inhibited by 1,25-dihydroxyvitamin D. *Exp Physiol* 2014.
114. Barbacci E, Reber M, Ott MO*, et al.* Variant hepatocyte nuclear factor 1 is required for visceral endoderm specification. *Development* 1999; **126:** 4795-4805.

115. Gresh L, Fischer E, Reimann A*, et al.* A transcriptional network in polycystic kidney disease. *The EMBO journal* 2004; **23:** 1657-1668.
116. Hiesberger T, Bai Y, Shao X*, et al.* Mutation of hepatocyte nuclear factor-1beta inhibits Pkhd1 gene expression and produces renal cysts in mice. *The Journal of clinical investigation* 2004; **113:** 814-825.
117. Faguer S, Decramer S, Devuyst O*, et al.* Expression of renal cystic genes in patients with HNF1B mutations. *Nephron Clinical practice* 2012; **120:** c71-78.
118. Gong Y, Ma Z, Patel V*, et al.* HNF-1beta regulates transcription of the PKD modifier gene Kif12. *Journal of the American Society of Nephrology : JASN* 2009; **20:** 41-47.
119. Arystarkhova E, Donnet C, Asinovski NK*, et al.* Differential regulation of renal Na,K-ATPase by splice variants of the gamma subunit. *J Biol Chem* 2002; **277:** 10162-10172.
120. Pu HX, Cluzeaud F, Goldshleger R*, et al.* Functional role and immunocytochemical localization of the gamma a and gamma b forms of the Na,K-ATPase gamma subunit. *The Journal of biological chemistry* 2001; **276:** 20370-20378.
121. Mundade R, Ozer HG, Wei H*, et al.* Role of ChIP-seq in the discovery of transcription factor binding sites, differential gene regulation mechanism, epigenetic marks and beyond. *Cell Cycle* 2014; **13:** 2847-2852.
122. Park PJ. ChIP-seq: advantages and challenges of a maturing technology. *Nature reviews Genetics* 2009; **10:** 669-680.
123. Todeschini AL, Georges A, Veitia RA. Transcription factors: specific DNA binding and specific gene regulation. *Trends Genet* 2014; **30:** 211-219.
124. Wang Z, Gerstein M, Snyder M. RNA-Seq: a revolutionary tool for transcriptomics. *Nature reviews Genetics* 2009; **10:** 57-63.

2 Loss of transcriptional activation of the potassium channel Kir5.1 by HNF1β drives autosomal dominant tubulointerstitial kidney disease

Andreas Kompatscher[1]*, Jeroen H.F. de Baaij[1]*, Karam Aboudehen[3], Anke P.W.M. Hoefnagels[1], Peter Igarashi[3], René J.M. Bindels[1], Gertjan J.C. Veenstra[2] & Joost G.J. Hoenderop[1]

[1]Department of Physiology, Radboud Institute for Molecular Life Sciences, Radboud university medical center; [2]Department of Molecular Developmental Biology, Radboud Institute for Molecular Life Sciences, Radboud University Nijmegen [3]Department of Medicine, University of Minnesota Medical School, Minneapolis, Minnesota, USA

*A.K. and J.H.F.d.B. contributed equally to this work.

Kidney International, 2017, 92(5):1145-1156

Abstract

HNF1β is an essential transcription factor for the development and functioning of the kidney. Mutations in HNF1β cause autosomal dominant tubulointerstitial kidney disease (ADTKD-HNF1β), which is characterized by renal cysts and maturity-onset diabetes of the young (MODY). Moreover, patients suffer from a severe electrolyte phenotype consisting of hypomagnesemia and hypokalemia. Until now, genes that are regulated by HNF1β are only partially known and do not fully explain the phenotype of the patients. Therefore, we conducted chIP-seq in immortalized mouse kidney cells (mpkDCT) to identify HNF1β binding sites at a genome-wide scale.

In total 7,421 HNF1β binding sites were identified, including several genes involved in electrolyte transport and diabetes. A highly specific and conserved HNF1β site was identified in the promoter of *Kcnj16*, encoding the potassium channel Kir5.1. Luciferase-promoter assays showed a 2.2 fold increase in *Kcnj16* expression when HNF1β was present. Expression of the Hnf1β p.Lys156Glu mutant that was previously identified in a ADTKD-HNF1β patient, did not activate *Kcnj16* expression. Knock down of *Hnf1β* in mpkDCT cells significantly reduced the expression of *Kcnj16* (Kir5.1) and *Kcnj10* (Kir4.1) by 38% and 37%, respectively. These results were confirmed in a HNF1β renal knockout mouse, exhibiting downregulation of *Kcnj16*, *Kcnj10* and *Slc12a3* transcripts in the kidney by 78%, 83% and 76%, respectively, compared to HNF1β wild-type mice.

In conclusion, HNF1β has been identified as a transcriptional activator of *Kcnj16*. Consequently patients with *HNF1β* mutations may have a reduced Kir5.1 activity in the kidney, resulting in hypokalemia and hypomagnesemia.

Keywords: HNF1β, Kir4.1, Kir5.1, ADTKD-HNF1β, hypomagnesemia, potassium, magnesium, chIP-seq

Introduction

Heterozygous deletion or mutation of hepatocyte nuclear factor 1 homeobox B (*HNF1β*) causes autosomal dominant tubulointerstitial kidney disease (ADTKD-HNF1β, OMIM: 137920),[1] comprising a wide variety of renal and extra-renal disorders. Although the symptoms have incomplete penetrance, the most common clinical phenotype is renal malformation combined with maturity-onset diabetes of the young (MODY5).[1-5] However, patients can also present with genital tract malformations,[6, 7] pancreatic hypoplasia,[8] abnormal liver functioning,[9] electrolyte disturbances,[4, 10] and hyperparathyroidism.[11] This makes ADTKD-HNF1β a multi-systemic disorder with a highly heterogeneous phenotype that is difficult to diagnose in the clinic.

Careful phenotyping of the electrolyte disturbances observed in ADTKD-HNF1β patients led several clinicians to conclude that the phenotype is reminiscent of Gitelman syndrome (OMIM: 263800). The shared symptoms include hypomagnesemia and hypokalemia, although hypocalciuria and metabolic alkalosis are less frequently observed.[4, 5, 10, 12] In Gitelman syndrome, inactivating mutations in the sodium-chloride-cotransporter (NCC) decrease Na^+ and Mg^{2+} transport in the DCT and increase K^+ secretion further downstream.[13, 14] Similarly, in SeSAME/EAST syndrome (OMIM: 612780) loss of function mutations in the Kir4.1/Kir5.1 inward-rectifying K^+ channel are causative for hypomagnesemia and hypokalemia.[15-17] Whether mutations in HNF1β affect NCC or Kir4.1/Kir5.1 remains to be elucidated.

Over the last decade, several transcriptional targets of HNF1β have been identified, including *UMOD*, *PKHD1* and *FXYD2*.[18-20] Specifically *FXYD2* has been implicated in the electrolyte disturbances observed in ADTKD-HNF1β. *FXYD2* encodes for the γ-subunit of the Na^+-K^+-ATPase and as such regulates the basolateral membrane potential.[4, 20] Indeed, heterozygous mutations in *FXYD2* are known to cause autosomal dominant hypomagnesemia with hypocalciuria (OMIM: 154020).[21, 22] Whether the regulation of *FXYD2* by HNF1β is sufficient to explain the symptoms in ADTKD-HNF1β is being questioned.[23] Current studies on HNF1β binding sites depend mainly on bio-informatical identification of the HNF1β recognition sequence in gene promoters. The complete genome-wide spectrum of HNF1β binding sites in the distal convoluted tubule (DCT) is not known.

The aim of our study was to elucidate the role of HNF1β in DCT electrolyte reabsorption. To this end, a genome-wide DNA binding profile for HNF1β was acquired by performing a chromatin immunoprecipitation followed by next generation sequencing (chIP-seq). Kir5.1 was identified as a prime candidate and its regulation by HNF1β was characterized by luciferase promoter assays and siRNA knock down experiments. Moreover, using renal-specific HNF1β knockout mice, the transcriptional effects of HNF1β were examined in the kidney.

Results

HNF1β is expressed in the distal convoluted tubule

Immunohistochemistry of mouse kidney was performed to examine the HNF1β localization and expression. HNF1β was located to the nuclei of tubular cells (Figure 1), and was absent in the interstitium and glomerulus. HNF1β is expressed with DCT marker Parvalbumin in the distal convoluted tubule.

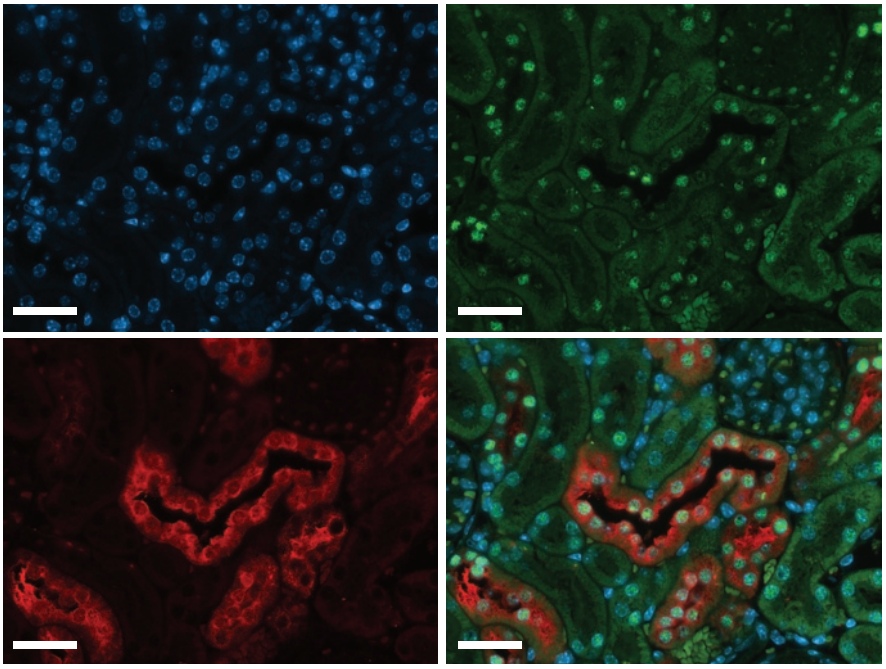

Figure 1 | HNF1β is expressed in the distal convoluted tubule

Immunohistochemical stainings of mouse kidney sections were co-stained with anti-HNF1β in green (top right), anti-Parvalbumin in red, (lower left) and 4', 6-diamidino-2-phenylindole (DAPI) in blue (top left). A merged image is shown in the lower right. Scale bar: 100 μm.

HNF1β chIP-seq binding sites are specific for the HNF1β motif

Genome-wide HNF1β binding sites were identified by performing chromatin-immunoprecipitation and sequencing (chIP-seq) on mpkDCT cells. Chromatin was isolated, cross-linked and immunoprecipitated with an anti-HNF1β antibody. After de-cross-

linking, samples underwent next-generation sequencing. Binding sites were found by comparing enriched immunoprecipitated genomic sequences to an untreated input control (genomic background). In total, 7421 HNF1β binding sites were significantly enriched over background (false discovery rate (FDR); q<0.001). Of which 4530 genes contained an HNF1β peak within 50kb of their respective transcription start sites (TSS). To determine whether these binding sites are near actively transcribed genes, a chIP-seq with an antibody against histone 3 lysine 4 trimethyl (H3K4me3) was performed. Of note: H3K4me3 is a histone marker for active TSS [24]. 43.5% of all HNF1β binding sites could be assigned to actively transcribed genes, determined by the presence of H3K4 trimethylation. 28.5% of HNF1β binding peaks were linked to H3K4me3 negative genes and the remaining 28% were located to intergene regions (Figure 2A). The nucleotide sequence of HNF1β binding sites in our analysis corresponds to the database motif nRTTAATnATTAACn for HNF1β binding (JASPAR database ID: MA0153.2), showing high specificity and sensitivity of the chIP-seq (Figure 2B-D). Furthermore, HNF1β bindings sites were identified in promoters of several known targets of HNF1β, for example *Pkhd1* and *Pcbd1* (Figure 2E).

HNF1β peaks are significantly enriched in putative promoter regions

Cis-regulatory element annotation system (CEAS) was used to quantify peak distribution along the genome (Figure 3A). This method assesses the percentage of Hnf1β binding sites found in upstream promoters, distal sites or the gene body [25]. A significant 1.78 fold (p<0.001) enrichment in HNF1β peaks was observed in a range of 3 kb upstream from the TSS of putative promoter regions, compared to genomic background (Figure 3A). No enrichment was found in regions <3 kb distal from the TSS. HNF1β peak enrichment was significantly lower in the gene body, which consists of the coding exons, introns, 5'UTR and 3'UTR. Hierarchical clustering with Euclidean distance metric was performed to assess the amount of overlap of HNF1β peaks with H3K4me3 peaks. Within a window of ±10 kb surrounding H3K4me3 peaks, most HNF1β binding sites were located either upstream or more distal from enriched H3K4 trimethylation binding sites indicating limited overlap with H3K4 trimethylation positive promoter regions (Figure 3B).

HNF1β shows enrichment of the MODY and type II diabetes pathways

Kyoto Encyclopedia of Genes and Genomes (KEGG) pathway analysis was performed on genes positive for HNF1β binding sites.[26] A significant enrichment for MODY and type II diabetes pathway was detected (Figure 4A). Interestingly, HNF1β peaks were located near the transcription start sites of genes related to diabetes, including *Hnf1α*, *Irs1* and *Irs2* (Figure 5). Subsequent gene ontology (GO) analysis showed enrichment of 'ion binding' (GO:0043167), 'calcium' (GO:0005509) and 'magnesium ion binding' (GO:0000287) GO-terms (Figure 5B).

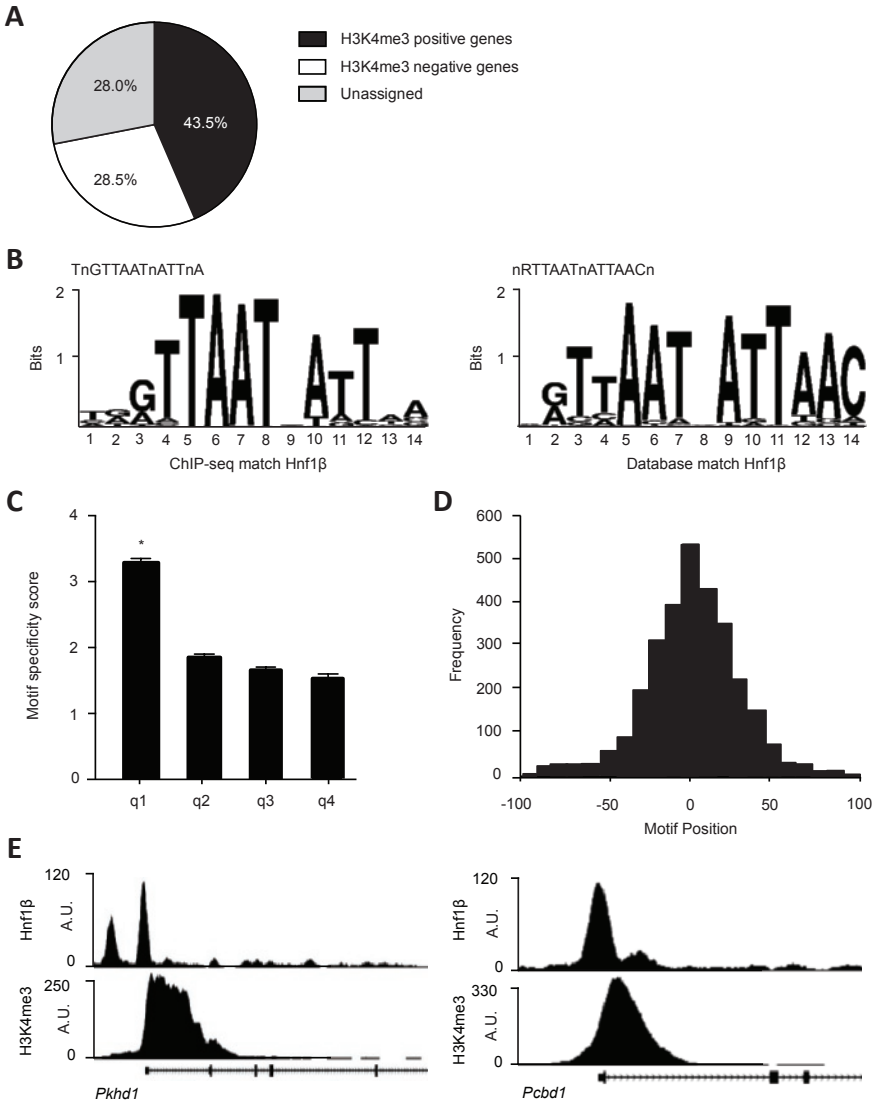

Figure 2 | HNF1β chIP-seq binding sites are specific for the HNF1β motif and known HNF1β target genes

A) Pie chart showing HNF1β peaks assigned to genes in a 50 kb window around the TSS. In total 7421 peaks were called (q<0.001). The percentage of H3K4me3 positive genes is depicted in black, H3K4me3 negative genes are shown in white and peaks that could not be assigned to a gene are portrayed in the grey segment. B) Left, sequence logo of the HNF1β motif found with the GimmeMotifs algorithm in our chIP-seq dataset. Right, HNF1β sequence logo acquired

from the JASPAR database (ID: MA0153.2). C) Histogram showing the HNF1β motif specificity score in relation to HNF1β peak height. Peaks were sorted by peak height in descending order and divided into quartiles (q1-4). Data (n=1855 per quartile) represent the mean ± SEM HNF1β motif specificity score. One-way ANOVA with Holm-Sidak correction, *, p<0.05. D) Positional preference plot indicates HNF1β peak frequency in relation to the motif position. The x-axis is the relative distance to the central position of the analyzed motif. E) HNF1β and H3K4me3 binding profile for two known targets of HNF1β, respectively *Pkhd1* (left) and *Pcbd1* (right).

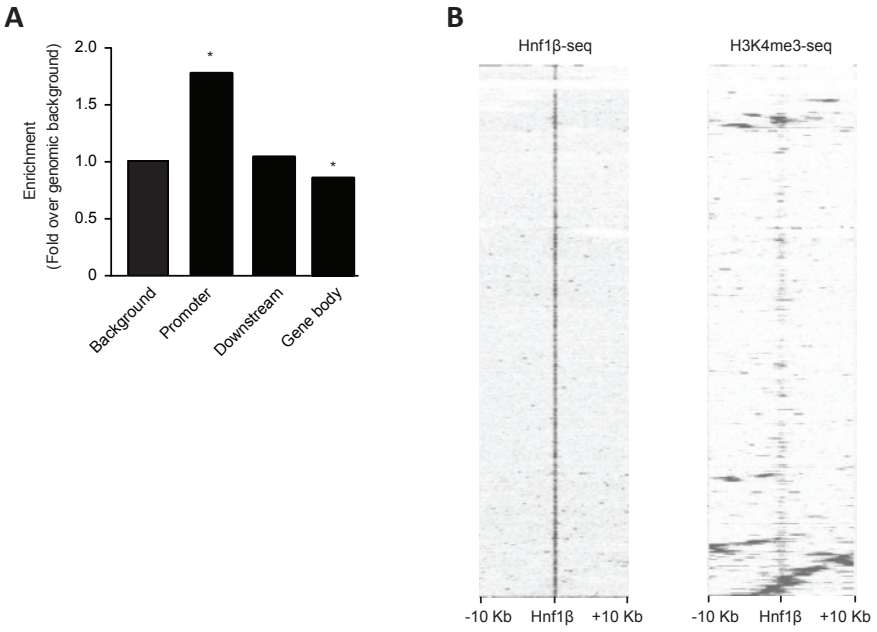

Figure 3 | HNF1β peaks are significantly enriched in putative promoter regions

A) Distribution of HNF1β peak location relative to RefSeq genes. Promoter indicates all HNF1β peaks that are <3 kb upstream from the TSS. Downstream refers to enrichment of HNF1β peaks over genomic background in <3 kb downstream from the TSS. A significantly lower enrichment of HNF1β peaks over genomic background is shown in the gene body. The gene body includes all exons, introns, 5' UTR and 3' UTR. One-sided binominal test *, p<0.01. B) Heatmap of HNF1β and H3K4me3 chIP-seq signal in a 10 kb window around HNF1β peak regions using hierarchical clustering with Euclidean distance metric. Rows in the heatmap represent individual peak regions. Left, all HNF1β peaks are centered in the middle of the map. Most HNF1β peaks are located >10 kb upstream or distal locations from H3K4me3 positive promoters.

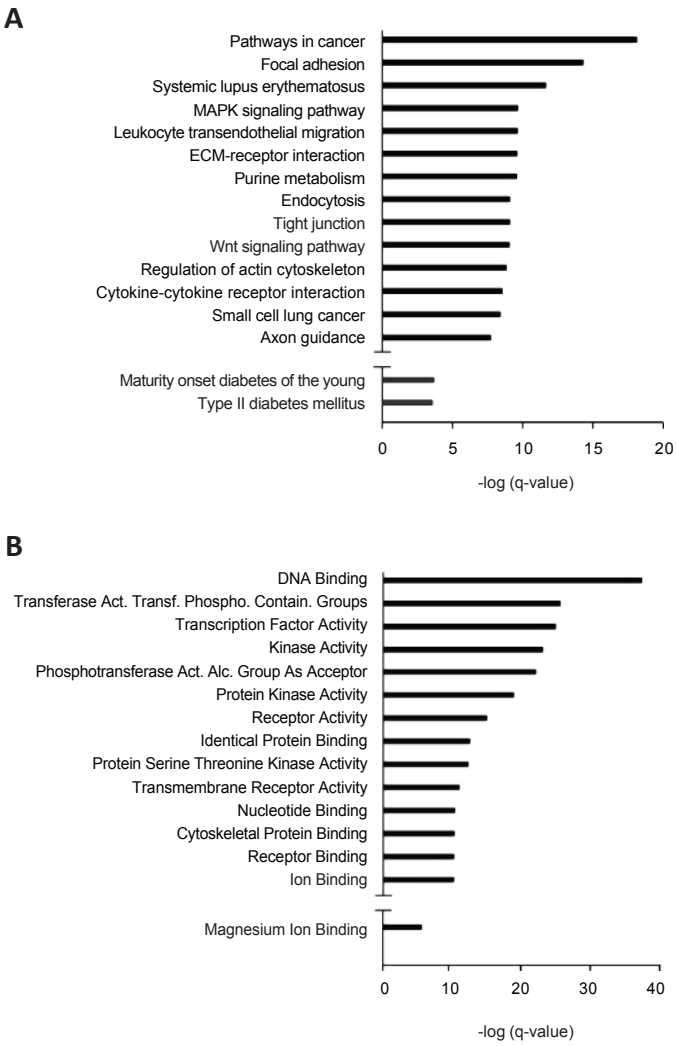

Figure 4 | HNF1β chIP-seq shows enrichment of the MODY and type II diabetes pathways and has novel bindings sites in known cystic and diabetes genes

A) KEGG pathway analysis was performed on genes with a HNF1β binding site in a window of 50 kb surrounding the TSS. The x-axis shows the –log q-value for each identified KEGG pathway. The q-value is adjusted with a FDR correction. B) GO-term molecular function analysis was performed on genes that had an Hnf1β peak in a window of 50 kb surrounding the TSS. The x-axis shows the –log q-value for each significant pathway. The q-value is adjusted for multiple comparisons with a FDR correction.

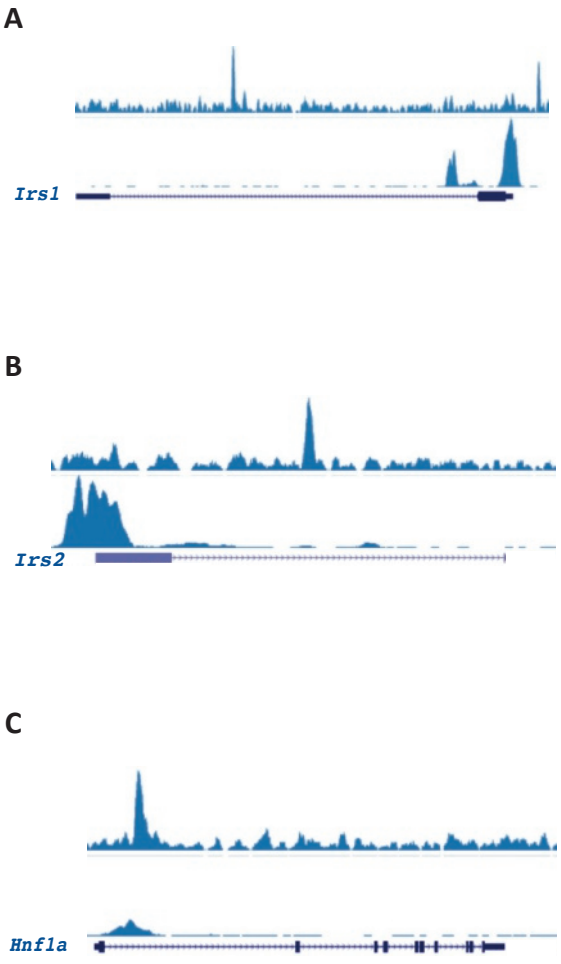

Figure 5 | Novel HNF1β binding sites are found in known diabetes genes

A-C) Screenshots of the UCSC genome browser for *Hnf1α*, *Irs1* and *Irs2* reveals HNF1β binding sites (upper track) near the H3K4me3 enriched transcription start sites (bottom track) of these genes.

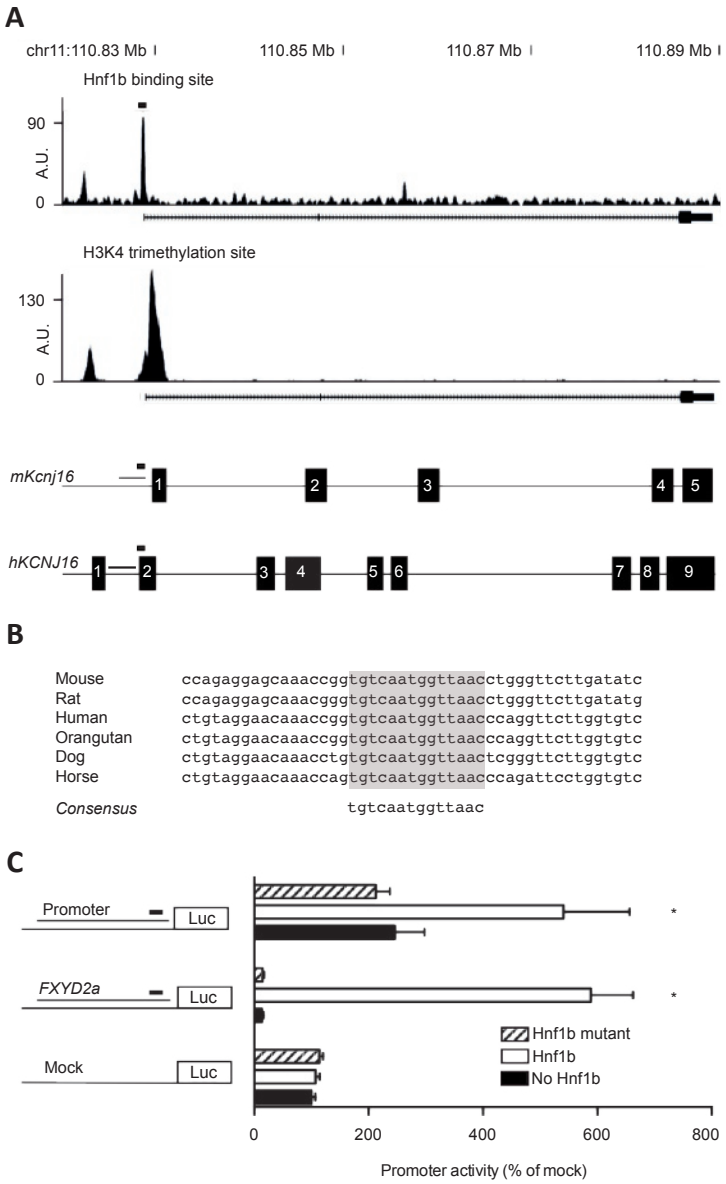

Figure 6 | HNF1β enhances activation of the *Kcnj16* promoter

A) HNF1β binding profile for Kir5.1 in mpkDCT cells. Underneath displays a linear representation of the location of the promoter, HNF1β binding site and H3K4 trimethylation site in relation to the exons of Kir5.1 for both mouse and human. A black rectangle denotes the HNF1β binding

site. B) Alignment of the HNF1β peak at -60 bp from the TSS of different species revealed a highly conserved binding site. C) HEK293 cells were transiently transfected with a luciferase construct carrying the *Kcnj16* promoter with the HNF1β binding site. Luciferase constructs with *Fxyd2a* were transfected as a positive control and an empty vector was added as negative control. Promoter activity was tested with (white bars), without (black bars) or with mutant (striped bars) HNF1β stimulation. Data (n=3) represent mean ± SEM. *, $p<0.05$, compared with non-stimulated condition.

HNF1β enhances activation of the *Kcnj16* promoter

Since patients with ADTKD-HNF1β suffer from a Gitelman-like phenotype, genes involved in Mg^{2+}, Na^{+} and K^{+} reabsorption were specifically analyzed. A highly enriched peak was located in the promoter of *Kcnj16* (Kir5.1), which is an important subunit of the Kir4.1/Kir5.1 inward rectifying K^{+} channel (Figure 6A). The peak was found 60 base pairs (bp) in front of the TSS and displays high nucleotide conservation (Figure 6B). Furthermore, it shows relatively high motif conservation with a motif specificity score of 5.26, obtained by the 'screen motif' algorithm.[27] Placing this binding site in the 15% of HNF1β peaks (n=7421) with the highest motif specificity scores (Supplemental table 1). To confirm the reproducibility of HNF1β binding, the binding site was validated separately with chromatin immunoprecipitation and real time quantitative

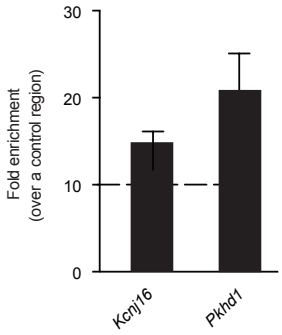

Figure 7 | The novel HNF1β binding site in the *Kcnj16* promoter is significantly enriched in mpkDCT cells

HNF1β chIP samples of mpkDCT samples were used to verify the HNF1β binding site in the Kcnj16 promoter. The *Pkhd1* binding site was used as a positive control. Samples were measured by quantitative RT-PCR. Data represent mean ± SEM and are expressed as fold enrichment over background. The cutoff for sufficient enrichment of the binding site was set at 10 fold enrichment over background. The background signal was determined at genomic coordinates GRCm38 chr15:99578842-99579015.

PCR and demonstrated 15-fold enrichment over background (Figure 7). Subsequently, luciferase constructs containing the human promoter for *KCNJ16* including the HNF1β binding site were expressed in Human Embryonic Kidney cells (HEK293). HNF1β increased *KCNJ16* promoter activity 2.2-fold compared to mock transfected cells (Figure 6C). Subsequently, we examined the effect of a HNF1β p.Lys156Glu mutant that was previously reported in a patient with renal cysts and MODY.[4, 28] HNF1β p.Lys156Glu did not raise *KCNJ16* or *FXYD2a* promoter activity.

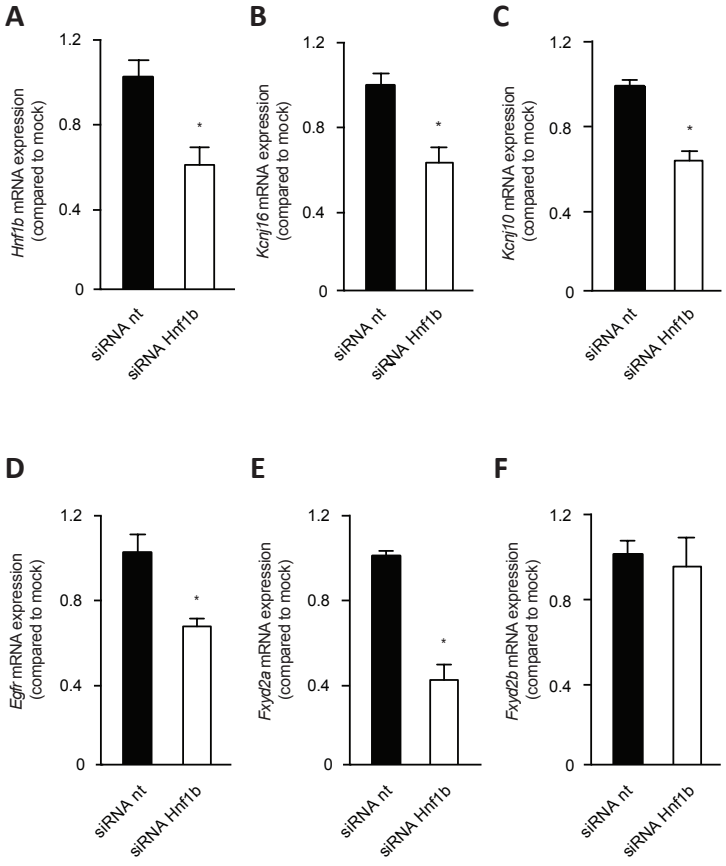

Figure 8 | Knockdown of *Hnf1β* causes downregulation of *Kcnj16* and *Kcnj10*

A-F) The mRNA expression levels of *Hnf1β* (A), *Kcnj16* (B), *Kcnj10* (C), *Egfr* (D), *Fxyd2a* (E), *Fxyd2b* (F) in mpkDCT cells treated with either non-targeting (nt) (black bars) or Hnf1β targeting (white bars) siRNAs. Samples were measured by quantitative RT-PCR and normalized for *Gapdh* expression. Data (n=3) represent mean ± SEM and are expressed as the fold difference when compared to the expression in siRNA nt.

Knockdown of HNF1β downregulates *Kcnj16* and *Kcnj10*

To further substantiate the transcriptional activation of *Kcnj16* by HNF1β, mpkDCT cells were transfected with siRNA targeting *Hnf1β.* RT-PCR analysis demonstrated a significant 42±28% decrease in *Hnf1β* transcript compared to a non-targeting siRNA (Figure 8A). *Kcnj16* mRNA levels were significantly decreased by 38±23%, (Figure 8B). Moreover, the expression of *Kcnj10,* encoding Kir4.1, and the EGF-receptor (*Egfr*) were downregulated with 37±13% and 36±23% respectively (Figure 8C and D). Transient receptor potential cation channel, subfamily M member 6 (*Trpm6*) and Epidermal growth factor (*Egf*) expression were not significantly altered (Figure 9). *Fxyd2a* was significantly downregulated by 60±20% in the absence of HNF1β, whereas *Fxyd2b* transcript levels were not affected (Figure 8E and F). Due too low *Slc12a3* transcript levels in the mpkDCT cells available to us, we were not able to reliably measure *Slc12a3* transcript abundance.

HNF1β regulates *Kcnj16*, *Kcnj10* and *Slc12a3* in a HNF1β mutant mouse model

To further substantiate that genes involved in electrolyte handling in the DCT are regulated by HNF1β, RT-PCR analysis for the expression of several genes was performed on RNA isolated from kidneys of Ksp-Cre;*Hnf1β*$^{flox/flox}$ mice (n=3). In these mice, *Hnf1β* is specifically inactivated in renal distal tubules.[29] This kidney-specific inactivation of *Hnf1β* significantly ($p<0.05$) decreased the transcript expression of

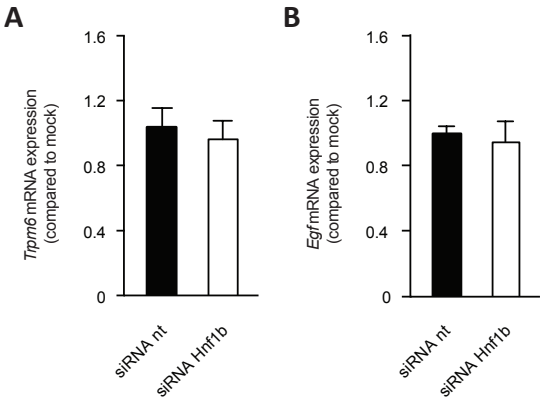

Figure 9 | Knockdown of *Hnf1β* has no effect on the transcription of *Trpm6* and *Egf*

A-B) The mRNA expression levels of *Trpm6* (A) and *Egf* (B) in mpkDCT cells treated with either non-targeting (nt) (black bars) or Hnf1β targeting (white bars) siRNAs. Samples were measured by quantitative RT-PCR and normalized for *Gapdh* expression. Data (n=3) represent mean ± SEM and are expressed as the fold difference when compared to the expression in siRNA nt.

Kcnj16, *Kcnj10* and *Slc12a3* in the kidney by 78±30%, 83±30% and 76±22%, respectively (Figure 10A, B and C). The expression of well-know HNF1β target *Pkhd1* was determined as a positive control and shown to be significantly reduced in HNF1β$^{fl+/fl+}$ mice by 66±12% (Figure 10D). No significant reduction was observed for other DCT genes, including *Trpm6* and the *Egfr* (Figure 10E and F). To exclude hypothrophy of

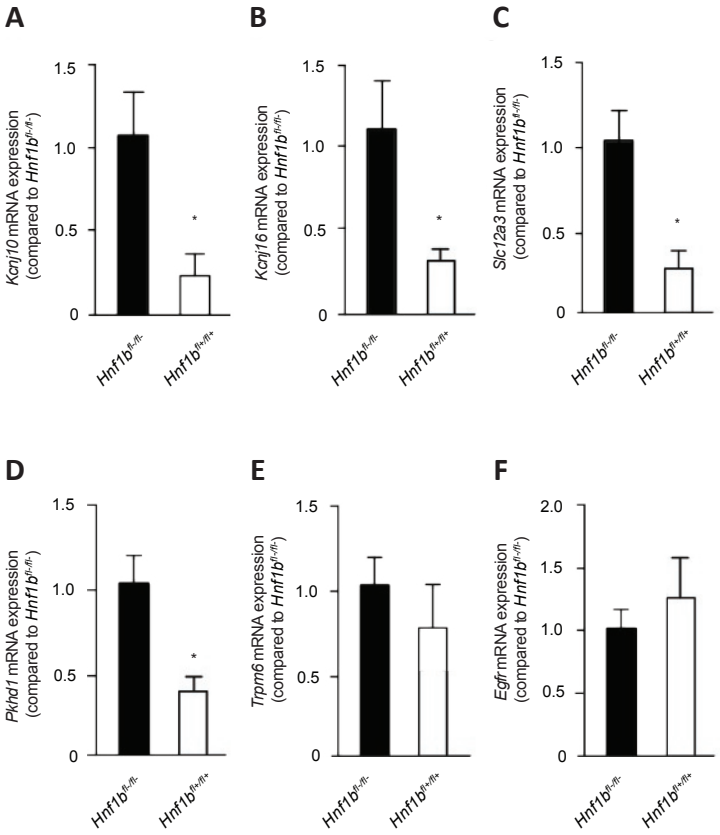

Figure 10 | *Kcnj16*, *Kcnj10* and *Slc12a3* transcripts are reduced in a HNF1β mutant mouse model

A-F) The mRNA expression levels of *Hnf1β* (A), *Kcnj16* (B), *Kcnj10* (C), *Egfr* (D), *Fxyd2a* (E), *Fxyd2b* (F) in Ksp-Cre;*Hnf1β$^{flox/flox}$* mouse kidneys. The black bars represent *Hnf1β$^{fl-/fl-}$* wild-type mice, while the white bars represent *Hnf1β$^{fl+/fl+}$* knockout mice. Samples were measured by quantitative RT-PCR and normalized for 18s ribosomal RNA expression. Data (n=3) represent mean ± SEM and are expressed as the fold difference when compared to the expression in *Hnf1β$^{fl-/fl-}$* wild-type mice.

the DCT as a cause for the decrease in transcript abundance, kidney slices from Ksp-Cre;*Hnf1β*$^{flox/flox}$ mice were stained for the DCT-specific marker parvalbumin. A qualitative assessment did not detect differences between *Hnf1β*$^{fl-/fl-}$ wild type and *Hnf1β*$^{fl+/fl+}$ mutant mice (Figure 11).

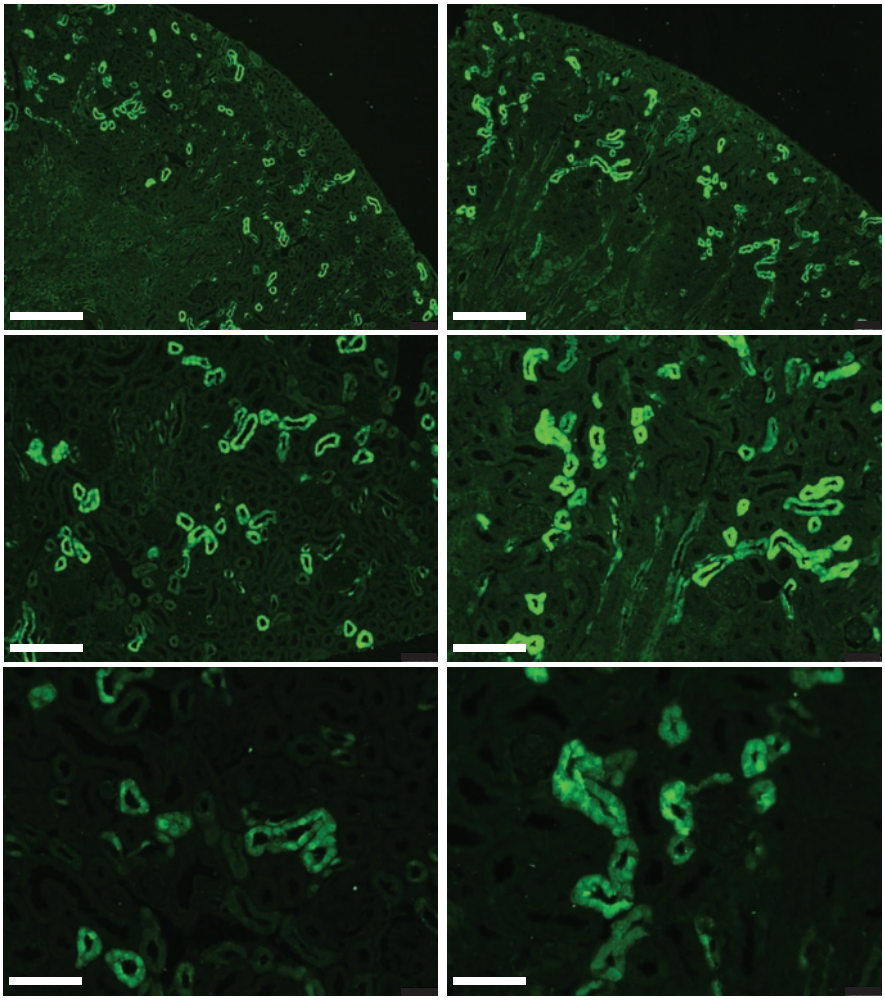

Figure 11 | No difference in DCT marker Parvalbumin abundance and intensity between *Hnf1β*$^{fl-/fl-}$ wild type and *Hnf1β*$^{fl+/fl+}$ knockout mice

Representative images are displayed of kidney slices derived from a *Hnf1β*$^{fl-/fl-}$ wild type (left) and a *Hnf1β*$^{fl+/fl+}$ knockout mouse (right) at various magnifications 10x (top), 20x (middle) and 40x (bottom). Parvalbumin is shown in green and DAPI in blue. Scale bars are respectively 150 µm (top), 100 µm (middle) and 50 µm (bottom).

Discussion

The present study provides a genome-wide screening of HNF1β binding sites in a mouse DCT cell line. Our results indicate that HNF1β induces transcription of *Kcnj16* (Kir5.1) and thereby regulates ion reabsorption in the DCT. This conclusion is based on the following findings: *i*) a highly enriched and conserved HNF1β-binding site was found in the promoter region of *Kcnj16*; *ii*) HNF1β, and not a HNF1β mutant, enhanced the promoter activity of *Kcnj16* in a luciferase assay; *iii*) knock down of *Hnf1β* in mpkDCT cells resulted in decreased expression of *Kcnj16* (Kir5.1) and *Kcnj10* (Kir4.1); *iv*) reduced expression of *Kcnj16* and *Kcnj10* transcript in HNF1β renal knockout mice compared to wild-type mice.

ChIP-seq was used to elucidate HNF1β binding sites at a genome-wide scale allowing the identification of novel HNF1β-regulated genes in the kidney. In total ~7400 binding sites were identified of which most were attributed to putative promoter regions. The strong overlap of the nucleotide binding sequence in our experiments with the signature HNF1β-binding sequence indicates the high specificity of the data set (JASPAR database ID: MA0153.2). Moreover, HNF1β-binding peaks were located near known HNF1β target genes *Pkhd1* and *Pcbd1*.[19, 30] Among others, MODY genes were enriched in the KEGG pathway analysis. Although our experiments were aimed at studying renal electrolyte transport, the genome-wide scale and high specificity of this dataset also allowed for the identification of HNF1β-binding sites near genes related to diabetes (e.g. *Irs1*, *Irs2*). The complete dataset is available via GEO (Accession: GSE77397).

The main result of our study is the identification of Kir5.1 as a novel target of HNF1β-induced transcription. Kir5.1 was first cloned in 1994 and subsequently shown to form heteromeric complexes with Kir4.1 in the kidney, rendering the channel pH sensitive.[31, 32] Kir5.1 has no channel properties *per se* and requires Kir4.x subunits for functioning.[31] In kidney, Kir4.1-Kir5.1 complexes are expressed in the DCT and cortical collecting duct, where they regulate Na^+-K^+-ATPase activity by recycling K^+ at the basolateral membrane.[33, 34]

The HNF1β binding site in the *Kir5.1* promoter is highly conserved among species and is 15-fold enriched in our chIP-seq dataset. HNF1β clearly increased the Kir5.1 promoter activity, indicating a direct transcriptional regulation of *Kir5.1* in mpkDCT cells. Importantly, expression of the HNF1β-p.Lys156Glu mutant, that was identified in ADTKD-HNF1β patients, did not activate *Kir5.1* transcription.[11] It is likely that this point mutation, which is located in the DNA binding domain of *HNF1β*, causes a dominant-interfering effect, hampering the binding of HNF1β to the DNA. In literature no evidence is reported for an altered phenotype between intragenic *HNF1β* mutations or whole-gene deletions, which would be consistent with haploinsufficiency as the underlying disease mechanism.[35, 36] However, more recent data revealed that

patients with an intragenic *HNF1β* mutation suffer from significantly increased renal impairment and have a reduced glomerular filtration rate (GFR) compared to patients with a whole-gene deletion.[37, 38] This indicates that in the case of intragenic *HNF1β* mutations, there might be an additional interfering effect of the mutant on the function of the *HNF1β* WT allele. The physiological effect of HNF1β binding to the *Kir5.1* promoter was further investigated and confirmed in a HNF1β knockdown experiment. *Kir5.1* expression decreased in mpkDCT cells after transfection with siRNA targeting *Hnf1β*.

To understand the physiological role of HNF1β-dependent regulation of Kir5.1 mouse models are important tools. Our renal-specific HNF1β knockout animals confirmed the *in vitro* data, since *Kcnj16* (Kir5.1) mRNA expression was reduced in HNF1β knockout mice in comparison to wild type mice. Given the early postnatal lethality of the animals, urinary measurements to examine physiological effects of Kir5.1 knockdown are not possible in the HNF1β mouse model.[18] However, Kir5.1$^{-/-}$ mice were reported to suffer from urinary K^+ and Mg^{2+} wasting, which was partially reflected in lower plasma K^+.[39] Although, a mechanism that explains urinary wasting of both Mg^{2+} and K^+ in the Kir5.1$^{-/-}$ mouse remains elusive. Indeed, both urinary Mg^{2+} and K^+ wasting are key features of ADTKD-HNF1β patients.

In addition to Kir5.1, HNF1β knockout animals also displayed reduced transcripts of Kir4.1 and NCC. These results suggest that the HNF1β phenotype is more extensive than Kir5.1 downregulation alone. Our results did not identify the cause for reduced Kir4.1 or NCC expression. The chIP-seq experiments showed that HNF1β binding sites are not present in or near the promoter region of *Slc12a3* or *Kcnj10* and therefore direct regulation of NCC and Kir4.1 expression by HNF1β seems unlikely. Reduced K^+ channel Kir4.1/Kir5.1 expression may impair electrolyte transport at the basolateral membrane of the DCT, resulting in reduced NCC activity and transcription. This is in line with Kir4.1 knockout mice that demonstrate decreased abundance and functioning of NCC, altogether resulting in hypokalemia and renal Mg^{2+} wasting.[40] Furthermore, Kir4.1-deficient mice displayed a blunted response to hydrochlorothiazides confirming reduced NCC activity. Interestingly, ADTKD-HNF1β patients display a similar decreased response to hydrochlorothiazide,[41] further pointing towards NCC involvement in HNF1β disease. From both the clinical and animal experiments, it cannot be excluded that DCT size is affected. However, histological analysis of the renal-specific HNF1β knockout animals demonstrates that morphological defects are mainly located in the renal medulla leaving the cortex largely unaffected.[18] Moreover, *Trpm6* expression is not significantly altered in the HNF1β knockout mice and no differences in DCT marker parvalbumin abundance or intensity was detected when comparing HNF1β wild type and knockout animals, suggesting normal DCT development (Figure 11). Decreased electrolyte reabsorption in DCT, caused by a decreased functioning of the Kir4.1/Kir5.1 potassium channel, could induce an

effacement of the basolateral membrane of the DCT, as observed in the renal biopsy of an EAST patient.[15] It is, therefore, conceivable that aberrant Kir4.1/Kir5.1 channel functioning can cause changes in DCT morphology. Although this has, as of yet, not been reported in HNF1β patients.

The strength of our study is the genome-wide approach to identify novel HNF1β binding sites. Performing a chIP-seq assay allowed for a highly specific identification of all HNF1β binding sites within the DCT. Furthermore, by including a kidney-specific HNF1β knockout mouse model, our findings were confirmed *in vivo*, which further substantiated the *in vitro* findings. An important limitation of this study is the early postnatal lethality of the kidney-specific HNF1β knockout animals. DCT-specific knockout of HNF1β would be necessary to further examine the role of HNF1β in the DCT. However, these animals are currently not available.

In conclusion, by using a genome-wide screen for HNF1β targets in a DCT specific cell line, a novel HNF1β binding site was identified in the *Kcnj16* promoter. We established that HNF1β regulates *Kcnj16* gene transcription *in vitro* and *in vivo*. Therefore, our findings provide valuable new insights inside the mechanism behind the electrolyte imbalance in ADTKD-HNF1β patients.

Methods

Cell lines and animals

HEK293 cells were grown in Dulbecco's modified Eagle's medium (Lonza, Leusden, The Netherlands) containing 10% (v/v) fetal calf serum (FCS), 2 mM L-glutamine at 37 °C in a humidity controlled incubator with 5% (v/v) CO_2. MpkDCT4a were cultured as described previously.[42] Distal tubule-specific inactivation of HNF1β was achieved using Cre/LoxP recombination by crossing Ksp-cadherin Cre mice with *Hnf1β*$^{flox/flox}$.[18] Cre/LoxP activity varies along the nephron and ensures HNF1β inactivation for 27% in the proximal tubule, 99% in the thick ascending limb (TAL), 92% in the DCT/CNT and 100% in the collecting duct.[43] All animal procedures were performed in accordance with the guidelines of the Institutional Animal Care and Use Committees of the University of Texas Southwestern Medical Center and the University of Minnesota Medical School.

Immunohistochemistry (IHC)

Immunohistochemistry was performed as previously described.[44] In short, stainings for Hnf1β were performed on 4 µm sections of formalin fixed and paraffin embedded mouse kidney samples. Sections were incubated for 16 hours at 4 °C in rabbit anti-HNF1β (Santa Cruz Biotechnology, Santa Cruz, CA) 1:1000 and goat anti-Parvalbumin 1:2000 (Santa Cruz Biotechnology, Santa Cruz, CA). For detection, samples

were incubated with an Alexa 594-conjugated donkey anti-goat antibody 1:300 (Thermo Scientific, Amsterdam, The Netherlands) and a biotin-conjugated swine anti-rabbit antibody 1:2000. Subsequently, samples were incubated with streptavidin-HRP 1:100 and fluorescein-tyramide 1:50 using the TSA Fluorescein System (PerkinElmer, Groningen, The Netherlands). Cell nuclei were stained with DAPI (1:20,000) for 10 min at RT. Images were taken with an AxioCam MRm camera (Zeiss, Sliedrecht, The Netherlands). For the IHC in HNF1β$^{flox/flox}$ mice, kidneys were isolated at p14 and fixed in 4% paraformaldehyde and then embedded in paraffin. Sections were incubated for 16 hrs at 4 °C in goat anti-parvalbumin 1:50 (Santa Cruz Biotechnology, Santa Cruz, CA) and goat donkey-goat alexa 488 1:1000 (Invitrogen, Breda, The Netherlands) for 2 hrs at room temperature. Cell nuclei were mounted and stained with ProLong Gold antifade containing DAPI (Invitrogen). Slides were visualized under a Leica DM5500 B upright microscope with DFC7000 T camera (Leica).

ChIP-seq

Chromatin was isolated from mpkDCT4a cells by fixing with 1% (v/v) formaldehyde (Ultra-Pure) (Thermo scientific) for 15 min at RT. Cells were washed and permeabilized in 0.25% (v/v) triton-X-100 and 0.05% (v/v) SDS. Samples were sonicated in a Diagenode bioruptor (Diagenode, Ougrée, Belgium), 50 times 30 seconds on 30 seconds off at high intensity. Chromatin samples were then immunoprecipitated with Protein A/G beads (Santa Cruz Biotechnology, Santa Cruz, CA) in either 5µg rabbit anti-Hnf1β (Santa Cruz Biotechnology, Santa Cruz, CA) or rabbit anti-H3K4me3 (Abcam, Cambridge, UK) for 16 hours at 4 °C. Samples were de-crosslinked in 5 M NaCl at 65 °C for 5 hours. De-crosslinked samples were then purified with phenol-chloroform. Sample preparation was performed according to the manufacturers protocol (Illumina, Eindhoven, The Netherlands). In short, adaptor sequences were linked to the generated chIP samples. The library was size selected (200-250 bp) and amplified by PCR. Sequencing was completed on an Illumina HiSeq 2000 (Illumina, Eindhoven, The Netherlands). Peak calling was executed with Macs2, q-value (False discovery rate, FDR) 0.001. Hnf1β peak distribution within genomic features was accomplished with CEAS as a part of the Galaxy/Cistrome toolbox.[25, 27] Promoters were defined as <3 kb regions upstream of the TSS. Whereas downstream regions were <3 kb downstream of the TSS. The gene body includes all exons, introns, 5' UTR and 3' UTR. Significant enrichment over background was tested with a one-sided binominal test. Hierarchical clustering with Euclidean distance metric was done for HNF1β and H3K4me3 sequence reads in a window of ±10 kb surrounding HNF1β peaks. Motif analysis was performed with the GimmeMotifs algorithm as described previously.[45] All motifs found by the GimmeMotifs algorithm are described in Table 1. Motif specificity scores were obtained by performing a motif screen with the 'screen

motif' algorithm from the Galaxy/Cistrome toolbox. [27] All matching motifs underneath HNF1β peaks were given a specificity score based on the resemblance to the positional weight matrix of the HNF1β motif derived from the JASPAR database (ID: MA0153.2). [27] As HNF1β has a tendency to bind ATAT repeats, some motifs besides the HNF1β motif were enriched. However these additional motifs had lower specificity scores, proving less significant than the HNF1β motif (Table 1).

GO-term and KEGG pathway analysis

Gene set enrichment analysis (GSEA) software and the Molecular Signature Database (MSigDB) was used to obtain gene enrichment for both KEGG pathway and GO-term gene sets.[46] A total of 2717 genes containing an HNF1β peak within 50 kb from their respective TSS were used in the analysis. Gene set overlap was calculated for KEGG pathway analysis and GO 'molecular function' gene sets. Statistical significance ($q<0.05$) was determined using hypergeometric testing with a FDR correction.

Cloning

The human *Kcnj16* promoter region (-998 bp upstream, +113 bp downstream from the TSS) containing the HNF1β binding site was amplified from a human BAC-clone (RPCI-11.c 79M2, Source biosciences, Nottingham, UK) using a high fidelity DNA polymerase (Phusion, Thermofisher, Amsterdam, The Netherlands). The PCR product was digested with restriction enzymes KpnI and XmaI (New England Biolabs Ltd, Leiden, The Netherlands). The sequence was than ligated into a pGL3b vector in front of the luciferase gene using T4 DNA ligase (New England Biolabs Ltd, Leiden, The Netherlands). Primers used were; forward 5'-TCTAACAACCGTCAAACAGCAAC-3' and reverse 5'- GCTAGGTGCTTTCAGCTGGG-3'. Human *HNF1β* full-length cDNA was amplified by PCR from *HNF1β* pCMV-SPORT6 (clone IRATp970A0421D), ImaGenes), and subcloned into the pCINeo IRES GFP expression vector. *HNF1β* p.Lys156Glu was obtained by site-directed mutagenesis (Stratagene, La Jolla, USA).[20]

Luciferase assay

HEK293 cells were transiently transfected with 700 ng of the promoter firefly luciferase constructs using polyethylenimine cationic polymer (PEI) (Invitrogen, Breda, The Netherlands) (ratio 1µg DNA to 6 µl PEI). Cells were transfected with a pGL3b-empty, pGL3b-*hFXYD2a*, pGL3b-*hKCNJ16*-promoter, or pGL3b-*hKCNJ16*-promoter-bindingsite construct. All four conditions were additionally transfected with 50 ng of the pCINEO-empty, pCINEO-*hHNF1β*, or pCINEO-*hHNF1β* p.Lys156Glu mutant construct. For standardization of the transfection efficiency, 20 ng of Renilla luciferase plasmid CMV-*pRL* was used as a reference in all conditions. Firefly and Renilla luciferase activities were measured with the Dual-Luciferase Reporter Assay (Promega, Fitchburg, MA).

Table 1 | Motifs found by the GimmeMotifs algorithm underneath HNF1β binding sites

ID	Consensus	Database match	P-value
GimmeMotifs_13	TAAATAAATAAATAAATAAATAAAT	Foxg1_DBD_ATAAACAAGTRTAAACA	0.98
GimmeMotifs_14	AwwTAwwTAwwTAwwTAwwTA	POU6F2_DBD_WTAATKAGCTMATTAW	0.39
GimmeMotifs_15	TAAATAAATA	Foxc1_DBD_GTAAAYAAACA	P>0.01
GimmeMotifs_16	TnGTTAATnATTnA	HNF1β_full_NRTTAATNATTAACN	P>0.01
GimmeMotifs_3	sArGmCAGC	TGIF1_DBD_TGACAGSTGTCA	P>0.01
GimmeMotifs_8	CCAGrAsAGs	MA0092.1_Hand1::Tcfe2a	0.08
GimmeMotifs_7	rGCTACAGwG	Osr2_pwm_primary_SCI09	P>0.01
GimmeMotifs_17	TTAATnATTAAy	HNF1A_full_NRTTAATNATTAACN	P>0.01
GimmeMotifs_1	CyCTsyCyy	Esrra_pwm_secondary_SCI09	P>0.01
GimmeMotifs_12	GTCTGAAGAC	BATF3_DBD_TGATGACGTCATCA	0.05
GimmeMotifs_4	CAGGCTGGCC	MA0112.2_ESR1	p>0.01
GimmeMotifs_6	mTkkAnTnrwAnkkAAnnGAATGGAATGnAnTrkAwwGkwATGGmATr	Zfp410_pwm_primary_SCI09	0.18
GimmeMotifs_10	AGTACACTG	SOX10_full_AACAATRTKCAGWGTT	P>0.01
GimmeMotifs_2	AGCCCTGGC	Zfp691_pwm_primary_RC_SCI09	P>0.01
GimmeMotifs_9	ynrCCAsyAGrkGGCrsyn	MA0139.1_CTCF	0.0
GimmeMotifs_5	CCTGGAAC	MA0144.1_Stat3	P>0.01
GimmeMotifs_11	CCCCmAAmCAmCCmCmmmC	MA0073.1_RREB1	0.0
GimmeMotifs_18	GGAAGGAAGGAAGGAAGG	MA0149.1_EWSR1-FLI1	0.0

ID; name assigned to the found motif by the GimmeMotifs algorithm. Consensus; the motif sequence found underneath HNF1β binding sites. Database match; depicts the protein and motif from the JASPAR database that optimally fits with the HNF1β dataset motif. P-value; shows whether the HNF1β dataset consensus significantly matches with the JASPAR database motif.

Quantitative Real-Time Polymerase Chain Reaction

MpkDCT cells were transiently transfected with 100 pmol of siRNA targeting *Hnf1β* mRNA (Dharmacon, Lafayette, USA).[47] Cells were transfected using lipofectamine 2000 (Invitrogen, Breda, The Netherlands) adding 3 µl for each condition. After 48 hours, Total RNA isolation was performed with TRizol (Invitrogen, Breda, The Netherlands). 1.5 µg of RNA was used for reverse transcription using a M-MLV transcriptase protocol as described by the manufacturer (Invitrogen, Breda, The Netherlands). The cDNA was used to determine mRNA expression levels by CF96 Real-Time PCR detection system (Bio-Rad, Veenendaal, The Netherlands) for target genes of interest and of the housekeeping gene glyceraldehyde 3-phosphate dehydrogenase (*Gapdh*), as an endogenous control. Real-Time PCR primers are reported in Table 2.

Table 2 | Primer Sequences for RT-qPCR

	Forward	Reverse
18S RNA	5'- GTAACCCGTTGAACCCCATT-3'	5'- CCATCCAATCGGTAGTAGCG-3'
Gapdh	5'-TAACATCAAATGGGGTGAGG-3'	5'-GGTTCACACCCATCACAAAC-3'
Kcnj16	5'-GACTTCCGACCAAACCATGTG-3'	5'-GTCATCCTCCCTTCACTGTC-3'
Kcnj10	5'- CCGCGATTTATCAGAGC-3'	5'- AGATCCTTGAGGTAGAGGAA-3'
Egfr	5'- CAGAACTGGGCTTAGGGAAC-3'	5'- GGACGATGTCCCTCCACTG-3'
Fxyd2a	5'- GAACAGTGGTGGCAGTGCCAAG-3'	5'- GATCTGTCAGCGAACAGTG-3'
Fxyd2b	5'- GTACCTGGGTGGCAGTGCCAAG-3'	5'- CTACCATGGACAGGTGGTA-3'
Trpm6	5'-AAAGCCATGCGAGTTATCAGC-3'	5'-CTTCACAATGAAAACCTGCCC-3'
proEgf	5'-GAGTTGCCCTGACTCTACCG-3'	5'-CCACCATTGAGGCAGTATCC-3'
Slc12a3	5'-CTTCGGCCACTGGCATTCTG-3'	5'-GATGGCAAGGTAGGAGATGG-3'

18S RNA, 18S Ribosomal RNA; *Gapdh*, glyceraldehyde 3-phosphate dehydrogenase; *Kcnj16*, ATP-sensitive inward rectifier potassium channel 16; *Kcnj10*, ATP-sensitive inward rectifier potassium channel 10; *Egfr*, epidermal growth factor receptor; *Fxyd2a-b*, FXYD domain containing ion transport regulator 2a-b; *Trpm6*, transient receptor potential cation channel, subfamily M, member 6; *Egf*, epidermal growth factor; *Slc12a3*, solute carrier family 12, member 3.

Real-time qPCR on Ksp-Cre;*Hnf1β*$^{flox/flox}$ kidneys.

Total RNA from postnatal day 28 adult wild–type or HNF1β mutant mouse kidneys was extracted using the RNeasy Mini Kit (Qiagen, Germantown, MD) according to the manufacturer's protocol. RNA was treated with DNAse (Invitrogen, Breda, The Netherlands) and cDNA was synthesized using superscript III first strand synthesis kit

(Invitrogen, Breda, The Netherlands). cDNA was diluted 1:20 and 10 µl was used in the real time qPCR reaction. Real-time qPCR was performed with the iTAG Universal SYBER Green Supermix (Bio-Rad, Veenendaal, The Netherlands) using the CFX Connect Real-Time System (Bio-Rad, Veenendaal, The Netherlands). 18S ribosomal RNA was used as an endogenous control. Real-Time PCR primers are listed in Table 2.

Data analysis

All results presented are based on at least three separate experiments. Values are expressed as mean ± SEM. Statistical significance ($P<0.05$) was determined using one-tailed Students T-test or one-way ANOVA with Holm-Sidak procedure. Data was deposited in NCBI GEO (Accession: GSE77397).

Disclosure

This work was supported by grants from the Netherlands Organization for Scientific Research (NWO VICI 016.130.668) and the EURenOmics project from the European Union seventh Framework Programme (FP7/2007–2013, agreement no. 305608). Dr. Jeroen de Baaij is supported by grants from NWO (Rubicon 825.14.021) and the Dutch Kidney Foundation (Kolff 14OKG17). Dr. Peter Igarashi is supported by a grant from the National Institutes of Health (grant no. R37DK042921). The authors declare that they have no conflict of interest.

Acknowledgements

The authors thank Dr. Svetlana Avdulov for excellent technical assistance.

References

1. Horikawa Y, Iwasaki N, Hara M*, et al.* Mutation in hepatocyte nuclear factor-1 beta gene (TCF2) associated with MODY. *Nature genetics* 1997; **17:** 384-385.
2. Bingham C, Bulman MP, Ellard S*, et al.* Mutations in the hepatocyte nuclear factor-1beta gene are associated with familial hypoplastic glomerulocystic kidney disease. *American journal of human genetics* 2001; **68:** 219-224.
3. Bingham C, Hattersley AT. Renal cysts and diabetes syndrome resulting from mutations in hepatocyte nuclear factor-1beta. *Nephrology, dialysis, transplantation : official publication of the European Dialysis and Transplant Association - European Renal Association* 2004; **19:** 2703-2708.
4. Adalat S, Woolf AS, Johnstone KA*, et al.* HNF1B mutations associate with hypomagnesemia and renal magnesium wasting. *J Am Soc Nephrol* 2009; **20:** 1123-1131.
5. Verhave JC, Bech AP, Wetzels JF*, et al.* Hepatocyte Nuclear Factor 1beta-Associated Kidney Disease: More than Renal Cysts and Diabetes. *Journal of the American Society of Nephrology : JASN* 2015.
6. Lindner TH, Njolstad PR, Horikawa Y*, et al.* A novel syndrome of diabetes mellitus, renal dysfunction and genital malformation associated with a partial deletion of the pseudo-POU domain of hepatocyte nuclear factor-1beta. *Human molecular genetics* 1999; **8:** 2001-2008.
7. Bingham C, Ellard S, Cole TR*, et al.* Solitary functioning kidney and diverse genital tract malformations associated with hepatocyte nuclear factor-1beta mutations. *Kidney international* 2002; **61:** 1243-1251.
8. Haldorsen IS, Vesterhus M, Raeder H*, et al.* Lack of pancreatic body and tail in HNF1B mutation carriers. *Diabetic medicine : a journal of the British Diabetic Association* 2008; **25:** 782-787.
9. Iwasaki N, Ogata M, Tomonaga O*, et al.* Liver and kidney function in Japanese patients with maturity-onset diabetes of the young. *Diabetes care* 1998; **21:** 2144-2148.
10. van der Made CI, Hoorn EJ, de la Faille R*, et al.* Hypomagnesemia as First Clinical Manifestation of ADTKD-HNF1B: A Case Series and Literature Review. *American journal of nephrology* 2015; **42:** 85-90.
11. Ferre S, Bongers EM, Sonneveld R*, et al.* Early development of hyperparathyroidism due to loss of PTH transcriptional repression in patients with HNF1beta mutations? *The Journal of clinical endocrinology and metabolism* 2013; **98:** 4089-4096.
12. Clissold RL, Hamilton AJ, Hattersley AT*, et al.* HNF1B-associated renal and extra-renal disease-an expanding clinical spectrum. *Nature reviews Nephrology* 2015; **11:** 102-112.
13. Cruz DN, Simon DB, Nelson-Williams C*, et al.* Mutations in the Na-Cl cotransporter reduce blood pressure in humans. *Hypertension* 2001; **37:** 1458-1464.
14. Subramanya AR, Ellison DH. Distal convoluted tubule. *Clinical journal of the American Society of Nephrology : CJASN* 2014; **9:** 2147-2163.
15. Reichold M, Zdebik AA, Lieberer E*, et al.* KCNJ10 gene mutations causing EAST syndrome (epilepsy, ataxia, sensorineural deafness, and tubulopathy) disrupt channel function. *Proceedings of the National Academy of Sciences of the United States of America* 2010; **107:** 14490-14495.
16. Bandulik S, Schmidt K, Bockenhauer D*, et al.* The salt-wasting phenotype of EAST syndrome, a disease with multifaceted symptoms linked to the KCNJ10 K+ channel. *Pflugers Archiv : European journal of physiology* 2011; **461:** 423-435.
17. Zhang C, Wang L, Zhang J*, et al.* KCNJ10 determines the expression of the apical Na-Cl cotransporter (NCC) in the early distal convoluted tubule (DCT1). *Proc Natl Acad Sci U S A* 2014; **111:** 11864-11869.
18. Gresh L, Fischer E, Reimann A*, et al.* A transcriptional network in polycystic kidney disease. *EMBO J* 2004; **23:** 1657-1668.
19. Hiesberger T, Bai Y, Shao X*, et al.* Mutation of hepatocyte nuclear factor-1beta inhibits Pkhd1 gene expression and produces renal cysts in mice. *The Journal of clinical investigation* 2004; **113:** 814-825.
20. Ferre S, Veenstra GJ, Bouwmeester R*, et al.* HNF-1B specifically regulates the transcription of the gammaa-subunit of the Na+/K+-ATPase. *Biochemical and biophysical research communications* 2011; **404:** 284-290.
21. Meij IC, Koenderink JB, van Bokhoven H*, et al.* Dominant isolated renal magnesium loss is caused by misrouting of the Na(+),K(+)-ATPase gamma-subunit. *Nature genetics* 2000; **26:** 265-266.

22. de Baaij JH, Dorresteijn EM, Hennekam EA*, et al.* Recurrent FXYD2 p.Gly41Arg mutation in patients with isolated dominant hypomagnesaemia. *Nephrology, dialysis, transplantation : official publication of the European Dialysis and Transplant Association - European Renal Association* 2015.
23. de Baaij JH, Hoenderop JG, Bindels RJ. Magnesium in man: implications for health and disease. *Physiological reviews* 2015; **95:** 1-46.
24. Santos-Rosa H, Schneider R, Bannister AJ*, et al.* Active genes are tri-methylated at K4 of histone H3. *Nature* 2002; **419:** 407-411.
25. Shin H, Liu T, Manrai AK*, et al.* CEAS: cis-regulatory element annotation system. *Bioinformatics* 2009; **25:** 2605-2606.
26. Ogata H, Goto S, Sato K*, et al.* KEGG: Kyoto Encyclopedia of Genes and Genomes. *Nucleic Acids Res* 1999; **27:** 29-34.
27. Liu T, Ortiz JA, Taing L*, et al.* Cistrome: an integrative platform for transcriptional regulation studies. *Genome biology* 2011; **12:** R83.
28. Edghill EL, Bingham C, Slingerland AS*, et al.* Hepatocyte nuclear factor-1 beta mutations cause neonatal diabetes and intrauterine growth retardation: support for a critical role of HNF-1beta in human pancreatic development. *Diabetic medicine : a journal of the British Diabetic Association* 2006; **23:** 1301-1306.
29. Aboudehen K, Kim MS, Mitsche M*, et al.* Transcription Factor Hepatocyte Nuclear Factor-1beta Regulates Renal Cholesterol Metabolism. *J Am Soc Nephrol* 2015.
30. Ferre S, de Baaij JH, Ferreira P*, et al.* Mutations in PCBD1 cause hypomagnesemia and renal magnesium wasting. *Journal of the American Society of Nephrology : JASN* 2014; **25:** 574-586.
31. Lagrutta AA, Bond CT, Xia XM*, et al.* Inward rectifier potassium channels. Cloning, expression and structure-function studies. *Jpn Heart J* 1996; **37:** 651-660.
32. Tucker SJ, Imbrici P, Salvatore L*, et al.* pH dependence of the inwardly rectifying potassium channel, Kir5.1, and localization in renal tubular epithelia. *J Biol Chem* 2000; **275:** 16404-16407.
33. Lourdel S, Paulais M, Cluzeaud F*, et al.* An inward rectifier K(+) channel at the basolateral membrane of the mouse distal convoluted tubule: similarities with Kir4-Kir5.1 heteromeric channels. *J Physiol* 2002; **538:** 391-404.
34. Zaika OL, Mamenko M, Palygin O*, et al.* Direct inhibition of basolateral Kir4.1/5.1 and Kir4.1 channels in the cortical collecting duct by dopamine. *Am J Physiol Renal Physiol* 2013; **305:** F1277-1287.
35. Edghill EL, Oram RA, Owens M*, et al.* Hepatocyte nuclear factor-1beta gene deletions--a common cause of renal disease. *Nephrology, dialysis, transplantation : official publication of the European Dialysis and Transplant Association - European Renal Association* 2008; **23:** 627-635.
36. Bellanne-Chantelot C, Clauin S, Chauveau D*, et al.* Large genomic rearrangements in the hepatocyte nuclear factor-1beta (TCF2) gene are the most frequent cause of maturity-onset diabetes of the young type 5. *Diabetes* 2005; **54:** 3126-3132.
37. Heidet L, Decramer S, Pawtowski A*, et al.* Spectrum of HNF1B mutations in a large cohort of patients who harbor renal diseases. *Clinical journal of the American Society of Nephrology : CJASN* 2010; **5:** 1079-1090.
38. Clissold RL, Shaw-Smith C, Turnpenny P*, et al.* Chromosome 17q12 microdeletions but not intragenic HNF1B mutations link developmental kidney disease and psychiatric disorder. *Kidney international* 2016; **90:** 203-211.
39. Paulais M, Bloch-Faure M, Picard N*, et al.* Renal phenotype in mice lacking the Kir5.1 (Kcnj16) K+ channel subunit contrasts with that observed in SeSAME/EAST syndrome. *Proceedings of the National Academy of Sciences of the United States of America* 2011; **108:** 10361-10366.
40. Cuevas CA, Su XT, Wang MX*, et al.* Potassium Sensing by Renal Distal Tubules Requires Kir4.1. *Journal of the American Society of Nephrology : JASN* 2017.
41. Bech AP, Wetzels JF, Bongers EM*, et al.* Thiazide Responsiveness Testing in Patients With Renal Magnesium Wasting and Correlation With Genetic Analysis: A Diagnostic Test Study. *American journal of kidney diseases : the official journal of the National Kidney Foundation* 2016; **68:** 168-170.
42. Diepens RJ, den Dekker E, Bens M*, et al.* Characterization of a murine renal distal convoluted tubule cell line for the study of transcellular calcium transport. *American journal of physiology Renal physiology* 2004; **286:** F483-489.

43. Li L, Zepeda-Orozco D, Black R*, et al.* Autophagy Is a Component of Epithelial Cell Fate in Obstructive Uropathy. *Am J Pathol* 2010; **176:** 1767-1778.
44. de Baaij JH, Blanchard MG, Lavrijsen M*, et al.* P2X4 receptor regulation of transient receptor potential melastatin type 6 (TRPM6) Mg2+ channels. *Pflugers Archiv : European journal of physiology* 2014; **466:** 1941-1952.
45. van Heeringen SJ, Veenstra GJ. GimmeMotifs: a de novo motif prediction pipeline for ChIP-sequencing experiments. *Bioinformatics* 2011; **27:** 270-271.
46. Subramanian A, Tamayo P, Mootha VK*, et al.* Gene set enrichment analysis: a knowledge-based approach for interpreting genome-wide expression profiles. *Proc Natl Acad Sci U S A* 2005; **102:** 15545-15550.
47. Tanaka T, Tomaru Y, Nomura Y*, et al.* Comprehensive search for HNF-1beta-regulated genes in mouse hepatoma cells perturbed by transcription regulatory factor-targeted RNAi. *Nucleic acids research* 2004; **32:** 2740-2750.

3 Transcription factor HNF1β regulates expression of the calcium-sensing receptor in the thick ascending limb of the kidney

Andreas Kompatscher[1]*, Jeroen H.F. de Baaij[1]*, Karam Aboudehen[3], Shayan Farahani[3], Lex H.J. van Son[1], Susanne Milatz[4], Nina Himmerkus[4], Gertjan C. Veenstra[2], Rene J.M. Bindels[1] and Joost G.J. Hoenderop[1]

[1]Department of Physiology, Radboud Institute for Molecular Life Sciences, Radboud University Medical Center; [2]Department of Molecular Developmental Biology, Radboud Institute for Molecular Life Sciences, Radboud University Nijmegen; [3]Department of Medicine, University of Minnesota Medical School, Minneapolis, Minnesota, USA; [4] Institute of Physiology, Christian-Albrechts-University of Kiel, Kiel, Germany

*A.K. and J.H.F.d.B. contributed equally to this work.

Am J Physiol Renal Physiology, 2018, 315:F24-F35

Abstract

Mutations in HNF1β cause autosomal dominant tubulointerstitial kidney disease (ADTKD-HNF1β), and patients tend to develop renal cysts, maturity-onset diabetes of the young (MODY), and suffer from electrolyte disturbances, including hypomagnesemia, hypokalemia and hypocalciuria. Previous HNF1β research focused on the renal distal convoluted tubule (DCT) to elucidate the ADTKD-HNF1β electrolyte phenotype, although 70% of Mg^{2+} is reabsorbed in the thick ascending limb of Henle's loop (TAL). An important regulator of Mg^{2+} reabsorption in the TAL is the calcium-sensing receptor (CaSR).

This study used several methods to elucidate the role of HNF1β in electrolyte reabsorption in the TAL. HNF1β ChIP-seq data revealed a conserved HNF1β binding site in the second intron of the *CaSR* gene. Luciferase-promoter assays displayed a 5.8 fold increase in *CaSR* expression when HNF1β was present. Expression of the HNF1β p.Lys156Glu mutant, which prevents DNA binding, abolished *CaSR* expression. *Hnf1β* knockdown in an immortalized TAL cell line (MKTAL) reduced expression of the *CaSR* and *Cldn14* (Claudin14) by 56% and 48%, respectively, while *Cldn10b* expression was upregulated 5.0 fold. These results were confirmed in a kidney-specific HNF1β knockout mouse, which exhibited downregulation of the *Casr* by 81%. *Cldn19* and *Cldn10b* expression levels were also decreased by 37% and 83%, respectively, whereas *Cldn3* was upregulated by 4.6 fold.

In conclusion, HNF1β is a transcriptional activator of the *CaSR*. Consequently, patients with *HNF1β* mutations may have reduced CaSR activity in the kidney, which could explain cyst progression and hyperabsorption of Ca^{2+} and Mg^{2+} in the TAL resulting in hypocalciuria.

Keywords: kidney, calcium-sensing receptor, HNF1β, TAL, hypomagnesemia,

Introduction

Autosomal dominant tubulo-interstitial kidney disease (ADTKD-HNF1β, OMIM: 137920) is caused by the deletion of or heterozygous mutations in hepatocyte nuclear factor 1 homeobox β (*HNF1β*).[1, 2] Patients suffer from a complex and heterogeneous phenotype characterized by renal malformations and maturity onset diabetes of the young subtype 5 (MODY5).[1-6] Interestingly, approximately 50% of ADTKD-HNF1β patients experience impaired renal electrolyte handling resulting in hypomagnesemia, hypokalemia and hypocalciuria.[5, 7-9]

HNF1β is ubiquitously expressed in the epithelial cells of all nephron segments.[10] In the distal convoluted tubule (DCT), HNF1β regulates the expression of the Kir4.1-Kir5.1 K^+ channel and the γ-subunit of the Na^+-K^+-ATPase (FXYD2).[11, 12] Kidney-specific (Ksp) *Hnf1β* knockout (KO) mice display reduced *Kcnj10* (Kir4.1) and *Kcnj16* (Kir5.1) expression levels, resulting in lower Na^+-Cl^--cotransporter (NCC) transcript levels.[13] These findings explain why ADTKD-HNF1β resembles Gitelman syndrome (OMIM: 263800), seizures, sensorineural deafness, ataxia, mental retardation, and electrolyte imbalance; or epilepsy, ataxia, sensorineural deafness, and renal tubulopathy;(SeSAME-EAST, OMIM: 612780) or isolated dominant hypomagnesemia (IDH, OMIM: 15040). These are caused by NCC, Kir4.1, and FXYD2 mutations, respectively.[14-16]

HNF1β is ubiquitously expressed along the nephron, including the thick ascending limb of Henle's loop (TAL). Here, HNF1β regulates the expression of uromodulin (UMOD), which is a cystic disease gene responsible for ADTKD-UMOD (OMIM: 191845).[17] The TAL plays a dominant role in Na^+, Ca^{2+} and Mg^{2+} reabsorption.[11, 18] In this segment, the furosemide-sensitive Na^+-K^+-$2Cl^-$-cotransporter (NKCC2) facilitates transcellular Na^+ reabsorption. A strong lumen positive potential drives the paracellular transport of divalent cations, which is maintained by the paracellular backflow of Na^+ and the recycling of K^+ into the lumen by the renal outer medullary potassium channel (ROMK). A highly regulated tight junction complex consisting of claudins 3, 14, 16 and 19 forms a pore to facilitate the paracellular reabsorption of Ca^{2+} and Mg^{2+}. The ion permeability and selectivity of this tight junction complex depends on the particular expression of each of the claudin-subunits.[19, 20] Whereas claudin16 and claudin19 are cation-permeable, claudin14 is generally considered cation-blocking, shifting the preference of the claudin16-19 pore to Na^+ instead of Ca^{2+} and Mg^{2+}.

Over the last few years, the calcium-sensing receptor (CaSR) was identified as regulator of the claudin complex.[19, 21] Several studies described the role of the CaSR in electrolyte transport in the TAL.[21, 22] Patients with gain-of function mutations in the CaSR develop autosomal dominant hypocalcemia (ADH, OMIM: 601198), and subsequently, renal Mg^{2+} wasting, hypomagnesemia, and hypocalcemia with hypoparathyroidism.[23] Loss-of-function mutations cause familial hypocalciuric hypercalcemia (FHH, OMIM: 145980), which is characterized by hyperabsorption of Ca^{2+}

and Mg^{2+}, and reduced levels of these ions in the urine.[24] Recent research shows how CaSR activation regulates claudin expression, by initiating a cellular cascade that results in the decreased expression of two specific microRNAs, Mir-9 and Mir-374, which in turn raise claudin14 protein levels.[19, 21, 25] As a consequence, Ca^{2+} and Mg^{2+} reabsorption in the TAL are decreased, which was observed in mice treated with the CaSR-agonist cinacalcet.[21]

Although HNF1β is highly expressed in the TAL, the role of HNF1β in electrolyte reabsorption in this segment has never been examined. The aim of the present study was to investigate the function of HNF1β in the TAL. The CaSR was identified as a prime candidate for HNF1β transcriptional regulation by screening HNF1β chromatin immunoprecipitation and sequencing (ChIP-seq) data. Transcriptional regulation of the *CaSR* by HNF1β was assessed by luciferase assays and siRNA knockdown experiments in mouse kidney TAL cells (MKTAL). Quantitative PCR analysis was performed on HNF1β mutant mice kidney tissue to determine differences in *CaSR* expression *in vivo*.

Results

Expression of HNF1β in the TAL

Immunohistochemistry was performed on mouse kidney slices to investigate HNF1β expression and localization in the TAL. HNF1β localizes to the nuclei of tubular cells and is co-expressed with the TAL-specific marker uromodulin (Figure 1).

HNF1β regulates the expression of the Calcium-sensing receptor

Analysis of previously published HNF1β chIP-seq data in an immortalized mouse DCT cell line revealed a highly enriched binding site for HNF1β in the second intron of the *Casr* gene (Figure 2A).[11] The binding site is located +16,611 nucleotides from the *Casr* transcriptional start site (TSS), and displays elevated nucleotide conservation (Figure 2B). The binding site has a motif conservation score of 6.38 as calculated by the screen motif algorithm, indicating high conservation, and placing it in the top 5% of most conserved HNF1β peaks (n=7421) found in the HNF1β chIP-seq dataset.[11, 26] Reproducibility of this binding site was validated by performing chIP-RT-qPCR, resulting in a 24-fold enrichment over the genomic background, which was comparable to the HNF1β binding site in the fibrocystin precursor (*Pkhd1)* gene that was used as a positive control (Figure 2C). Subsequently, luciferase assays were performed on HEK293 cells containing the human promoter for the *CaSR,* including the HNF1β binding site. HNF1β overexpression raised promoter activity significantly by 5.8-fold ($P<0.05$) compared to cells that lacked HNF1β expression (Figure 2D). Overexpression of the HNF1β p.Lys156Glu mutant that was previously reported in a patient with renal

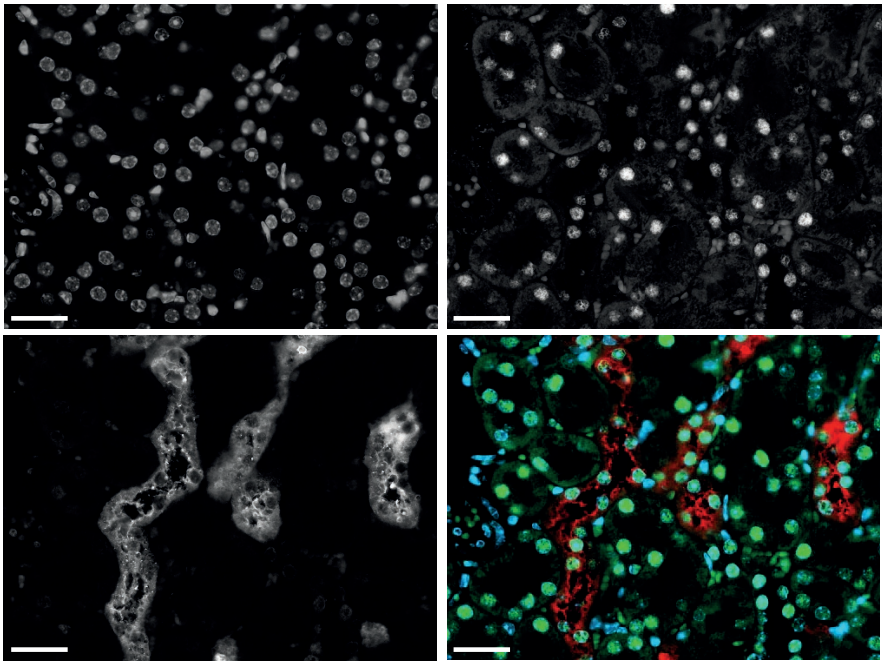

Figure 1 | HNF1β is expressed in the thick ascending limb

Immunohistochemical stainings of mouse kidney sections were co-stained with anti-HNF1β (top right, grayscale), anti-uromodulin (lower left, grayscale) and 4', 6-diamidino-2-phenylindole (DAPI) (top left, gray scale). A merged image is shown in the lower right with HNF1β in green, uromodulin in red and DAPI in blue. Scale bar: 100 µm

cysts and MODY, abolished the rise in promoter activity.[5, 27] No significant changes were observed in mock-transfected cells. Luciferase experiments with the alternative *CaSR* promoter 2 did not show HNF1β-induced *CaSR* transcription (Figure 2E). Removal of the HNF1β binding site abolishes any significant HNF1β-induced increase in *CaSR* promoter activity (Figure 2C).

siRNA-mediated knockdown of HNF1β downregulates *Casr*, *Cldn14* and upregulates *Cldn10b* transcript levels *in vitro*

To further elucidate the role of HNF1β in the transcriptional regulation of the CaSR, MKTAL cells were transfected with siRNA targeting HNF1β. Real-time quantitative PCR (RT-qPCR) analysis revealed a significant decrease of 59±11 % in *Hnf1β* transcript levels compared to non-targeting siRNA-transfected cells (Figure 3A). A similar significant

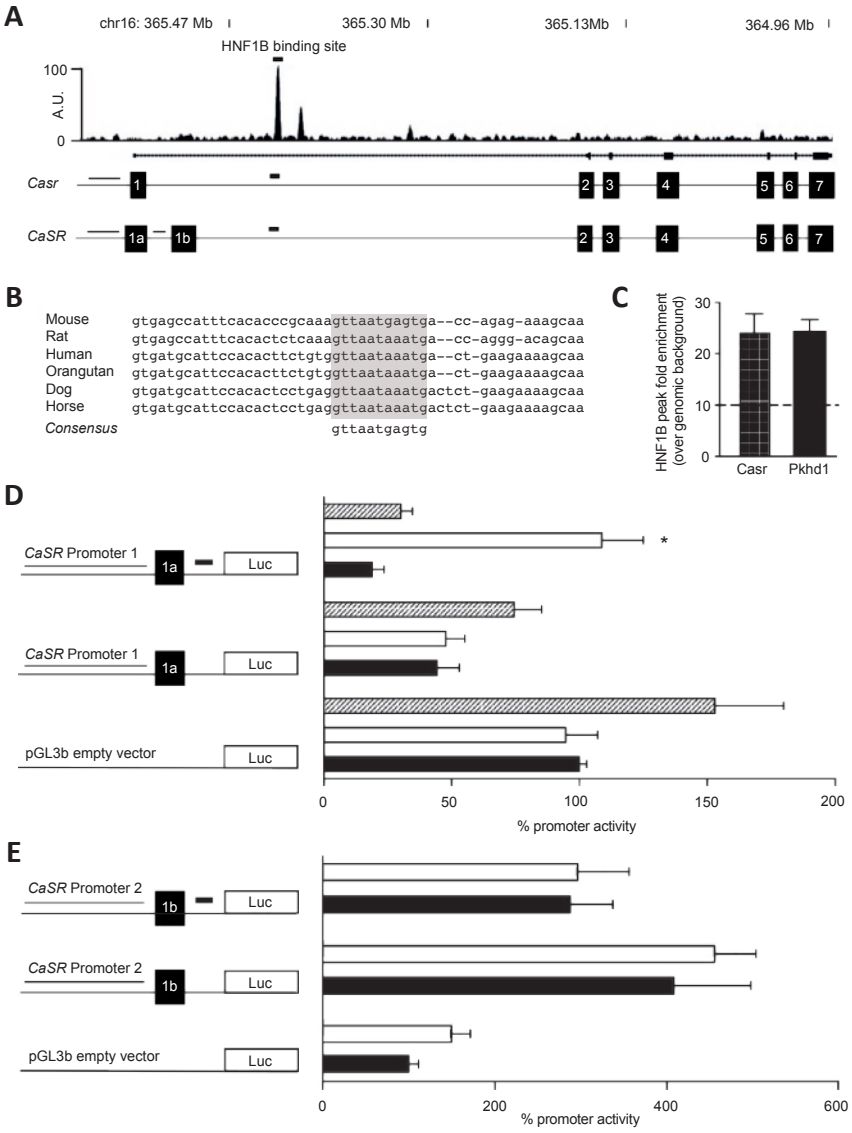

Figure 2 | HNF1β increases activation of the Calcium-sensing receptor promoter

A) HNF1β binding profile for the *Casr* in mpkDCT cells. Below is a linear representation of the location of the promoter and HNF1β binding site in relation to the exons of the *CaSR* for both mouse and human. A black rectangle denotes the HNF1β binding site. A black line denotes the promoter region. B) Alignment of the HNF1β peak at +16.611 bp from the TSS of several different species reveals a highly conserved binding site. C) HNF1β chIP samples of mpkDCT

samples were used to verify the HNF1β binding site in the *CaSR* promoter. The *Pkhd1* binding site was used as a positive control. Samples were measured by quantitative RT-PCR. Data represent mean ± SEM and are expressed as fold enrichment over background. The cutoff for sufficient enrichment of the binding site was set at 10 fold enrichment over background. The background signal was determined at genomic coordinates GRCm38 chr15:99578842-99579015 D) HEK293 cells were transiently transfected with a luciferase construct carrying the human *CaSR* promoter 1, *CaSR* exon 1a and also containing the HNF1β binding site (black square). Luciferase constructs carrying the *CaSR* promoter lacking the HNF1β binding site and an empty vector were added as negative controls. Promoter activity was tested with (white bars), without (black bars) or with mutant (striped bars) HNF1β stimulation. E) HEK293 cells were transiently transfected with a luciferase construct carrying the human *CaSR* promoter 2, *CaSR* exon 1B and also containing the HNF1β binding site. An empty vector was added as negative control. Promoter activity was tested with (white bars) or without (black bars) HNF1β stimulation. Data (n=3) represent mean ± SEM. *, $p<0.05$, compared to the non-stimulated condition

Table 1 | MKTAL cells are not selective for Na^+, Mg^{2+} or Ca^{2+}

Native cells	P_{Na}/P_{Cl}	P_{Mg}/P_{Na}	P_{Ca}/P_{Na}
MKTAL1	1.14 ± 0.04	1.93 ± 0.03	2.00 ± 0.01
MKTAL2	1.16 ± 0.03	1.93 ± 0.02	2.01 ± 0.04
MKTAL3	1.22 ± 0.03	2.12 ± 0.20	2.15 ± 0.04
siRNA nt	P_{Na}/P_{Cl}	P_{Mg}/P_{Na}	P_{Ca}/P_{Na}
MKTAL1	1.17 ± 0.03	1.99 ± 0.02	1.99 ± 0.03
MKTAL2	1.16 ± 0.05	1.95 ± 0.01	1.95 ± 0.06
MKTAL3	1.20 ± 0.03	1.98 ± 0.04	1.98 ± 0.08
siRNA *Hnf1β*	P_{Na}/P_{Cl}	P_{Mg}/P_{Na}	P_{Ca}/P_{Na}
MKTAL1	1.18 ± 0.02	1.96 ± 0.03	2.00 ± 0.04
MKTAL2	1.19 ± 0.03	1.95 ± 0.05	2.05 ± 0.06
MKTAL3	1.19 ± 0.03	1.91 ± 0.02	1.91 ± 0.05

Three independent experiments, each containing three separate measurements (N=3) are represented. The 'native cells' column displays the untransfected MKTAL cells. siRNA nt represents the non-targeting siRNA condition, whereas the siRNA *Hnf1β* column shows cells that were transfected with siRNAs targeting *Hnf1β* mRNA. P_{Na}/P_{Cl}, P_{Mg}/P_{Na} and P_{Ca}/P_{Na} are ratios of ion permeability. Data is expressed as Mean ± Standard Deviation (SD).

decrease of 56±18 % was observed for the *Casr* (Figure 3B). *Kcnj16* mRNA levels were taken along as a positive control. As expected, *Kcnj16* transcript levels were significantly decreased by 65±19 % (Figure 3C).[11] In addition, mRNA levels of *Cldn10b, 16, 19* and *14* were investigated, as these tight junction proteins are involved in the reabsorption of Ca^{2+} and Mg^{2+} in the TAL. Transcript levels of *Cldn14* were significantly downregulated by 48±14 % (Figure 3F). However, no significant changes were found

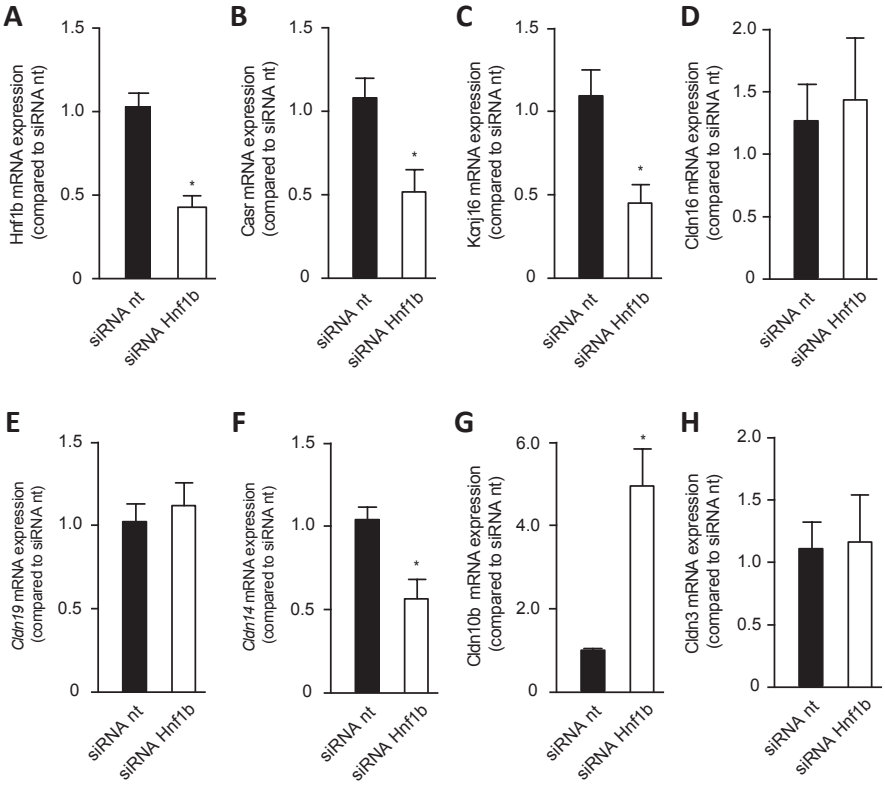

Figure 3 | siRNA mediated knockdown of Hnf1β causes downregulation of the *Casr*, *Cldn14*, and upregulates *Cldn10b* expression levels in an immortalized TAL cell line

A-G) The mRNA expression levels of Hnf1β (A), Casr (B), Kcnj16 (C), Cldn16 (D), Cldn19 (E), Cldn14 (F) and Cldn10b (G) in MKTAL cells treated with either non-targeting (nt) (black bars) or Hnf1β targeting (white bars) siRNAs. Samples were measured by quantitative RT-qPCR and normalized to GAPDH expression. Data (n=3) represent mean ± SEM, *, $p<0.05$ and are expressed as the fold difference compared to the expression in siRNA nt

in the abundances of *Cldn16*, *Cldn19, Cldn3* mRNA (Figure 3D, E & H). Interestingly, RT-qPCR measurements for *Cldn10b* revealed a 5-fold ($p<0.05$) increase in transcript levels in *Hnf1β* deficient cells (Figure 3G). *Cldn10a* expression levels were not detectable in the MKTAL cell line. Ussing chamber experiments were performed to assess the consequences of *Hnf1β* deficiency for Ca^{2+} and Mg^{2+} transport in MKTAL cells. Measurements in native MKTAL cells displayed no significant changes in Na^{+}, Mg^{2+} and Ca^{2+} permeability (Table 1). Transfection of MKTAL cells with *Hnf1β* targeting siRNAs resulted in no significant changes in cation permeability (Table 1).

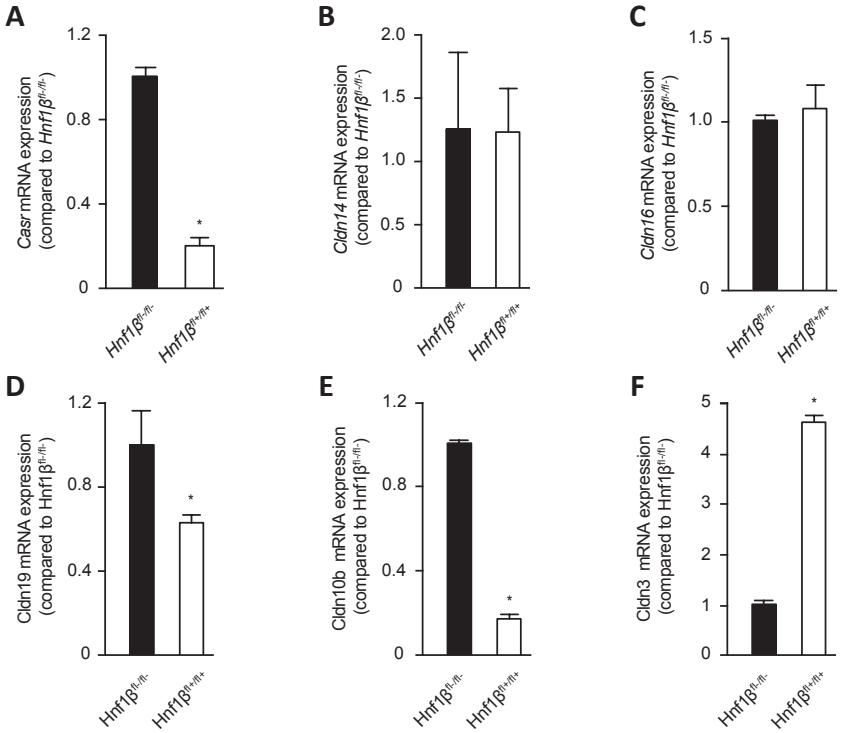

Figure 4 | *Casr* and *Cldn10b* transcripts are reduced, whereas *Cldn3* mRNA levels were increased in a HNF1β mutant mouse model

A-F) The mRNA expression levels of *Hnf1β* (A), *Cldn14* (B), *Cldn16* (C), *Cldn19* (D), *Cldn10b* (E), *Cldn3* (F) in Ksp-Cre;*Hnf1β*$^{flox/flox}$ mouse kidneys. The black bars represent *Hnf1β*$^{fl-/fl-}$ wild-type mice, while the white bars represent *Hnf1β*$^{fl+/fl+}$ knockout mice. Samples were measured by quantitative RT-qPCR and normalized for U6 spliceosome RNA expression. Data (n=3) represent mean ± SEM, *, $p<0.05$ and are expressed as the fold difference when compared to the expression in *Hnf1β*$^{fl-/fl-}$ wild-type mice.

Expression of *Casr*, *Cldn19* and *Cldn3* is regulated by HNF1β *in vivo*

We confirmed our findings that HNF1β regulates *CaSR* transcription and thereby affects electrolyte reabsorption in the TAL by performing RT-qPCR on RNA isolated from kidney-specific (Ksp)-Cre;*Hnf1β*$^{flox/flox}$ mouse kidneys (n=3). In these mice, Ksp-cre induced knockout of *Hnf1β* ensures that *Hnf1β* is inactivated in 99 % of all TAL segments.[28] This specific lack of *Hnf1β* in the TAL causes a significant ($P<0.05$) decrease of 81±6 % in *Casr* mRNA abundance (Figure 4A). *Cldn14*, one of the critical downstream targets of the CaSR, was not significantly affected by the decrease in *Casr* abundance (Figure 4B). Similarly, *Cldn16* mRNA levels were not significantly altered (Figure 4C). Contrary to the *in vitro* data (Figure 3E & G), *Cldn19* and *Cldn10b* were significantly downregulated by 37±6 % and 83±2 %, respectively, in *Hnf1β* mutant mice (Figure 4D and E). Interestingly, *Cldn3*, a component of the divalent cation selective pore in the TAL, exhibited a significant 4.6-fold increase in *Hnf1β*$^{fl+/fl+}$ mice compared to *Hnf1β*$^{fl-/fl-}$ mice (Figure 4F).

Discussion

Our findings provide novel insights into the role of HNF1β in the TAL. HNF1β is ubiquitously expressed throughout the kidney.[11] It is therefore likely that problems with electrolyte homeostasis in ADTKD-HNF1β patients cannot be attributed to only one segment of the nephron. We have demonstrated that HNF1β induces the expression of the *CaSR* gene in the TAL. An enriched and conserved binding site of HNF1β was found in the second intron of the *CaSR* gene. Subsequent luciferase assays revealed that HNF1β enhances *CaSR* promoter activity. The absence of the HNF1β binding site or overexpression of mutant HNF1β protein was sufficient to abolish this stimulatory effect. SiRNA knockdown of HNF1β in MKTAL cells decreased *Casr* expression significantly compared to a non-targeted control siRNA. RT-qPCR analysis in Ksp-cre *Hnf1β* KO mice revealed a similar decrease of *CaSR* expression in the kidney.

The CaSR is a G-protein-coupled receptor (GPCR) that is sensitive to extracellular Ca^{2+}, and, to a lesser extent, Mg^{2+} ions.[29, 30] The receptor plays a major role in the maintenance of the plasma Ca^{2+} concentration by regulating the circulating levels of parathyroid hormone and directly affecting Ca^{2+} reabsorption in the kidney.[31]. Intracellular signaling is initiated upon Ca^{2+} binding to the large extracellular domain. CaSR-dependent signaling activates phospholipase C activity that results in an accumulation of inositol 1,4,5-trisphosphate and a rapid increase of the cytosolic Ca^{2+} concentration.[32-34] Although it has been shown that the *CaSR* promoter is responsive to 1,25-dihydroxyvitamin D_3, proinflammatory cytokines and the transcription factor glial cells missing-2 (GCM2), this is the first report of regulation of the CaSR by HNF1β.[35]

The *CaSR* gene has eight exons, of which exons 2 to 7 contain the coding sequence for the CaSR protein (GenBank U20759). Interestingly, the gene harbors two alternative first exons (1A and 1B) that encode different 5'-UTRs, both splicing to the common exon 2.[36, 37] The human *CaSR* gene has two promoters driving the transcription of alternative exons 1A and 1B. Our data demonstrated that HNF1β regulates promoter 1 activity, whereas promoter 2 is unaffected. The *CaSR* is highly expressed in the parathyroid gland and the renal tubular system, including the TAL.[38] Northern blot analysis of human parathyroid glands shows exclusive exon 1A use.[36] Moreover, nephrolithiasis is associated with the transcription of promoter 1.[39] These data suggest that promoter 1-driven exon1A transcription is most important for Ca^{2+} and Mg^{2+} transport. Therefore, HNF1β-regulated promoter 1 activity may be of particular importance for renal electrolyte homeostasis.

In TAL, the CaSR has been implicated in the regulation of NKCC2 activity and *CLDN14* expression.[21, 22] Previous studies in mice have shown that extracellular Ca^{2+} increases *Cldn14* mRNA levels through CaSR-mediated increases of intracellular Ca^{2+}. This reduces the expression of two miRNAs, Mir-9 and Mir-374. As a consequence of this downregulation, *Cldn14* mRNA levels are decreased.[21] In our model, we expected to observe a decrease in *Cldn14* due to the decreased CaSR activity following Hnf1β-mediated downregulation. A decrease in *Cldn14* expression was indeed observed in our MKTAL cell model, when *Hnf1β* expression was suppressed. However, there was no significant decrease in *Cldn14* expression levels in Ksp-Cre;*Hnf1β*$^{flox/flox}$ mouse kidneys. *Cldn14* expression is normally low in mice on a normal Ca^{2+} diet;[19, 25] previous studies have shown that an increase in dietary Ca^{2+} is required to ensure *Cldn14* upregulation.[19, 25, 40, 41] Our data confirms low basal expression levels of *Cldn14*. Previous research showed that wildtype mice treated with the CaSR agonist cinacalcet had increased expression of *Cldn14*.[21] Subjecting HNF1β mutant mice to cinacalcet is not possible, as these mice suffer from early postnatal lethality, which limits any further investigation.[17]

There are some disparities between the *in vitro* and *in vivo* expression levels of *Cldn10b*, *Cldn19* and *Cldn3* (figure 3EGH and 4DEF). Although these discrepancies cannot completely be explained, it is expected that this is a limitation of the MKTAL cell model. It has recently been shown that the mosaic claudin expression in the TAL results in several types highly organized and spatially separated paracellular permeation pathways *in vivo*.[20, 42] This complex physiological organization is not mimicked in MKTAL cells, which just express one type of paracellular shunt. Moreover, MKTAL cells cannot take into account the compensatory effects of other tubule segments affected by a reduction in HNF1β. The ion permeability measurements performed in Ussing chambers determined that MKTAL cells are not suitable for permeability studies, because the cells were not selective for Na^+, Mg^{2+} or Ca^{2+} (Table 1). The P_{Na}/P_{Cl} values did not exceed 1.2, whereas cortical TAL and medullary TAL

should have at least a P_{Na}/P_{Cl} of around 4 and 8 respectively to accurately mimic the ion transport selectivity in these segments.[42] Furthermore, targeting HNF1β expression in MKTAL cells did not elicit the expected decrease in Na^+ and increase in Mg^{2+} and Ca^{2+} permeability. Taken together, our experiments indicate that the MKTAL cell line is not a sufficient model to study ion transport. What does remain evident is the clear reduction of *Casr* expression after loss of HNF1β in both *in vitro* and *in vivo* models,

Patients that suffer from ADTKD-HNF1β often have kidney cyst formation.[8, 43] A study in mice with rodent nephronophthisis shows that stimulating the CaSR with calcimimetics reduced cyst progression.[44] A lack of *CaSR* expression due to a HNF1β mutation might contribute to cyst formation. It would therefore be interesting to treat ADTKD-HNF1β patients with calcimimetics to induce CaSR activity and reduce cyst progression. In some cases ADTKD-HNF1β patients develop nephrolithiasis.[45] Curiously, a single-nucleotide polymorphism (SNP) in the *CaSR* promoter 1 has been associated with nephrolithiasis.[39] The SNP was more frequent in stone formers vs controls, and homozygous SNP carriers had lower *CaSR* mRNA levels in the kidney medulla.[39] Our finding that HNF1β controls *CaSR* transcription may therefore be of clinical interest for reducing cyst and kidney stone formation. However, more research is needed to elucidate what effect the loss of HNF1β has on ion transport in the TAL and what the consequences are for the ADTKD-HNF1β patient.

In conclusion, a HNF1β binding site was identified in the second intron of the *CaSR* gene. Our data indicate that HNF1β positively regulates gene transcription of the *CaSR in vitro* and *in vivo*. Thereby providing a novel insight into the potential role of HNF1β in electrolyte transport that is not only confined to the DCT, but also relevant to TAL function.

Materials and Methods

Cell lines

Human embryonic kidney cells (HEK293) were grown in Dulbecco's Modified Eagle's Medium (DMEM) (Lonza, Leusden, The Netherlands) containing 10 % (v/v) fetal calf serum (FCS) and 2 mM L-glutamine, at 37 °C in a humidity controlled incubator with 5% (v/v) CO_2. The immortalized TAL cell line (MKTAL) was derived from microdissected medullary TAL tubules.[46] MKTAL cells were cultured in DMEM/HAM-F12 (1:1) (Lonza, Leusden, The Netherlands) containing 5% (v/v) FCS and 2 mM L-glutamine, at 37°C in a humidity controlled incubator with 5% (v/v) CO_2.[46]

Animal experimentation

Renal-specific inactivation of HNF1β was achieved using Cre/LoxP recombination by crossing Ksp-cadherin Cre mice with *HNF1β*$^{flox/flox}$.[17] Cre/LoxP activity varies along the nephron and ensured HNF1β inactivation along 27 % of the proximal tubule, 99 % of the TAL, 92 % of the DCT/connecting tubule, and 100 % of the collecting duct.[28] Mice were housed in standard cages with bedding material consisting of straw and paper in a temperature- and light-controlled room with standard pellet chow and deionized drinking water available *ad libitum*. Animals were sacrificed at postnatal day 28. An equal number of male and female mice were used for all procedures. All animal procedures were performed in accordance with the guidelines of the Institutional Animal Care and Use Committees of the University of Texas Southwestern Medical Center and the University of Minnesota Medical School. The animal protocol number is 1503-32434.

Immunohistochemistry (IHC)

Immunohistochemistry was performed as previously described.[11] In short, stainings for HNF1β were achieved on 4 µm sections of mouse kidney samples fixed in formalin and embedded in paraffin. Sections were incubated for 1 hour at 4 °C in rabbit anti-HNF1β (Santa Cruz Biotechnology, Santa Cruz, CA, USA) at a dilution of 1:1,000 and mouse anti-Tamm-Horsfall at 1:2,000 (Santa Cruz Biotechnology). For detection, samples were incubated with an Alexa 594-conjugated goat anti-mouse antibody 1:300 (Thermo Scientific, Amsterdam, The Netherlands) and a biotin-conjugated swine anti-rabbit antibody 1:2,000. Subsequently, samples were incubated with streptavidin-HRP 1:100 and fluorescein-tyramide 1:50 using the TSA Fluorescein System (PerkinElmer, Groningen, The Netherlands). Cell nuclei were stained with DAPI-Fluoromount-GÒ mounting medium (Southern Biotech, Uithoorn, The Netherlands) at room temperature (RT) for 5 minutes. Images were taken with an AxioCam MRm camera (Zeiss, Sliedrecht, The Netherlands) at 40x magnification. Zeiss Zen 2012 (Zeiss, Sliedrecht, The Netherlands) software was used to acquire the images.

Cloning

The human *CaSR* promoter 1 region (-2622 bp, -539 bp upstream) from the transcription start site (TSS) and the *CaSR* promoter 2 region (-972 bp, -242 bp upstream) were amplified from a human bacterial artificial chromosome (BAC) clone (Human RPCI-11.c 79M2; chr3: 121,868,424-122,055,369, Source biosciences, Nottingham, UK) using a high fidelity DNA polymerase (Phusion, Thermofisher, Amsterdam, The Netherlands). The HNF1β binding site region (+16,290 bp to +16,864 bp) was amplified from the same human BAC-clone. The *CaSR* promoter 1 and promoter 2 PCR products were digested with restriction enzymes KpnI and NheI, whereas the HNF1β binding region was digested with NheI and XhoI (New England Biolabs Ltd, Leiden, The Netherlands).

The *CaSR* promoter sequences were ligated first into the pGL3b vector, followed by the HNF1β binding region. Both sequences were cloned upstream of the luciferase gene using T4 DNA ligase (New England Biolabs Ltd, Leiden, The Netherlands). Primers used for the *CaSR* promoter 1 region were; forward 5'-TAAAGCTTCTAGCCACAGCG-3' and reverse 5'- CTCATTCTGCAAGACTCAGGTC-3'. The following primers were used for the *CaSR* promoter 2 PCR; forward 5'-TAAGAGTTTGGGCACGCG-3' and reverse 5'-GTTCCCCGGTCCTACCTG-3'. For the HNF1β binding region the subsequent primers were used; forward 5'- GAAGCACAGATTATTACGGAGATCTC-3' and reverse 5'-CAT-GTCCCTGACCTAATTTGAG-3'. Human *HNF1β* full-length cDNA was amplified by PCR from *HNF1β* pCMV-SPORT6 (clone IRATp970A0421D), ImaGenes), and subcloned into the pCINeo IRES GFP expression vector. HNF1β p.Lys156Glu was obtained by site-directed mutagenesis (Stratagene, La Jolla, USA).[47]

Luciferase assay

Human embryonic kidney 293 (HEK293) cells were transiently transfected with 700 ng of the promoter firefly luciferase constructs using polyethylenimine cationic polymer (PEI) (Invitrogen, Breda, The Netherlands) (ratio 1µg DNA to 6 µl PEI). Cells were transfected with either a pGL3b-empty, pGL3b-*hCaSR*-promoter-1, pGL3b-*hCaSR*-promoter-2, pGL3b-*hCaSR*-promoter-1 or pGL3b-*hCaSR*-promoter-2-HNF1β-binding-region construct. All three conditions were additionally transfected with 50 ng of the pCINEO-empty, pCINEO-*hHNF1β*, or pCINEO-*hHNF1β* p.Lys156Glu mutant construct. In the case of the *CaSR* promoter 2 experiments only pCINEO-empty and pCINEO-*hHNF1β* constructs were used. For standardization of the transfection efficiency, 20 ng of Renilla luciferase plasmid *pRL* under a human cytomegalovirus promoter (CMV) was used as a reference in all conditions. Firefly and Renilla luciferase activities were measured with the Dual-Luciferase Reporter Assay (Promega, Fitchburg, MA, USA).

Real-Time quantitative PCR

MKTAL cells were transiently transfected with 100 pmol of a siRNA smart pool against *Hnf1β* (Dharmacon, Lafayette, USA).[48] Cells were transfected using lipofectamine 2000 (Invitrogen, Breda, The Netherlands) adding 3 µl for each condition. After 48 hours, Total RNA isolation was performed with TRizol (Invitrogen, Breda, The Netherlands). 1.5 µg of RNA was used for reverse transcription using a Moloney Murine Leukemia Virus (M-MLV) reverse transcriptase protocol as described by the manufacturer (Invitrogen, Breda, The Netherlands). The cDNA was used to determine mRNA expression levels by CF96 Real-Time PCR detection system (Bio-Rad, Veenendaal, The Netherlands) for target genes of interest and of the housekeeping gene glyceraldehyde 3-phosphate dehydrogenase (*Gapdh*), as an endogenous control. RT-qPCR primers are reported in Table 1.

Table 1 | RT-qPCR primer sequences

Gene	Forward	Reverse
U6	5'-GTAACCCGTTGAACCCCATT-3'	5'-CCATCCAATCGGTAGTAGCG-3'
Gapdh	5'-TAACATCAAATGGGGTGAGG-3'	5'-GGTTCACACCCATCACAAAC-3'
Kcnj16	5'-GACTTCCGACCAAACCATGTG-3'	5'-GTCATCCTCCCTTCACTGTC-3'
Casr	5'-CTTTCCTATCCATTTTGGAGTAGCA-3'	5'-GCAAAGATCATGGCTTGTAACCA-3'
Cldn16	5'-GTTGCAGGGACCACATTAC-3'	5'-GAGGAGCGTTCGACGTAAAC-3'
Cldn19	5'-GGTTCCTTTCTCTGCTGCAC-3'	5'-CGGGCAACTTAACAACAGG-3'
Cldn10b	5'-GGAGTTCCCCTCCATGCT-3'	5'-GCAAAAATGGAACCGAAAAA-3'
Cldn14	5'-GTCCAGCTCCTAGGCTTCCT-3'	5'-CATCCACAGTCCCTTCAGGT-3'
Hnf1β	5'-CATTGCACAGAGCCTCAACACC-3'	5'-GTTGAGAGAACTGGACGGGCTG-3'
Cldn3	5'-GCACCCACCAAGATCCTCTA-3'	5'-GTAGTCCTTGCGGTCGTAGG-3'
Pkhd1 **(chIP)**	5'-AGAAAAATGTAAGCAGCCCTTTC-3'	5'-GAGTGAAAGTTCACAAATGACCAC-3'
Casr **(chIP)**	5'-CACAAAGCCCATGATGAATG-3'	5'-GTGTGGCTTGGGCTAGTCTC-3'

U6, U6 spliceosomal RNA; *Gapdh*, glyceraldehyde 3-phosphate dehydrogenase; *Kcnj16*, ATP-sensitive inward rectifier potassium channel 16; *Kcnj16*, ATP-sensitive inward rectifier potassium channel 16; *Casr*; calcium-sensing receptor, *Cldn16*; Claudin16, *Cldn19*; Claudin19, *Cldn10b*; Claudin10b, *Cldn14*; Claudin14, *Hnf1β*; hepatocyte nuclear factor 1 homeobox β, *Cldn3*; Claudin3, *Pkhd1* (chIP); Fibrocystin

Real-time qPCR on Ksp-Cre;*Hnf1β*$^{flox/flox}$ kidneys

Total RNA from postnatal day 28 adult wild–type or HNF1β mutant mouse kidneys was extracted using the RNeasy Mini Kit (Qiagen, Germantown, MD, USA) according to the manufacturer's protocol. RNA was treated with DNAse (Invitrogen, Breda, The Netherlands) and cDNA was synthesized using superscript III first strand synthesis kit (Invitrogen, Breda, The Netherlands). cDNA was diluted 1:20 and 10 µl was used in the RT-qPCR reaction. RT-qPCR was performed with the iTAG Universal SYBER Green Supermix (Bio-Rad, Veenendaal, The Netherlands) using the CFX Connect Real-Time System (Bio-Rad, Veenendaal, The Netherlands). U6 spliceosomal RNA was used as an endogenous control. Real-Time PCR primers are listed in Table 1.

Ussing chamber

After seeding MKTAL cells on transwell membranes, confluence was monitored by measuring TEER (trans epithelial electrical resistance) daily with an EVOM^2 chamber (World precision instruments, Sarasota, USA). MKTAL cells were transfected with 100 pmol siRNA for 24 hours, a day before these cells reached their TEER plateau (30-40 Ω*cm^2). Measurements in the Ussing chamber were performed 24 hours after transfection of the MKTAL cells. Experimental and control solutions were preheated

to 37°C before pouring them in liquid reservoirs connected to the Ussing chamber. Two additional heaters were interposed between the fluid reservoirs and the chamber. The flow rate was approximately 10 mL/min. Transepithelial voltage was recorded using agarbridges (2.5 (w/v) agar in 1M KCl and chlorinated silver electrodes connected to an Ussing-Amplifier UPG3. A 10 µA current pulse was applied every 10 s and the resulting voltage reflection was used to calculated transepithelial resistance according to Ohm's law. Paracellular permeability properties were assess similar to by generating a NaCl diffusion potential reducing the NaCl concentration to 30 mM first at the apical then on the basolateral side and by generating bi-ionic diffusion potentials replacing NaCl by either $MgCl_2$ or $CaCl_2$. All three permeability ratios for P_{Na}/P_{Cl}, P_{Mg}/P_{Na} and P_{Ca}/P_{Na} were calculated with the Goldman-Hodgkin-Katz equation and a simplified Kimizuka-Koketsu equation, respectively. [40, 49] Osmolality for all solutions was ~300 mOsm and pH was set at 7.4 using HCl. The composition of the solutions used was the following; Ringer's solution (control solution): 145 mM NaCl, 0.4 mM KH_2PO_4, 1.6 mM KH_2PO_4, 5 mM glucose, 1 mM $MgCl_2$, 1.3 mM Ca-gluconate; Low Na^+ solution: 30 mM NaCl, 0.4 mM KH_2PO_4, 1.6 mM KH_2PO_4, 5 mM glucose, 1 mM $MgCl_2$, 230 mM mannitol, and 1.3 mM Ca-gluconate; Ca^{2+} solution: 3.6 mM KCl, 5 mM glucose, 75 mM mannitol, 72.5 mM $CaCl_2$, and 3 mM HEPES; Mg^{2+} solution: 3.6 mM KCl, 5 mM glucose, 72.5 mM $MgCl_2$, 71 mM mannitol, 1.3 mM Ca-gluconate, and 3 mM HEPES.

Chromatin-immunoprecipitation and quantative PCR (ChIP-qPCR)

Chromatin was isolated from an immortalized DCT cell line (mpkDCT4a) cells by fixing with 1% (v/v) formaldehyde (Ultra-Pure) (Thermo scientific) for 15 min at RT. Cells were washed and permeabilized in 0.25% (v/v) triton-X-100 and 0.05% (v/v) SDS. Samples were sonicated in a Diagenode bioruptor (Diagenode, Ougrée, Belgium), 50 times 30 seconds on 30 seconds off at high intensity. Chromatin samples were then immunoprecipitated with Protein A/G beads (Santa Cruz Biotechnology, Santa Cruz, CA) in 5µg rabbit anti-HNF1β (Santa Cruz Biotechnology, Santa Cruz, CA) for 16 hours at 4 °C. Samples were de-crosslinked in 5 M NaCl at 65 °C for 5 hours. De-crosslinked samples were then purified with phenol-chloroform. cDNA was synthesized from isolated RNA and RT-qPCR was performed as described above. RT-qPCR primers targeting the HNF1β bindingsites found in the *Casr* and *Pkhd1* gene are represented in Table 1.

Data analysis

All results presented are based on at least three independent experiments. Values are expressed as mean ± SEM. Statistical significance ($P<0.05$) was determined using one-tailed students T-test or one-way ANOVA with Dunnett's multiple comparison procedure. ChIP-seq data can be accessed through NCBI GEO (Accession: GSE77397).

Disclosure

This work was supported by grants from the Netherlands Organization for Scientific Research (NWO VICI 016.130.668). Dr. Jeroen de Baaij is supported by a grant from NWO (Veni 016.186.012) and the Dutch Kidney Foundation (Kolff 14OKG17). The authors disclose that they have no conflicts of interest with the contents of this article.

Acknowledgements

The authors thank Dr. Pascal Houillier for kindly providing us with the MKTAL cell line. We would also like to thank Markus Bösch for excellent technical assistance.

References

1. Horikawa Y, Iwasaki N, Hara M*, et al.* Mutation in hepatocyte nuclear factor-1 beta gene (TCF2) associated with MODY. *Nature genetics* 1997; **17:** 384-385.
2. Lindner TH, Njolstad PR, Horikawa Y*, et al.* A novel syndrome of diabetes mellitus, renal dysfunction and genital malformation associated with a partial deletion of the pseudo-POU domain of hepatocyte nuclear factor-1beta. *Human molecular genetics* 1999; **8:** 2001-2008.
3. Bingham C, Bulman MP, Ellard S*, et al.* Mutations in the hepatocyte nuclear factor-1beta gene are associated with familial hypoplastic glomerulocystic kidney disease. *American journal of human genetics* 2001; **68:** 219-224.
4. Bingham C, Hattersley AT. Renal cysts and diabetes syndrome resulting from mutations in hepatocyte nuclear factor-1beta. *Nephrology, dialysis, transplantation : official publication of the European Dialysis and Transplant Association - European Renal Association* 2004; **19:** 2703-2708.
5. Adalat S, Woolf AS, Johnstone KA*, et al.* HNF1B mutations associate with hypomagnesemia and renal magnesium wasting. *Journal of the American Society of Nephrology : JASN* 2009; **20:** 1123-1131.
6. Verhave JC, Bech AP, Wetzels JF*, et al.* Hepatocyte Nuclear Factor 1beta-Associated Kidney Disease: More than Renal Cysts and Diabetes. *Journal of the American Society of Nephrology : JASN* 2016; **27:** 345-353.
7. Verhave JC, Bech AP, Wetzels JF*, et al.* Hepatocyte Nuclear Factor 1beta-Associated Kidney Disease: More than Renal Cysts and Diabetes. *Journal of the American Society of Nephrology : JASN* 2015.
8. van der Made CI, Hoorn EJ, de la Faille R*, et al.* Hypomagnesemia as First Clinical Manifestation of ADTKD-HNF1B: A Case Series and Literature Review. *American journal of nephrology* 2015; **42:** 85-90.
9. Clissold RL, Hamilton AJ, Hattersley AT*, et al.* HNF1B-associated renal and extra-renal disease-an expanding clinical spectrum. *Nature reviews Nephrology* 2015; **11:** 102-112.
10. Coffinier C, Barra J, Babinet C*, et al.* Expression of the vHNF1/HNF1beta homeoprotein gene during mouse organogenesis. *Mech Dev* 1999; **89:** 211-213.
11. Kompatscher A, de Baaij JHF, Aboudehen K*, et al.* Loss of transcriptional activation of the potassium channel Kir5.1 by HNF1beta drives autosomal dominant tubulointerstitial kidney disease. *Kidney international* 2017; **92:** 1145-1156.
12. Ferre S, Veenstra GJ, Bouwmeester R*, et al.* HNF-1B specifically regulates the transcription of the gammaa-subunit of the Na+/K+-ATPase. *Biochemical and biophysical research communications* 2011; **404:** 284-290.
13. Cuevas CA, Su XT, Wang MX*, et al.* Potassium Sensing by Renal Distal Tubules Requires Kir4.1. *Journal of the American Society of Nephrology : JASN* 2017.
14. Gitelman HJ, Graham JB, Welt LG. A new familial disorder characterized by hypokalemia and hypomagnesemia. *Trans Assoc Am Physicians* 1966; **79:** 221-235.
15. Bockenhauer D, Feather S, Stanescu HC*, et al.* Epilepsy, ataxia, sensorineural deafness, tubulopathy, and KCNJ10 mutations. *N Engl J Med* 2009; **360:** 1960-1970.
16. de Baaij JH, Dorresteijn EM, Hennekam EA*, et al.* Recurrent FXYD2 p.Gly41Arg mutation in patients with isolated dominant hypomagnesaemia. *Nephrology, dialysis, transplantation : official publication of the European Dialysis and Transplant Association - European Renal Association* 2015.
17. Gresh L, Fischer E, Reimann A*, et al.* A transcriptional network in polycystic kidney disease. *The EMBO journal* 2004; **23:** 1657-1668.
18. de Baaij JH, Hoenderop JG, Bindels RJ. Magnesium in man: implications for health and disease. *Physiological reviews* 2015; **95:** 1-46.
19. Gong Y, Renigunta V, Himmerkus N*, et al.* Claudin-14 regulates renal Ca(+)(+) transport in response to CaSR signalling via a novel microRNA pathway. *The EMBO journal* 2012; **31:** 1999-2012.
20. Milatz S, Himmerkus N, Wulfmeyer VC*, et al.* Mosaic expression of claudins in thick ascending limbs of Henle results in spatial separation of paracellular Na+ and Mg2+ transport. *Proceedings of the National Academy of Sciences of the United States of America* 2017; **114:** E219-E227.
21. Gong Y, Hou J. Claudin-14 underlies Ca(+)(+)-sensing receptor-mediated Ca(+)(+) metabolism via NFAT-microRNA-based mechanisms. *Journal of the American Society of Nephrology : JASN* 2014; **25:** 745-760.

22. Gamba G, Friedman PA. Thick ascending limb: the Na(+):K (+):2Cl (-) co-transporter, NKCC2, and the calcium-sensing receptor, CaSR. *Pflugers Archiv : European journal of physiology* 2009; **458:** 61-76.
23. Thakker RV. Genetic developments in hypoparathyroidism. *Lancet* 2001; **357:** 974-976.
24. Hannan FM, Nesbit MA, Turner JJ*, et al.* Comparison of human chromosome 19q13 and syntenic region on mouse chromosome 7 reveals absence, in man, of 11.6 Mb containing four mouse calcium-sensing receptor-related sequences: relevance to familial benign hypocalciuric hypercalcaemia type 3. *European journal of human genetics : EJHG* 2010; **18:** 442-447.
25. Dimke H, Desai P, Borovac J*, et al.* Activation of the Ca(2+)-sensing receptor increases renal claudin-14 expression and urinary Ca(2+) excretion. *American journal of physiology Renal physiology* 2013; **304:** F761-769.
26. Liu T, Ortiz JA, Taing L*, et al.* Cistrome: an integrative platform for transcriptional regulation studies. *Genome biology* 2011; **12:** R83.
27. Edghill EL, Bingham C, Slingerland AS*, et al.* Hepatocyte nuclear factor-1 beta mutations cause neonatal diabetes and intrauterine growth retardation: support for a critical role of HNF-1beta in human pancreatic development. *Diabetic medicine : a journal of the British Diabetic Association* 2006; **23:** 1301-1306.
28. Li L, Zepeda-Orozco D, Black R*, et al.* Autophagy Is a Component of Epithelial Cell Fate in Obstructive Uropathy. *Am J Pathol* 2010; **176:** 1767-1778.
29. Brown EM, Gamba G, Riccardi D*, et al.* Cloning and characterization of an extracellular Ca(2+)-sensing receptor from bovine parathyroid. *Nature* 1993; **366:** 575-580.
30. Hebert SC. Extracellular calcium-sensing receptor: implications for calcium and magnesium handling in the kidney. *Kidney international* 1996; **50:** 2129-2139.
31. Houillier P. Calcium-sensing in the kidney. *Current opinion in nephrology and hypertension* 2013; **22:** 566-571.
32. Chakravarti B, Chattopadhyay N, Brown EM. Signaling Through the Extracellular Calcium-Sensing Receptor (CaSR). In: Islam MS (ed). *Calcium Signaling*. Springer Netherlands: Dordrecht, 2012, pp 103-142.
33. Brown E, Enyedi P, LeBoff M*, et al.* High extracellular Ca2+ and Mg2+ stimulate accumulation of inositol phosphates in bovine parathyroid cells. *FEBS Lett* 1987; **218:** 113-118.
34. Brown EM, Pollak M, Chou YH*, et al.* Cloning and functional characterization of extracellular Ca(2+)-sensing receptors from parathyroid and kidney. *Bone* 1995; **17:** 7S-11S.
35. Hendy GN, Canaff L, Cole DE. The CASR gene: alternative splicing and transcriptional control, and calcium-sensing receptor (CaSR) protein: structure and ligand binding sites. *Best practice & research Clinical endocrinology & metabolism* 2013; **27:** 285-301.
36. Chikatsu N, Fukumoto S, Takeuchi Y*, et al.* Cloning and characterization of two promoters for the human calcium-sensing receptor (CaSR) and changes of CaSR expression in parathyroid adenomas. *The Journal of biological chemistry* 2000; **275:** 7553-7557.
37. Garrett JE, Capuano IV, Hammerland LG*, et al.* Molecular cloning and functional expression of human parathyroid calcium receptor cDNAs. *The Journal of biological chemistry* 1995; **270:** 12919-12925.
38. Loupy A, Ramakrishnan SK, Wootla B*, et al.* PTH-independent regulation of blood calcium concentration by the calcium-sensing receptor. *The Journal of clinical investigation* 2012; **122:** 3355-3367.
39. Vezzoli G, Terranegra A, Aloia A*, et al.* Decreased transcriptional activity of calcium-sensing receptor gene promoter 1 is associated with calcium nephrolithiasis. *The Journal of clinical endocrinology and metabolism* 2013; **98:** 3839-3847.
40. Plain A, Wulfmeyer VC, Milatz S*, et al.* Corticomedullary difference in the effects of dietary Ca(2)(+) on tight junction properties in thick ascending limbs of Henle's loop. *Pflugers Archiv : European journal of physiology* 2016; **468:** 293-303.
41. Gong Y, Himmerkus N, Plain A*, et al.* Epigenetic regulation of microRNAs controlling CLDN14 expression as a mechanism for renal calcium handling. *Journal of the American Society of Nephrology : JASN* 2015; **26:** 663-676.
42. Bleich M, Wulfmeyer VC, Himmerkus N*, et al.* Heterogeneity of tight junctions in the thick ascending limb. *Ann N Y Acad Sci* 2017.
43. Faguer S, Chassaing N, Bandin F*, et al.* The HNF1B score is a simple tool to select patients for HNF1B gene analysis. *Kidney international* 2014; **86:** 1007-1015.

44. Chen NX, Moe SM, Eggleston-Gulyas T*, et al.* Calcimimetics inhibit renal pathology in rodent nephronophthisis. *Kidney international* 2011; **80:** 612-619.
45. Faguer S, Decramer S, Chassaing N*, et al.* Diagnosis, management, and prognosis of HNF1B nephropathy in adulthood. *Kidney international* 2011; **80:** 768-776.
46. Bourgeois S, Rossignol P, Grelac F*, et al.* Differentiated thick ascending limb (TAL) cultured cells derived from SV40 transgenic mice express functional apical NHE2 isoform: effect of nitric oxide. *Pflugers Archiv : European journal of physiology* 2003; **446:** 672-683.
47. Ferre S, Bongers EM, Sonneveld R*, et al.* Early development of hyperparathyroidism due to loss of PTH transcriptional repression in patients with HNF1beta mutations? *The Journal of clinical endocrinology and metabolism* 2013; **98:** 4089-4096.
48. Tanaka T, Tomaru Y, Nomura Y*, et al.* Comprehensive search for HNF-1beta-regulated genes in mouse hepatoma cells perturbed by transcription regulatory factor-targeted RNAi. *Nucleic acids research* 2004; **32:** 2740-2750.
49. Li H, Sheppard DN, Hug MJ. Transepithelial electrical measurements with the Ussing chamber. *J Cyst Fibros* 2004; **3 Suppl 2:** 123-126.

4 FAM111A interacts with transcription factor STAT1: Implications for Ca^{2+} and Mg^{2+} reabsorption in Kenny-Caffey syndrome type 2

Andreas Kompatscher[1], Jeroen H.F. de Baaij[1], Gertjan J.C. Veenstra[2], René J.M. Bindels[1] & Joost G.J. Hoenderop[1]

[1]Department of Physiology, Radboud Institute for Molecular Life Sciences, Radboud university medical centre; [2]Department of Molecular Developmental Biology, Radboud Institute for Molecular Life Sciences, Radboud University Nijmegen

In preparation

Abstract

Mutations in family with sequence similarity 111, member A (*FAM111A*) cause Kenny-Caffey syndrome type 2 (KCS2). KCS2 is characterized by severe proportionate short stature, gracile bones dysplasia and other morphological symptoms. Patients also suffer from hypoparathyroidism combined with a hypocalcemia and hypomagnesemia, which explains the growth retardation and other morphological and endocrine symptoms. FAM111A is a protein known for having anti-viral properties and a function in cell replication. However, the role of FAM111A in renal electrolyte transport and parathyroid hormone (PTH) secretion remains unclear.

To elucidate the function of FAM111A that explains its role in electrolyte reabsorption. *Fam111a* was knocked down 50% using siRNAs in an immortalized mouse distal convoluted cell line. Transcriptome analysis in these cells culminated in a list of 78 upregulated and 39 downregulated genes (Fold change >1.32). Pathway analysis of the upregulated genes showed significantly enriched anti-viral pathways. Green Fluorescent Protein (GFP)-pulldown experiments confirmed signal transducer and activator of transcription 1 (*Stat1)* as a potential binding partner of FAM111A. *Stat1* was also upregulated 2.0±0.8 fold after *Fam111a* knockdown in mpkDCT cells and part of the anti-viral pathways established in the KEGG pathway analysis. STAT1 is known as a transcriptional activator of the calcium sensing receptor (CaSR). The CaSR is an important regulator of Ca^{2+} and Mg^{2+} reabsorption in the kidney and PTH secretion in the parathyroid.

It might, therefore, be possible that increased STAT1 expression due to aberrant FAM111A functioning could be responsible for the phenotype of the KCS2 patient.

Introduction

Kenny-Caffey syndrome (KCS, OMIM; #127000, #244460) is a complex disease with a wide variety of morphological, neurological and endocrinological manifestations. Symptoms shared by all KCS patients are a severe proportionate short stature, gracile bones dysplasia, mid-face hypoplasia, delayed closure of the anterior fontanel, frontal bossing, eye abnormalities and hypocalcemia owing to hypoparathyroidism.[1-4] KCS is classified in two subtypes based on clinical features and inheritance pattern. KCS type 1 patients (KCS1, OMIM; #244460) develop mental and prenatal growth retardation. Mutations in the tubulin-folding cofactor E (*TBCE*) gene cause KCS1, which follows a recessive inheritance pattern.[4, 5 6] Cases with normal intelligence and an autosomal dominant inheritance pattern suffer from KCS type 2 (KCS2, OMIM; #127000).[7] Sequencing of several patients with KCS2 identified that mutations in the *family with sequence similarity 111, member A* (*FAM111A*) gene are responsible for the KCS2 disorder.[8] In a Japanese KCS2 cohort, p.Arg569His was established as a hotspot mutation.[9] Mutations in *FAM111A* were also identified in five patients suffering from osteocraniostenosis (OCS, OMIM; #602361), a similar but more severe disorder than KCS2 resulting in early life lethality.[8]

A common feature in KCS2 is the distinct electrolyte deficiencies observed in these patients, characterized by hypocalcemia, hypomagnesemia and hypokalemia, combined with a hypoparathryoidism.[8] Together these symptoms explain the growth retardation, gracile bones syndrome and other morphological and endocrine symptoms.[8-10] The distal convoluted tubule (DCT) and thick ascending limb of Henle's loop (TAL) are segments that are crucial for Ca^{2+} and Mg^{2+} reabsorption in the kidney. In one patient, Ca^{2+} and Mg^{2+} restriction tests were performed which determined that the hypomagnesemia was primary to the hypoparathyroidism.[9] The role of FAM111A in the DCT and TAL segments could, therefore, determine the molecular mechanism behind KCS2 syndrome. However, the relation between FAM111A function and renal Ca^{2+} and Mg^{2+} reabsorption has never been investigated.

FAM111A encodes a protein of 611 amino acids and has homology with trypsin-like peptidases.[11] The protein has been identified as an interactor with the large T antigen of the SV40 virus indicating that FAM111A has anti-viral properties.[11] More recent studies concluded that FAM111A is a binding partner of proliferating cell nuclear factor antigen 1 (*PCNA1*).[12] Depletion of FAM111A by RNA interference indeed decreased PCNA loading onto the chromatin. As a consequence, FAM111A-depleted cells start replication significantly slower than control cells.[12] *In sillico*, modeling of FAM111A mutations elucidated that the Arg569His hotspot mutation potentially disturbs an enzymatic pocket, which could result in FAM111A function loss.[8]

In this study, the role of FAM111A in renal electrolyte handling was investigated. *FAM111A* knockdown in an immortalized mouse distal convoluted cell line (mpkDCT)

and subsequent RNA-sequencing (RNA-seq) was used to reveal novel transcriptional pathways that explain the physiological role of FAM111A in electrolyte handling in the kidney. In addition, an eGFP-pull down experiment was performed to elucidate potential binding partners of FAM111A that could further determine its molecular function in the context of the KCS2 syndrome.

Results

Fam111a mRNA is ubiquitously expressed

Fam111a mRNA levels were measured in various mouse tissues (Figure 1A). *Fam111a* was ubiquitously expressed. The highest expression was present in spleen, lung and inguinal fat with differences in mRNA levels of 231 ± 21, 50 ± 6 and 59 ± 28 fold, respectively, compared to kidney. Since the DCT segment of the nephron is crucial for Mg^{2+} reabsorption, mouse DCT tubules were acquired by complex object parametric analyzer and sorter (COPAS) cell sorter isolation to measure *Fam111a* expression levels. *Fam111a* mRNA was present in the sorted DCT and unsorted tubules to a similar extent (Figure 1B). *Trpm6* is exclusively expressed in the DCT and used as a positive control (Figure 1C). As expected, *Trpm6* expression was significantly increased 6 ± 2 fold in sorted DCT tubules compared to unsorted tubules.

Knockdown of *Fam111a* does not change mRNA expression of Ca^{2+} and Mg^{2+} transport genes

To understand the role of *Fam111a* in electrolyte handling in the kidney, mRNA expression levels of various genes involved in Ca^{2+} and Mg^{2+} transport were measured. To this end, *Fam111a* was significantly knocked down by 44 ± 13% in mpkDCT using siRNAs (Figure 2A). However, *Fam111a* knockdown did not result in significant changes in expression of the epithelial Mg^{2+} channel *Trpm6*, basolateral Mg^{2+} transporter *Slc41a1* or magnesiotropic gene *Cnnm2* (Figure 2A). Neither were significant differences observed in mRNA expression levels of *pro- epidermal growth factor (EGF)* or the EGF receptor (*EGFR*), which are known to enhance *Trpm6* channel activity (Figure 2A).

To examine a potential role of FAM111A in TAL, *Fam111a* was knocked down by 68 ± 8% in an immortalized mouse kidney TAL cell line (MKTAL) (Figure 2B). The expression of the tight junction proteins Claudin16 (*Cldn16*), Claudin19 (*Cldn19*), Claudin14 (*Cldn14)* or the *Casr* was not significantly affected by knock down of *Fam111a* (Figure 2B).

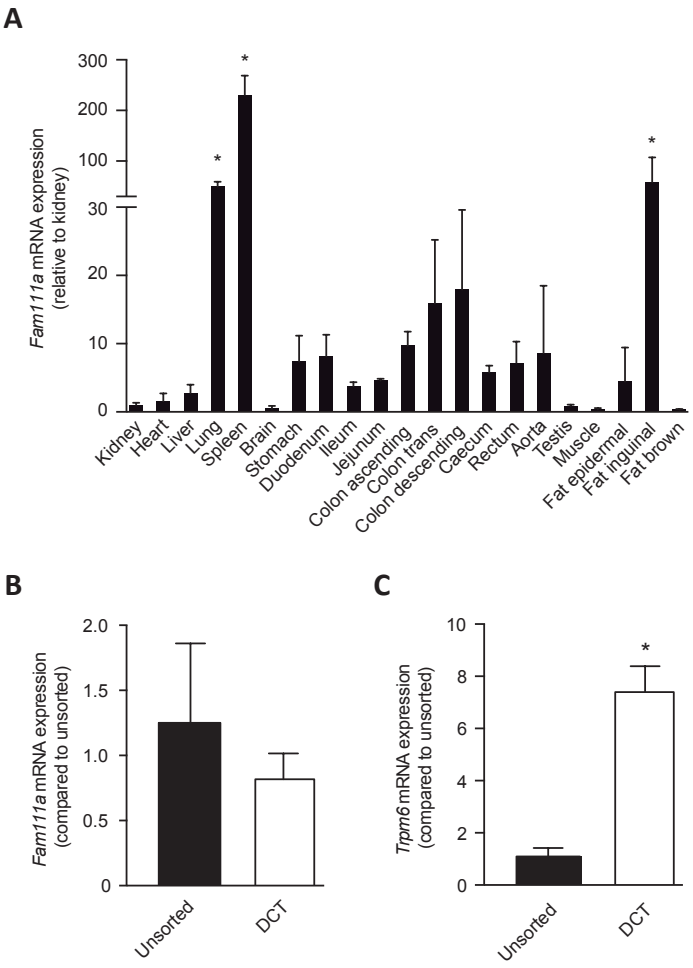

Figure 1 | *Fam111a* mRNA is ubiquitously expressed

A) Data displays *Fam111a* mRNA expression in various mouse tissues relative to kidney. Samples were measured in wild-type mice (n=3) by quantitative RT-PCR and normalized for *Gapdh* expression. Data (n=3) represent mean ± SEM and are expressed as the fold difference compared to the expression of *Fam111a* in kidney. B-C) The mRNA expression levels of *Fam111a* B) or *Trpm6* C) were measured in unsorted (black bar) or sorted DCT tubules (white bar). Samples were measured by RT-qPCR and normalized for *Gapdh* expression. Data (n=3) represent mean ± SEM expressed as the fold difference compared to the expression in unsorted tubules.

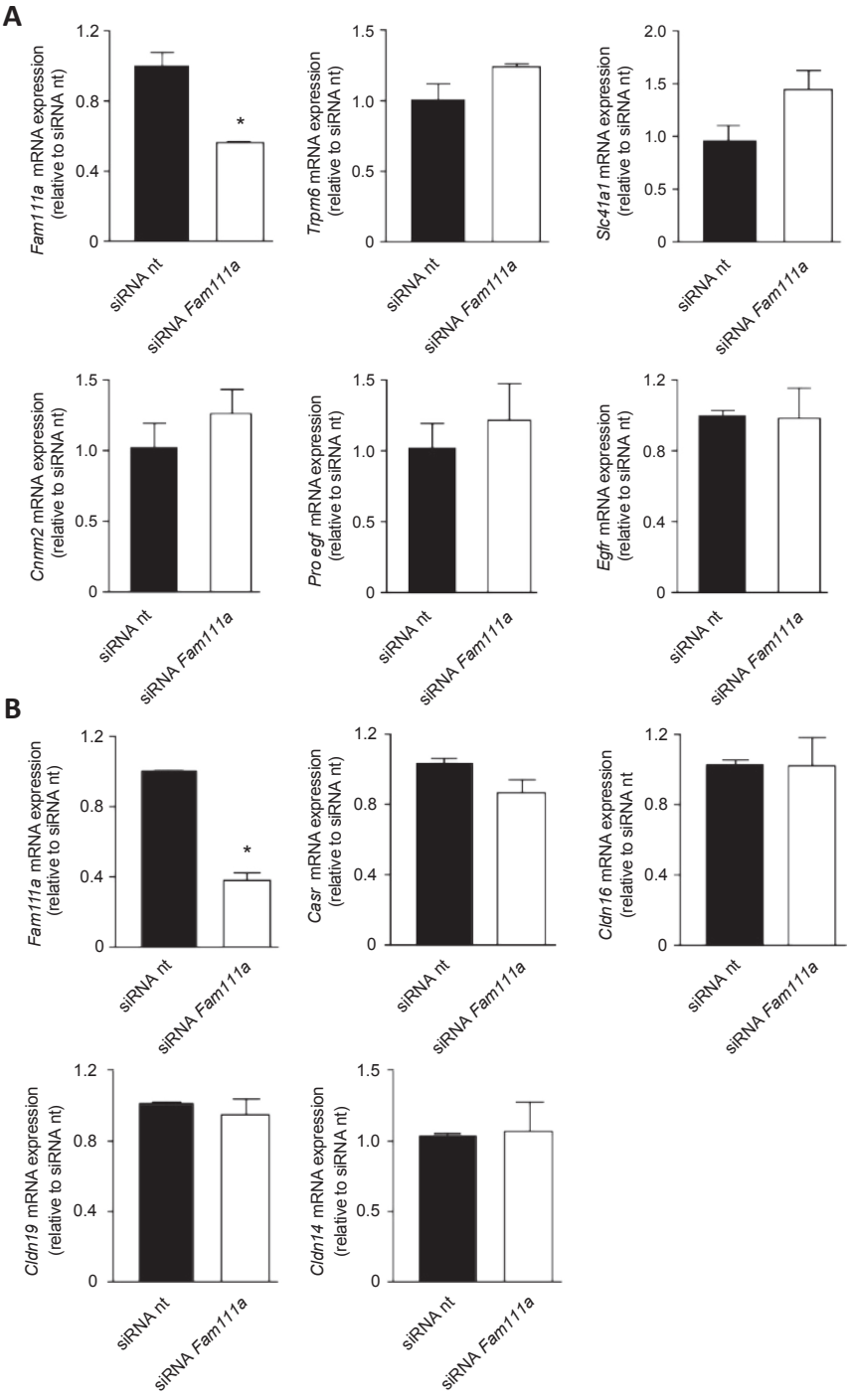
A
Fam111a mRNA expression (relative to siRNA nt)
1.2
0.8
0.4
0
*
siRNA nt
siRNA Fam111a
Trpm6 mRNA expression (relative to siRNA nt)
1.5
1.0
0.5
0
Slc41a1 mRNA expression (relative to siRNA nt)
2.0
1.5
1.0
0.5
0
Cnnm2 mRNA expression (relative to siRNA nt)
Pro egf mRNA expression (relative to siRNA nt)
Egfr mRNA expression (relative to siRNA nt)
B
Casr mRNA expression (relative to siRNA nt)
Cldn16 mRNA expression (relative to siRNA nt)
Cldn19 mRNA expression (relative to siRNA nt)
Cldn14 mRNA expression (relative to siRNA nt)

Figure 2 | Knockdown of *Fam111a* does not change mRNA expression of Ca^{2+} and Mg^{2+} transport genes

A) The mRNA expression levels of *Fam111a*, *Trpm6*, *Slc41a1*, *Cnnm2*, *Proegf* and *Egf* in mpkDCT cells treated with either non-targeting (nt) (black bars) or *Fam111a* targeting (white bars) siRNAs. B) The mRNA expression levels of *Fam111a*, *Casr*, *Cldn16*, *Cldn19* and *Cldn14* in MKTAL cells treated with either non-targeting (nt) (black bars) or *Fam111a* targeting (white bars) siRNAs. Samples were measured by quantitative RT-PCR and normalized for *Gapdh* expression. Data (n=3) represent mean ± SEM, *, P>0.05 and are expressed as the fold difference compared to the expression in siRNA nt.

Fam111a down regulation activates anti-viral pathways

As our targeted-approach did not identify genes that are regulated by FAM111A, a genome-wide approach was used. An RNA-seq was performed on mpkDCT cells to identify which genes in the kidney are regulated by FAM111A and related to ion transport. SiRNAs targeting *Fam111a* decreased endogenous *Fam111a* expression significantly with 58 ± 5% compared to a non-targeting control condition (siRNA nt) (Figure 3A). A principal component analysis (PCA) demonstrated that the siRNA *Fam111a* samples form a separate cluster from the siRNA nt samples along the PC1 axis, which explains most (70%) of the variance observed in the dataset (Figure 3B). This indicates higher variance between the siRNA nt and the siRNA *Fam111a* conditions than within the groups. Differential expression of 21,041 genes was assessed (Figure 3C), resulting in the identification of 519 up- and 298 significantly down-regulated genes (false discovery rate (FDR); $p<0.05$) (supplemental table 1). A >1.3 fold change cut-off was used to select for biologically relevant targets culminating in a list of 78 upregulated (Table 1) and 37 downregulated genes (Table 2). The genes with the most substantial expression differences were *Inmt* with a 1.68 fold upregulation and, as expected, *Fam111a* with a 1.95 fold downregulation (Table 1 and 2).

KEGG pathway analysis demonstrated that several anti-viral pathways (Herpes simplex infection, mmu05168; Hepatitis C, mmu05160; Influenza A, mmu05164) where significantly upregulated (Table 3). The affected genes in these pathways were interferon regulatory factor 7 (*Irf7*), interferon-induced protein with tetratricopeptide repeats 1 (*Ifit1*), ribonuclease L (2', 5'-oligoisoadenylate synthetase-dependent) (*Rnasel*), toll-like receptor 3 (*Tlr3*), transporter 1, ATP-binding cassette, sub-family B (MDR/TAP) (*Tap1*) and signal transducer and activator of transcription 1 (*Stat1*). KEGG pathway analysis for the downregulated genes determined that the p53-signaling (04115) pathway was affected. Due to the limited amount of differentially expressed genes this result did not reach statistical significance. *Stat1* upregulation after *Fam111a* knockdown was verified by RT-qPCR in mouse DCT cells. *Fam111a* was significantly knocked down by 50 ± 13%, while *Stat1* expression was significantly upregulated by 2.0 ± 0.8 fold (Figure 3D).

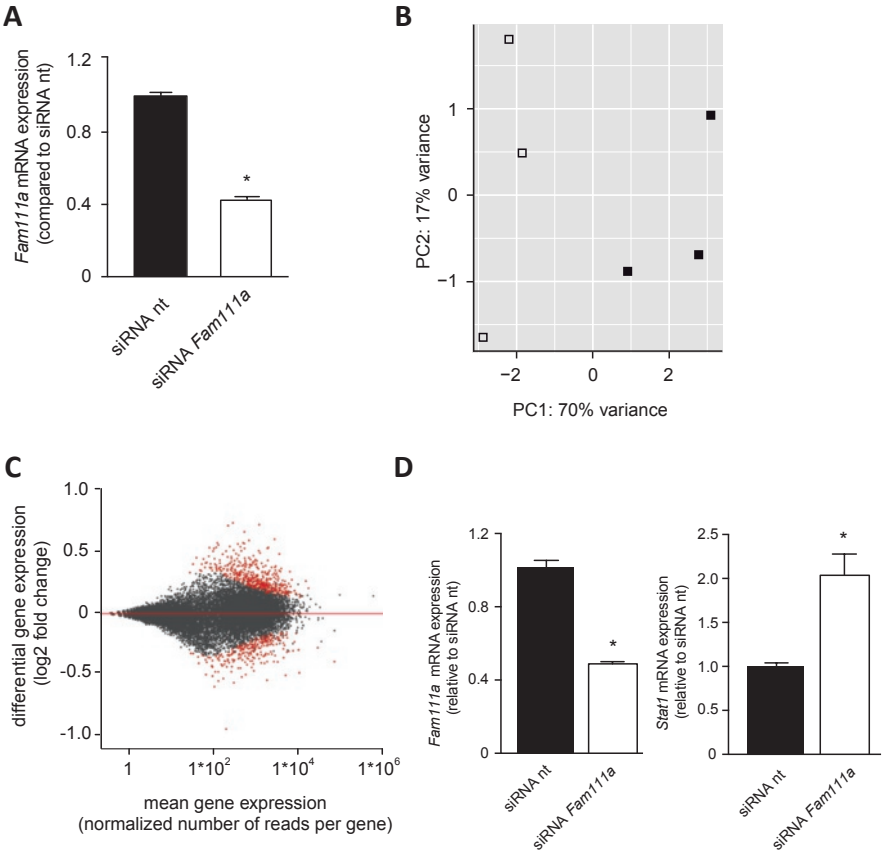

Figure 3 | *Fam111a* downregulation activates anti-viral pathways

A) The mRNA expression levels of *Fam111a* in mpkDCT cells treated with either non-targeting (nt) (black bars) or *Fam111a* targeting (white bars) siRNAs that were destined for RNA-seq. Samples were measured by quantitative RT-PCR and normalized for *Gapdh* expression. Data (n=3) represent mean ± SEM and are expressed as the fold difference compared to the expression in siRNA nt. B) The principal component analysis (PCA) plot exhibits the two variables that explain most of the variance present in the data. Principal component 1 (PC1) explains 70%, whereas PC2 explains 17% of the variance found in all samples (n=3 control samples, n=3 siRNA *Fam111a* samples) of the RNA-seq dataset. Samples are plotted based on the amount of variance that both PCs explain in the RNA-seq of that sample. Control samples are depicted as white squares, siRNA *Fam111a* samples are shown as black squares. C) The MA plot displays the overall mean expression for every tested gene and the relative differential gene expression of the siRNA *Fam111a* samples compared to the non-targeting control samples expressed as a Log2 fold change. The mean expression is expressed as the normalized number of reads per gene. Red data points depict genes that are significantly differentially expressed in

the siRNA *Fam111a* condition compared to the control samples (FDR; P<0.05, corrected for multiple comparison with Benjamini-Hochberg). D) The mRNA expression levels of *Fam111a* or *Stat1* in mpkDCT cells treated with either non-targeting (nt) (black bars) or *Fam111a* targeting (white bars). Data (n=3) represent mean ± SEM and are expressed as the fold difference compared to the expression in siRNA nt. Samples were measured by RT-qPCR and normalized for *Gapdh* expression.

Table 1 | Upregulated genes due to decreased *Fam111a* expression in mpkDCT cells

Gene name	Mean of normalized counts across samples	Differential gene expression (Fold change)	P-value (FDR, <0.01)
Inmt	271	1.68	1.5E-11
Aqp1	1155	1.67	8.0E-18
Kank4	207	1.66	1.3E-09
Hsd11b2	510	1.60	1.5E-09
Npnt	2715	1.53	1.5E-17
Fras1	658	1.52	2.6E-10
Vnn1	114	1.50	3.4E-05
Nrp2	473	1.50	1.5E-09
Ifit3b	511	1.50	2.0E-07
Ube2l6	355	1.49	1.7E-06
Prr5l	121	1.49	6.6E-05
Kazn	226	1.47	1.8E-05
Dhx58	411	1.47	8.5E-06
Peli3	107	1.47	1.6E-04
Nrip3	73	1.46	2.9E-04
Neurl1b	1933	1.46	8.9E-13
Sema3a	95	1.46	3.2E-04
Ifitm3	1826	1.45	9.9E-09
Tspan13	514	1.45	1.4E-08
Masp1	281	1.44	8.5E-06
Rasgrp2	90	1.44	7.4E-04
Aebp1	430	1.43	1.9E-06
Nup210	1131	1.43	4.4E-11
Lipg	186	1.43	1.9E-04
Irf7	1218	1.42	1.7E-06
Bsnd	320	1.41	1.3E-05
Tmem8	153	1.41	4.4E-04

Table 1 | Continued

Gene name	Mean of normalized counts across samples	Differential gene expression (Fold change)	P-value (FDR, <0.01)
Lgals3bp	3528	1.41	3.5E-09
Stard8	370	1.40	6.2E-05
Chchd10	844	1.40	1.6E-05
Dgat2	71	1.39	2.6E-03
Afap1l1	249	1.39	1.6E-04
Fam53b	201	1.39	4.9E-04
Cxcl12	36	1.38	NA
Them6	657	1.38	7.0E-06
Cmpk2	519	1.38	1.9E-04
Crybg1	97	1.37	3.9E-03
Ppargc1b	53	1.37	4.3E-03
Tap1	341	1.37	8.8E-05
Pcsk5	250	1.37	4.3E-04
Lynx1	711	1.36	3.6E-06
Ppargc1a	936	1.36	2.0E-06
Dmd	131	1.36	3.4E-03
Ifit1	1875	1.36	2.3E-03
Fyco1	534	1.36	6.4E-06
Hcn2	296	1.36	4.3E-04
Gpd1l	1019	1.35	8.7E-08
Uap1l1	902	1.35	1.9E-05
Gnai1	378	1.35	9.7E-05
Itgb3	249	1.35	1.1E-03
Oxct1	818	1.35	7.0E-07
Gal3st1	64	1.35	8.6E-03
B3gnt7	60	1.34	1.0E-02
Stat1	549	1.34	2.1E-04
Tlr3	411	1.34	4.3E-04
Ifi27l2a	132	1.34	7.3E-03
Arfgef3	226	1.34	2.0E-03
Usp18	1322	1.34	3.9E-05
Aldh6a1	530	1.34	1.6E-04
Cpped1	820	1.34	2.9E-06
Rhcg	231	1.34	3.9E-03

Table 1 | Continued

Gene name	Mean of normalized counts across samples	Differential gene expression (Fold change)	P-value (FDR, <0.01)
Slc27a6	78	1.33	1.1E-02
Wipf3	30	1.33	NA
Frem2	48	1.33	1.1E-02
Gfra1	99	1.33	1.0E-02
Pltp	290	1.33	2.1E-03
Fam84b	985	1.33	1.4E-06
Slc45a4	682	1.33	1.4E-05
Rnasel	205	1.33	3.7E-03
Iigp1	570	1.33	1.4E-02
Ifi30	731	1.33	1.7E-04
Fam20c	936	1.33	3.4E-06
Arhgdib	491	1.32	1.1E-03
Rsad2	722	1.32	1.4E-02
Me3	108	1.32	1.3E-02
Nptxr	273	1.32	1.6E-03
Bpnt1	767	1.32	2.0E-05
Adora1	369	1.32	7.6E-04

Columns indicate Gene name, list of HGNC gene symbols; mean of normalized counts for all samples; differential gene expression between siRNA *Fam111a* and siRNA non-targeting expressed as fold change; P-value, false discovery rate (FDR) $p<0.05$, and corrected for multiple testing with the Benjamini-Hochberg correction.

Table 2 | Downregulated genes due to decreased *Fam111a* expression in mpkDCT cells

Gene name	Mean of normalized counts across samples	Differential gene expression (Fold change)	P-value (FDR, <0.01)
Fam111a	186	1.94	6.1E-16
Sprr1a	97	1.53	2.4E-05
Creb5	285	1.49	1.4E-06
Mettl7b	121	1.48	1.1E-04
Ankrd1	1790	1.47	3.8E-12
Gm38357	158	1.45	1.2E-04
Serpine1	442	1.44	1.4E-06
Col4a2	5009	1.43	1.5E-20

Table 2 | Continued

Gene name	Mean of normalized counts across samples	Differential gene expression (Fold change)	P-value (FDR, <0.01)
Gm42899	61	1.42	9.3E-04
Zdhhc21	549	1.42	3.2E-06
Akap12	10704	1.40	2.1E-11
AC087890.1	120	1.40	2.0E-03
Gm45223	101	1.40	2.2E-03
Ano1	248	1.40	1.4E-04
Zbtb37	860	1.39	3.4E-06
Pmaip1	363	1.37	3.4E-05
Zswim6	413	1.37	5.2E-05
Slc13a2os	87	1.36	5.0E-03
AC160637.1	763	1.36	5.1E-05
A930004J17Rik	192	1.36	1.5E-03
Slc39a3	255	1.36	4.9E-04
AC131586.1	83	1.35	7.2E-03
Gm37420	86	1.35	7.3E-03
Mtm1	149	1.35	3.3E-03
Galnt3	151	1.35	4.6E-03
Amn1	592	1.34	2.5E-04
Gm37472	143	1.34	7.3E-03
Gm37238	169	1.34	6.5E-03
Ctgf	841	1.34	3.4E-05
Tgfbi	41	1.33	NA
Rhob	1545	1.33	1.4E-06
Clock	1300	1.33	2.1E-06
Rbm4	218	1.33	5.6E-03
AC140397.1	63	1.33	1.3E-02
Sbds	532	1.32	4.8E-05
Gm21781	278	1.32	8.0E-03
Mfap3l	3227	1.32	7.0E-12

Gene name, list of HGNC gene symbols; mean of normalized counts for all samples; differential gene expression between siRNA *Fam111a* and siRNA non-targeting expressed as fold change; P-value, FDR $p<0.05$, and corrected for multiple testing with the Benjamini-Hochberg correction.

Table 3 | Deregulated pathways in mpkDCT cells with decreased *Fam111a* expression

KEGG pathways (upregulated genes)	Count	p-value
Herpes simplex infection	6	<0.01
Hepatitis C	5	<0.01
Influenza A	5	0.01
Renin secretion	3	0.05
Chemokine signaling pathway	4	0.08
Toll-like receptor signaling pathway	3	0.09
KEGG pathways (downregulated genes)	**Count**	**P-value**
p53 signaling pathway	2	0.07

KEGG pathways analysis with up and downregulated genes P<0.01, Fold change >1.3. Columns indicate KEGG pathway, number of genes and P-value. KEGG, Kyoto Encyclopedia of Genes and Genomes.

FAM111A binds to transcriptional activator STAT1

eGFP-pull down experiments were performed to determine potential binding partners of FAM111A. A HeLa FRT-flp-in cell line was produced that stably expresses eGFP-FAM111A or eGFP-FAM111A R569H hotspot mutation to assess whether protein interactions are affected by this patient mutation. Proper expression of eGFP-FAM111A wildtype and R569H mutant protein was verified on immunoblot at the expected height of 100 kD (Figure 4A). A protein sample of cells expressing eGFP only was used as a positive control and displays eGFP (27 kD) expression at a height of ~34 kD.

An eGFP-pulldown on an 'eGFP only' expressing HeLa cell line was used as a control for non-specific binding. As expected, FAM111A was demonstrated to be significantly bound to itself, acting as a validation of the specificity of the GFP-pull down experiment (Figure 4B and C). STAT1 was the only protein that met the minimum requirements (FDR; p<0.015, Log2 fold change >6) as a potential interacting partner of the FAM111A wild-type protein. The FAM111A R569H mutant did not abolish the interaction with STAT1 (Figure 4C). The results of the FAM111A mutant pull down identified cysteine and glycine-rich protein 1 (CSRP1) to be significantly more present in the negative control compared to the FAM111A mutant (FDR; p<0.015, Log2 fold change >6) (Figure 4C).

Further examinations into FAM111A binding partners demonstrated five proteins (RPL23, RPF2, ELF6, KRT2 and RBM8A) with a higher affinity for binding to the FAM111A wildtype compared to the FAM111A mutant protein (FDR; p<0.025, Log2 fold change >1.6) (Figure 4D).

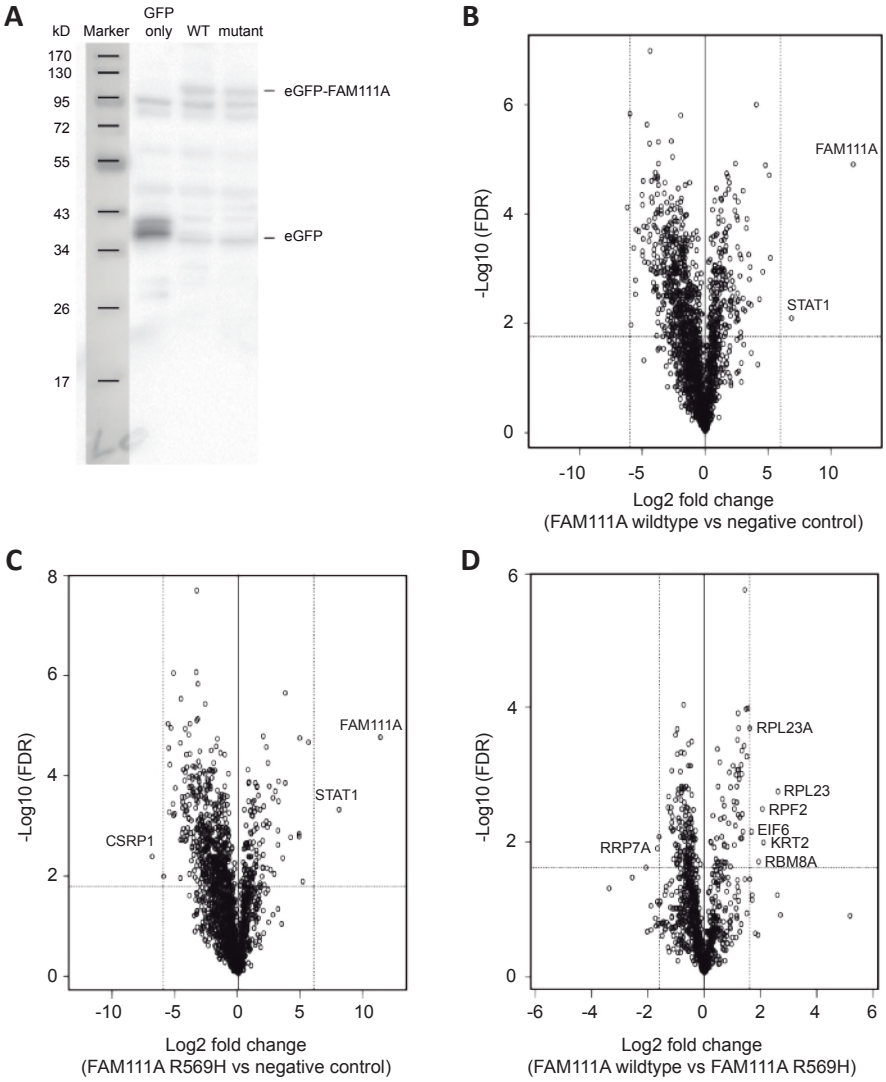

Figure 4 | FAM111A binds to transcriptional activator STAT1

A) Immunoblot of protein lysate from HeLa cells stably expressing eGFP-FAM111A. The blot is stained for eGFP detecting 'eGFP only' (27 kD), eGFP-FAM111A (97 kD) and eGFP-FAM111A R569H (97 kD). Marker (ez-run prestained marker (ThermoScientific, Breda, The Netherlands) represents protein size in kilo Dalton (kD). B-D) The volcano plots display proteins that are bound to either FAM111A wild-type or FAM111A R569H versus an empty control sample or FAM111A wild-type versus FAM111A R569H. All samples are expressed as a Log2 fold change.

A positive Log2 fold change represents higher affinity to FAM111A wild-type or R569H versus the empty control B-C) or FAM111A R569H D). The statistical significance of the Log2 fold change is expressed as –Log10 FDR. The thresholds for binding are set at >6 Log2 fold change, FDR p<0.015 B), >6 Log2 fold change, FDR p<0.015 C), >1.6 Log2 fold change, FDR p<0.025 D).

Discussion

The aim of this study was to elucidate the molecular mechanism explaining the disturbed electrolyte balance seen in KCS2 patients. Transcriptome analysis of a mouse DCT cell line demonstrated that decreased *Fam111a* expression upregulates several anti-viral pathways. One of the upregulated genes found in these anti-viral pathways was *Stat1*. eGFP-pull down experiments further substantiated that STAT1 is a binding partner of FAM111A. These experiments demonstrated that FAM111A might be a novel partner for STAT1 functioning, which could be conducive to the development of the KCS2 patient phenotype.

STAT1 is a key transcription factor that activates genes involved in cell proliferation, apoptosis and immunological processes.[13, 14] STAT1 activity is regulated by the Janus (JAK) kinase family, which is essential for activating interferon (IFN)-α induced anti-viral responses.[15, 16] In humans, loss-of-function mutations in *STAT1* increased susceptibly to mycobacterial and viral infections.[17] This phenotype was reflected in a STAT1 knockout (KO) mouse model, which manifested as compromised innate immunity to viral disease.[18] *Fam111a* knockdown indeed resulted in the upregulation of anti-viral pathways. A co-operating role of FAM111A-STAT1 complexes fits with previous literature on FAM111A, as depletion of FAM111A via RNA interference in CV-1P cells induced viral gene expression and replication.[11] FAM111A was actively bound by the viral SV40 large T antigen c-terminus to reduce host range restriction activity of FAM111A allowing for increased viral RNA replication.[11] It is, therefore, plausible that depletion or limited availability of FAM111A can act as a signal for the upregulation of other anti-viral genes like STAT1. Indeed, STAT1 upregulation was confirmed in cells lacking *Fam111a* (Figure 3D).

The interaction of FAM111A with STAT1 may also contribute to the electrolyte phenotype of KCS2 patients. STAT1 is a transcriptional activator of the CaSR,[19] which is an important factor in Ca^{2+} and Mg^{2+} transport in the TAL by regulating *Cldn14* expression.[20] The hypocalcemia found in critically ill patients suffering from burn injuries and sepsis is associated with CaSR upregulation activated by the STAT1/STAT3 pathway in response to Interleukin-6 (IL-6) signaling.[21, 22] Indeed, rats that were injected with interleukin (IL)-6, activating the STAT1/3 pathway, displayed significant decreases in serum PTH, $1,25(OH)_2D_3$ (VitD) and Ca^{2+} levels.[23, 24] These results are in line with the KCS2 patient's hypoparathyroidism, hypocalcemia and hypomagnesemia,

because increased expression of the *Casr* reduces Ca^{2+} and Mg^{2+} reabsorption in the kidney. The CaSR also directly regulates PTH release. Therefore, future studies should examine extra-renal effects of FAM111A. CaSR gain-of-function mutations are known to reduce PTH release aggravating the loss of Ca^{2+} and Mg^{2+} in the kidney and reducing Ca^{2+} resorption in bone.[25] It is, therefore, important to investigate the function of FAM111A in parathyroid tissue to delineate potential direct effects on PTH secretion.

Based on our data, siRNA-mediated knockdown of FAM111A did not result in increased *Casr* and *Cldn14* expression levels in MKTAL cells (Figure 2B). This could be due to insufficient knockdown of *Fam111a*. However, it cannot be excluded that the electrolyte phenotype of KCS2 patients is explained by STAT1-independent effects. Patients with heterozygous STAT1 gain-of-function mutations suffer from a different phenotype then KCS2, characterized by impaired IL-17 immunity causing chronic mucocutaneous candidiasis.[17] This shows that STAT1 and FAM111A have different functional effects. Careful characterization of a FAM111A KO mouse model may help to determine STAT1-dependent and STAT1-independent effects. Furthermore, the binding of STAT1 to FAM111A requires confirmation in a co-immunoprecipitation (CO-IP) experiment. Other point mutations and deletions found in KCS2 patients could subsequently be investigated by CO-IP to determine whether these affect STAT1 binding to FAM111A.[8, 26] This study focuses mainly on FAM111A functioning in the kidney. However, the results from the tissue panel (Figure 1A) indicated that, although *Fam111a* is present in the kidney, there seems to be a vastly increased expression of *Fam111a* in spleen, lung and linguinal fat. For spleen and lung, this is likely due to FAM111As' anti-viral properties. As spleen holds a large reservoir of monocytes and both lung and spleen have an important role in combating infections.[27, 28] Despite these high relative expression levels of *Fam111* in these tissues, the total mRNA level of *Fam111a* in kidney was detected at 25 PCR cycles by RT-qPCR. Meaning that *Fam111a* is expressed in sufficient quantities to participate in biological processes in the kidney.

In this study, we identified STAT1 as a new binding partner of FAM111A. Although the precise mechanism responsible for this binding is yet unclear, it is apparent that a decrease in *Fam111a* abundance in a mouse DCT cell line increases *Stat1* expression levels. STAT1 is an important activator of *Casr* receptor transcription and could affect Ca^{2+} and Mg^{2+} reabsorption in the kidney and PTH release in the parathyroid. The KCS2 patient phenotype could therefore be caused by abnormal STAT1 expression and functioning due to mutations and deletions in its binding partner FAM111A.

Methods

Cell lines

Human embryonic kidney cells (HEK293) were grown in Dulbecco's modified Eagle's medium (Lonza, Leusden, The Netherlands) containing 10% (v/v) fetal calf serum (FCS), 2 mM L-glutamine at 37 °C in a humidity controlled incubator with 5% (v/v) CO_2. HeLa cells were cultured in DMEM (Lonza) containing 10% (v/v) FCS, 2 mM L-glutamine and 3 µg/ml blasticidin. MpkDCT4a were cultured as described previously.[29] The immortalized mouse kidney TAL cell line (MKTAL) was derived from microdissected medullary TAL tubules.[30] MKTAL cells were cultured in DMEM/HAM-F12 (1:1) (Lonza, Leusden, The Netherlands) containing 5% (v/v) FCS and 2 mM L-glutamine, at 37°C in a humidity controlled incubator with 5% (v/v) CO_2.[30]

Tissue panel

Tissues were harvested from C57BL/6 wildtype mice and homogenized using a tissue homogenizer. Total RNA was isolated as described in the Real-Time quantitative PCR section (RT-qPCR). Primers for *Fam111a* are described in Table 4. Tubules were sorted with a COPAS Biosort cell sorter (Union biometrica, Geel, Belgium) as described in a previous study.[31]

Real-Time quantitative PCR

MpkDCT4a and MKTAL cells were transiently transfected with 100 pmol of a siRNA smart pool against *Fam111a* (Dharmacon, Lafayette, USA). Cells were transfected using lipofectamine 2000 (Invitrogen, Breda, The Netherlands) adding 3 µl for each condition. After 48 hours, Total RNA isolation was performed with TRizol (Invitrogen, Breda, The Netherlands). 1.5 µg of RNA was used for reverse transcription using a Moloney Murine Leukemia Virus (M-MLV) reverse transcriptase protocol as described by the manufacturer (Invitrogen, Breda, The Netherlands). The cDNA was used to determine mRNA expression levels by CF96 Real-Time PCR detection system (Bio-Rad, Veenendaal, The Netherlands) for target genes of interest and of the housekeeping gene glyceraldehyde 3-phosphate dehydrogenase (*Gapdh*), as an endogenous control. RT-qPCR primers are reported in Table 4.

Cloning

Human FAM111A full-length cDNA was amplified by PCR from human cDNA clone (clone IRAUp969C0699D), ImaGenes), and subcloned into the pcDNA/FRT-TAP eGFP expression vector using a high fidelity DNA polymerase (Phusion, Thermofisher, Amsterdam, The Netherlands). The PCR product was digested with restriction enzymes KpnI and XhoI (New England Biolabs Ltd, Leiden, The Netherlands). The sequence was than ligated into a pcDNA/FRT-TAP vector behind the eGFP using T4

Table 4 | Primer Sequences for RT-qPCR

	Forward	Reverse
Gapdh	5'-TAACATCAAATGGGGTGAGG-3'	5'-GGTTCACACCCATCACAAAC-3'
Fam111a	5'-TAACATCAAATGGGGTGAGG-3'	5'-GGTTCACACCCATCACAAAC-3'
Trpm6	5'-AAAGCCATGCGAGTTATCAGC-3'	5'-CTTCACAATGAAAACCTGCCC-3'
Slc41a1	5'-CCGCGATTTATCAGAGC-3'	5'- AGATCCTTGAGGTAGAGGAA-3'
Cnmm2	5'-GCCTTTAAGCAGACGGACAG-3'	5'-GATGGGCTAAACGCTTCTAC-3'
proEgf	5'-GAGTTGCCCTGACTCTACCG-3'	5'-CCACCATTGAGGCAGTATCC-3'
Egfr	5'- CAGAACTGGGCTTAGGGAAC-3'	5'- GGACGATGTCCCTCCACTG-3'
Casr	5'-CTTTCCTATCCATTTTGGAGTAGCA-3'	5'-GCAAAGATCATGGCTTGTAACCA-3'
Cldn16	5'-GTTGCAGGGACCACATTAC-3'	5'-GAGGAGCGTTCGACGTAAAC-3'
Cldn19	5'-GGTTCCTTTCTCTGCTGCAC-3'	5'-CGGGCAACTTAACAACAGG-3'
Cldn14	5'-GTCCAGCTCCTAGGCTTCCT-3'	5'-CATCCACAGTCCCTTCAGGT-3'

Gapdh, glyceraldehyde 3-phosphate dehydrogenase; *Trpm6*, transient receptor potential cation channel, subfamily M, member 6; *Slc41a1*, solute carrier family 41 member 1; *Cnnm2*, Cyclin M2; pro*Egf*, epidermal growth factor; *Egfr*, epidermal growth factor receptor; *Casr*, calcium-sensing receptor; *Cldn16*, Claudin16; *Cldn19*, Claudin19; Cldn14, Claudin14

DNA ligase to create the eGFP-FAM111A fusion protein (New England Biolabs Ltd, Leiden, The Netherlands). Primers used were; forward 5'- ATGCCACCAGCTGTAAGAAGCAGAGGTC-3' and reverse 5'- ATCTCGAG*TCA*CAAGTCCTCATCACTCATCATTTC-3'. FAM111A p.Arg569His was obtained by site-directed mutagenesis (Stratagene, La Jolla, USA).[32] Primers used for mutagenesis were; forward 5'-CCAAGATATGAAACTTAAGCTCACACATAGTGAGAATAGTAG-3' and reverse 5'-CTACTATTCTCACTATGTGTGAGCTTAAGTTTCATATCTTGG-3'.

Stable eGFP-FAM111A HeLa cell line

300,000 HeLa flp-in cells were seeded into a 6-well plate. After 12 hrs, the medium was changed to HeLa cell medium without blasticidin (Sigma-Aldrich, Zwijndrecht, The Netherlands). Cells were transiently transfected with 2 µg of pcDNA5-flp-in eGFP-FAM111A or pcDNA5-flp-in eGFP-FAM111A R569H constructs with 200 ng pOG44 Flp-recombinase expression vector. 3 µl of lipofectamine 2000 (Invitrogen, Breda, The Netherlands) was used for each 1 µg of DNA. After 24 hrs, 100 µg/ml was added to the HeLa medium to start the selection procedure. eGFP-FAM111A expression was induced by adding 1 µg/ml of tetracycline to the cells.

Immunoblotting

Cells expressing eGFP-FAM111A, eGFP-FAM111A R569H or 'eGFP only' were lysed in lysis buffer (50 mM Tris/HCl pH 7.5, 1 mM EDTA, 1 mM EGTA, 1 mM Na-Orthovandate, 5 mM NaF, 5 mM glycerolphosphate 0.27 M sucrose and 1 tablet of complete protease inhibitor cocktail (Roche) containing 1% (v/v) Triton X-100. Protein concentrations were measured with a colorimetric Pierce BCA protein assay kit (ThermoFisher scientific, Breda, The Netherlands) according to the manufacturer's protocol. In short, samples were loaded on a 96 well plate, incubated for 30 minutes at 37 °C and measured at 562 nm with a Biorad Benchmark plus microplate photospectrometer (Biorad, Veenendaal, The Netherlands). Samples were set to 1 µg/µl of protein.

Protein lysates were denatured in Laemmli containing 100 mM Dithiothreitol (DTT) for 5 minutes at 95 °C. Samples were then subjected to SDS-PAGE and Immunoblots were incubated with a rabbit polyclonal anti-GFP antibody (ab290, 1:5,000) (Abcam, Cambridge, UK) in 5% (w/v) milk o/n at 4 °C. Then, immunoblots were incubated 45 minutes at RT in 5% (w/v) milk with peroxidase conjugated goat anti-rabbit (1:10,000) secondary antibodies (Sigma-Aldrich, Zwijndrecht, The Netherlands).

RNA-seq

mpkDCT cells were transiently transfected with 100 pmol of a siRNA smart pool against FAM111A or a non-targeting control (Dharmacon, Lafayette, USA). Total RNA was isolated with the RNeasy micro kit according to the manufacturer's protocol (Qiagen, Venlo, The Netherlands). *Fam111a* knockdown was confirmed by RT-qPCR. RNA quality was assessed on an Experion bioanalyzer (Bio-rad, Veenendaal, The Netherlands). RNA integrity numbers (RIN) for all samples were >9. Library preparation was performed on 4 control and 4 experimental samples with a KAPA hyper prep kit according to the manufacturer's protocol (Roche, Woerden, The Netherlands).

In short, 1 µg of Poly(A) RNA was captured with magnetic oligo-dT beads. Total RNA was fragmented for 6 min at 94 ºC. The total RNA is converted to double-stranded cDNA by 1st and 2nd strand cDNA synthesis followed by A-tailing. Seperate adapters are ligated to the cDNA fragments for each library sample. The libraries were then amplified by PCR for 9 cycles. The library was size selected (200-250 bp) on an E-gel (Thermo Fisher Scientific, Amsterdam, The Netherlands). No PCR induced bias was found using RT-qPCR. Sample quality and size was confirmed on an Experion bioanalyzer. Samples were sequenced with paired end (2X 42bp) on an Illumina NexSeq 500 (Illumina, Eindhoven, The Netherlands).

Data analysis was performed as follows. Raw sequencing data was demultiplexed with Illumina software to obtain fastq files. Fastq files were mapped on the mm10 mouse genome with GRCm38 vM16 annotation from gene code using STAR v2.5.3a.[33] The quantMode TranscriptomeSAM GeneCounts option was used to quantify the count table containing the number of reads per gene. The gene count table was

imported in DESeq2 and analyzed as a pairwise comparison using the default Wald statistics to normalize the data and test for significance.[34] Results were revised for multiple testing using the Benjamini-Hochberg correction.

Label free pulldown

HeLa cells stably expressing eGFP-FAM111A or eGFP-FAM111A R569H were seeded in 12 cm ø Petri dishes. Tetracycline (1 µg/ml) was added to the medium at 80-90% *confluency*. After 16 hrs, cells were harvested to achieve optimal protein production. Label-free eGFP-pulldowns were performed in triplicate as described in Smits *et al.*[35] For GFP-pulldowns, 1 mg of nuclear extract was incubated with 7.5ul beads (GFP-TRAP; Chromotek, Planegg-Martinsried, Germany) in incubation buffer (300 mM NaCl, 20 mM HEPES KOH pH 7.9, 20% v/v glycerol, 2 mM $MgCl_2$, 0.2 mM EDTA, 0.25% v/v NP-40, complete protease inhibitors, and 0.5 mM DTT) in the presence of 50 µg/ml ethidium bromide (Sigma-Aldrich, Zwijndrecht, The Netherlands) to prevent indirect DNA mediated interactions. Beads were washed two times with incubation buffer (0.5% v/v NP-40), two times with phosphate-buffered saline (PBS) (0.5% v/v NP-40) and finally two times with PBS. Subsequently, the proteins were subjected to on-bead trypsin (Promega, Leiden, The Netherlands) digestion and peptides were acidified and desalted using C18-Stagetips.[35] Protein yield was determined using a Bradford assay (Sigma-Aldrich, Zwijndrecht, The Netherlands) before moving on to mass spectrometry.

Mass spectrometry and data analysis

Before mass spectrometry analysis, peptides were eluted from the C-18 stagetips and recorded with LC-MS/MS Orbitrap Fusion Tribrid mass spectrometer (ThermoFisher Scientific, Breda, The Netherlands) at top speed mode of 3 seconds cycle.[36] Raw data were analyzed by MaxQuant (1.5.1.0)[37] using default settings and searching against the Human Uniprot database downloaded on December 2015. Statistical outliers for the eGFP-pulldown of the Hela empty WT compared to FAM111A WT or FAM111A mutant samples were determined using a two-tailed *t*-test. A correction for multiple testing was applied by using a permutation-based FDR method in Perseus (MaxQuant package). Differential proteins between Hela empty WT and FAM111A WT or FAM111A mutant samples were presented in a volcano plot with FDR <0.015 and fold change >6. Statistical cut-offs were chosen such that no proteins were present as outliers on the empty vector control side of the volcano plot.

Data analysis

All results presented are based on at least three different experiments. Values are expressed as mean ± SEM. Statistical significance ($P<0.05$) was determined using one-tailed Students T-test or one-way ANOVA with Holm-Sidak procedure unless otherwise specified.

Disclosure

This work was supported by grants of the Netherlands Organization for Scientific Research (NWO VICI 016.130.668). Dr. Jeroen de Baaij is supported by grants from NWO (Rubicon 825.14.021) and the Dutch Kidney Foundation (Kolff 14OKG17). The authors declare that they have no conflict of interest.

Acknowledgements

The authors thank Lex van Son, Willem Bosman, Matteo Perino, Pascal Jansen and Marijke Baltissen for excellent technical assistance.

References

1. Kenny FM, Linarelli L. Dwarfism and cortical thickening of tubular bones. Transient hypocalcemia in a mother and son. *Am J Dis Child* 1966; **111:** 201-207.
2. Caffey J. Congenital stenosis of medullary spaces in tubular bones and calvaria in two proportionate dwarfs--mother and son; coupled with transitory hypocalcemic tetany. *Am J Roentgenol Radium Ther Nucl Med* 1967; **100:** 1-11.
3. Fanconi S, Fischer JA, Wieland P*, et al.* Kenny syndrome: evidence for idiopathic hypoparathyroidism in two patients and for abnormal parathyroid hormone in one. *J Pediatr* 1986; **109:** 469-475.
4. Lee WK, Vargas A, Barnes J*, et al.* The Kenny-Caffey syndrome: growth retardation and hypocalcemia in a young boy. *Am J Med Genet* 1983; **14:** 773-782.
5. Sabry MA, Zaki M, Abul Hassan SJ*, et al.* Kenny-Caffey syndrome is part of the CATCH 22 haploinsufficiency cluster. *J Med Genet* 1998; **35:** 31-36.
6. Parvari R, Hershkovitz E, Grossman N*, et al.* Mutation of TBCE causes hypoparathyroidism-retardation-dysmorphism and autosomal recessive Kenny-Caffey syndrome. *Nat Genet* 2002; **32:** 448-452.
7. Franceschini P, Testa A, Bogetti G*, et al.* Kenny-Caffey syndrome in two sibs born to consanguineous parents: evidence for an autosomal recessive variant. *Am J Med Genet* 1992; **42:** 112-116.
8. Unger S, Gorna MW, Le Bechec A*, et al.* FAM111A mutations result in hypoparathyroidism and impaired skeletal development. *Am J Hum Genet* 2013; **92:** 990-995.
9. Isojima T, Doi K, Mitsui J*, et al.* A recurrent de novo FAM111A mutation causes Kenny-Caffey syndrome type 2. *J Bone Miner Res* 2014; **29:** 992-998.
10. Nikkel SM, Ahmed A, Smith A*, et al.* Mother-to-daughter transmission of Kenny-Caffey syndrome associated with the recurrent, dominant FAM111A mutation p.Arg569His. *Clin Genet* 2014; **86:** 394-395.
11. Fine DA, Rozenblatt-Rosen O, Padi M*, et al.* Identification of FAM111A as an SV40 host range restriction and adenovirus helper factor. *PLoS Pathog* 2012; **8:** e1002949.
12. Alabert C, Bukowski-Wills JC, Lee SB*, et al.* Nascent chromatin capture proteomics determines chromatin dynamics during DNA replication and identifies unknown fork components. *Nat Cell Biol* 2014; **16:** 281-293.
13. Stark GR, Darnell JE, Jr. The JAK-STAT pathway at twenty. *Immunity* 2012; **36:** 503-514.
14. Chen K, Liu J, Liu S*, et al.* Methyltransferase SETD2-Mediated Methylation of STAT1 Is Critical for Interferon Antiviral Activity. *Cell* 2017; **170:** 492-506 e414.
15. Beadling C, Guschin D, Witthuhn BA*, et al.* Activation of JAK kinases and STAT proteins by interleukin-2 and interferon alpha, but not the T cell antigen receptor, in human T lymphocytes. *EMBO J* 1994; **13:** 5605-5615.
16. Schindler C, Shuai K, Prezioso VR*, et al.* Interferon-dependent tyrosine phosphorylation of a latent cytoplasmic transcription factor. *Science* 1992; **257:** 809-813.
17. Liu L, Okada S, Kong XF*, et al.* Gain-of-function human STAT1 mutations impair IL-17 immunity and underlie chronic mucocutaneous candidiasis. *J Exp Med* 2011; **208:** 1635-1648.
18. Durbin JE, Hackenmiller R, Simon MC*, et al.* Targeted disruption of the mouse Stat1 gene results in compromised innate immunity to viral disease. *Cell* 1996; **84:** 443-450.
19. Hendy GN, Canaff L, Cole DE. The CASR gene: alternative splicing and transcriptional control, and calcium-sensing receptor (CaSR) protein: structure and ligand binding sites. *Best practice & research Clinical endocrinology & metabolism* 2013; **27:** 285-301.
20. Gong Y, Renigunta V, Himmerkus N*, et al.* Claudin-14 regulates renal Ca(+)(+) transport in response to CaSR signalling via a novel microRNA pathway. *The EMBO journal* 2012; **31:** 1999-2012.
21. Murphey ED, Chattopadhyay N, Bai M*, et al.* Up-regulation of the parathyroid calcium-sensing receptor after burn injury in sheep: a potential contributory factor to postburn hypocalcemia. *Crit Care Med* 2000; **28:** 3885-3890.
22. Steele T, Kolamunnage-Dona R, Downey C*, et al.* Assessment and clinical course of hypocalcemia in critical illness. *Crit Care* 2013; **17:** R106.

23. Canaff L, Hendy GN. Calcium-sensing receptor gene transcription is up-regulated by the proinflammatory cytokine, interleukin-1beta. Role of the NF-kappaB PATHWAY and kappaB elements. *J Biol Chem* 2005; **280:** 14177-14188.
24. Canaff L, Zhou X, Hendy GN. The proinflammatory cytokine, interleukin-6, up-regulates calcium-sensing receptor gene transcription via Stat1/3 and Sp1/3. *J Biol Chem* 2008; **283:** 13586-13600.
25. Vargas-Poussou R. Functional Characterization of a Calcium-Sensing Receptor Mutation in Severe Autosomal Dominant Hypocalcemia with a Bartter-Like Syndrome. *Journal of the American Society of Nephrology* 2002; **13:** 2259-2266.
26. Abraham MB, Li D, Tang D*, et al.* Short stature and hypoparathyroidism in a child with Kenny-Caffey syndrome type 2 due to a novel mutation in FAM111A gene. *Int J Pediatr Endocrinol* 2017; **2017:** 1.
27. Iijima S. Sporadic isolated congenital asplenia with fulminant pneumococcal meningitis: a case report and updated literature review. *BMC Infect Dis* 2017; **17:** 777.
28. Sanders CJ, Doherty PC, Thomas PG. Respiratory epithelial cells in innate immunity to influenza virus infection. *Cell Tissue Res* 2011; **343:** 13-21.
29. Diepens RJ, den Dekker E, Bens M*, et al.* Characterization of a murine renal distal convoluted tubule cell line for the study of transcellular calcium transport. *American journal of physiology Renal physiology* 2004; **286:** F483-489.
30. Bourgeois S, Rossignol P, Grelac F*, et al.* Differentiated thick ascending limb (TAL) cultured cells derived from SV40 transgenic mice express functional apical NHE2 isoform: effect of nitric oxide. *Pflugers Archiv : European journal of physiology* 2003; **446:** 672-683.
31. de Baaij JH, Groot Koerkamp MJ, Lavrijsen M*, et al.* Elucidation of the distal convoluted tubule transcriptome identifies new candidate genes involved in renal Mg(2+) handling. *American journal of physiology Renal physiology* 2013; **305:** F1563-1573.
32. Ferre S, Veenstra GJ, Bouwmeester R*, et al.* HNF-1B specifically regulates the transcription of the gammaa-subunit of the Na+/K+-ATPase. *Biochemical and biophysical research communications* 2011; **404:** 284-290.
33. Dobin A, Davis CA, Schlesinger F*, et al.* STAR: ultrafast universal RNA-seq aligner. *Bioinformatics* 2013; **29:** 15-21.
34. Love MI, Huber W, Anders S. Moderated estimation of fold change and dispersion for RNA-seq data with DESeq2. *Genome Biol* 2014; **15:** 550.
35. Smits AH, Jansen PW, Poser I*, et al.* Stoichiometry of chromatin-associated protein complexes revealed by label-free quantitative mass spectrometry-based proteomics. *Nucleic Acids Res* 2013; **41:** e28.
36. Rappsilber J, Mann M, Ishihama Y. Protocol for micro-purification, enrichment, pre-fractionation and storage of peptides for proteomics using StageTips. *Nat Protoc* 2007; **2:** 1896-1906.
37. Cox J, Mann M. MaxQuant enables high peptide identification rates, individualized p.p.b.-range mass accuracies and proteome-wide protein quantification. *Nat Biotechnol* 2008; **26:** 1367-1372.

5 P2X6 knockout mice exhibit normal electrolyte homeostasis

Jeroen H.F. de Baaij[1*], Andreas Kompatscher[1*], Daan Viering[1], Caro Bos[1], René J.M. Bindels[1] and Joost G.J. Hoenderop[1]

[1]Department of Physiology, Radboud Institute for Molecular Life Sciences, Radboud university medical center, Nijmegen, The Netherlands

*A.K. and J.H.F.d.B. contributed equally to this work.

PLoS One, 2016, 11(6):e0156803

Abstract

ATP-mediated signaling is an important regulator of electrolyte transport in the kidney. The purinergic cation channel P2X6 has been previously localized to the distal convoluted tubule (DCT), a nephron segment important for Mg^{2+} and Na^{+} reabsorption, but its role in ion transport remains unknown. In this study, *P2x6* knockout *(P2x6$^{-/-}$)* mice were generated to investigate the role of P2X6 in renal electrolyte transport. The *P2x6$^{-/-}$* animals displayed a normal phenotype and did not differ physiologically from wild type mice. Differences in serum concentration and 24-hrs urine excretion of Na^{+}, K^{+}, Mg^{2+} and Ca^{2+} were not detected between *P2x6$^{+/+}$*, *P2x6$^{+/-}$* and *P2x6$^{-/-}$* mice. Quantitative PCR was applied to examine potential compensatory changes in renal expression levels of other *P2x* subunits and electrolyte transporters, including *P2x1-5, P2x7, Trpm6*, *Ncc*, *Egf*, *Cldn16*, *Scnn1*, *Slc12a3, Slc41a1, Slc41a3, Cnnm2, Kcnj10 and Fxyd2*. Additionally, protein levels of P2X2 and P2X4 were assessed in *P2x6$^{+/+}$* and *P2x6$^{-/-}$* mouse kidneys. However, significant changes in expression were not detected. Furthermore, no compensatory changes in gene expression could be demonstrated in heart material isolated from *P2x6$^{-/-}$* mice. Except for a significant ($P<0.05$) upregulation of *P2x2* in the heart of *P2x6$^{-/-}$* mice compared to the *P2x6$^{+/+}$* mice. Thus, our data suggests that purinergic signaling via P2X6 is not significantly involved in the regulation of renal electrolyte handling under normal physiological conditions.

Keywords: P2X6, ATP, DCT, Purinergic cation channel, Kidney

Introduction

Adenosine triphosphate (ATP) is an important mediator of cellular communication. In normal physiological conditions, extracellular ATP is involved in a wide variety of cell signaling processes including the recruitment of leukocytes and platelets to damaged cells and sites of increased cell death.[1-3] In the kidney, ATP-mediated purinergic signaling has been linked to renal inflammation [4] and fibrosis.[5] Purinergic signaling is also involved in the regulation of Na^+ and water transport [6], which means it is one of the factors involved in the onset of hypertension.[7-10]

ATP activates both P2X and P2Y receptors.[11] Whereas P2Y receptors are G protein-coupled receptors, P2X receptors form ATP-sensitive ion channels that are expressed at the surface of epithelial cells throughout the body.[12-14] P2X subunits assemble in homo- or heterotrimers with large extracellular loops forming ATP binding sites.[12, 15] Activation of P2X receptors by extracellular ATP results in the non-selective influx of cations into the cell. The P2X family of receptors consists of seven subtypes (P2X1-7).[12, 16] Within the kidney, P2X receptors are commonly described as inhibitors of ion transport.[6] In mouse collecting duct (CD) cells, ATP release inhibits ENaC mediated Na^+ uptake [9], which has been linked to P2X2, P2X4, P2X2/6 and P2X4/6 activity. P2 channel activity has also been implicated in the inhibition of water uptake via AQP2.[17]

Recent studies demonstrated that P2X receptors regulate electrolyte reabsorption in the distal convoluted tubule (DCT).[18, 19] A screening of *P2x* receptors expression levels revealed that P2X4 and P2X6 are the predominant P2X subtypes in the DCT.[18] P2X6 forms heteromers with P2X4.[19, 20] Recently, P2X4 homomers were found to directly inhibit the apical Mg^{2+} channel transient receptor potential cation channel subfamily M, member 6 (TRPM6). In the DCT, TRPM6 is the main channel for Mg^{2+} reabsorption, and extracellular ATP inhibits Mg^{2+} uptake by increasing P2X-mediated Ca^{2+} influx.[21] However, the role of P2X6 in the regulation of Mg^{2+} transport is still unknown.

The aim of the present study was, therefore, to determine the function of P2X6 in renal electrolyte handling. To this end, *P2x6*$^{-/-}$ mice were generated and functionally characterized by measuring serum levels and 24-hour urine excretion of Na^+, Mg^{2+}, K^+ and Ca^{2+}. Potential compensatory mechanisms for loss of *P2x6* gene function were measured by RT-qPCR analysis.

Results

Breeding of *P2x6*$^{-/-}$ mice

To assess the function of P2X6 *in vivo*, *P2x6*$^{-/-}$ mice were generated (Figure 1A). Inactivation of the *P2x6* gene was achieved by inserting a LacZ knockout (KO) cassette in exon 2 of the gene. The breeding of *P2x6*$^{+/-}$ mice resulted in a normal Mendelian inheritance pattern in offspring. Of a total of 116 mice, 23% were genotyped *P2x6*$^{+/+}$, 49% *P2x6*$^{+/-}$ and 28% *P2x6*$^{-/-}$. All offspring were genotyped for the insertion of the knockout cassette and presence of the wild type *P2x6* allele (Figure 1B). Mouse heart cDNA was used to establish the presence of full-length *P2x6* transcripts in *P2x6*$^{+/+}$ mice and the complete absence of *P2x6* expression or potential alternatively spliced transcripts in *P2x6*$^{-/-}$ animals (Figure 1C). The expected PCR products were present in *P2x6*$^{+/+}$ mice and not detectable in the *P2x6*$^{-/-}$ animals.

Normal behavior in *P2x6*$^{-/-}$ mice

P2x6$^{+/+}$, *P2x6*$^{+/-}$ and *P2x6*$^{-/-}$ mice were subjected to an inspection of behavior and phenotype according to the guidelines for assessing the health and condition of mice [22]. All genotypes had a body condition scoring (BCS) of 3, indicating that all animals were in optimal condition. No changes in breathing, grooming and fur quality were observed. Mice exhibited no problems with any voluntary movement or with supporting their own body weight. Both eyes and ears were normal in all genotypes. All mice displayed normal open field behavior. No Fighting wounds could be detected after thorough examination and there were no mice with a rectal or vaginal prolapse.

Normal renal electrolyte handling in *P2x6*$^{-/-}$ mice

To investigate the role of P2X6 in renal electrolyte handling, blood, 24 hrs urine and feces were collected using metabolic cages. No significant differences in body weight, food and water intake were identified between *P2x6*$^{+/+}$, *P2x6*$^{+/-}$ and *P2x6*$^{-/-}$ mice littermates (Table 1). Furthermore, urine production did not significantly change between the three mice groups. A similar trend was observed in the feces production, which was not significantly altered. Because P2X6 is localized to the DCT, changes in electrolyte handling were expected for Na^+ and Mg^{2+}. However, measurements of serum (Figure 2A and E) and 24 hrs urinary excretion (Figure 2B and f) showed that all groups have similar Na^+ or Mg^{2+} concentrations and excretion rates, respectively. Furthermore, serum and 24 hrs urine excretion of Ca^{2+} and K^+ remained unchanged regardless of genotype (Figure 2C, D, G and H).

Gene expression of renal electrolyte transporters is not altered in *P2x6*$^{-/-}$ mice

Since P2x6 has been implicated in regulating both Na^+ and Mg^{2+} transport in the kidney. The renal expression of several sodium and magnesiotropic genes was analyzed in the two mice groups using RT-qPCR (Figure 3). Significant changes in the renal transcript levels of the apically expressed magnesium channel *Trpm6 were not detected*, neither where there expression differences for *Egf*, which regulates Trpm6 activity (Figure 3A and B) [23]. *Cldn16* was measured to investigate whether paracellular Mg^{2+} transport in the thick ascending limb of Henle's loop (TAL) was affected in the P2x6$^{-/-}$ mice. However no significant changes in *Cldn16* transcript levels were detected (Figure 3C). Since the epithelial Na^+ channel (ENaC) activity is inhibited by purinergic signaling [9], its transcript levels were measured. *Scnn1* expression, encoding ENaC was the same in *P2x6*$^{+/+}$ and *P2x6*$^{-/-}$ litter mates (Figureure 3E and F). Other Na^+ and Mg^{2+} related genes expressed in the DCT cell such as *Slc12a3*, *Cnnm2*, *Kcnj10, Slc41a1*, *Slc41a3* and *Fxyd2* were also analyzed (Figure 4), since P2x6 was localized to this nephron segment. Again, there was no marked difference in expression levels between the two mice groups. To investigate whether other P2x subunits would compensate for the inactivation of P2x6, the genes encoding *P2x1-5* and *7* were also analyzed for changes in expression, but no quantifiable changes could be found (Figure 5). To ensure that the putative binding partners of P2X6, namely P2X2 and P2X4, did not compensate for the loss of *P2x6* at the protein level, Western blots for P2X2 and P2X4 were performed using membrane and cytosol fractions of *P2x6*$^{+/+}$ and *P2x6*$^{-/-}$ mouse kidneys. P2X4 was detected in both the membrane and cytosol, whereas P2X2 was only detected in the membrane fraction. Both proteins displayed a band at the expected height of ~54 kD (Figure 6A). After quantification no significant differences were found between *P2x6*$^{+/+}$ and *P2x6*$^{-/-}$ mice (Figure 6B).

Table 1 | Metabolic Parameters of P2x6 Mice.

	P2x6$^{+/+}$	*P2x6*$^{+/-}$	*P2x6*$^{-/-}$
Body weight (g)	21.5 ± 0.9	21.9 ± 1.0	21.6 ± 1.0
Water intake (mL)	4.1 ± 0.1	4.8 ± 0.2	4.7 ± 0.2
Food intake (g)	3.4 ± 0.3	3.9 ± 0.1	3.9 ± 0.1
Urine volume (mL)	1.2 ± 0.1	1.2 ± 0.1	1.3 ± 0.1
Feces weight (g)	1.4 ± 0.1	1.6 ± 0.0	1.7 ± 0.1

Body weight, water intake, food intake, urine volume and feces weight was assessed after housing the animals for 48 hrs in metabolic cages. Numbers represent the mean ± SEM.

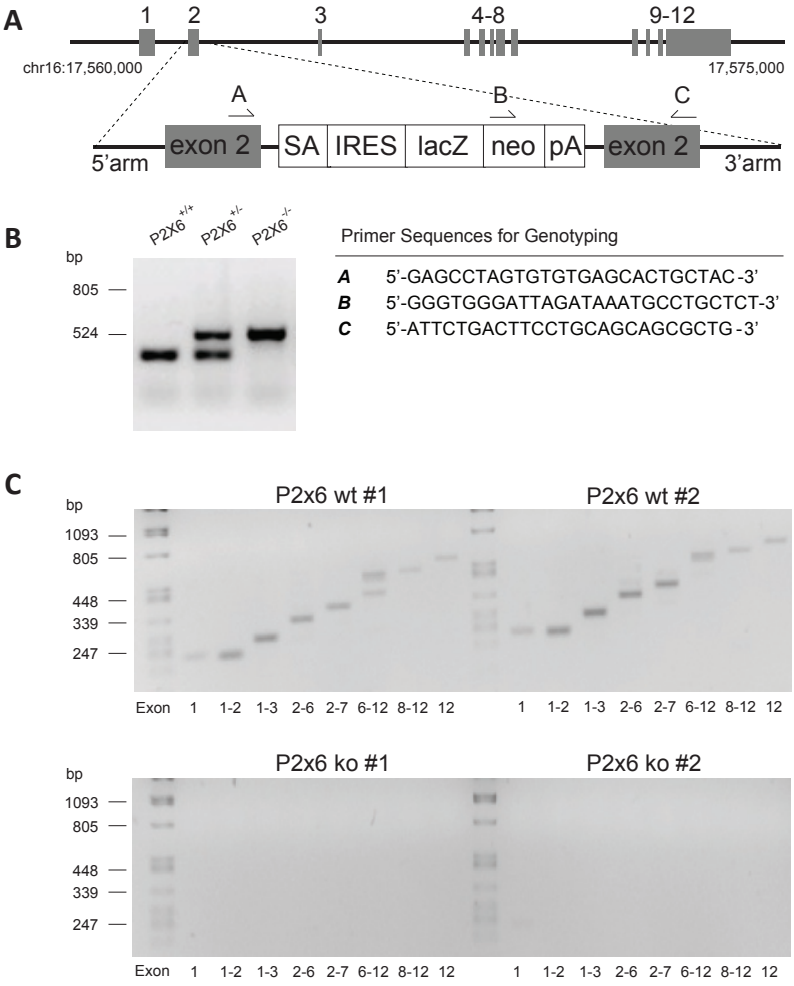

Figure 1 | Characteristics of the *P2x6*$^{-/-}$ mouse

A) Targeted insertion of the knockout (KO) cassette. Top: *P2x6* locus on chromosome 16. Bottom: targeted allele in which the KO cassette is inserted within exon 2. Grey boxes indicate exons, arrows depict genotype primers. A-C) SA: Splice acceptor site, IRES: internal ribosome entry site, LacZ: ß-galactosidase, NEO: neomycin cassette, pA: polyA. B) Identification of the mouse genotype by PCR analysis of ear-derived DNA. The PCR product size ± 478 bp shows the presence of the wild-type allele (+/+), using primers A and C; the PCR product sized ± 800 bp shows the KO allele (-/-) using primers B and C. Both alleles are detected in heterozygous animals (+/-). c) cDNA isolated from murine heart samples were used to amplify exons 1-12 of *P2x6* with PCR. The top agarose gels show the PCR products for exons 1-12 in two *P2x6*$^{+/+}$ animals. The lower gels represent the PCR products for exons 1-12 in two *P2x6*$^{-/-}$ animals.

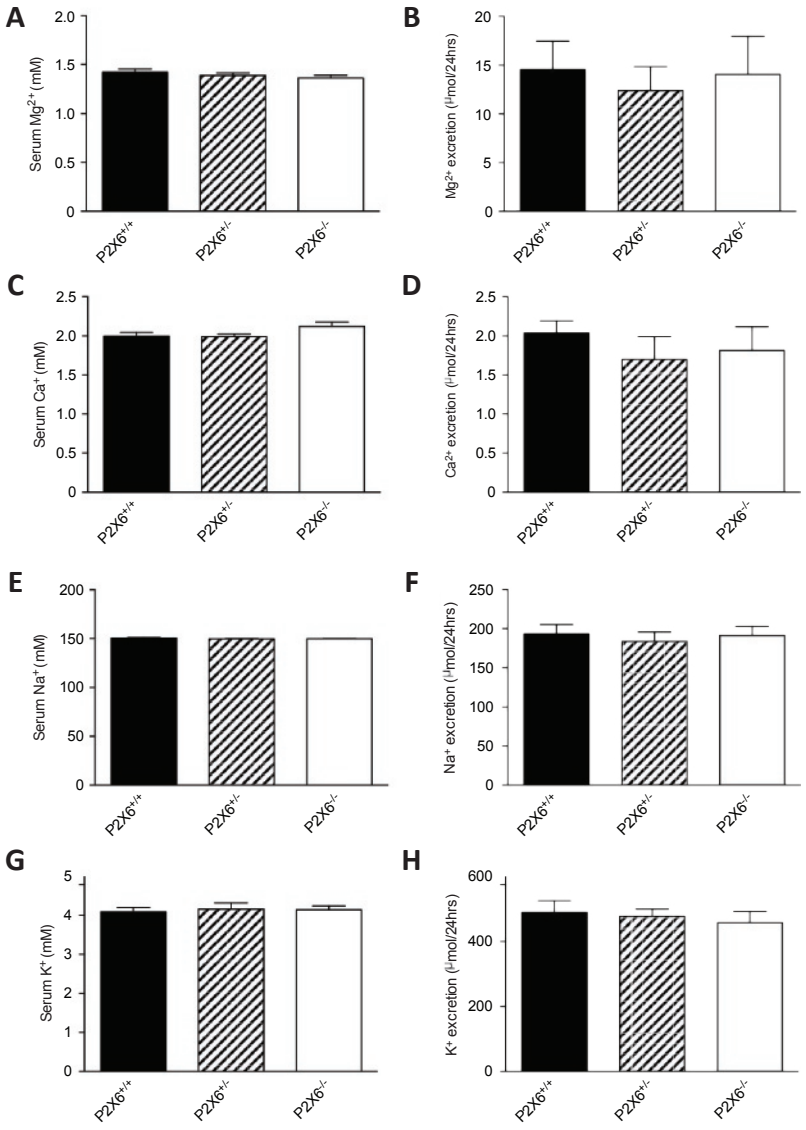

Figure 2 | Normal renal electrolyte handling in *P2x6*$^{-/-}$ mice

A) Serum Mg^{2+} concentrations of wildtype, heterozygous and knockout P2x6 mice. B) 24 hrs urinary Mg^{2+} excretion of wildtype, heterozygous and knockout P2x6 mice. C) Serum Ca^{2+} concentrations. D) 24 hrs urinary Ca^{2+} excretion. E) Serum Na^{+} concentrations. F) 24 hrs urinary Na^{+} excretion. G) Serum K^{+} concentrations. H) 24 hrs urinary K^{+} excretion. Values (n=10) are presented as means ± SEM.

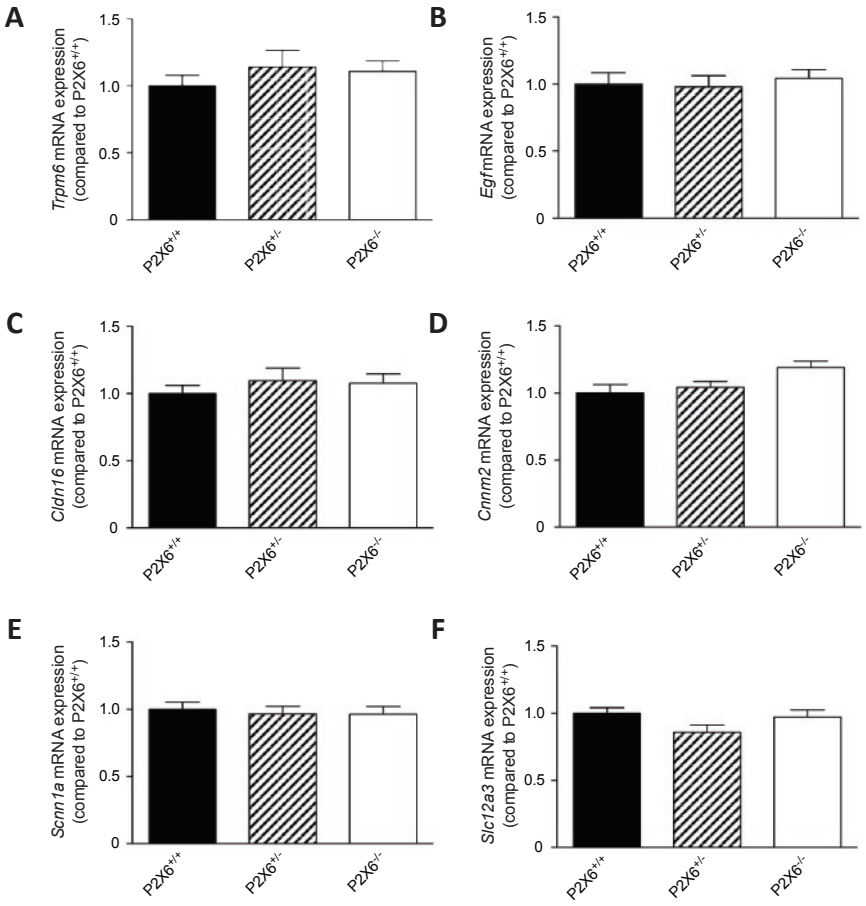

Figure 3 | Gene expression of renal electrolyte transporters was not altered in *P2x6*$^{-/-}$ mice

A-F) The mRNA expression levels of *Trpm6* (A), *Egf* (B), *Cldn16* (C), *Cnnm2* (D), *Scnn1a* (E), *Slc12a3* (F) in kidney of *P2x6*$^{+/+}$ (Black bars), *P2x6*$^{+/-}$ (Striped bars), *P2x6*$^{-/-}$ (white bars) mice were measured by quantitative RT-PCR and normalized for *Gapdh* expression. Data (n=10) represent mean ± SEM and are expressed as the fold difference when compared to the expression in *P2x6*$^{+/+}$ mice.

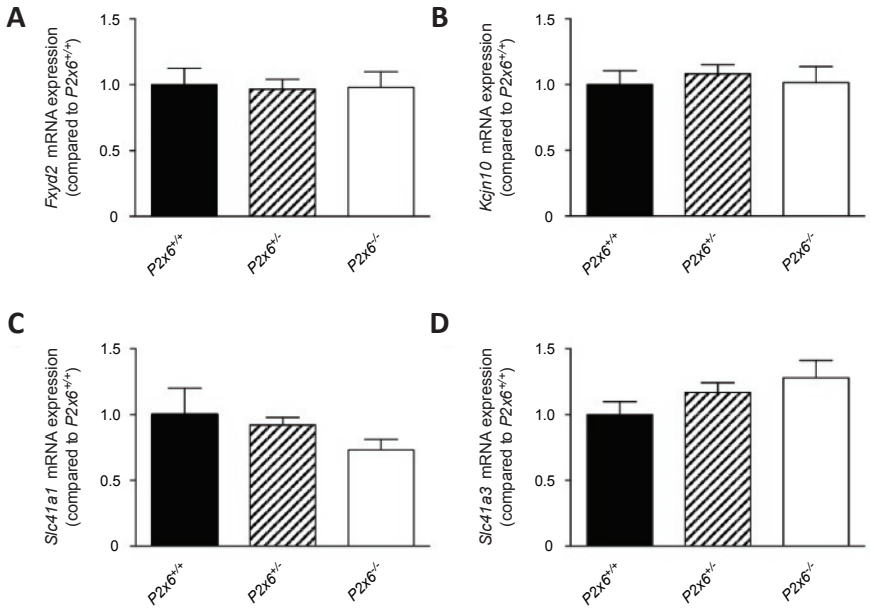

Figure 4 | *P2x* subunit expression in response to the loss of *P2x6* function in the kidney

A-F) The mRNA expression levels of *P2x1* (A), *P2x2* (B), *P2x3* (C), *P2x4* (D), *P2x5* (E), *P2x7* (F), in kidney of $P2x6^{+/+}$ (Black bars), $P2x6^{+/-}$ (Striped bars), $P2x6^{-/-}$ (white bars) mice were measured by quantitative RT-qPCR and normalized for *Gapdh* expression. Data (n=10) represent mean ± SEM and are expressed as the fold difference when compared to the expression in $P2x6^{+/+}$ mice.

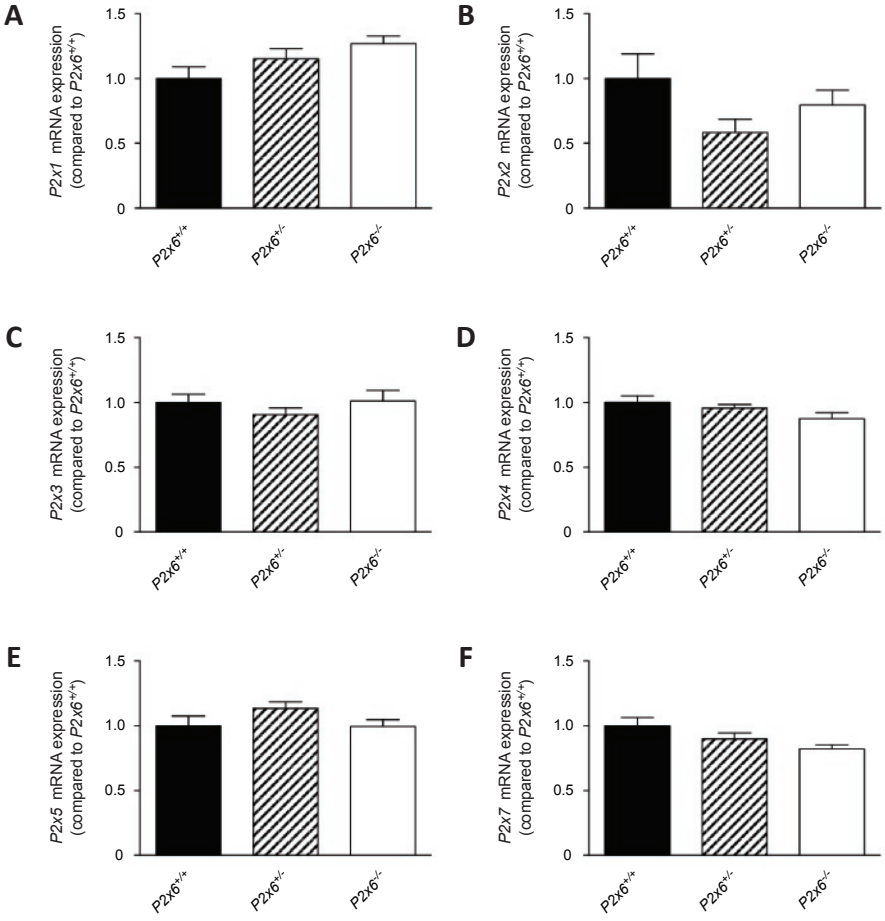

Figure 5 | Basolaterally expressed compensatory mechanisms for the loss of P2X6 function in the kidney

A-D) The mRNA expression levels of *Fxyd2* (A), *Kcjn10* (B), *Slc41a1* (C), *Slc41a3* (D) in kidney of *P2x6*$^{+/+}$ (Black bars), *P2x6*$^{+/-}$ (Striped bars), *P2x6*$^{-/-}$ (white bars) mice were measured by quantitative RT-qPCR and normalized for *Gapdh* expression. Data (n=10) represent mean ± SEM and are expressed as the fold difference when compared to the expression in *P2x6*$^{+/+}$ mice.

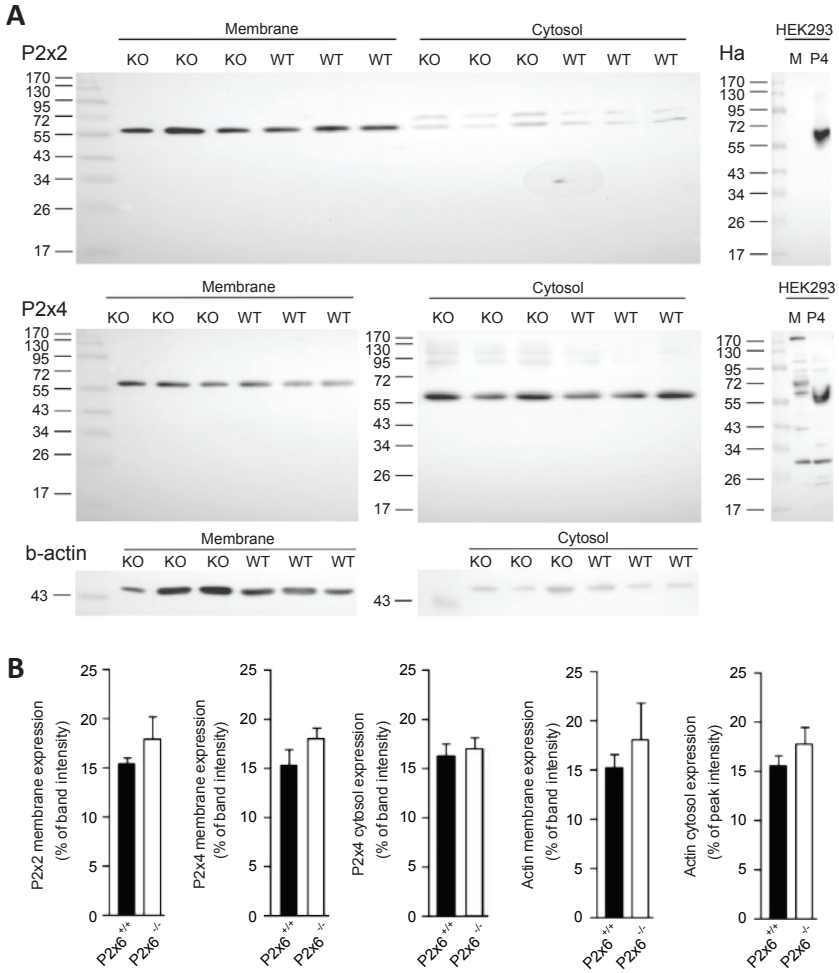

Figure 6 | Protein abundance of P2X2 and P2X4 in response to the loss of P2X6

A) Western blots of membrane and cytosol fractions of *P2x6*$^{-/-}$ (KO) and *P2x6*$^{+/+}$ (WT) mice. The upper blot shows the immune-staining for P2X2 in mouse kidney material. To the right a western blot of HEK293 cells transiently transfected with HA-tagged P2X4 (P4) and mock (M) constructs is displayed. Middle, two western blots below are immune-stained for P2X4, left depicts *P2x6*$^{-/-}$ (KO) and *P2x6*$^{+/+}$ (WT) material stained for P2X4, right represents a P2X4 blot on HEK293 material transiently transfected with human P2X4 and a mock construct. Bottom, displays a ß-actin immune-staining used as a loading control. Ladders (ez-run prestained marker (ThermoScientific, Breda, The Netherlands) represent protein size in kilo Dalton (kD). B) Protein expression levels for the P2X2 membrane lysate, P2X4 membrane lysate, P2X4 cytosol lysate, ß-actin membrane and ß-actin cytosol lysates in *P2x6*$^{-/-}$ and *P2x6*$^{+/+}$ mice. Data (n=3) represents mean ± SEM and are expressed as the % of total band intensity.

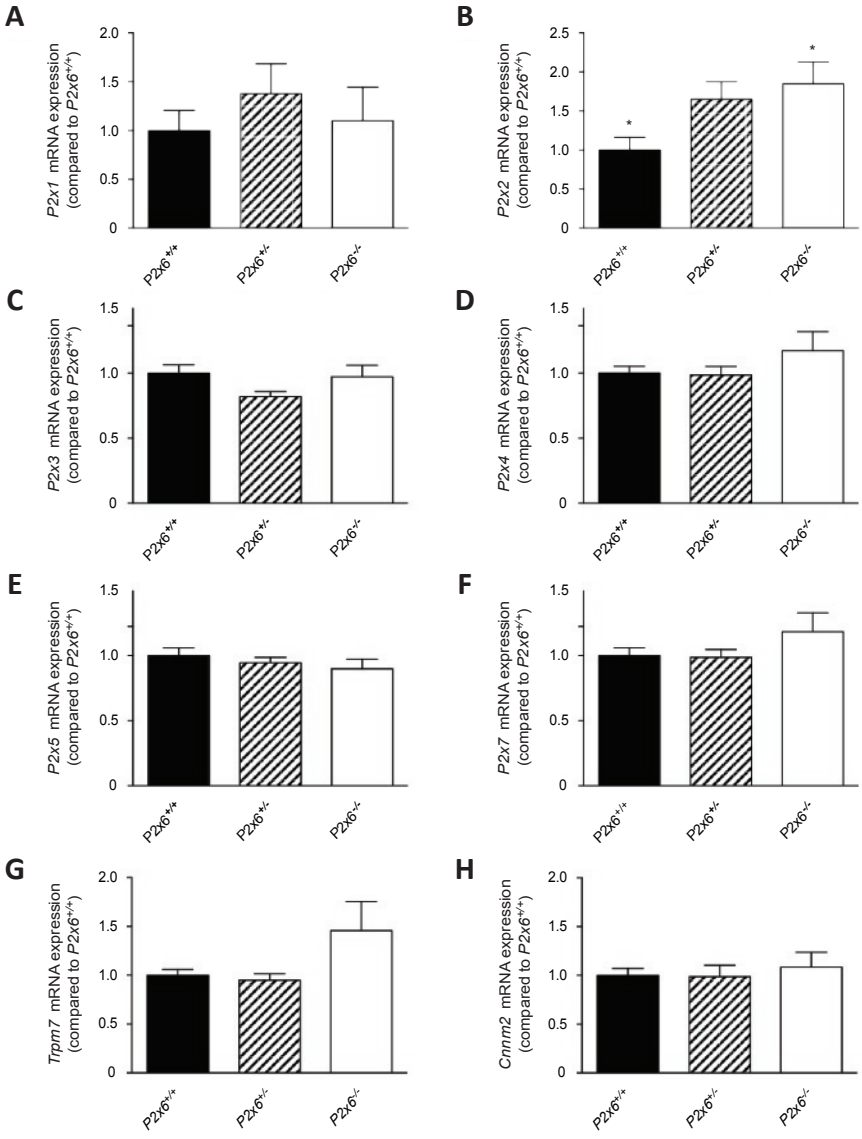

Figure 7 | Compensatory mechanisms for the loss of P2X6 function in the heart

A-H) The mRNA expression levels of *P2x1* (A), *P2x2* (B), *P2x3* (C), *P2x4* (D), *P2x5* (E), *P2x7* (F), *Trpm7* (G), *Cnnm2* (H), in heart of $P2x6^{+/+}$ (Black bars), $P2x6^{+/-}$ (Striped bars), $P2x6^{-/-}$ (white bars) mice were measured by quantitative RT-qPCR and normalized for *Gapdh* expression. Data represent mean (n=10) ± SEM and are expressed as the fold difference when compared to the expression in $P2x6^{+/+}$ mice. * P<0.05 indicates a significant difference from $P2x6^{+/+}$ mice.

Increased P2x2 expression in *P2x6*$^{-/-}$ heart

Since upregulation of P2X6 has been linked to chronic heart disease [24], RT-qPCR analysis was performed on heart tissue of *P2x6*$^{-/-}$ mice. As in the kidney, expression of the magnesiotropic genes *Trpm7* and *Cnnm2* remained unchanged. The *P2x2* subunit was however significantly upregulated two-fold ($P<0.05$) in the *P2x6*$^{-/-}$ heart material compared to *P2x6*$^{+/+}$ mice. *P2x* subunits 1, 3-5 & 7 did not show significant differences in gene expression (Figure 7).

Discussion

This study demonstrated that P2X6 knockout mice have a normal phenotype, suggesting that P2X6 does not play a significant role in renal electrolyte handling. *P2x6*$^{-/-}$ mice were physiologically similar to their wild-type littermates in terms of behavior, weight, food or water intake. No significant changes in serum concentrations or urinary excretion were observed for Na^+, K^+, Ca^{2+} and Mg^{2+} in *P2x6* null mice. Furthermore, loss of P2X6 function did not induce compensatory gene expression of any P2X purinergic receptors or other ion transporters that were investigated in the kidney. Likewise, no changes in P2X2 and P2X4 protein levels were detected in the kidneys of the *P2x6* null mice compared to wild type littermates. Together, these results suggest that P2X6 is not involved in renal electrolyte handling under normal physiological conditions.

P2X receptors have been established as important negative regulators of ion transport in the kidney.[25] Specifically, homomers of P2X4 receptors and heteromeric complexes of P2X4 and P2X6 have been implicated in the reabsorption of Na^+ and Mg^{2+}.[9, 26] In microdissected tubules of the TAL, extracellular ATP inhibited Na^+ currents in a P2X-dependent manner.[10] P2X4 receptors also result in diminished TRPM6-mediated currents when overexpressed in HEK293 cells.[18] Moreover, several studies showed that P2X4 homomers and P2X4/6 heteromers inhibit ENaC in the CD, decreasing Na^+ reabsorption.[17 26] Although this vast amount of *in vitro* studies shows the importance of ATP in the regulation of renal ion channel activity, the physiological consequences remain undecided. In this study, we revealed that loss of P2X6 does not impair electrolyte handling *in vivo*, since renal electrolyte handling is unaffected in *P2x6*$^{-/-}$ mice. Moreover, previous studies demonstrated that *P2x4*$^{-/-}$ mice also displayed normal renal Mg^{2+} excretion.[18] These findings question the *in vivo* role of P2X receptors for renal electrolyte handling.

There are several explanations for the absence of a renal phenotype in *P2x6*$^{-/-}$. First, the loss of P2X6 function may be compensated for by other P2x subunits. P2X6 functions in complexes with P2X2 or P2X4 and their function may counterbalance the loss of P2X6. However, our expression profile did not show differences in *P2x2* and

P2x4 expression at the transcriptional and protein level in *P2x6*$^{-/-}$ mice. Second, *P2x6*$^{-/-}$ mice might need to be challenged to reveal disturbances in Na^+ or Mg^{2+} handling. For instance, in rat cardiomyocytes, *P2x6* expression is low under normal physiological condition.[27, 28] However, studies in patients have shown that P2X6 expression significantly increases after an ischemic cardiac event.[24] This latter study demonstrated that when the system is pathologically challenged, P2X6 expression can be induced. In our study, compensatory mechanisms, e.g. upregulation of other *P2x* subunits in the heart, were not detected in the *P2x6*$^{-/-}$ mice, except for a significant increase in *P2x2* transcript. For now, which pathogenic factors would stimulate renal P2X6 expression are unknown. A transcriptome-wide screening, where mice were challenged with Mg^{2+}-deficient diets, found no differences in *P2x4* and *P2x6* expression in the DCT.[29] Third, the mouse may not provide a good model to study the role of P2X purinoreceptors in the DCT. Although previous studies have shown that *P2x6* is the predominantly expressed *P2x* transcript in the DCT together with *P2x4*, P2X4 protein expression could not be confirmed in the DCT.[18] These findings together with our results shed doubt on the presence of functional P2X4/P2X6 trimers in the DCT.

Over the last decade, the function of P2X6 has been widely debated.[19, 30, 31] Although recombinant homomeric P2X6 complexes have been reported to reach the plasma membrane in transiently transfected HEK293 cells [32], Others have shown that P2X6 requires the presence of P2X4 or P2X2 to become functional at the cell surface.[30, 33-35] This has been attributed to P2X6 lacking charged residues in the N-terminus, which prevents trafficking of the protein to the membrane.[19] Recent studies suggest that P2X6 may function as a nuclear regulator of post-transcriptional modifications in neurons.[31] However, nuclear localization has not been identified in other tissues.[36] Further *in vitro* studies are required to examine the function of P2X6.

In conclusion, *P2x6*$^{-/-}$ mice exhibit an apparent normal physiological behavior and renal electrolyte handling under normal conditions. Serum Na^+, Mg^{2+}, K^+ and Ca^{2+} concentrations were not significantly different compared to wild type littermates and compensatory expression of relevant electrolyte transporters was absent. Thus, P2X6 is likely not significantly involved in the regulation of renal electrolyte handling under normal physiological conditions. Our results, therefore, question the essential role of P2X6 in normal electrolyte homeostasis.

Methods

P2X6$^{-/-}$ mice

All experiments were performed in compliance with the Central Animal Laboratory Nijmegen and the animal ethics board of the Radboud University Nijmegen (DEC #2013-185). *P2x6*$^{+/-}$ mice (mus musculus), from a mixed background, (B6J-129P2-P2RX6) were provided by The Mary Lyon Centre, Oxfordshire, UK. The acquired *P2x6*$^{-/-}$ mice were backcrossed once with C57BL/6 wild-type. 6-10 littermates were housed in standard cages with bedding material consisting of straw and paper in a temperature- and light-controlled room with standard pellet chow and deionized drinking water available *ad libitum* (ARRIVE guidelines). To confirm full loss of *P2x6*, PCR amplification of the complete *P2x6* transcript was performed in isolated mouse heart cDNA. PCR products were designed to be exon-exon junction spanning and amplify several exons in a range of 145-564 bp in ascending order. PCRs were performed with Amplitaq Gold 360 mastermix (Invitrogen, Bleiswijk, The Netherlands) in a Biometra T3000 (Westburg, Leusden, The Netherlands). Primer sequences are described in Table 1.

Phenotyping

Phenotyping was performed on *P2x6*$^{+/+}$, *P2x6*$^{+/-}$ and *P2x6*$^{-/-}$ mice to assess differences in behavior and phenotype. Body condition scoring (BCS) was performed as described previously.[22] Mice were checked for abnormal breathing, grooming and fur condition. Additionally, mice were closely monitored for the ability to support their own body weight and whether they lacked voluntary movement of the fore and hind limbs. Eyes and ears were visually inspected for abnormalities. All mice were thoroughly investigated for fighting wounds. Furthermore, animals were checked for bearing a possible rectal or vaginal prolapse. Activity and curiosity of the animals was verified by assessing open-field behavior as described previously.[22]

Experimental set-up

The experimental sample size was determined by a power calculation ($N \geq 2\sigma(Z\alpha+Z\beta)^2/\delta 2$), based on an estimated urinary Mg^{2+} excretion of 65 ± 35 µmol/day.[37] A difference of 70% (45 µmol/day) (δ) with a standard deviation of 75% (48 µmol/day) (σ) in urinary Mg^{2+} excretion was expected, combined with a power of 80% (β) and a significance threshold of 5% (α) this results in a minimum sample size of 10 animals (N) per group. For the experiment, 30 adult male mice (10 *P2x6*$^{-/-}$ (knock-out), 10 *P2x6*$^{+/-}$ (heterozygous) and 10 *P2x6*$^{+/+}$ (wild-type)) were housed individually in mouse metabolic cages during the last 48 hrs for urine and feces collection (24 hrs adaptation, 24 hrs sampling). Littermates were allocated to an experimental group based on genotype. Animals were 8-10 weeks old. Blood samples were collected by orbita

Table 2 | Primer Sequences for RT-qPCR

	Forward	Reverse
Gapdh	5'-TAACATCAAATGGGGTGAGG-3'	5'-GGTTCACACCCATCACAAAC-3'
P2x1	5'-CCGAAGCCTTGCTGAGAA-3'	5'-GGTTTGCAGTGCCGTACAT-3'
P2x2	5'-CACCACCACTCGAACTCTCA-3'	5'-GGTACGCACCTTGTCGAACT-3'
P2x3	5'-GGTGGCTGCCTTCACTTC-3'	5'-TCAGCCCCTTTGAGGAAA-3'
P2x4	5'-TTGGCTCTGGCTTGGCGCTC-3'	5'-TCTCCGGAAAGACCCTGCTCG-3'
P2x5	5'-GAGCGAGTTTTACCGAGACAAG-3'	5'-GATGAACCCTCTCCAGTGGC-3'
P2x7	5'-GGGGGTTTACCCCTACTGTAA-3'	5'-GCTCGTCGACAAAGGACAC-3'
Trpm6	5'-AAAGCCATGCGAGTTATCAGC-3'	5'-CTTCACAATGAAAACCTGCCC-3'
Cnnm2	5'-GGAGGATACGAACGACGTG-3'	5'-TTGATGTTCTGCCCGTACAC-3'
Egf	5'-GAGTTGCCCTGACTCTACCG-3'	5'-CCACCATTGAGGCAGTATCC-3'
Cldn16	5'-GTTGCAGGGACCACATTAC-3'	5'-GAGGAGCGTTCGACGTAAAC-3'
Slc12a3	5'-CTTCGGCCACTGGCATTCTG-3'	5'-GATGGCAAGGTAGGAGATGG-3'
Scnn1a	5'-CATGCCTGGAGTCAACAATG-3'	5'-CCATAAAAGCAGGCTCATCC-3'
Trpm7	5'-GGTTCCTCCTGTGGTGCCTT-3'	5'-CCCCATGTCGTCTCTGTCGT-3'
Fxyd2	5'-TCAGCCTTTCTTGTGACTGG-3'	5'-GGTCTTCCTGTGGCCTCTACT-3 '
Kcjn10	5'-CCGCGATTTATCAGAGC-3'	5'-AGATCCTTGAGGTAGAGGA A-3'
Slc41a1	5'-CATCCCACACGCCTTCCTGC-3'	5'-CGGCTGGCCTGCACAGCCAC-3 '
Slc41a3	5'-TGAAGGGAAACCTGGAAATG-3'	5'-GGTTGCTGCTGATGATTTTG-3'

Gapdh, glyceraldehyde 3-phosphate dehydrogenase; P2x1-5, 7, P2X purinoreceptors 1-5, 7; Trpm6, transient receptor potential cation channel, subfamily M, member 6; Cnnm2, cyclin and CBS domain divalent metal cation transport mediator 2; Egf, epidermal growth factor; Cldn16, claudin 16; Slc12a3, solute carrier family 12, member 3; Scnn1, Amiloride-sensitive sodium channel subunit; Trpm7, transient receptor potential cation channel, subfamily M, member 7; Fxyd2, FXYD domain containing ion transport regulator 2; Kcnj10, ATP-sensitive inward rectifier potassium channel 10; Slc41a1, solute carrier family 41, member 1; Slc41a3, solute carrier family 41, member 3.

extraction in isoflurane-anesthetized mice during the day. The primary outcome measure was changes in urinary Mg^{2+} excretion levels between experimental groups. Secondary measures were differences in other electrolytes, such as Na^{+}, K^{+} and Ca^{2+}. After being anesthetized with 4% (v/v) isoflurane, all thirty mice were sacrificed. Blood samples, kidneys and hearts were collected and the organs were immediately frozen in liquid nitrogen.

Expression profiling

Total RNA was isolated using TRIzol total RNA isolation agent (Invitrogen, Bleiswijk, the Netherlands) according to the manufacturer's protocol. Obtained RNA was treated with DNase (Promega, Fitchburg, WI, USA) to remove genomic DNA. Subsequently, reverse transcription of the mRNA by M-MLV reverse transcriptase (Invitrogen, Bleiswijk, the Netherlands) was performed for 1 hr at 37 °C. Gene expression levels were determined by RT-qPCR on a BioRad (Hercules, CA, USA) analyzer using SYBR Green and normalized for glyceraldehyde 3-phosphate dehydrogenase (*Gapdh)* expression levels. Primer sequences are provided in Table 2.

Electrolyte measurements

Serum and urinary total Mg^{2+} and Ca^{2+} concentrations were determined using a xylidyl blue colorimetric assay kit according to the manufacturer's protocol (Roche/Hitachi, Tokyo, Japan). In short, serum Mg^{2+} and Ca^{2+} were measured photometrically via the decrease in xylidyl blue absorbance. 1 M Mg^{2+} and Ca^{2+} standards (Sigma Aldrich, Zwijndrecht, The Netherlands) were used to generate standard dilution curves. The assay was calibrated using a Mg^{2+} Precinorm (Sigma Aldrich, Zwijndrecht, The Netherlands) with a concentration of 0.76 mM Mg^{2+}. Samples were measured on a Nanodrop 2000c spectrophotometer (Thermo Scientific, Breda, The Netherlands) at 600 nm. 20 µl of urine was acidified by adding 4 µl 1M HCl and diluted 30x with MQ before performing the Mg^{2+} and Ca^{2+} assays. All feces were dissolved in 5 ml 65 % v/v sulfuric acid and incubated for 10 min. at 50 °C and then diluted 50 times in MQ before use. Serum and urinary Na^{+} and K^{+} concentration were determined by the Radboudumc clinical lab on an automated system according to the manufacturer's protocol (Abbott Diagnostics, Belgium).

Isolation of membrane and cytosol fractions

Membrane and cytosol fractions were isolated from kidney tissue of *P2x6*$^{-/-}$ and *P2x6*$^{+/+}$ littermates by ultracentrifugation. To this end, half of a mouse kidney was first homogenized using a homogenizer (bedrijf) in 1 ml of lysis buffer (50 mM Tris pH 7.5, 1 mM EDTA, 1 mM EGTA, 1 mM NaOrthovandate, 5 mM NaF, 5 mM glycerolphosphate 0.27 M sucrose) containing 1 tablet of complete protease inhibitor cocktail (Roche) and 0.1 % b-mercapto-ethanol without detergents. Samples were than centrifugated at 3000 g for 10 minutes at 4 °C. The supernatant was then centrifugated at 100,000 g for 1 hour at 4 °C in a Sorvall™ WX Floor Ultra Centrifuge (Thermo Scientific, Asheville, NC, USA) with a 70.1Ti rotor. The supernatant was taken and proteins in the cytosolic fraction were solubilized by adding 1% NP-40. The remaining pellet was resuspended in 1 ml lysis buffer without b-mercapto-ethanol and centrifuged at 100,000 g for 15 minutes at 4 °C to get rid of all cytosolic parts. The remaining pellet consists of the membrane fraction and is subsequently resuspended

in 100 µl lysis buffer containing 1% NP-40 and b-mercapto-ethanol. To remove any debris, membrane fractions were spun a final time at 12,000 g for 10 minutes at 4 °C. The remaining supernatant was used for further experiments.

Cell culture and transfection

Human embryonic kidney cells (HEK293) were grown in Dulbecco's modified Eagle's medium (Lonza, Leusden, The Netherlands) containing 10% (v/v) fetal calf serum (FCS), 2 mM L-glutamine at 37 °C in a humidity controlled incubator with 5% (v/v) CO_2. The cells were transiently transfected with the respective construct using Lipofectamine 2000 (Invitrogen Bleiswijk, The Netherlands) in a 1 µg DNA to 2 µl lipofectamine ratio and analyzed on Western blot, 48 hours after transfection. Cell samples were lysed in lysis buffer (50 mM Tris pH 7.5, 1 mM EDTA, 1 mM EGTA, 1 mM NaOrthovandate, 5 mM NaF, 5 mM glycerolphosphate 0.27 M sucrose and 1 tablet of complete protease inhibitor cocktail (Roche)) containing 1% (v/v) Triton X-100.

BCA protein measurements and western blotting

Protein concentrations were measured with a colorimetric Pierce BCA protein assay kit (ThermoFisher scientific, Breda, The Netherlands) according to the manufacturer's protocol. In short, samples were loaded on a 96 well plate, incubated for 30 minutes at 37 °C and measured at 562 nm with a Bio-rad Benchmark plus microplate photo-spectrometer (Bio-rad, Veenendaal, The Netherlands). Protein lysates of membrane and cytsolic fractions of $P2x6^{-/-}$ and $P2x6^{+/+}$ mouse kidney samples were denatured in Laemmli containing 100 mM DTT for 30 minutes at 37 °C. Samples were then subjected to SDS-PAGE and Western blots were incubated with a rabbit anti-mouse P2x2 antibody (Alomone Labs, Jerusalem, Israel, 1:500) or a rabbit anti-mouse P2x4 (H-40, Santa Cruz biotechnology, Santa Cruz CA, USA, 1:500) in 5% milk o/n at 4 °C. Then, immunoblots were incubated 45 minutes at RT with peroxidase conjugated goat anti-rabbit secondary antibodies (Sigma-Aldrich, Zwijndrecht, The Netherlands, 1:10,000). β-actin was used as a loading control and samples were stained in 5% milk o/n at 4 °C with anti-mouse β-actin (Sigma-Aldrich, Zwijndrecht, The Netherlands, 1:10,000). HEK293 cells, which were transiently transfected with HA-tagged pCINEO-hP2X4-IRES-GFP and pCINEO-mock-IRES-GFP constructs, were subjected to the same procedure as described above.

Statistical analysis

All results are depicted as mean ± standard error of the mean (SEM). The statistical analyses were conducted by one-way ANOVA, followed by a Tukey's post hoc test when comparing the three treatment groups (n=10 for each group). Difference in means with P values < 0.05 were considered statistically significant.

Disclosure

This work was supported by grants from the Netherlands Organization for Scientific Research (NWO VICI 016.130.668) and the EURenOmics project from the European Union seventh Framework Programme (FP7/2007–2013, agreement no. 305608). Dr. Jeroen de Baaij is supported by grants from NWO (Rubicon 825.14.021) and the Dutch Kidney Foundation (Kolff 14OKG17). The authors declare that they have no conflict of interest.

Acknowledgements

The authors thank Hans Meijer, Marla Lavrijsen, Dr. Maxime Blanchard, Dr. Anke Lameris and Bryan van den Broek for excellent technical assistance.

References

1. Di Virgilio F, Chiozzi P, Ferrari D*, et al.* Nucleotide receptors: an emerging family of regulatory molecules in blood cells. *Blood* 2001; **97:** 587-600.
2. Filippini A, Taffs RE, Sitkovsky MV. Extracellular ATP in T-lymphocyte activation: possible role in effector functions. *Proceedings of the National Academy of Sciences of the United States of America* 1990; **87:** 8267-8271.
3. Booth JW, Tam FW, Unwin RJ. P2 purinoceptors: Renal pathophysiology and therapeutic potential. *Clin Nephrol* 2012; **78:** 154-163.
4. Arulkumaran N, Turner CM, Sixma ML*, et al.* Purinergic signaling in inflammatory renal disease. *Frontiers in physiology* 2013; **4:** 194.
5. Kim MJ, Turner CM, Hewitt R*, et al.* Exaggerated renal fibrosis in P2X4 receptor-deficient mice following unilateral ureteric obstruction. *Nephrology, dialysis, transplantation : official publication of the European Dialysis and Transplant Association - European Renal Association* 2014; **29:** 1350-1361.
6. Leipziger J. Luminal nucleotides are tonic inhibitors of renal tubular transport. *Current opinion in nephrology and hypertension* 2011; **20:** 518-522.
7. Stokes L, Scurrah K, Ellis JA*, et al.* A loss-of-function polymorphism in the human P2X4 receptor is associated with increased pulse pressure. *Hypertension* 2011; **58:** 1086-1092.
8. Menzies RI, Unwin RJ, Bailey MA. Renal P2 receptors and hypertension. *Acta Physiol (Oxf)* 2015; **213:** 232-241.
9. Wildman SS, Marks J, Turner CM*, et al.* Sodium-dependent regulation of renal amiloride-sensitive currents by apical P2 receptors. *Journal of the American Society of Nephrology : JASN* 2008; **19:** 731-742.
10. Marques RD, de Bruijn PI, Sorensen MV*, et al.* Basolateral P2X receptors mediate inhibition of NaCl transport in mouse medullary thick ascending limb (mTAL). *American journal of physiology Renal physiology* 2012; **302:** F487-494.
11. Cusack NJ, Hourani SM. Subtypes of P2-purinoceptors. Studies using analogues of ATP. *Ann N Y Acad Sci* 1990; **603:** 172-181.
12. Coddou C, Yan Z, Obsil T*, et al.* Activation and regulation of purinergic P2X receptor channels. *Pharmacol Rev* 2011; **63:** 641-683.
13. Orriss IR, Key ML, Brandao-Burch A*, et al.* The regulation of osteoblast function and bone mineralisation by extracellular nucleotides: The role of p2x receptors. *Bone* 2012; **51:** 389-400.
14. Surprenant A, North RA. Signaling at purinergic P2X receptors. *Annu Rev Physiol* 2009; **71:** 333-359.
15. Kawate T, Michel JC, Birdsong WT*, et al.* Crystal structure of the ATP-gated P2X(4) ion channel in the closed state. *Nature* 2009; **460:** 592-598.
16. North RA, Surprenant A. Pharmacology of cloned P2X receptors. *Annu Rev Pharmacol Toxicol* 2000; **40:** 563-580.
17. Wildman SS, Boone M, Peppiatt-Wildman CM*, et al.* Nucleotides downregulate aquaporin 2 via activation of apical P2 receptors. *Journal of the American Society of Nephrology : JASN* 2009; **20:** 1480-1490.
18. de Baaij JH, Blanchard MG, Lavrijsen M*, et al.* P2X4 receptor regulation of transient receptor potential melastatin type 6 (TRPM6) Mg2+ channels. *Pflugers Archiv : European journal of physiology* 2014; **466:** 1941-1952.
19. Ormond SJ, Barrera NP, Qureshi OS*, et al.* An uncharged region within the N terminus of the P2X6 receptor inhibits its assembly and exit from the endoplasmic reticulum. *Molecular pharmacology* 2006; **69:** 1692-1700.
20. Le KT, Babinski K, Seguela P. Central P2X4 and P2X6 channel subunits coassemble into a novel heteromeric ATP receptor. *The Journal of neuroscience : the official journal of the Society for Neuroscience* 1998; **18:** 7152-7159.
21. Dai LJ, Kang HS, Kerstan D*, et al.* ATP inhibits Mg(2+) uptake in MDCT cells via P2X purinoceptors. *American journal of physiology Renal physiology* 2001; **281:** F833-840.
22. Charmaine J. Foltz D, Dipl. ACLAM, and Mollie Ullman-Cullere B, MS. Guidelines for Assessing the Health and Condition of Mice. *Lab Animal* 1999; **28:** 28-

23. Thebault S, Alexander RT, Tiel Groenestege WM*, et al.* EGF increases TRPM6 activity and surface expression. *Journal of the American Society of Nephrology : JASN* 2009; **20:** 78-85.
24. Banfi C, Ferrario S, De Vincenti O*, et al.* P2 receptors in human heart: upregulation of P2X6 in patients undergoing heart transplantation, interaction with TNFalpha and potential role in myocardial cell death. *Journal of molecular and cellular cardiology* 2005; **39:** 929-939.
25. Praetorius HA, Leipziger J. Intrarenal purinergic signaling in the control of renal tubular transport. *Annu Rev Physiol* 2010; **72:** 377-393.
26. Wildman SS, King BF. P2X receptors: epithelial ion channels and regulators of salt and water transport. *Nephron Physiol* 2008; **108:** p60-67.
27. Musa H, Tellez JO, Chandler NJ*, et al.* P2 purinergic receptor mRNA in rat and human sinoatrial node and other heart regions. *Naunyn Schmiedebergs Arch Pharmacol* 2009; **379:** 541-549.
28. Cheung KK, Marques-da-Silva C, Vairo L*, et al.* Pharmacological and molecular characterization of functional P2 receptors in rat embryonic cardiomyocytes. *Purinergic signalling* 2015; **11:** 127-138.
29. de Baaij JH, Groot Koerkamp MJ, Lavrijsen M*, et al.* Elucidation of the distal convoluted tubule transcriptome identifies new candidate genes involved in renal Mg(2+) handling. *American journal of physiology Renal physiology* 2013; **305:** F1563-1573.
30. Barrera NP, Ormond SJ, Henderson RM*, et al.* Atomic force microscopy imaging demonstrates that P2X2 receptors are trimers but that P2X6 receptor subunits do not oligomerize. *The Journal of biological chemistry* 2005; **280:** 10759-10765.
31. Diaz-Hernandez JI, Sebastian-Serrano A, Gomez-Villafuertes R*, et al.* Age-Related Nuclear Translocation of P2X6 Subunit Modifies Splicing Activity Interacting with Splicing Factor 3A1. *PloS one* 2015; **10:** e0123121.
32. Jones CA, Vial C, Sellers LA*, et al.* Functional regulation of P2X6 receptors by N-linked glycosylation: identification of a novel alpha beta-methylene ATP-sensitive phenotype. *Molecular pharmacology* 2004; **65:** 979-985.
33. Collo G, North RA, Kawashima E*, et al.* Cloning OF P2X5 and P2X6 receptors and the distribution and properties of an extended family of ATP-gated ion channels. *The Journal of neuroscience : the official journal of the Society for Neuroscience* 1996; **16:** 2495-2507.
34. Torres GE, Egan TM, Voigt MM. Hetero-oligomeric assembly of P2X receptor subunits. Specificities exist with regard to possible partners. *The Journal of biological chemistry* 1999; **274:** 6653-6659.
35. Bobanovic LK, Royle SJ, Murrell-Lagnado RD. P2X receptor trafficking in neurons is subunit specific. *The Journal of neuroscience : the official journal of the Society for Neuroscience* 2002; **22:** 4814-4824.
36. Uhlen M, Fagerberg L, Hallstrom BM*, et al.* Proteomics. Tissue-based map of the human proteome. *Science* 2015; **347:** 1260419.
37. Sprinthall RC. *Basic Statistical Analysis* 9th edn. Pearson Education, 2011.

6 General discussion and summary

Introduction

Mineral homeostasis is crucial for many physiological processes in the body like enzymatic activity, cell metabolism, bone formation and neuronal excitability. Ca^{2+} and Mg^{2+} concentrations are therefore tightly regulated by the kidney, parathyroid glands, intestine and bone. The kidney determines the final concentration of these ions by reabsorbing Ca^{2+} and Mg^{2+} from the pro-urine into the blood. This reabsorption process is facilitated by paracellular and transcellular epithelial transport in the PT, thick ascending limb of Henle's loop (TAL) and distal convoluted tubule (DCT) of the kidney. The capacity to mediate ion transport in these segments depends on the amount, availability, composition and activity of membrane transporters, channels and tight junctions. Membrane transporters and channels facilitate transcellular epithelial transport in the kidney. Endocrine signaling molecules, like parathyroid hormone (PTH) and 1,25-dihydroxyvitamin D_3 (VitD), regulate the activity of these transporters and channels in the whole kidney. Whereas, paracrine signaling molecules like ATP, regulate ion transport on a local cellular level. The other rate-limiting factor of both transcellular and paracellular ion transport is the amount of ion transporters, channels and tight junctions at the plasma membrane. Two key mechanisms are: the recruiting and recycling of these elements to the plasma membrane via vesicle trafficking, a fast response and the regulation of transcription and translation of additional transport proteins to facilitate a change in ion transport capacity, a slow response. The aim of this thesis was to elucidate new transcriptional networks that regulate Mg^{2+} and Ca^{2+} transport in the kidney. In particular, *i*) in **chapter 2** a genome-wide dataset of HNF1β binding sites in the DCT was established; *ii*) Kir5.1 was identified as a target of HNF1β elucidating a new regulatory pathway of Mg^{2+} transport in the DCT; *iii*) **chapter 3** investigates the identification of the *CaSR* gene as a new transcriptional target of HNF1β, providing insight in a novel transcriptional mechanism for Ca^{2+} and Mg^{2+} reabsorption in the TAL; *iv)* **chapter 4** established that FAM111A is a binding partner of transcription factor STAT1, which revealed a novel regulatory role for FAM111A in Ca^{2+} and Mg^{2+} reabsorption in the body; *v)* additionally, **chapter 5** demonstrated that the P2X purinoreceptor subunit P2X6 is not involved in renal ion transport based on the characterization of a *P2x6* knockout (KO) mouse model.

P2X6 functioning in and outside the kidney

Inside the kidney

P2X receptors are important regulators of Ca^{2+} and Mg^{2+} transport in both TAL and DCT. In an initial report by Dai and colleagues, ATP was shown to regulate Mg^{2+} transport via P2X purinoreceptors.[1] P2X receptors are ATP-activated ion channels with a cation selective pore and are mainly permeable for Ca^{2+}, although monovalent cations can also pass through. P2X receptors can form both homotrimers and heterotrimers. Expression pattern analysis of mouse *P2x* subunits 1-7 revealed that only *P2x4* and *P2x6* transcripts are highly expressed in the DCT.[2, 3] However, immunohistological co-localization analysis of P2X4 with NCC in mouse kidney sections revealed that only *P2x6* is exclusively expressed in the DCT.[3] The exclusive expression of P2X6 in DCT made it an interesting candidate to further investigate its potential role in the regulation of Mg^{2+} transport in the DCT.

To examine the aforementioned role of P2X6, a *P2x6*$^{-/-}$ knockout mouse was developed and in **chapter 5** a detailed characterization of this mouse is presented.[4] Knocking out *P2x6* in mice did, however, not result in a measurable electrolyte phenotype in serum or urine. Possible compensatory mechanisms were ruled out, as none of the common magnesio- or calciotropic genes in the kidney were affected by the loss of *P2x6*. On the functional level, previous work confirmed that co-expression of P2X6 with TRPM6, in an *in vitro* cell model, did not have an effect on TRPM6 activity after ATP stimulation. This fits with preceding *in vitro* studies, which state that P2X6 cannot form homotrimers and requires P2X2 or P2X4 subunits to reach the plasma membrane and become a functional ion channel.[5-7] The lack of an effect on electrolyte transport and the absence of any transcriptional changes in magnesio- and calciotropic genes in the *P2x6*$^{-/-}$ mouse lead to the conclusion that the P2X6 subunit has no role in renal electrolyte transport. The physiological role of P2X6 beyond the kidney remains elusive.

Outside the kidney

Data from the *P2x6*$^{-/-}$ mouse showed a decrease of *P2x2* expression in the heart. Indeed P2X6 forms heterotrimers with P2X2 and only then becomes a functional P2X receptor at the plasmamembrane.[8, 9] Previous research describes that P2X6 and no other P2 receptors are upregulated in chronic hear disease. It is argued that increased P2X6 activity raises intracellular Ca^{2+} levels resulting in cell death, which contributes to the elevated risk of cardiac arrest.[10] Although *P2x6*$^{-/-}$ mice did not appear to suffer from heart problems, P2X2 subunits were significantly upregulated, as a potential compensatory mechanism to increase ATP-mediated Ca^{2+} signaling in the heart. Another study showed how P2X6 subunits might have an additional function in brain.[11] They described P2X6 accumulation in hippocampal neurons in an age-dependent

way, which then interacts with the splicing factor 3A1 resulting in decreased mRNA splicing in these cells.[11] It is, therefore, possible that the primary function of P2X6 is not related to ATP-mediated Ca^{2+} signaling, but involved in regulating splicing factor 3A1s' function in mRNA splicing. The *P2x6*$^{-/-}$ mouse model can be used to further study the physiological effects of P2X6 loss on hippocampal neuron functioning in an age-dependent manner. Subsequently, it is interesting to examine the exact role of P2X6 in the heart as well.

HNF1β: key regulator of renal Mg^{2+} reabsorption

Mutations and deletion of hepatocyte nuclear factor 1 homeobox β (HNF1β) is one of the most common genetic causes for genital tract malformations (CAKUT) and cyst formation in the kidney.[12-15] Most HNF1β patients tend to additionally develop an electrolyte phenotype characterized by hypomagnesemia, hypocalciuria and hypokalemic metabolic alkalosis.[16-18] HNF1β has been identified as a transcriptional regulator of many cystic disease genes.[19-22] However, the role of HNF1β in regulating electrolyte transport in the kidney has not been thoroughly investigated. HNF1β was identified as a transcriptional activator of the *FXYD2* gene, encoding the y-subunit of the Na^+-K^+-ATPase, and is essential for the reabsorption of Mg^{2+} in DCT.[23] [24] Mutations in *FXYD2* indeed cause hypomagnesemia and hypocalcemia in patients.[25, 26] Close investigation of the literature, however, reveals that HNF1β is specifically responsible for the regulation of the *FXYD2a* splice variant of *FXYD2*.[23] *FXYD2* gene expression in DCT is however limited to the *FXYD2b* splice variant.[27, 28] Consequently, HNF1β mediated *FYXD2a* expression in the DCT cannot be responsible for the lack of Mg^{2+} reabsorption in HNF1β patients.[27]

In **chapter 2,** all genome-wide binding sites of HNF1β were, for the first time, identified in an immortalized DCT cell line (mpkDCT). In DCT, the potassium inwardly-rectifying channel, subfamily J, member 16 (*KCNJ16* gene), encoding for the Kir5.1 K^+ channel subunit, was identified and validated as a target for HNF1β-mediated regulation. *Hnf1β* knockdown experiments resulted in a loss of *Kcnj16* gene transcription both *in vitro* and *in vivo*. The potassium inwardly-rectifying channel, subfamily J, member 10 (*KCNJ10*) gene coding for the Kir4.1 K^+ channel subunit was likewise affected.

HNF1β chIP-sequencing unravels novel transcriptional networks

Over the years various studies investigated the complex transcriptional networks of HNF1β, slowly elucidating parts of its vast web of target genes in the kidney and other organs. In 2004, Gresh *et al.* identified multiple cystic disease genes, namely *Pkhd1*, *Pkd2* and *Umod*, as HNF1β targets using chIP-qPCR in a kidney specific HNF1β KO mouse.[19] A related study using chIP-qPCR in a mouse inner medullary collecting duct

(IMCD3) cell line argues that HNF1β is not a typical transcription factor. Instead of releasing from the chromatin during post-mitotic silencing, HNF1β remains bound to certain parts of the chromatin and is postulated to act like a bookmarking factor to rapidly reactivate target genes after mitosis.[29] Although, this idea has not been explored further.

The aforementioned findings identified parts of the role of HNF1β in renal cyst formation and cell cycle regulation, but there are several big downsides to chIP-qPCR, which limits its usefulness for further research: *i)* ChIP-qPCR is highly labor intensive as potential HNF1β sites have to be identified *in silico* and then tested *in vitro* or *in vivo; ii)* this severely limits the amount of potential target genes that can be tested for HNF1β binding sites; *iii)* potential HNF1β binding sites outside of the promoter of the target gene can be missed; *iv)* most importantly this approach is highly biased as genes of interest have to be chosen *a priori*. Indeed after genome-wide screening methods became available a chIP-chIP for HNF1β in IMCD3 immediately revealed cystic disease gene *Kif12* as a novel target of HNF1β.[22]

A limitation of chIP-chIP is that it does not cover the whole genome.[30] With chIP-chIP, immunoprecipitated chromatin was hybridized to promoter tiling arrays that cover 1.5 kb of the promoter regions of 26,842 mouse genes.[22] This severely limits the identification of intronic or intergenic enhancer sites obscuring the identification of HNF1β targets. The solution to the problem is chIP-sequencing. This method is truly genome-wide and has a much improved signal to noise-ratio compared to chIP-chIP.[31] The first HNF1β chIP-seq was performed in the collecting duct (CD) cell line IMCD3 and identified 4,725 mRNAs and 85 miRNAs with HNF1β bindings located in a 50 kb range from their respective transcription start sites (TSS). Most HNF1β peaks could be mapped close to or within gene bodies.[32] Our study in mpkDCT cells revealed a remarkably similar set of 4,530 genes containing HNF1β binding sites in a 50 kb range from the TSS of which 43.5% were present near transcriptional active genes. Aboudehen *et al.* combined the differentially expressed genes from a RNA-seq of renal epithelial (53A) cells expressing mutant HNF1β with HNF1β target genes identified in the chIP-seq.[32] Metabolic pathways were highly regulated by HNF1β and further research showed that specifically cholesterol metabolism was affected. A similar approach was used in a CD-specific *Hnf1β* KO mouse. RNA-seq was performed on CD material from the CD-specific *Hnf1β* KO mouse model. This revealed differentially expressed genes related to osmoregulation between CD-specific *Hnf1β* KO and wildtype mice. The chIP-seq data from the IMCD3 cells was used to investigate, which of these differentially expressed genes from the RNA-seq data contained HNF1β binding sites.[33] Such a combined analysis could also be used to identify with more specificity the pathways in DCT that are directly affected by HNF1β. However, constructing a HNF1β mutant mpkDCT cell line is highly challenging. Current innovations in gene knock-in technology, like CRISPR-CAS9, could potentially solve this problem.

The chIP-seq performed in IMCD3 cells also identified HNF1β binding sites near 85 miRNAs. A follow-up study determined that HNF1β regulates a long-coding RNA containing the mir-200 family.[34] Mir-200 is known to coordinate Pkd1 expression, which demonstrates another regulatory pathway that connects HNF1β to cyst formation.[34] It would be of interest to analyze which miRNAs have HNF1β binding sites near them in the mpkDCT chIP-seq. This could be combined with a DCT-wide screening of differentially expressed miRNAs in mice that are subjected to a low versus normal Mg^{2+} diet. This approach could reveal HNF1β-regulated miRNAs with a role in Mg^{2+} transport regulation.

HNF1β also plays an important role in kidney development, especially uretric bud branching and in the initiation of nephrogenesis.[35, 36] A recent RNA-seq of E15 kidney material from HNF1β KO mice identified that HNF1β controls specifically epithelial organization and cell polarity during ureteric bud branching and collecting duct morphogenesis.[37] Loss of cell polarity and epithelial organization are often linked to cilia genes like *PKHD1* and *PKD1&2*, which are incidentally cystic disease and HNF1β target genes.[20, 21, 38] The role of HNF1β in ureteric bud branching and CD morphogenesis fits with the fact that loss of HNF1β after birth does not result in cystic kidneys anymore.[29] Consequently, the regulation of cystic disease genes by HNF1β is mainly important during nephrogenesis. Of particular interest was the result of a HNF1β chIP-seq performed on E14.5 mouse kidney material, which validates HNF1β targets like *Kcnj16* found in our chIP-seq data.[37] *Kcnj16* was also downregulated in the aforementioned RNA-seq further confirming the results in **chapter 2**. Except of a list of genes containing HNF1β binding sites; more details on this chIP-seq were not available.

HNF1β regulates the Kir5.1 K^+ subunit; consequences for Mg^{2+} transport in DCT

The results of **chapter 2** demonstrate that HNF1β directly regulates *Kcnj16* while *Kcnj10* is indirectly controlled. The consequences for Mg^{2+} reabsorption in DCT are, therefore, as follows. We postulate that the decreased availability of Kir4.1/Kir5.1 K^+ channels at the basolateral side of DCT diminishes K^+ extrusion and subsequently decreases Na^+-K^+-ATPase activity, depolarizing the basolateral membrane. As a consequence, this would lead to diminish extrusion of Cl^- via the CLC-Kb channel (Figure 1). An increase in intracellular Cl^- decreases the activity of the WNK-SPAK kinase pathway, which in turn reduces phosphorylation of the hydrochlorothiazide-sensitive Na^+-Cl^- co-transporter (NCC) and limits its activity.[39] NCC activity is required for proper reabsorption of Mg^{2+} via Mg^{2+} channel TRPM6 (Figure 1). This is illustrated in Gitelman syndrome and SeSAME-EAST syndrome, where patients suffer from hypomagnesemia and a hypokalemic metabolic alkalosis due to decreased NCC functioning or activity in the DCT.[40, 41 42-44] Both Gitelman and SeSAME-EAST syndrome

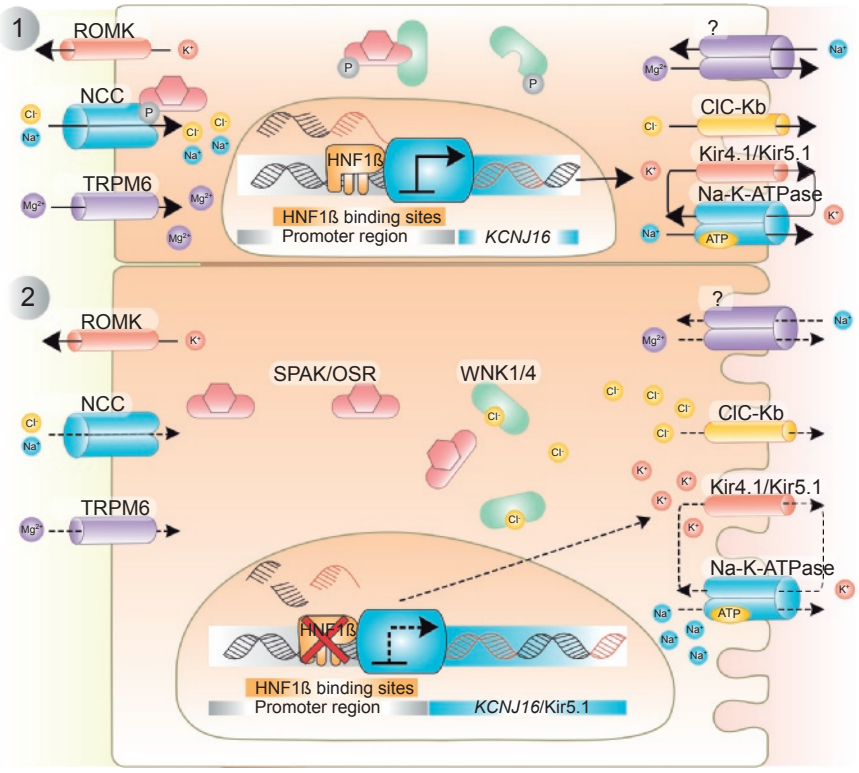

Figure 1 | A model of HNF1β deficiency and the consequences for Mg^{2+} reabsorption in the DCT

1) In the physiological normal situation HNF1β facilitates expression of Kir5.1, which results in normal functioning of the Na^+-K^+-ATPase. This in turn results in proper extrusion of Cl^- from the cell. Loss of Cl^- autophosphorylates WNK kinases and causes phosphorylation of the SPAK/OSR1 complex. In turn, SPAK/OSR1 phosphorylates NCC inducing NCC activity. NCC activity increases Mg^{2+} reabsorption via Mg^{2+} channel TRPM6. 2) Mutations and loss of HNF1β result in decreased Kir5.1 expression. This causes hyperpolarization of the basolateral membrane reducing Cl^- extrusion. Increased intracellular Cl^- will bind and inihibit autophosphorylation of the WNK kinases, which reduces SPAK/OSR1 activity. Reduced activity of this pathway limits NCC phosphorylation and decreases NCC activity. This reduces Mg^{2+} reabsorption via TRPM6.

have a comparable electrolyte disorder to ADTKD-HNF1B patients, alluding to the similar mechanism underlying these diseases.

Kidney-specific Kir4.1 KO mice mimic to a degree the phenotype observed in SeSAME-EAST and ADTKD-HNF1β patients. Mice lacking Kir4.1 expression in the kidney suffer from a hypokalemic metabolic alkalosis with urinary Na^+, K^+, Ca^{2+} and Mg^{2+} wasting.[45] The loss of basolateral K^+ extrusion in DCT suppressed the activity of the WNK-SPAK kinase, which is an important activator of NCC (Figure 1).[46-48] Indeed phosphorylated (active) and total NCC levels were reduced in the Kir4.1 KO mice.[45] This fits with the decreased *NCC* mRNA levels observed in the kidney specific *Hnf1β* KO mice.[49]

ADTKD-HNF1β patients are, therefore, likely to exhibit decreased renal expression of Kir4.1/Kir5.1 K^+ channels and NCC, which should manifest in a decreased response to hydrochlorothiazide (HCTZ). Indeed a recent publication detected a blunted response to HCTZ diuretics in HNF1β patients.[50] This further strengthens the hypothesis that loss of K^+ recycling in the DCT is the underlying mechanism behind the electrolyte imbalance observed in ADTKD-HNF1β patients.

A point of contention in our studies is that a direct regulatory effect of HNF1β on *Kcnj16* (Kir5.1) was detected and only an indirect effect on *Kcnj10* (Kir4.1) gene expression.[49] Mice that are only Kir5.1 deficient display an inverted phenotype to SeSAME-EAST and ADTKD-HNF1β.[51] These mice do suffer from a hypokalemia but combined with an acidosis rather than an alkalosis, and hypercalciuria instead of hypocalciuria. Furthermore, renal NCC activity was increased rather than decreased.[51] In normal conditions, the Kir4.1/Kir5.1 channel is the dominant K^+ channel present in DCT.[51-53] However, in the absence of Kir5.1, the formation of Kir4.1 monomer channels increases K^+ extrusion at the basolateral membrane resulting in the aforementioned Kir5.1 KO mice phenotype.[51, 54, 55] Likewise, a study in salt-sensitive (SS) *Kir5.1* KO rats reported that loss of Kir5.1 increased Kir4.1 mRNA and protein expression.[56] However, immunohistochemical stainings displayed that most Kir4.1 subunits were retained in the cytosol and were not routed to the plasma membrane. Patch-clamp experiments confirmed a decrease in K^+ conductance in the basolateral membrane of DCT. Together, the electrolyte imbalance in *Kir5.1* KO SS rats is similar to the phenotype seen in SeSAME-EAST and ADTKD-HNF1β patients. It is relevant to investigate not only why *Kir4.1* expression is decreased in *ksp-cre Hnf1β* KO mice, but also whether Kir4.1 protein trafficking to the plasma membrane is affected.

It remains unclear why *Kir4.1* mRNA expression in DCT is decreased after HNF1β knockdown. No direct HNF1β binding sites were detected in or near the *Kcnj10* gene, which tends to rule out direct regulation by HNF1β. However, transcription factors are not required to bind within a promoter sequence to affect gene transcription. To elucidate whether HNF1β binds the *Kcnj10* promoter, circularized chromosome conformation capture (4C) can be used to map the interacting DNA sites with the Kir4.1 target promoter.[57, 58] Allowing for the identification of far-off HNF1B binding

sites or HNF1B binding partners. CHIA-PET is a technique that combines High-throughput sequencing (Hi-S) and ChIP-seq, allowing for the detection of *de novo* long-range chromatin interactions mediated by a target protein like HNF1β.[59] This would also allow for the identification of far-off distal HNF1β binding sites and their interacting target genes, which is not possible with standard chIP-seq techniques. Further research is, therefore, needed to elucidate the long-range enhancer and repressor sites of HNF1β to determine which target genes are affected.

HNF1β: key regulator of Ca^{2+} and Mg^{2+} transport in the TAL

HNF1β is ubiquitously expressed throughout the kidney. However, research concerned with investigating the transcriptional pathways behind the HNF1B related electrolyte imbalance is confined to the DCT. With the exception of a study that identified HNF1β as a repressor of parathyroid hormone (PTH) expression, explaining the development of hyperparathyroidism in a subpopulation of HNF1β patients.[17] The ADTKD-HNF1β phenotype remains, however, reminiscent of typical DCT-based electrolyte syndromes like SeSAME-EAST and Gitelman syndrome.

Although, one aspect of the ADTKD-HNF1β electrolyte disorder, namely the hypocalciuria observed in ADTKD-HNF1β patients, is difficult to explain with a strictly DCT-based hypothesis. As, Ca^{2+} is actively reabsorbed downstream from the DCT, which is not affected by changes in NCC-mediated transport.[41] A plausible explanation for the hypocalciuria in ADTKD-HNF1β focuses on compensatory mechanisms in the PT, where increased active Na^+ reabsorption drives passive Ca^{2+} reaborption, due to decreased NCC activity in the DCT (Figure 2).[41]

Another segment relevant for Ca^{2+} and Mg^{2+} reabsorption is the TAL. A significant lumen-positive voltage is maintained in the cortical TAL (cTAL) by uptake of Na^+ by the furosemide-sensitive Na^+-K^+-$2Cl^-$ cotransporter (NKCC2). Passive reabsorption of Na^+ through Na^+ selective Cldn10b tight junctions in the medullary TAL (mTAL) and cTAL also contributes to this lumen-positive voltage in the cTAL.[60, 61] This process facilitates paracellular uptake of Ca^{2+} and Mg^{2+} in cTAL.[62] Here, reabsorption of Na^+, like in the DCT, is dependent on proper K^+ recycling via the Kir4.1/Kir5.1 K^+ channel and the Na^+-K^+-ATPase to maintain a hyperpolarized basolateral membrane. Similarly to DCT, a lack of Kir4.1/Kir5.1 K^+ channels reduced phosphorylated and total NKCC2 (pNKCC2) in *Kir4.1* KO mice.[45] Subjecting these animals to furosemide did, however, not affect Na^+ reabsorption in TAL.[63] Furosemide treatment in *Kir5.1* KO mice identified a normal Na^+, K^+ and Ca^{2+} response and NKCC2 levels were increased in salt-sensitive (SS) *Kir5.1* KO rats.[51, 56] It seems that loss of Kir4.1/Kir5.1 K^+ channels does not affect passive reabsorption of Ca^{2+} and Mg^{2+} via aberrant Na^+ reabsorption in the TAL.[45]

HNF1β regulates expression of the Ca^{2+}-sensing receptor in TAL and the parathyroid glands

Chapter 3 describes how HNF1β regulates the expression of the calcium-sensing receptor (CaSR), an important regulator of Ca^{2+} and Mg^{2+} in the kidney. The CaSR is a G-protein coupled receptor (GPCR) and localized along the basolateral membrane of TAL and parathyroid gland.[64] Intracellular signaling is triggered when Ca^{2+} binds to the large extracellular domains of the CaSR. These extracellular domains have a high affinity for Ca^{2+} in the mM range, and to a lesser degree also respond to Mg^{2+}.[64] Activation of the CaSR elevates levels of intracellular Ca^{2+}, which subsequently decreases the uptake of Ca^{2+} and Mg^{2+} in TAL.[65] In the parathyroid glands, activation of the CaSR reduces PTH release, which also lowers the uptake of Ca^{2+} in the kidney.[66]

CaSR gene transcription is known to be responsive to VitD, proinflammatory cytokines and the transcription factor glial cells missing-2 (GCM2) however, the connection to HNF1B is novel.[67] Two promoters regulate CaSR expression, each controlling a separate alternative exon (exon 1A or 1B) coding for a different '5 UTR, which then splices to a common segment encoded in exon 2 of the coding region.[68 69] In human kidney, the predominant CaSR transcripts are controlled by promoter 1 and HNF1β specifically regulates the activity of that promoter.[68-70] Promoter 1-controlled CaSR expression is also dominant in the parathyroid meaning that CaSR expression in the parathyroid is regulated by HNF1β. Absence or aberrant functioning of HNF1β cause a decrease in *CaSR* transcript availability, weakening the sensitivity for extracellular Ca^{2+} and Mg^{2+} sensing at the basolateral side of TAL and parathyroid glands.

In the parathyroid gland, CaSR activity is an important repressor of parathyroid horomone (PTH) release. Additionally, it has been shown that HNF1β is a direct repressor of PTH expression.[17] A loss of HNF1β would, therefore, raise PTH expression levels and via the additional loss of CaSR expression would increase PTH release. Subsequently, this stimulates reabsorption of Ca^{2+} in the kidney and facilitates Ca^{2+} release from bone. This could explain the hypocalciuria observed in HNF1β patients. Indeed, a subset of ADTKD-HNF1β patients develops hyperparathyroidism and it has been reported that PTH levels in HNF1β patients are elevated compared to controls.[16, 17, 71] This can have consequences for both Ca^{2+} and Mg^{2+} uptake in the kidney. It is known that PTH stimulates the activity of Ca^{2+} channel transient receptor potential vanilloid 5 (TRPV5), increasing Ca^{2+} reabsorption in the late DCT and connecting tubule (CNT).[72] Furthermore, it has been shown that PTH also decreases NCC activity, which can negatively influence Mg^{2+} reabsorption in DCT.[73]

Potential treatment options for ADTKD-HNF1β patients would be VitD supplementation to suppress PTH expression and to decrease Ca^{2+} reabsorption in the kidney. Administration of calcimimetics, like CaSR agonist cinacalcet, can boost CaSR signaling.[74, 75] This subsequently decreases PTH release, which in turn could remedy

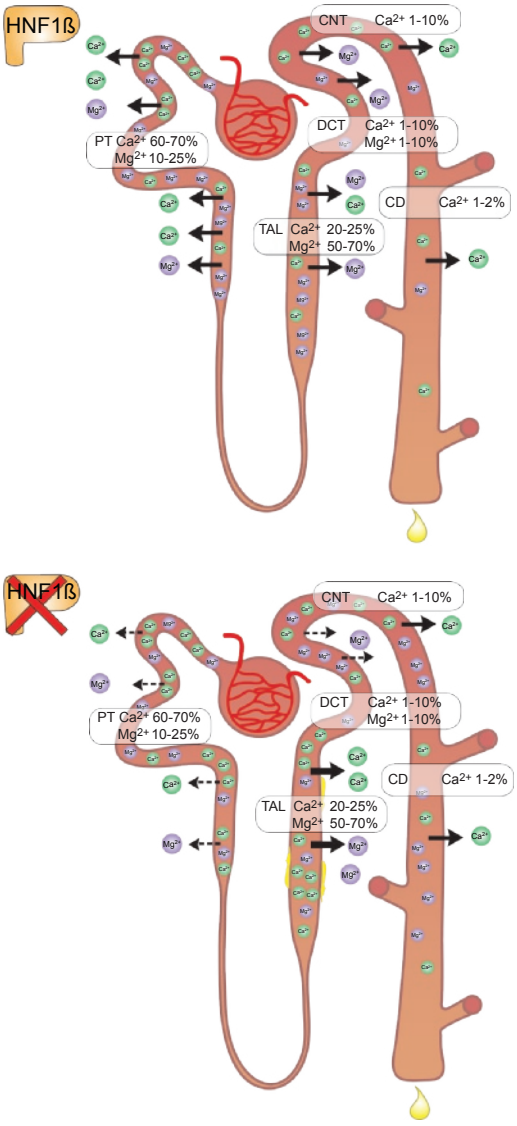

Figure 2 | A model of HNF1β deficiency and the consequences for Ca^{2+} and Mg^{2+} reabsorption along the nephron

Loss of HNF1β along the nephron increases reabsorption of Ca^{2+} and Mg^{2+} in the thick ascending limb of Henle's loop (TAL). As a consequence uptake of mainly Ca^{2+} is decreased in the PT. This increases the Ca^{2+} load in the TAL, which increases the chance for nephrocalcinosis (yellow plaques). Loss of HNF1β reduces uptake of Mg^{2+} in the DCT. Yellow plagues show Ca^{2+} oxalate deposits, indicative of nephrocalcinosis.

the hypocalciuria. VitD will additionally stimulate CaSR expression directly as both CaSR promoter 1 and 2 harbor 1,25-dihydroxyvitamin D_3 receptor (VDR) responsive elements.[76, 77] It is, however, unknown whether these VitD responsive elements interact with HNF1β. In addition, it also remains unclear whether hyperparathyroidism is a primary or secondary symptom of HNF1β dysfunction. As increased PTH levels can be a consequence of direct defects in Ca^{2+} reabsorption in the kidney.

HNF1β regulation of the Ca^{2+}-sensing receptor in the TAL; Consequences for Ca^{2+} and Mg^{2+} reabsorption along the kidney tubule

In **chapter 3** we show that loss of HNF1β decreases CaSR transcription in TAL (Figure 3). Patients with inactivating mutations in the CaSR suffer from familial hypocalciuric hypercalcemia (FHH; OMIM #145980), which is characterized by hypermagnesemia, hypercalcemia, hypomagnesiuria and hypocalciuria. ADTKD-HNF1β patients also suffer from a hypocalciuria, which could be the consequence of decreased CaSR abundance and signaling in the kidney. Previous research identified that CaSR activity is causative of Cldn14 upregulation in the tight junctions of TAL.[78] This is induced by CaSR-mediated repression of two miRNAs, Mir-9 and Mir-374, which subsequently upregulate Ca^{2+} and Mg^{2+} excretion.[78-80] SiRNA-mediated knockdown of *HNF1β* revealed an anticipated decrease in mouse *Casr* transcript and *Cldn14* mRNA levels in an immortalized TAL cell line. *Cldn14* levels did not change in a kidney-specific *Hnf1β* KO mouse, although a significant reduction of *Casr* transcript was observed. *Cldn14* mRNA levels were extremely low in both wildtype and *Hnf1β* KO mice. These observations fit with previous research, as mice require a high Ca^{2+} diet before *Cldn14* mRNA levels become detectable.[78, 80-82] Lacking *Cldn14*, the increased influx of Ca^{2+} and Mg^{2+} is expected to trigger other compensatory mechanism to decrease divalent cation influx. Indeed, in the *ksp-cre Hnf1β* KO mice, *Cldn19* and *Cldn10b* expression was significantly reduced, whereas *Cldn3* expression was upregulated. Claudin19 forms together with Claudin16, the pore that facilitates the paracellular uptake of Ca^{2+} and Mg^{2+} in cTAL.[83] It is, therefore, plausible to assume that in response to reduced CaSR signaling, *Cldn19* expression is diminshed to avoid Ca^{2+} precipitations.

Claudin10b forms monomeric tight junctions in mTAL, which are selective for Na^+.[61] A reduction in Claudin10b tight junctions would decrease Na^+ reabsorption in the medullary part of the TAL.[60] Loss of *Cldn10b* in *ksp-cre Cldn10* KO mice showed that these mice suffer from hyperabsorption of Ca^{2+} and Mg^{2+}.[84] Whereas the increased reabsorption of Mg^{2+} in the TAL caused hypermagnesemia, Ca^{2+} levels were unaffected, even causing a slight hypocalcemia. This can be explained by different absorption rates for Ca^{2+} and Mg^{2+} along the tubule. The bulk of Mg^{2+} (~70%) is reabsorbed in TAL compared to ~20% of Ca^{2+}. Decreasing the reabsorption of Ca^{2+} in the PT can diminish the effects of hyperabsorption of Ca^{2+} in the TAL. However, this subsequently increases the Ca^{2+} load in TAL resulting in nephrocalcinosis in the mTAL,

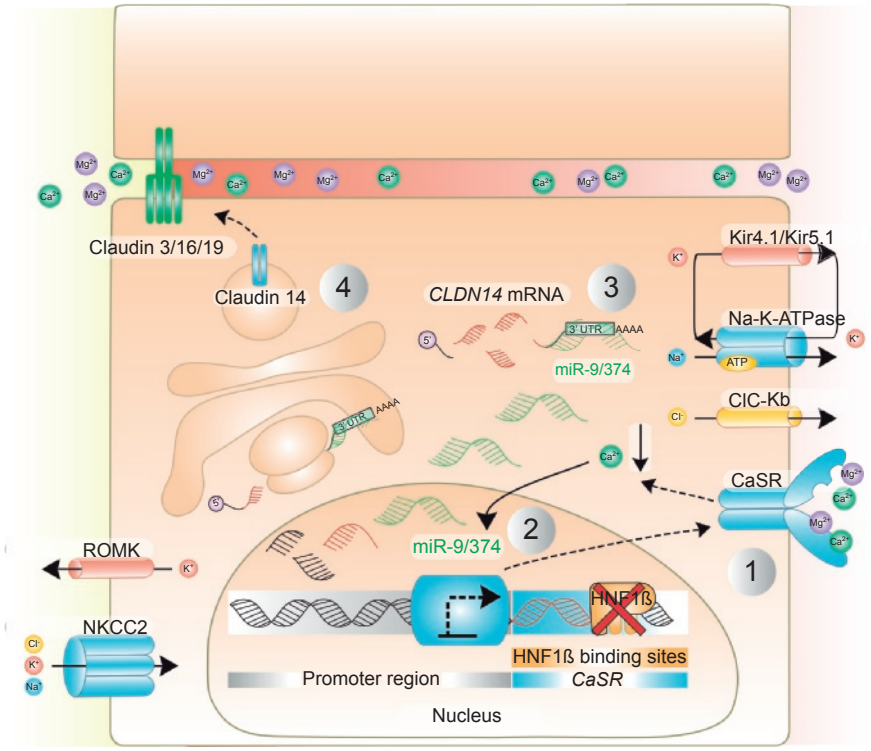

Figure 3 | A model of HNF1β deficiency and the consequences for Ca^{2+} and Mg^{2+} reabsorption in the TAL

1) Mutations and loss of HNF1β result in decreased CaSR expression. This diminishes CaSR activity and reduces intracellular Ca^{2+} signaling. 2) Reduced intracellular Ca^{2+} signaling increases the expression of miR-9 & miR-374. 3) miR-9&374 bind to the *CLDN14* mRNA and facilitates breakdown, reducing *CLDN14* mRNA translation into protein. 4) The decreased availability of Claudin14 protein increases Ca^{2+} and Mg^{2+} transport through the Claudin3/16/19 tight junction complex.

which has been observed in *ksp-cre Cldn10* KO mice.[84] Observations in patients with *CLDN10* mutations confirmed the decrease in Ca^{2+} and Mg^{2+} excretion, due to insufficient Na^{+} reabsorption in TAL.[85] It seems, therefore, credible that in HNF1β patients the lack of CaSR and *CLDN10b* expression can result in an increased Ca^{2+} load and hyperabsorption of Ca^{2+} in TAL. Indeed, HNF1β patients are known to develop hypocalciuria and reports of HNF1β patients developing nephrolithiasis have been

documented, which is a common consequence of nephrocalcinosis (Figure 2).[71] Patients suffering from inactivating mutations in the CaSR are also prone to develop nephrolithiasis. A study in stone formers versus control patients revealed that a SNP in promoter 1 of the CaSR is highly associated with nephrolithiasis, the exact promoter whose activity is regulated by HNF1β.[86]

Although a plausible hypothesis has been established on how loss of HNF1β causes hypocalciuria due to aberrant Ca^{2+} transport in TAL. It remains unclear how an increase in reabsorption of Mg^{2+} in the TAL results in hypomagnesemia in HNF1β patients. More detailed investigations are required to elucidate how Mg^{2+} reabsorption is affected by the loss of HNF1β in TAL.

HNF1β: models to study electrolyte transport in ADTKD-HNF1β

A distinct problem arises when comparing the electrolyte disorder observed in HNF1β patients with purely tubular nephropathies like Gitelman syndrome, SeSAME-EAST or TAL electrolyte disorders. HNF1β patients suffer from a highly heterogeneous disease, which entails the regular occurrence of cysts and or developmental problems in the kidney. These complications can be the cause of secondary symptoms like the electrolyte imbalance observed in ADTKD-HNF1β patients.

HNF1β mouse models

Current mouse models, in which HNF1β has been knocked out along the nephron, are not sufficient to exclude cyst progression as a cause for the electrolyte disorder. Cyst formation is extremely aggressive in the *ksp-cre Hnf1β* KO mice causing 75% lethality after day 21.[19] The high early life lethality in these mice prevents the accurate measurement of urine electrolyte excretion. Knocking out *Hnf1β* in a specific nephron segment, like the collecting duct, established that cyst progression can be delayed significantly, starting at p28, and mice can be monitored for 2 years.[33] It is, therefore, necessary to develop TAL and DCT–specific *Hnf1β* KO mouse models to disentangle the effect of cyst progression from the electrolyte phenotype in ADTKD-HNF1β. This is, however, highly challenging since TAL or DCT-cre specific mice are not yet available. Another option would be an inducible *Hnf1β* KO model. Indeed, induction after postnatal day 10 avoids the cystic phenotype and *Hnf1β* KO mice develop normally.[29] It would be of great interest to measure electrolytes in these latter mice to investigate whether the typical HNF1β electrolyte disorder is persistent in a non-cystic model.

HNF1β in vitro models

An alternative to avoid the high amount of co-morbidity in HNF1β-related diseases would be to study HNF1β-mediated transcriptional regulation in *in vitro* models for

TAL or DCT. In our research, both MKTAL and mpkDCT cell lines were used. The MKTAL cell line was derived from mouse thick ascending limb tubules, specifically from the inner strip of the outer medulla.[87] This cell line sufficiently expresses the *CaSR* and all *Cldns* important for Ca^{2+}, Mg^{2+} and Na^{+} transport at the transcript level. However, immunohistochemical data (Kompatscher et al., unpublished data) revealed that MKTAL cells, grown either on glass coverslips or polarized in transwell plates, had a distinct lack of Claudin16 and Claudin10b staining. As nearly all tight junctions were exclusively occupied by Claudin19 and Claudin3. Furthermore, these cells lacked *Slc12a1* (NKCC2) expression. Although, previous work in MKTAL cells did reveal *Slc12a1* expression at the mRNA level.[87] Measurements of MKTAL cells in an Ussing chamber indeed displayed a Na^{+} permeability that was not sensitive to furosemide and was not selective for Ca^{2+}, Mg^{2+} or Na^{+}.[88] This makes MKTAL cells unsuited to study functional electrolyte transport. Effects of extracellular Ca^{2+} on *Cldn14*, Mir-9 and Mir-374 expression levels have, however, been measured in MKTAL cells.[78] The MKTAL cell model is, therefore, a useful tool to study Ca^{2+}-mediated transcriptional pathways regulating *Cldn* expression in TAL.

There are several cell models available to investigate DCT cells *in vitro*. The initial immortalized murine DCT cell line (mDCT) was frequently used to study Na^{+}, Ca^{2+} and Mg^{2+} influx.[89, 90] Although these cells express NCC, genes directly involved in Mg^{2+} transport, like TRPM6, are poorly expressed and it turned out to be difficult to measure Mg^{2+} influx in these cells. As an alternative, Vandewalle and colleagues established an immortalized DCT cell line derived from microdissected mouse DCT, named the mpkDCT cell line.[91] Several studies reported thiazide-sensitive NCC-mediated Na^{+} transport in this cell line.[92-94] A recent subclone, the mDCT15 cell line more closely resembles the native DCT condition with intact WNK-SPAK, PTH and insulin signaling.[73, 95-97] Both latter cell lines seem good models to study, for example, HNF1β-mediated regulation of NCC activity. The lack of native NCC protein expression in the mpkDCT cell and mDCT15 subclone (Kompatscher et al., unpublished), however, severely limits the study of HNF1Bs' effect on NCC activity. It remains, therefore, necessary to develop an *in vitro* model that more closely resembles the native DCT cell state containing all relevant transporters and channels to study Mg^{2+} transport in the absence of HNF1β.

The role of FAM111A in Ca^{2+} and Mg^{2+} reabsorption

Mutations in FAM111A are responsible for the autosomal dominant Kenny-Caffey syndrome type 2.[98] Patients suffer from severe short stature, gracile bones, hypoparathyroidism, hypocalcemia and hypomagnesemia.[99, 100] A previous study shows that the hypomagnesemia could be the primary symptom in the KCS2 syndrome.[101]

Both the DCT and TAL segments of the kidney are crucial for Mg^{2+} reabsorption. The aim of **chapter 4** was therefore to investigate the role of FAM111A in the kidney. RNA-seq analysis of an immortalized DCT cell line revealed that transcription factor *Stat1* was upregulated in the absence of *Fam111a*. This was later confirmed by RT-qPCR in *Fam111a* knockdown experiments. Furthermore, STAT1 was identified as a potential binding partner of FAM111A.

As of yet the function of FAM111A remains quite elusive. An earlier study determined that FAM111A has anti-viral properties.[102] Pathway analysis, performed on the RNA-seq data of **chapter 4**, indeed confirmed enrichment in several anti-viral pathways, including the upregulation of the *Stat1* gene. It was however surprising to find that STAT1 was the only confirmed FAM111A binding partner. As a recent study concluded that FAM111A was an important binding partner of proliferating cell nuclear factor antigen 1 (*PCNA1*).[103] Cells that were lacking FAM111A displayed low levels of chromatin-bound PCNA and impaired replication. GFP-tagged FAM111A also co-localized with PCNA on replication sites and GST-pulldown experiments displayed FAM111A directly interacting with PCNA.[103] However, PCNA was not identified as a binding partner of FAM111A in our eGFP-pulldown experiments and it remained unclear why PCNA binding was not observed. Despite these discrepant results, the binding of STAT1 to FAM111A remains of high interest for further investigation.

Transcription factor STAT1 is known as a transcriptional activator of the CaSR,[68] and could conceivably contribute to the KCS2 syndrome. A first clue can be found in patients suffering from severe burns and sepsis, which are prone to develop hypocalcemia due to CaSR upregulation induced by the STAT1/STAT3 pathway in response to Interleukin-6 (IL-6) signaling.[104, 105] Increased expression of STAT1 due to aberrant FAM111A functioning could therefore induce a similar response in KCS2 patients by increasing CaSR expression in the TAL. Activating mutations in the CaSR are well known to cause autosomal dominant hypocalcemia (ADH: OMIM 601198) together with hypomagnesemia and hypoparathyroidism.[106] A phenotype that closely resembles the electrolyte disorder seen in KCS2 patients. As increased CaSR signaling decreases PTH release from the parathyroid, which subsequently reduces Ca^{2+} and Mg^{2+} reabsorption in the kidney and resorption in bone.

First, it is crucial to establish whether STAT1 is an actual binding partner of FAM111A by performing co-immunoprecipitation experiments.[98, 107] Additionally, this provides the means to assess the effect on STAT1 binding of other point mutation and deletions found in KCS2 patients. The eGFP-pulldown experiment in **chapter 4** determined that the FAM111A R569H hotspot mutation did not affect binding of STAT1 to FAM111A. However, the mutation could still affect FAM111A-STAT1 functioning. Overexpressing the R569H mutant in a cell model could elucidate the effect of the FAM111A mutant on STAT1 expression and activity. The MKTAL cell model would be ideal as CaSR expression levels could also be determined. However,

this cell line is notoriously difficult to transfect (Kompatscher et al. unpublished data). Furthermore, knockdown of *Fam111a* in the MKTAL cell line did not increase *Casr* expression. This could mean that FAM111A does not affect CaSR expression. However, an *in vitro* cell model like the MKTAL cell line has limitations. Especially when it comes to assessing ion transport in these cells. Since it was not possible to measure changes in ion selectivity and permeability in the MKTAL cells using an Ussing chamber setup.[88] To fully elucidate the role of FAM111A in Ca^{2+} and Mg^{2+} handling a KO mouse model is required.

Careful phenotyping of a FAM111A KO mouse model will be crucial to determine whether serum Ca^{2+}, Mg^{2+} and PTH levels mimic the situation in KCS2 patients. To assess whether there is a renal defect, 24-hour urine should be collected to determine potential renal Ca^{2+} and Mg^{2+} wasting. As a renal defect would confirm that the loss of Ca^{2+} and Mg^{2+} in KCS2 originates from the kidney. *Stat1* and *Casr* levels can also be easily determined in FAM111A KO mice, which should be significantly increased. Parathyroid tissue can also be harvested to assess *Stat1* and *Casr* mRNA levels. Rescue experiments with CaSR anatagonists like NPS-2143 could establish whether the low Ca^{2+} and Mg^{2+} symptoms are fully STAT1-CaSR dependent or whether there are other mechanisms involved.[108] Additional transcriptome analysis of parathyroid and kidney tissue would provide an overview of additional pathways that might be affected by the complete loss of FAM111A in mice. There is a risk that the FAM111A KO mice will suffer from early life lethality. This was observed in patients with osteocraniostenosis, which have more pronounced defects in FAM111A.[98] In this case, heterozygous FAM111A KO mice should be assessed to investigate whether these mice develop a mild KCS2 phenotype.

Nonetheless, a first step has been taken to understand FAM111As' role in KCS2 syndrome. Further *in vitro* experiments are required to validate the novel interaction with STAT1. Additionally, a FAM111A KO mouse model is necessary to discern the effects of FAM111A loss on Ca^{2+} and Mg^{2+} uptake in the intestines, reabsorption in the kidney and regulation from the parathyroid.

Future perspectives

Ion transport in the nephron is highly dependent on the activity and availability of ion channels and transporters. Much is known about the factors regulating the activity of these channels. In contrast, little research is directed towards elucidating the transcriptional networks that regulate the expression of ion channels and transporters in the kidney. The studies reported in this thesis give insight into these transcriptional mechanisms. This thesis focused on elucidating novel transcriptional targets of HNF1β. A chIP-seq for HNF1β on immortalized DCT material allowed for the

identification of two novel targets that are key regulators of Ca^{2+} and Mg^{2+} transport in both the DCT and TAL, respectively. Firmly establishing HNF1β as a master regulator of electrolyte transport in these segments. The next step would be to further elucidate these mechanisms and show that loss of HNF1β indeed causes a reduction in NCC activity and transcription. It is further relevant to investigate how transcription of the Kir4.1 subunit is affected due to loss of HNF1β, since direct regulation can be excluded. Accurate *in vitro* models for the DCT will be key in elucidating these pathways. Except for indirect regulation via transcription factor HNF1β, it is unknown what other transcription factors or miRNAs regulate directly the transcription and translation of key transporters and channels like NCC or TRPM6 in DCT. Powerful new sequencing technologies have been developed like 4C-seq that are able to determine all interacting regions of the genome with a certain target sequence. This allows for the identification of novel transcription factors and regulatory proteins that interact with this target sequence. This can be combined with reverse chIP-seq experiments were for example proteins interacting with the TRPM6 promoter sequence are pulled down and identified by mass-spectrometry.[109] These findings could enhance our understanding of the transcriptional mechanisms regulating these key ion transporters and channels.

In the TAL, our findings show that HNF1β regulates CaSR transcription. It is, however, unclear what the effect is on ion transport in TAL. Injecting HNF1β KO mice with CaSR agonist cinacalcet and measuring Ca^{2+} and Mg^{2+} values in blood and urine, might provide more insight in how the loss of HNF1β affects CaSR signaling and what effect this has on *Cldn* expression and tight junction formation. Although as discussed previously HNF1β KO models develop a severe cystic phenotype and early lethality, which hampers this type of study. An alternative would be to investigate the effect of HNF1β loss on CaSR signaling and paracellular transport in an *in vitro* model. However as of yet, an *in vitro* model to measure changes in paracellular Na^{+} and Mg^{2+} selectivity is not available.

In conclusion, elucidating the transcriptional networks that regulate Ca^{2+} and Mg^{2+} reabsorption in the kidney is key to understanding how and by which transcription factors, transporters and channels are regulated at the transcriptional level. This provides new targets and insights in treating highly heterogeneous and complex inherited diseases like ADTKD-HNF1β.

References

1. Dai LJ, Kang HS, Kerstan D*, et al.* ATP inhibits Mg(2+) uptake in MDCT cells via P2X purinoceptors. *American journal of physiology Renal physiology* 2001; **281:** F833-840.
2. de Baaij JH, Groot Koerkamp MJ, Lavrijsen M*, et al.* Elucidation of the distal convoluted tubule transcriptome identifies new candidate genes involved in renal Mg(2+) handling. *American journal of physiology Renal physiology* 2013; **305:** F1563-1573.
3. de Baaij JH, Blanchard MG, Lavrijsen M*, et al.* P2X4 receptor regulation of transient receptor potential melastatin type 6 (TRPM6) Mg2+ channels. *Pflugers Archiv : European journal of physiology* 2014; **466:** 1941-1952.
4. Wilkinson P, Sengerova J, Matteoni R*, et al.* EMMA--mouse mutant resources for the international scientific community. *Nucleic acids research* 2010; **38:** D570-576.
5. Le KT, Babinski K, Seguela P. Central P2X4 and P2X6 channel subunits coassemble into a novel heteromeric ATP receptor. *The Journal of neuroscience : the official journal of the Society for Neuroscience* 1998; **18:** 7152-7159.
6. Torres GE, Egan TM, Voigt MM. Hetero-oligomeric assembly of P2X receptor subunits. Specificities exist with regard to possible partners. *The Journal of biological chemistry* 1999; **274:** 6653-6659.
7. Antonio LS, Stewart AP, Varanda WA*, et al.* Identification of P2X2/P2X4/P2X6 heterotrimeric receptors using atomic force microscopy (AFM) imaging. *FEBS Lett* 2014; **588:** 2125-2128.
8. Ormond SJ, Barrera NP, Qureshi OS*, et al.* An uncharged region within the N terminus of the P2X6 receptor inhibits its assembly and exit from the endoplasmic reticulum. *Molecular pharmacology* 2006; **69:** 1692-1700.
9. Hausmann R, Bodnar M, Woltersdorf R*, et al.* ATP binding site mutagenesis reveals different subunit stoichiometry of functional P2X2/3 and P2X2/6 receptors. *The Journal of biological chemistry* 2012; **287:** 13930-13943.
10. Banfi C, Ferrario S, De Vincenti O*, et al.* P2 receptors in human heart: upregulation of P2X6 in patients undergoing heart transplantation, interaction with TNFalpha and potential role in myocardial cell death. *Journal of molecular and cellular cardiology* 2005; **39:** 929-939.
11. Diaz-Hernandez JI, Sebastian-Serrano A, Gomez-Villafuertes R*, et al.* Age-Related Nuclear Translocation of P2X6 Subunit Modifies Splicing Activity Interacting with Splicing Factor 3A1. *PloS one* 2015; **10:** e0123121.
12. Lindner TH, Njolstad PR, Horikawa Y*, et al.* A novel syndrome of diabetes mellitus, renal dysfunction and genital malformation associated with a partial deletion of the pseudo-POU domain of hepatocyte nuclear factor-1beta. *Human molecular genetics* 1999; **8:** 2001-2008.
13. Bingham C, Bulman MP, Ellard S*, et al.* Mutations in the hepatocyte nuclear factor-1beta gene are associated with familial hypoplastic glomerulocystic kidney disease. *American journal of human genetics* 2001; **68:** 219-224.
14. Bingham C, Ellard S, Cole TR*, et al.* Solitary functioning kidney and diverse genital tract malformations associated with hepatocyte nuclear factor-1beta mutations. *Kidney international* 2002; **61:** 1243-1251.
15. Thomas R, Sanna-Cherchi S, Warady BA*, et al.* HNF1B and PAX2 mutations are a common cause of renal hypodysplasia in the CKiD cohort. *Pediatric nephrology* 2011; **26:** 897-903.
16. Adalat S, Woolf AS, Johnstone KA*, et al.* HNF1B mutations associate with hypomagnesemia and renal magnesium wasting. *Journal of the American Society of Nephrology : JASN* 2009; **20:** 1123-1131.
17. Ferre S, Bongers EM, Sonneveld R*, et al.* Early development of hyperparathyroidism due to loss of PTH transcriptional repression in patients with HNF1beta mutations? *The Journal of clinical endocrinology and metabolism* 2013; **98:** 4089-4096.
18. van der Made CI, Hoorn EJ, de la Faille R*, et al.* Hypomagnesemia as First Clinical Manifestation of ADTKD-HNF1B: A Case Series and Literature Review. *American journal of nephrology* 2015; **42:** 85-90.
19. Gresh L, Fischer E, Reimann A*, et al.* A transcriptional network in polycystic kidney disease. *The EMBO journal* 2004; **23:** 1657-1668.
20. Williams SS, Cobo-Stark P, Hajarnis S*, et al.* Tissue-specific regulation of the mouse Pkhd1 (ARPKD) gene promoter. *American journal of physiology Renal physiology* 2014; **307:** F356-368.

21. Faguer S, Decramer S, Devuyst O*, et al.* Expression of renal cystic genes in patients with HNF1B mutations. *Nephron Clinical practice* 2012; **120:** c71-78.
22. Gong Y, Ma Z, Patel V*, et al.* HNF-1beta regulates transcription of the PKD modifier gene Kif12. *Journal of the American Society of Nephrology : JASN* 2009; **20:** 41-47.
23. Ferre S, Veenstra GJ, Bouwmeester R*, et al.* HNF-1B specifically regulates the transcription of the gammaa-subunit of the Na+/K+-ATPase. *Biochemical and biophysical research communications* 2011; **404:** 284-290.
24. Arystarkhova E, Wetzel RK, Asinovski NK*, et al.* The gamma subunit modulates Na(+) and K(+) affinity of the renal Na,K-ATPase. *The Journal of biological chemistry* 1999; **274:** 33183-33185.
25. Meij IC, Koenderink JB, van Bokhoven H*, et al.* Dominant isolated renal magnesium loss is caused by misrouting of the Na(+),K(+)-ATPase gamma-subunit. *Nature genetics* 2000; **26:** 265-266.
26. de Baaij JH, Dorresteijn EM, Hennekam EA*, et al.* Recurrent FXYD2 p.Gly41Arg mutation in patients with isolated dominant hypomagnesaemia. *Nephrology, dialysis, transplantation : official publication of the European Dialysis and Transplant Association - European Renal Association* 2015.
27. Arystarkhova E, Wetzel RK, Sweadner KJ. Distribution and oligomeric association of splice forms of Na(+)-K(+)-ATPase regulatory gamma-subunit in rat kidney. *American journal of physiology Renal physiology* 2002; **282:** F393-407.
28. Arystarkhova E, Sweadner KJ. Splice variants of the gamma subunit (FXYD2) and their significance in regulation of the Na, K-ATPase in kidney. *J Bioenerg Biomembr* 2005; **37:** 381-386.
29. Verdeguer F, Le Corre S, Fischer E*, et al.* A mitotic transcriptional switch in polycystic kidney disease. *Nature medicine* 2010; **16:** 106-110.
30. Massie CE, Mills IG. Mapping protein-DNA interactions using ChIP-sequencing. *Methods Mol Biol* 2012; **809:** 157-173.
31. Park PJ. ChIP-seq: advantages and challenges of a maturing technology. *Nature reviews Genetics* 2009; **10:** 669-680.
32. Aboudehen K, Kim MS, Mitsche M*, et al.* Transcription Factor Hepatocyte Nuclear Factor-1beta Regulates Renal Cholesterol Metabolism. *Journal of the American Society of Nephrology : JASN* 2016; **27:** 2408-2421.
33. Aboudehen K, Noureddine L, Cobo-Stark P*, et al.* Hepatocyte Nuclear Factor-1beta Regulates Urinary Concentration and Response to Hypertonicity. *Journal of the American Society of Nephrology : JASN* 2017; **28:** 2887-2900.
34. Hajarnis SS, Patel V, Aboudehen K*, et al.* Transcription Factor Hepatocyte Nuclear Factor-1beta (HNF-1beta) Regulates MicroRNA-200 Expression through a Long Noncoding RNA. *The Journal of biological chemistry* 2015; **290:** 24793-24805.
35. Lokmane L, Heliot C, Garcia-Villalba P*, et al.* vHNF1 functions in distinct regulatory circuits to control ureteric bud branching and early nephrogenesis. *Development* 2010; **137:** 347-357.
36. Heliot C, Desgrange A, Buisson I*, et al.* HNF1B controls proximal-intermediate nephron segment identity in vertebrates by regulating Notch signalling components and Irx1/2. *Development* 2013; **140:** 873-885.
37. Desgrange A, Heliot C, Skovorodkin I*, et al.* HNF1B controls epithelial organization and cell polarity during ureteric bud branching and collecting duct morphogenesis. *Development* 2017.
38. Fischer E, Legue E, Doyen A*, et al.* Defective planar cell polarity in polycystic kidney disease. *Nature genetics* 2006; **38:** 21-23.
39. Terker AS, Zhang C, McCormick JA*, et al.* Potassium modulates electrolyte balance and blood pressure through effects on distal cell voltage and chloride. *Cell Metab* 2015; **21:** 39-50.
40. Schultheis PJ, Lorenz JN, Meneton P*, et al.* Phenotype resembling Gitelman's syndrome in mice lacking the apical Na+-Cl- cotransporter of the distal convoluted tubule. *The Journal of biological chemistry* 1998; **273:** 29150-29155.
41. Nijenhuis T, Vallon V, van der Kemp AW*, et al.* Enhanced passive Ca2+ reabsorption and reduced Mg2+ channel abundance explains thiazide-induced hypocalciuria and hypomagnesemia. *The Journal of clinical investigation* 2005; **115:** 1651-1658.
42. Bockenhauer D, Feather S, Stanescu HC*, et al.* Epilepsy, ataxia, sensorineural deafness, tubulopathy, and KCNJ10 mutations. *N Engl J Med* 2009; **360:** 1960-1970.

43. Reichold M, Zdebik AA, Lieberer E*, et al.* KCNJ10 gene mutations causing EAST syndrome (epilepsy, ataxia, sensorineural deafness, and tubulopathy) disrupt channel function. *Proceedings of the National Academy of Sciences of the United States of America* 2010; **107:** 14490-14495.
44. Scholl UI, Choi M, Liu T*, et al.* Seizures, sensorineural deafness, ataxia, mental retardation, and electrolyte imbalance (SeSAME syndrome) caused by mutations in KCNJ10. *Proceedings of the National Academy of Sciences of the United States of America* 2009; **106:** 5842-5847.
45. Cuevas CA, Su XT, Wang MX*, et al.* Potassium Sensing by Renal Distal Tubules Requires Kir4.1. *Journal of the American Society of Nephrology : JASN* 2017.
46. McCormick JA, Mutig K, Nelson JH*, et al.* A SPAK isoform switch modulates renal salt transport and blood pressure. *Cell Metab* 2011; **14:** 352-364.
47. Grimm PR, Taneja TK, Liu J*, et al.* SPAK isoforms and OSR1 regulate sodium-chloride co-transporters in a nephron-specific manner. *The Journal of biological chemistry* 2012; **287:** 37673-37690.
48. Yang SS, Lo YF, Wu CC*, et al.* SPAK-knockout mice manifest Gitelman syndrome and impaired vaso-constriction. *Journal of the American Society of Nephrology : JASN* 2010; **21:** 1868-1877.
49. Kompatscher A, de Baaij JHF, Aboudehen K*, et al.* Loss of transcriptional activation of the potassium channel Kir5.1 by HNF1beta drives autosomal dominant tubulointerstitial kidney disease. *Kidney international* 2017; **92:** 1145-1156.
50. Bech AP, Wetzels JF, Bongers EM*, et al.* Thiazide Responsiveness Testing in Patients With Renal Magnesium Wasting and Correlation With Genetic Analysis: A Diagnostic Test Study. *American journal of kidney diseases : the official journal of the National Kidney Foundation* 2016; **68:** 168-170.
51. Paulais M, Bloch-Faure M, Picard N*, et al.* Renal phenotype in mice lacking the Kir5.1 (Kcnj16) K+ channel subunit contrasts with that observed in SeSAME/EAST syndrome. *Proceedings of the National Academy of Sciences of the United States of America* 2011; **108:** 10361-10366.
52. Lachheb S, Cluzeaud F, Bens M*, et al.* Kir4.1/Kir5.1 channel forms the major K+ channel in the basolateral membrane of mouse renal collecting duct principal cells. *American journal of physiology Renal physiology* 2008; **294:** F1398-1407.
53. Lourdel S, Paulais M, Cluzeaud F*, et al.* An inward rectifier K(+) channel at the basolateral membrane of the mouse distal convoluted tubule: similarities with Kir4-Kir5.1 heteromeric channels. *J Physiol* 2002; **538:** 391-404.
54. Tanemoto M, Kittaka N, Inanobe A*, et al.* In vivo formation of a proton-sensitive K+ channel by heteromeric subunit assembly of Kir5.1 with Kir4.1. *J Physiol* 2000; **525 Pt 3:** 587-592.
55. Yang Z, Xu H, Cui N*, et al.* Biophysical and molecular mechanisms underlying the modulation of heteromeric Kir4.1-Kir5.1 channels by CO2 and pH. *J Gen Physiol* 2000; **116:** 33-45.
56. Palygin O, Levchenko V, Ilatovskaya DV*, et al.* Essential role of Kir5.1 channels in renal salt handling and blood pressure control. *JCI Insight* 2017; **2**.
57. Zhao Z, Tavoosidana G, Sjolinder M*, et al.* Circular chromosome conformation capture (4C) uncovers extensive networks of epigenetically regulated intra- and interchromosomal interactions. *Nature genetics* 2006; **38:** 1341-1347.
58. Simonis M, Klous P, Splinter E*, et al.* Nuclear organization of active and inactive chromatin domains uncovered by chromosome conformation capture-on-chip (4C). *Nature genetics* 2006; **38:** 1348-1354.
59. Li G, Cai L, Chang H*, et al.* Chromatin Interaction Analysis with Paired-End Tag (ChIA-PET) sequencing technology and application. *BMC Genomics* 2014; **15 Suppl 12:** S11.
60. Milatz S, Himmerkus N, Wulfmeyer VC*, et al.* Mosaic expression of claudins in thick ascending limbs of Henle results in spatial separation of paracellular Na+ and Mg2+ transport. *Proceedings of the National Academy of Sciences of the United States of America* 2017; **114:** E219-E227.
61. Bleich M, Wulfmeyer VC, Himmerkus N*, et al.* Heterogeneity of tight junctions in the thick ascending limb. *Ann N Y Acad Sci* 2017.
62. Gunzel D, Haisch L, Pfaffenbach S*, et al.* Claudin function in the thick ascending limb of Henle's loop. *Ann N Y Acad Sci* 2009; **1165:** 152-162.
63. Zhang C, Wang L, Su XT*, et al.* KCNJ10 (Kir4.1) is expressed in the basolateral membrane of the cortical thick ascending limb. *American journal of physiology Renal physiology* 2015; **308:** F1288-1296.

64. Brown EM, Gamba G, Riccardi D*, et al.* Cloning and characterization of an extracellular Ca(2+)-sensing receptor from bovine parathyroid. *Nature* 1993; **366:** 575-580.
65. Chakravarti B, Chattopadhyay N, Brown EM. Signaling through the extracellular calcium-sensing receptor (CaSR). *Adv Exp Med Biol* 2012; **740:** 103-142.
66. Friedman PA, Gesek FA. Cellular calcium transport in renal epithelia: measurement, mechanisms, and regulation. *Physiological reviews* 1995; **75:** 429-471.
67. Houillier P. Calcium-sensing in the kidney. *Current opinion in nephrology and hypertension* 2013; **22:** 566-571.
68. Hendy GN, Canaff L, Cole DE. The CASR gene: alternative splicing and transcriptional control, and calcium-sensing receptor (CaSR) protein: structure and ligand binding sites. *Best practice & research Clinical endocrinology & metabolism* 2013; **27:** 285-301.
69. Chikatsu N, Fukumoto S, Takeuchi Y*, et al.* Cloning and characterization of two promoters for the human calcium-sensing receptor (CaSR) and changes of CaSR expression in parathyroid adenomas. *The Journal of biological chemistry* 2000; **275:** 7553-7557.
70. Aida K, Koishi S, Tawata M*, et al.* Molecular cloning of a putative Ca(2+)-sensing receptor cDNA from human kidney. *Biochemical and biophysical research communications* 1995; **214:** 524-529.
71. Faguer S, Decramer S, Chassaing N*, et al.* Diagnosis, management, and prognosis of HNF1B nephropathy in adulthood. *Kidney international* 2011; **80:** 768-776.
72. de Groot T, Lee K, Langeslag M*, et al.* Parathyroid hormone activates TRPV5 via PKA-dependent phosphorylation. *Journal of the American Society of Nephrology : JASN* 2009; **20:** 1693-1704.
73. Hoover RS, Tomilin V, Hanson L*, et al.* PTH modulation of NCC activity regulates TRPV5 Ca2+ reabsorption. *American journal of physiology Renal physiology* 2016; **310:** F144-151.
74. Nemeth EF, Steffey ME, Fox J. The parathyroid calcium receptor: a novel therapeutic target for treating hyperparathyroidism. *Pediatric nephrology* 1996; **10:** 275-279.
75. Goodman WG, Hladik GA, Turner SA*, et al.* The Calcimimetic agent AMG 073 lowers plasma parathyroid hormone levels in hemodialysis patients with secondary hyperparathyroidism. *Journal of the American Society of Nephrology : JASN* 2002; **13:** 1017-1024.
76. Canaff L, Hendy GN. Human calcium-sensing receptor gene. Vitamin D response elements in promoters P1 and P2 confer transcriptional responsiveness to 1,25-dihydroxyvitamin D. *The Journal of biological chemistry* 2002; **277:** 30337-30350.
77. Canaff L, Zhou X, Mosesova I*, et al.* Glial cells missing-2 (GCM2) transactivates the calcium-sensing receptor gene: effect of a dominant-negative GCM2 mutant associated with autosomal dominant hypoparathyroidism. *Hum Mutat* 2009; **30:** 85-92.
78. Gong Y, Renigunta V, Himmerkus N*, et al.* Claudin-14 regulates renal Ca(+)(+) transport in response to CaSR signalling via a novel microRNA pathway. *The EMBO journal* 2012; **31:** 1999-2012.
79. Gong Y, Hou J. Claudin-14 underlies Ca(+)(+)-sensing receptor-mediated Ca(+)(+) metabolism via NFAT-microRNA-based mechanisms. *Journal of the American Society of Nephrology : JASN* 2014; **25:** 745-760.
80. Dimke H, Desai P, Borovac J*, et al.* Activation of the Ca(2+)-sensing receptor increases renal claudin-14 expression and urinary Ca(2+) excretion. *American journal of physiology Renal physiology* 2013; **304:** F761-769.
81. Plain A, Wulfmeyer VC, Milatz S*, et al.* Corticomedullary difference in the effects of dietary Ca(2)(+) on tight junction properties in thick ascending limbs of Henle's loop. *Pflugers Archiv : European journal of physiology* 2016; **468:** 293-303.
82. Gong Y, Himmerkus N, Plain A*, et al.* Epigenetic regulation of microRNAs controlling CLDN14 expression as a mechanism for renal calcium handling. *Journal of the American Society of Nephrology : JASN* 2015; **26:** 663-676.
83. Hou J, Renigunta A, Gomes AS*, et al.* Claudin-16 and claudin-19 interaction is required for their assembly into tight junctions and for renal reabsorption of magnesium. *Proc Natl Acad Sci U S A* 2009; **106:** 15350-15355.
84. Breiderhoff T, Himmerkus N, Stuiver M*, et al.* Deletion of claudin-10 (Cldn10) in the thick ascending limb impairs paracellular sodium permeability and leads to hypermagnesemia and nephrocalcinosis. *Proceedings of the National Academy of Sciences of the United States of America* 2012; **109:** 14241-14246.

85. Bongers E, Shelton LM, Milatz S*, et al.* A Novel Hypokalemic-Alkalotic Salt-Losing Tubulopathy in Patients with CLDN10 Mutations. *Journal of the American Society of Nephrology : JASN* 2017; **28:** 3118-3128.
86. Vezzoli G, Terranegra A, Aloia A*, et al.* Decreased transcriptional activity of calcium-sensing receptor gene promoter 1 is associated with calcium nephrolithiasis. *The Journal of clinical endocrinology and metabolism* 2013; **98:** 3839-3847.
87. Bourgeois S, Rossignol P, Grelac F*, et al.* Differentiated thick ascending limb (TAL) cultured cells derived from SV40 transgenic mice express functional apical NHE2 isoform: effect of nitric oxide. *Pflugers Archiv : European journal of physiology* 2003; **446:** 672-683.
88. Kompatscher A, de Baaij JHF, Aboudehen K*, et al.* Transcription factor HNF1beta regulates expression of the calcium-sensing receptor in the thick ascending limb of the kidney. *American journal of physiology Renal physiology* 2018.
89. Gesek FA, Friedman PA. Mechanism of calcium transport stimulated by chlorothiazide in mouse distal convoluted tubule cells. *The Journal of clinical investigation* 1992; **90:** 429-438.
90. Pizzonia JH, Gesek FA, Kennedy SM*, et al.* Immunomagnetic separation, primary culture, and characterization of cortical thick ascending limb plus distal convoluted tubule cells from mouse kidney. *In Vitro Cell Dev Biol* 1991; **27A:** 409-416.
91. Duong Van Huyen JP, Bens M, Teulon J*, et al.* Vasopressin-stimulated chloride transport in transimmortalized mouse cell lines derived from the distal convoluted tubule and cortical and inner medullary collecting ducts. *Nephrology, dialysis, transplantation : official publication of the European Dialysis and Transplant Association - European Renal Association* 2001; **16:** 238-245.
92. Richardson C, Rafiqi FH, Karlsson HK*, et al.* Activation of the thiazide-sensitive Na+-Cl- cotransporter by the WNK-regulated kinases SPAK and OSR1. *Journal of cell science* 2008; **121:** 675-684.
93. San-Cristobal P, Pacheco-Alvarez D, Richardson C*, et al.* Angiotensin II signaling increases activity of the renal Na-Cl cotransporter through a WNK4-SPAK-dependent pathway. *Proceedings of the National Academy of Sciences of the United States of America* 2009; **106:** 4384-4389.
94. Sohara E, Rai T, Yang SS*, et al.* Acute insulin stimulation induces phosphorylation of the Na-Cl cotransporter in cultured distal mpkDCT cells and mouse kidney. *PloS one* 2011; **6:** e24277.
95. Ko B, Mistry AC, Hanson L*, et al.* A new model of the distal convoluted tubule. *American journal of physiology Renal physiology* 2012; **303:** F700-710.
96. Richards J, Ko B, All S*, et al.* A role for the circadian clock protein Per1 in the regulation of the NaCl co-transporter (NCC) and the with-no-lysine kinase (WNK) cascade in mouse distal convoluted tubule cells. *The Journal of biological chemistry* 2014; **289:** 11791-11806.
97. Ko B, Mistry A, Hanson L*, et al.* Mechanisms of angiotensin II stimulation of NCC are time-dependent in mDCT15 cells. *American journal of physiology Renal physiology* 2015; **308:** F720-727.
98. Unger S, Gorna MW, Le Bechec A*, et al.* FAM111A mutations result in hypoparathyroidism and impaired skeletal development. *Am J Hum Genet* 2013; **92:** 990-995.
99. Kenny FM, Linarelli L. Dwarfism and cortical thickening of tubular bones. Transient hypocalcemia in a mother and son. *Am J Dis Child* 1966; **111:** 201-207.
100. Caffey J. Congenital stenosis of medullary spaces in tubular bones and calvaria in two proportionate dwarfs--mother and son; coupled with transitory hypocalcemic tetany. *Am J Roentgenol Radium Ther Nucl Med* 1967; **100:** 1-11.
101. Isojima T, Doi K, Mitsui J*, et al.* A recurrent de novo FAM111A mutation causes Kenny-Caffey syndrome type 2. *J Bone Miner Res* 2014; **29:** 992-998.
102. Fine DA, Rozenblatt-Rosen O, Padi M*, et al.* Identification of FAM111A as an SV40 host range restriction and adenovirus helper factor. *PLoS Pathog* 2012; **8:** e1002949.
103. Alabert C, Bukowski-Wills JC, Lee SB*, et al.* Nascent chromatin capture proteomics determines chromatin dynamics during DNA replication and identifies unknown fork components. *Nat Cell Biol* 2014; **16:** 281-293.
104. Murphey ED, Chattopadhyay N, Bai M*, et al.* Up-regulation of the parathyroid calcium-sensing receptor after burn injury in sheep: a potential contributory factor to postburn hypocalcemia. *Crit Care Med* 2000; **28:** 3885-3890.

105. Steele T, Kolamunnage-Dona R, Downey C*, et al.* Assessment and clinical course of hypocalcemia in critical illness. *Crit Care* 2013; **17:** R106.
106. Thakker RV. Genetic developments in hypoparathyroidism. *Lancet* 2001; **357:** 974-976.
107. Abraham MB, Li D, Tang D*, et al.* Short stature and hypoparathyroidism in a child with Kenny-Caffey syndrome type 2 due to a novel mutation in FAM111A gene. *Int J Pediatr Endocrinol* 2017; **2017:** 1.
108. Hannan FM, Walls GV, Babinsky VN*, et al.* The Calcilytic Agent NPS 2143 Rectifies Hypocalcemia in a Mouse Model With an Activating Calcium-Sensing Receptor (CaSR) Mutation: Relevance to Autosomal Dominant Hypocalcemia Type 1 (ADH1). *Endocrinology* 2015; **156:** 3114-3121.
109. Dejardin J, Kingston RE. Purification of proteins associated with specific genomic Loci. *Cell* 2009; **136:** 175-186.

7 Nederlandse samenvatting

Inleiding

Een adequate Ca^{2+} en Mg^{2+} balans in het lichaam is essentieel voor het functioneren van verschillende intra- en extracellulaire processen, zoals enzymatische activiteit, metabolisme, botformatie en neuronale excitatie. Hierbij zijn de darmen verantwoordelijk voor de opname van Ca^{2+} en Mg^{2+} uit het voedsel, fungeert het bot als een reservoir voor de opslag van deze mineralen en bepalen de nieren hoeveel Ca^{2+} en Mg^{2+} uitgescheiden wordt via de urine. De bijschildklier dirigeert de afgifte van hormonen die opname en excretie van Ca^{2+} en Mg^{2+} reguleren uit het bot en de nieren.

In de nier wordt bloed gefiltreerd in de glomerulus waardoor Ca^{2+} en Mg^{2+} terechtkomen in de voorurine in de nierbuis. Deze nierbuis is opgedeeld in verscheidene segmenten, die op verschillende manieren ionen resorberen. Het overgrote deel van het Ca^{2+} en Mg^{2+} wordt tussen de cellen door (paracellulair) geresorbeerd in de proximale tubulus en het stijgende deel van de lis van Henle (TAL). Hierna wordt de definitieve uitscheiding van het Ca^{2+} en Mg^{2+} bepaald door deze ionen actief door het epitheel te transporteren (transcellulair). Voor Mg^{2+} vindt dit exclusief plaats in het distaal convoluut (DCT), terwijl Ca^{2+} transcellulair wordt geresorbeerd in de verbindingsbuis (CNT). De capaciteit voor iontransport van deze niersegmenten is afhankelijk van de hoeveelheid, samenstelling en activiteit van membraantransporteurs, ionkanalen en 'tight junction' eiwitten. Membraantransporteurs en ionkanalen zijn verantwoordelijk voor het transcellulaire transport van Ca^{2+} en Mg^{2+}. Terwijl het paracellulaire transport gereguleerd wordt door verschillende 'tight junction' eiwitten, die tussen de cellen een buisje vormen dat selectief is voor de opname van Na^{+} of Ca^{2+} en Mg^{2+}. De activiteit van membraantransporteurs en ionkanalen wordt nauwkeurig gereguleerd door signaalmoleculen, zoals paraathormoon (PTH) en 1,25-dihydroxyvitamine D_3 (VitD). Daarnaast worden lokaal moleculen zoals adenosine triphosphaat (ATP) afgegeven om het iontransport te stimuleren. Een bepalende factor in zowel het transcellulair als paracellulair iontransport is het aantal beschikbare membraantransporteurs, kanalen en 'tight junction' eiwitten in de plasmamembraan. De twee belangrijkste mechanismen om dit te reguleren zijn het rekruteren en recyclen van de eerder genoemde eiwitten naar de plasmamembraan uit een reservoir van eiwitten in het cytoplasma. Dit is een snelle response. Of het verhogen danwel verlagen van de productie van membraantransporteurs, ionkanalen en 'tight junction' eiwitten. Dit is een relatief trage response.

Het doel van dit proefschrift is om te onderzoeken hoe de productie van de eiwitten die bijdragen aan Ca^{2+} en Mg^{2+} transport in de nier, gereguleerd wordt. Eiwitten die verantwoordelijk zijn voor de aanmaak (transcriptie) van membraantransporteurs en ionkanalen worden transcriptiefactoren genoemd. Een transcriptiefactor bindt het DNA op de promotorsequentie van genen om zo de transcriptie in gang te zetten. In dit proefschrift ligt de nadruk vooral op de transcriptiefactor HNF1β,

aangezien patiënten met HNF1β deleties of mutaties lijden aan een verlaagde bloed Mg^{2+} spiegel. Het onderzoek is als volgt opgebouwd; *i*) In **hoofdstuk 2** worden alle potentiële doelwitten van HNF1β beschreven in het genoom; *ii*) Het K^+-kanaal *KCNJ16* (Kir5.1), een belangrijke speler in Mg^{2+} transport in het DCT, werd geïdentificeerd als een doelwit van de transcriptiefactor. Deze bevinding verklaart hoe HNF1β Mg^{2+} transport in het DCT reguleert; *iii*) in **hoofdstuk 3** werd het calcium-sensor receptor gen (*CaSR*) geïdentificeerd als een doelwit van HNF1β. Dit gaf nieuwe inzichten in het mechanisme waarop Ca^{2+} en Mg^{2+} geresorbeerd worden in de TAL; *iv*) in **hoofdstuk 4** werd de transcriptiefactor STAT1 geïdentificeerd als een potentiële bindingspartner van FAM111A. Deze bevinding geeft een nieuwe kijk op de functie van FAM111A met betrekking tot Ca^{2+} en Mg^{2+} resorptie in de nier; *v*) **hoofdstuk 5** toont aan dat het ATP-gevoelige P2X receptor kationkanaal P2X6 niet betrokken is bij iontransport in de nier. Een *P2x6* knock-out (KO) muismodel werd gebruikt om de gevolgen van een P2X6 tekort op het transport van Ca^{2+} en Mg^{2+} in de nier te onderzoeken.

Het ATP-gevoelige P2X6 kationkanaal is niet betrokken bij Ca^{2+} en Mg^{2+} resorptie in de nier

In **hoofdstuk 4** werd de fysiologische rol van het ATP-gevoelige P2X6 kationkanaal onderzocht met betrekking tot Mg^{2+} transport in het DCT van de nier. Uit eerder onderzoek is bekend dat P2X6 in de nier exclusief wordt aangemaakt in het DCT. *P2x6* komt eveneens verhoogt tot expressie in muizen op een laag Mg^{2+} dieet. Deze resultaten maken het plausibel dat P2X6 een bijdrage levert aan iontransport in het DCT. Het verlies van P2X6 in de muis had echter geen verlaging van bloed Ca^{2+} en Mg^{2+} waarden tot gevolg. Er werd ook geen significant verlies van Ca^{2+} en Mg^{2+} waargenomen in de urine. Daarbij was de productie van Ca^{2+}- en Mg^{2+}-gevoelige genen niet significant verschillend tussen de *P2x6* wildtype (WT) en *P2x6* KO muis. Op basis van deze studie kon een effect van P2X6 op de Ca^{2+} en Mg^{2+} transport in de nier worden uitgesloten. Wel werd er een verhoging van *P2x2* mRNA, een interactiepartner van P2X6, waargenomen in het hart. In hoeverre deze verhoging van *P2x2* mRNA compenseert voor het verlies van P2X6 en wat de functie van P2X6 is in het hart dient nog verder te worden uitgezocht. De eerder genoemde *P2x6* KO muis kan hier een bijdrage aan leveren.

De regulatie van Ca^{2+} en Mg^{2+} transport door transcriptiefactor HNF1β in het distaal convoluut van de nier

Patiënten met mutaties en deleties in transcriptiefactor HNF1β lijden aan het ADTKD-HNF1β syndroom. ADTKD-HNF1β patiënten hebben een bijzonder heterogeen fenotype bestaande uit de volgende symptomen; cystenieren, een overerfelijke vorm van diabetes, en in ~50% van de gevallen, verminderde bloed Mg^{2+} en K^+ waarden. Verder is er ook regelmatig sprake van verminderde uitscheiding van Ca^{2+}

in de urine. De rol van HNF1β in de vorming van cystenieren is veelvuldig onderzocht. Cystenieren in ADTKD-HNF1β patiënten ontstaan doordat HNF1β mutaties de transcriptie van genen als PKHD1, PKD2 en UMOD verstoren. Er is echter nog maar weinig bekend over hoe HNF1β het transport van, in het bijzonder Mg^{2+}, reguleert en waarom in ~50% van de HNF1β patiënten er een Mg^{2+} tekort in het bloed ontstaat. Het Mg^{2+} en K^+ tekort in ADTKD-HNF1β patiënten lijkt op het Gitelman syndroom; een aandoening die wordt veroorzaakt door een defect in de Na^+-Cl^- cotransporteur (NCC), die specifiek werkzaam is in het DCT.

In **hoofdstuk 2** werd HNF1β functie onderzocht in een DCT cellijn. Door een chromatine immunoprecipitatie (chIP) zijn alle plaatsen op het genoom waar HNF1β bindt geïsoleerd en geanalyseerd. In totaal zijn ~7,500 bindingsplaatsen van HNF1β geïdentificeerd, waarvan 4,530 in de nabijheid van de transcriptiestartlocatie (TSS) van genen op het genoom. De belangrijkste bevinding was de identificatie van een HNF1β-bindingsplaats in de promotor van het K^+-kanaal *KCNJ16,* dat codeert voor het eiwit Kir5.1. Om aan te tonen dat HNF1β de transcriptie van KCNJ16 reguleert, werd HNF1β eiwitproductie verstoord door het inbrengen van 'korte translatie verstorende RNAs' (siRNAs) in DCT cellen. De reductie van HNF1β expressie verminderde inderdaad de *KCNJ16* transcriptie in deze cellen. *KCNJ16* transcriptie was eveneens sterker verlaagd in een nierspecifieke HNF1β KO muis dan in HNF1β WT controle muizen.

Transcriptie van het verwante Kir4.1 K^+-kanaal was eveneens verstoord in zowel de siRNA behandelde DCT cellijn als de HNF1β KO muis. Kir4.1 vormt samen met Kir5.1 het functionele K^+-kanaal aan de bloedzijde (basolaterale kant) van het DCT. Een verminderde aanwezigheid van het K^+-kanaal leidt tot gereduceerde uitscheiding van K^+ aan de basolaterale zijde van het DCT. Voorgaand onderzoek wijst uit dat verminderde K^+- uitscheiding leidt tot verstoorde activiteit van de Na^+-Cl^- cotransporteur (NCC) aan de voorurine zijde (apicale membraan) van de DCT cel. Uit observaties in Gitelmansyndroom patiënten is bekend dat verminderde activiteit van NCC resulteert in een gereduceerde resorptie van Mg^{2+} via het Mg^{2+}-kanaal TRPM6. Het is daarom waarschijnlijk dat het Mg^{2+} en K^+ tekort in ADTKD-HNF1β patiënten veroorzaakt wordt door verlaagde transcriptie van Kir4.1/Kir5.1 K^+-kanalen. Onze resultaten wijzen uit dat HNF1β direct bind aan de Kir5.1 promotor en transcriptie van het kanaal stimuleert. Het is vooralsnog onbekend op welke wijze HNF1β de transcriptie van Kir4.1 reguleert.

De regulatie van Ca^{2+} en Mg^{2+} door de transcriptie factor HNF1β in de opstijgende lus van Henle (TAL)

ADTKD-HNF1β patiënten lijden, behalve aan verlaagde Mg^{2+} en K^+ bloed waarden, ook aan de vorming van Ca^{2+} afzettingen in de nierbuis (nefrocalcinose) doordat minder Ca^{2+} wordt uitgescheiden. Deze verstoring in Ca^{2+} resorptie kan niet volledig vanuit een defect in het DCT verklaard worden. Verder is HNF1β ook vertegenwoor-

digd in alle segmenten van de nierbuis. De TAL is het niersegment waar 70% van Mg^{2+} en 20% van Ca^{2+} wordt geresorbeerd. Verlies van HNF1β in de TAL zou kunnen leiden tot problemen met Ca^{2+} en Mg^{2+} resorptie, die symptomen als nefrocalcinosis kan verklaren.

In **hoofdstuk 3** werd het eerdere overzicht van HNF1β bindingsplaatsen in de DCT gebruikt om nieuwe genen die door HNF1β gereguleerd worden te identificeren. De meest veelbelovende bevinding was de identificatie van een HNF1β-bindingsplaats In het tweede intron van het calcium-sensor receptor (CaSR) gen. De CaSR functioneert als een sensor voor Ca^{2+} en Mg^{2+} aan de basolaterale zijde van de TAL. Als Ca^{2+} of Mg^{2+} bindt aan de CaSR wordt er een intracellulaire cascade in gang gezet die paracelullaire opname van Ca^{2+} en Mg^{2+} verlaagd. CaSR activiteit verhoogt de aanmaak van Claudine 14 (*Cldn14*), waardoor de affiniteit voor paracellulaire Na^{+} resorptie in de TAL toeneemt. Dit gaat ten koste van het Ca^{2+} en Mg^{2+} transport in de TAL. Op deze manier reguleert de CaSR de resorptie van Ca^{2+} en Mg^{2+} in het bloed.

HNF1β werd tot overexpressie gebracht in humane niercellen om aan te tonen dat HNF1β de transcriptie van de *CaSR* activeert. Alleen in de aanwezigheid van de HNF1β-bindingsplaats in de promotor van de CaSR was er verhoogde promotoractiviteit waarneembaar. De toevoeging van een HNF1β mutant die niet aan de HNF1β-bindingsplaats kon hechten, zorgde voor een significante vermindering in *CaSR* promotoractiviteit.

Deze resultaten werden bevestigd door de productie van het HNF1β eiwit te verstoren met siRNAs in een muis TAL cellijn, wat leidde tot de verwachtte daling in *Casr* mRNA. De afwezigheid van HNF1β zorgde ook voor een afname in *Cldn14* transcriptie in deze cellen. Om CaSR reductie te bevestigen *in vivo* werden experimenten in een nierspecifieke HNF1β KO muis uitgevoerd. Inderdaad CaSR transcriptie was aanzienlijk lager in de nier-specifieke HNF1β KO muis dan in de controle dieren. *Cldn14* mRNA liet echter geen afname zien, hoewel dit overeenkomt met eerder onderzoek. Alleen muizen met veel Ca^{2+} in hun dieet maken *Cldn14* aan om overmatige Ca^{2+} resorptie te remmen.

Afgezien van deze verschillen in claudine transcriptie tussen *in vitro* en *in vivo* experimenten is het duidelijk dat HNF1β bindt in het *CaSR* gen en zo de transcriptie van dit gen activeert. In ADTKD-HNF1β patiënten zou dit betekenen dat de CaSR verminderd aanwezig is in de TAL. Wat zou leiden tot een verhoogde opname van Ca^{2+} en Mg^{2+} in de TAL. Deze resultaten passen bij de verlaagde Ca^{2+} uitscheiding die wordt waargenomen in ADTKD-HNF1β patiënten.

Patiënten met ADTKD-HNF1β hebben last van nefrocalcinose. Eerder onderzoek wijst uit dat dragers van kleine genomische variaties (SNPs) in de promotorsequentie van de *CaSR* een verhoogde kans hebben op het ontwikkelen van nefrocalcinose, hetgeen wordt veroorzaakt door de verminderde aanmaak van het CaSR eiwit. Dit lijkt sterk op wat er gebeurd in ADTKD-HNF1β patiënten. Er is echter meer onderzoek

nodig naar de rol van HNF1β in Ca^{2+} en Mg^{2+} resorptie in de TAL. Hierdoor kunnen nieuwe behandelmethoden ontwikkeld worden voor ADTKD-HNF1β patiënten door bijvoorbeeld CaSR activiteit te remmen.

FAM111A is een potentiële regulator van de Ca^{2+} en Mg^{2+} resorptie in de nier

Patiënten met mutaties in FAM111A lijden aan het autosomaal dominant erfelijk Kenny-Caffey syndroom type 2 (KCS2). De meest voorkomende symptomen in deze patiënten zijn ernstige groeistoornissen, botdysplasie en sterk verminderde bloed Ca^{2+}, Mg^{2+} en paraathormoon waarden. De rol van FAM111A in het KCS2 syndroom is echter onbekend. Verstoorde resorptie van Ca^{2+} en Mg^{2+} in de nier kunnen de lage paraathormoon waarden, groeistoornissen en botdysplasie in KCS2 patiënten verklaren. Inderdaad Ca^{2+} en Mg^{2+} restrictie experimenten in patiënten tonen aan dat het Mg^{2+} tekort tot de primaire stoornis behoort in KCS2. Het onderliggende mechanisme achter dit tekort is echter nog onbekend.

In **hoofdstuk 5** werd daarom een transcriptoom analyse uitgevoerd op muis DCT cellen die behandeld waren met siRNAs tegen *Fam111a*. Deze verlaging in *Fam111a* leidde tot verhoogde expressie van verschillende antivirale genen waaronder transcriptiefactor *Stat1*, een eiwit die eveneens een rol heeft in de regulatie van het iontransport. Complementair aan de voorgaande studie werd een eiwit interactie-analyse uitgevoerd om interactiepartners van FAM111A in kaart te brengen. STAT1 kwam hier naar voren als een sterke FAM111A bindingspartner. In voorgaand onderzoek werd STAT1 geïdentificeerd als een activator van CaSR expressie. De verlaagde Ca^{2+} en Mg^{2+} waardes in het bloed van KCS2 patiënten zou daarom verklaard kunnen worden door verhoogde CaSR expressie ten gevolge van verminderde FAM111A functie. De CaSR speelt eveneens een belangrijke rol bij het uitscheiden van paraathormoon vanuit de bijschildklier. Een hormoon dat cruciaal is bij het reguleren van de excretie van Ca^{2+} en Mg^{2+} in de nieren en de opname van deze ionen in het bot. Deze mogelijke connectie tussen FAM111A en de CaSR zal echter experimenteel bewezen moeten worden voordat conclusies getrokken kunnen worden over de rol van FAM111A bij Ca^{2+} en Mg^{2+} resorptie.

Vervolgonderzoek zal moeten uitwijzen of FAM111A inderdaad bindt aan STAT1 en of de FAM111A mutaties deze verbinding verstoren. Verder zal onderzocht moeten worden of verhoogde STAT1 expressie inderdaad TAL transport van Ca^{2+} en Mg^{2+} beïnvloed en of dit via regulatie van de CaSR gebeurt. Een FAM111A KO muismodel kan meer inzicht verschaffen in de gevolgen van FAM111A deficiëntie voor ionresorptie in de nier. Transcriptoom analyse in de nier en bijschildklier van de FAM111A KO muis zou eveneens mechanismen kunnen blootleggen waarmee de rol van FAM111A in Ca^{2+} en Mg^{2+} resorptie verklaard kan worden.

Toekomstperspectieven

Dit proefschrift geeft nieuwe inzichten in de wijze waarop Ca^{2+} en Mg^{2+} resorptie gereguleerd wordt op transcriptioneel niveau in zowel de TAL als het DCT. Een gedetailleerde analyse in een muis DCT cellijn van alle bindingsplaatsen voor HNF1β, identificeerde twee nieuwe genen die gereguleerd worden door deze transcriptiefactor. Het Kir5.1 K^+-kanaal is belangrijk voor de adequate resorptie van Mg^{2+} in het DCT, terwijl de CaSR cruciaal is voor het reguleren van de paracellulaire opname van Ca^{2+} en Mg^{2+} in de TAL. In vervolgonderzoek is het belangrijk om de consequenties voor Ca^{2+} en Mg^{2+} resorptie verder te analyseren om zo meer inzicht te krijgen in het ziektebeeld van ADTKD-HNF1β patiënten.

Een volgende stap zou zijn om causaal te kunnen aantonen dat een tekort aan HNF1β inderdaad een verlaging van NCC activiteit en transcriptie veroorzaakt in de patiënten. Dit zou uitgevoerd kunnen worden door urine te verzamelen van deze patiënten. Om vervolgens uit deze urine de zogenaamde 'exosoom' membraanblaasjes te isoleren. Hierin kan dan de hoeveelheid NCC eiwit gemeten worden. De verwachting is dat ADTKD-HNF1β patiënten minder NCC bezitten door het tekort aan goedfunctionerend HNF1β in deze patiënten. Een tekort aan NCC verklaart de verminderde Mg^{2+} resorptie in deze patiënten in het DCT.

Verder is het zeer relevant om te onderzoeken hoe de transcriptie van het Kir4.1 K^+-kanaal beïnvloed wordt door HNF1β. Uit onderzoek in dit proefschrift blijkt dat directe regulatie via HNF1β kan worden uitgesloten. Een nieuwe techniek op het gebied van genoom-sequencing en massaspectrometrie 'reverse ChIP' (een omgekeerde chromatine-immunoprecipitatie) is in staat om alle eiwitten die aan een specifieke DNA sequentie binden te identificeren. Andere transcriptiefactoren die belangrijk zijn voor Kir4.1 transcriptie kunnen zo in kaart worden gebracht, waaronder mogelijke interactiepartners van HNF1β. Het is eveneens onbekend welke transcriptiefactoren de expressie van belangrijke DCT eiwitten zoals NCC en Mg^{2+}-kanaal TRPM6 reguleren. Met technieken als 'reverse ChIP' kan men de identiteit van deze factoren ophelderen om zo de mechanismen achter Ca^{2+} en Mg^{2+} resorptie in de nier te onthullen.

In het TAL segment van de nier, werd aangetoond dat HNF1β de transcriptie van de CaSR reguleert. Het is echter onduidelijk wat het effect is op Ca^{2+} en Mg^{2+} resorptie in de TAL. Hiervoor is het belangrijk om nauwkeurig te bepalen welke claudines in hun productie door HNF1β, direct of indirect, worden gereguleerd. Aangezien de claudines verantwoordelijk zijn voor het paracellulaire iontransport in de TAL. Het behandelen van HNF1β KO muizen met de CaSR agonist cinacalcet zou hier meer inzicht in kunnen geven. Door CaSR activiteit te stimuleren met deze agonist kan men het verlies van *CaSR* transcriptie door HNF1β herstellen en zo aantonen welke claudines nu worden beïnvloed door de CaSR en wat het effect is op Ca^{2+} en Mg^{2+} resorptie in de nier. Dit

soort dierstudies bestrijken lange periodes. Een probleem in de huidige HNF1β KO muismodellen is de vroege ontwikkeling van cystenieren, en als gevolg daarvan, vroege sterfte van deze dieren. Een alternatief zou een studie zijn in een bruikbaar TAL celmodel waar paracellulair iontransport gemeten kan worden. Dit celmodel moet nog ontwikkeld worden, waardoor deze iontransport studies nog niet mogelijk zijn. De ontwikkeling van nieuwe HNF1β KO muismodellen en bruikbare celmodellen is daarom noodzakelijk om het effect van transcriptiefactoren, zoals HNF1β, op iontransport verder te kunnen onderzoeken.

Het is noodzakelijk om complexe netwerken van transcriptie van membraan-transporteurs en kanalen verder te onderzoeken. Toekomstig onderzoek zal op deze wijze nieuwe mechanismen van genregulatie kunnen onthullen hetgeen inzicht geeft in de behandeling van zeer heterogene en complexe erfelijke aandoeningen als ADTKD-HNF1β en KCS2.

8

List of abbreviations
List of publications
Curriculum vitae
Research data management
RIMLS portfolio

List of abbreviations

$1,25(OH)_2D_3$	1,25-dihydroxyvitamin D_3
18S	18S ribosomal RNA
ADH	Autosomal dominant hypocalcemia
ADTKD	Autosomal dominant tubulo-interstitial kidney disease
ANOVA	Analysis of variance
ATP	Adenosine triphosphate
ATPase	Adenosine triphosphatase
BAC	Bacterial artificial chromosome
BCS	Body condition scoring
Bp	Base pair
Ca^{2+}	Calcium ion
CaSR	The calcium-sensing receptor
CAKUT	Genital tract malformation
CD	Collecting duct
CEAS	Cis-regulatory element annotation system
cDNA	Complementary DNA
CDK5	Cyclin-dependent kinase 5
ChIP-seq	Chromatin immunoprecipitation and sequencing
CKD	Chronic kidney disease
Cl^-	Chloride ion
ClC-Kb	Voltage-gated chloride channel
Cldn	Claudin
CLDN3	Gene encoding claudin 3
CLDN16	Gene encoding claudin 16
CLDN19	Gene encoding claudin 19
CLDN14	Gene encoding claudin 14
CLDN10a	Gene encoding claudin 10a
CLDN10b	Gene encoding claudin 10b
CMV	Cytomegalovirus
CNNM2	Cyclin M2
CNT	Connecting tubule
CO-IP	Coimmunoprecipitation
COPAS	Complex object parametric analyzer and sorter
CSRP1	Cysteine and glycine-rich protein 1
cTAL	Cortical thick ascending limb of Henle's loop
DAPI	4', 6-diamidino-2-phenylindole
DCT	Distal convoluted tubule
DMEM	Dulbecco's modified eagle's medium
DNA	Deoxyribonucleic acid
DTT	Dithiothreitol
EAST	Epilepsy, ataxia, sensorineuronal deafness and renal tubulopathy

EDTA	Ethylene diamine tetraacetic acid
eGFP	Enhanced green fluorescent protein
EGF	Epidermal growth factor
EGTA	Egtazic acid
EFGR	Epidermal growth factor receptor
eGFP	Enhanced green fluorescent protein
EGTA	Ethylene glycol tetraacetic acid
EIF6	Eukaryotic translation initiation factor 6
ENaC	Epithelial Na^+ channel
ER	Endoplasmatic reticulum
ERK	Extracellular signal-regulated kinase
FAM111A	Family with sequence similarity 111, member A
FCS	Fetal calf serum
FDR	False discovery rate
FHH	Familial hypocalciuric hypercalcemia
FHHNC	Familial hypomagnesemia with hypocalcuria and nephrocalcinosis
FXYD2a	*FXYD* domain containing ion transport regulator 2 variant a
FXYD2b	*FXYD* domain containing ion transport regulator 2 variant b
GAPDH	Glyceraldehyde 3-phosphate dehydrogenase
GCPR	G-protein coupled receptor
GCM2	Transcription factor glial cells missing-2
GEO	Gene expression omnibus
GFP	Green fluorescent protein
GFR	Glomerular filtration rate
GO	Gene ontology
HA	Human influenza hemaglutinin
H3K4me3	Histone H3 protein trimethylation of lysine 4
HAM-F12	HAM's F12 nutrient mixture
HCl	Hydrogen chloride
HEK293	Human embryonic kidney cells (293)
HeLa	Henrietta Lacks cervical tumor cells
HGNC	HUGO Gene Nomenclature Committee
HNF1α	Hepatocyte nuclear factor 1 homeobox alpha
HNF1β	Hepatocyte nuclear factor 1 homeobox beta
HSH	Severe hypomagnesemia and secondary hypocalcemia
HRP	Horseradish peroxide
IDH	Isolated dominant hypomagnesemia
IHC	Immunohistochemistry
IL-6	Interleukin 6
IR	Insulin receptor
IRES	Internal ribosome entry site
IRF7	Interferon regulatory factor 7
IFIT1	Interferon-induced protein with tetratricopeptide repeats 1

IFN-α	Interferon alpha
IRH	Isolated autosomal recessive hypomagnesemia
JAK	Janus kinase
K^+	Potassium ion
Kb	Kilobase
KCl	Potassium chloride
KCNJ10	ATP-sensitive inward rectifier potassium channel 10
KCNJ16	ATP-sensitive inward rectifier potassium channel 16
KCS	Kenny-Caffey syndrome
KCS2	Kenny-Caffey syndrome type 2
kD	Kilo Dalton
KEGG	Kyoto Encyclopedia of Genes and Genomes
Keratin 2A	KRT2
Kif12	Kinesin family member 12
Kir4.1	Inward rectifying K^+ channel subunit 4.1
Kir5.1	Inward rectifying K^+ channel subunit 5.1
KO	Knock-out
KOH	Potassium hydroxide
Ksp-cre	Ksp-cadherin cre recombinase
Kv1.1	Potassium voltage-gated channel subfamily A member 1
LacZ	β-galactosidase
LC-MS	Liquid chromatography–mass spectrometry
LT	Large T antigen
MA	Bland-Altman plot
mDCT	Mouse distal convoluted tubule
MDR/TAP	ATP-binding cassette, sub-family B
miR	microRNA
Mg^{2+}	Magnesium ion
MKTAL	Immortalized mouse medullary thick ascending limb cell line
mL	Milliliter
M-MLV	Moloney murine leukemia virus reverse transcriptase
mpkDCT(4a)	Immortalized mouse DCT cell line
MODY	Maturity onset diabetes of the young
MODY5	Maturity onset diabetes of the young type 5
mRNA	Messenger ribonucleic acid
mTAL	Medullary thick ascending limb of Henle's loop
MsigDB	Molecular Signature Database
mV	Millivolt
MS	Mass spectrometry
MQ	Milli-Q water
Na^+	Sodium ion
NaCl	Sodium chloride
NaF	Sodium fluoride

Na^+-K^+-ATPase	Na^+-K^+-adenosine triphosphatase pump
NCBI	National Center for Biotechnology Information
NCC	The thiazide-sensitive NaCl cotransporter
NCX1	The Na^+-Ca^{2+} exchanger
NEO	Neomycin resistance gene
NFAT	Nuclear factor of activated T-cells
NKCC2	The furosemide-sensitive Na^+-K^+-$2Cl^-$ co-transporter
NP-40	Nonidet 40
Nt	Non-targeting
OMIM	Online mendelian inheritance in man
OCS	Osteocraniostenosis
P	Probability value
pA	polyA
PT	Proximal tubule
PC	Principal component
PCA	Principal component analysis
PCR	Polymerase chain reaction
PCBD1	Pterin-4a-carbinolamine dehydratase/dimerization factor
PCNA1	Proliferating cell nuclear antigen 1
PEI	Polyethylenimine cationic polymer
pGL3b	Luciferase reporter vector
PKD2	Polycystin-2
PKHD1	Fibrocystin
PMCA1b	Ca^{2+}-ATPase
POU_H	Atypical POU homeodomain
POU_S	POU-specific domain
pNCC	Phosphorylated thiazide-sensitive NaCl cotransporter
PVDF	Polyvinylidene difluoride
P2X	ATP-regulated purinoreceptor cation channel
RL	Renilla luciferase
RNA	Ribonucleic acid
RNasel	Ribonuclease L
ROMK	The renal outer medullary potassium channel
RPF2	Ribosome production factor 2 homolog
RPL23	60S ribosomal protein L23
RT	Reverse transcriptase
RT-qPCR	Real-time quantitative PCR
RBM8A	RNA-binding protein 8A
SD	Standard deviation
SEM	Standard error of the mean
SeSAME	Seizures, sensorineural deafness, ataxia, mental retardation and electrolyte imbalance or epilepsy, ataxia, sensorineural deafness, tubulopathy
SCNN1a	α subunit of the epithelial sodium channel

SDS-PAGE	Sodium dodecyl sulfate polyacrylamide gel electrophoresis
SD	Standard deviation
SEM	Standard error of the mean
siRNA	Silencing RNA
SLC12A1	Solute carrier family 12 type 1
SLC12A3	Solute carrier family 12 type 3
SLC41A1	Solute carrier family 41 member 1
SLC41A3	Solute carrier family 41 member 3
SNP	Single-nucleotide polymorphism
STAT1	Signal transducer and activator of transcription 1
STAT3	Signal transducer and activator of transcription 3
SV40	Simian virus 40
TAL	Thick ascending limb of Henle's loop
TBCE	Tubulin-folding cofactor E
TEER	Trans epithelial electrical resistance
TF	Transcription factor
TLR3	Toll-like receptor 3
TRIS	Trisaminomethane
TRPM6	Transient receptor potential melastatin member 6
TRPM7	Transient receptor potential melastatin member 7
TRPV5	Transient receptor potential vanilloid 5
TSS	Transcription startsite
U6	U6 spliceosome
UCSC	University of California, Santa Cruz genome browser
UMOD	Uromodulin
UTR	Untranslated region
WT	Wildtype

List of publications

1. Kompatscher A*, de Baaij JHF*, Aboudehen K, Hoefnagels APWM, Igarashi P, Bindels RJM, Veenstra GC, Hoenderop JGJ. Transcriptional activation of Kir5.1 by HNF1β - implications for autosomal dominant tubulo-interstitial kidney disease. *Kidney Int.*, 2017, 92(5):1145-1156

2. Kompatscher A*, de Baaij JHF*, Aboudehen K, Farahani S, van Son LHJ, Milatz S, Himmerkus N, Veenstra GC, Bindels RJM, Hoenderop JGJ. Transcription factor HNF1β regulates expression of the calcium-sensing receptor in the thick ascending limb of the kidney. *Am J Physiol Renal Physiology,* 2018, 315:F27-F35

3. Kompatscher A, de Baaij JHF, Veenstra GC., Bindels RJM, Hoenderop JGJ. FAM111A interacts with transcription factor STAT1: Implications for Ca^{2+} and Mg^{2+} reabsorption in Kenny-Caffey syndrome type 2. *In preparation*

4. De Baaij JHF*, Kompatscher A*, Viering DH, Bos C, Bindels RJM, Hoenderop JGJ. P2X6 Knockout Mice Exhibit Normal Electrolyte Homeostasis, *PLOS ONE*, 2016, 11:6:e0156803

*Authors contributed equally to this work

Curriculum vitae

Andreas Kompatscher was born in Bolzano, Italy, on 9 February 1988. After graduating from high school in 2006 at Erfgooiers College in Huizen, The Netherlands, he studied Psychobiology from 2006-2010 at the University Of Amsterdam, obtaining his Bachelor's degree in 2010. From 2010-2012 he enrolled in the research Master Brain and Cognitive Sciences (Cognitive Science Center Amsterdam), at the University of Amsterdam, focusing on the Neuroscience track. For his first Master internship, he performed an internship at the department of Astrocyte Biology & Neurodegeneration at the Netherlands institute for Neuroscience under the supervision of Prof. dr. Elly Hol. During this internship, he investigated the role of the GFAP-delta splice variant as a marker for neuronal regeneration in astrocytes. His second Master internship, he performed in 2012 at the department of Functional Genomics in the Secretory Vesicle Trafficking and Recycling group under supervision of Prof. Dr. Matthijs Verhage and Dr. Heidi de Wit at the Free University in Amsterdam. Here he studied the role of Munc18 in modulating cortical F-actin and how this affects vesicle docking in chromaffin cells. In 2012, he obtained his Master's degree *Cum laude*. After his studies, Andreas joined the department of Physiology of the Radboud university medical center (Radboudumc) in 2013 as a technician working on elucidating the binding sites of transcription factor HNF1B before being extended in 2014 to a PhD position. Under the supervision of Prof. dr. René J.M. Bindels, Prof. dr. Joost G.J. Hoenderop and Dr. Jeroen H.F. de Baaij, he continued his studies, investigating the role of transcription factor HNF1B in renal magnesium handling. During his PhD period, Andreas attended and held oral and poster presentations at several (inter)national conferences including the Experimental Biology (EB) Meeting, Chicago, USA for which he was awarded a RIMLS travel award; Dutch Nephrology days, Veldhoven; Dutch Federation of Nephrology (NfN) day, and Radboud New Frontiers Symposia. Additionally, he successfully followed the PhD training program of the Radboud Institute for Molecular Life Sciences (RIMLS) and supervised 10 students from Biomedical Sciences, Medicine and Medical Biology, Bachelor's and Master's studies.

Research data management

The data obtained during my PhD at the Radboud University medical center (Radboudumc) are archived according to the Findable, Accessible, Interoperable and Reusable (FAIR) principles.[1] The generated primary and secondary data were have been stored on Labguru, a digital lab book client which is centrally stored and daily backed-up on the local Radboudumc server. Data was additionally backed-up on university servers belonging to the department. All data archives (view only) are stored on Labguru and accessible by the associated senior staff members. Mouse studies described in **Chapter 2, 3** and **5** were approved by the Central Animal Laboratory and the Animal Ethics Board of the associated universities. Published data generated or analyzed in this thesis are part of published articles and its additional files are available from the associated corresponding authors on request. All raw and processed chIP-seq data described in **Chapter 2** is available through the public functional genomics data repository GEO (gene expression omnibus). The RNA-seq data displayed in **Chapter 4** will be available in GEO after publication. To ensure general accessibility of the data, all filenames, primary and secondary data, metadata, descriptive files and program code and scripts used to provide the final results are documented according to the protocol of the department of Physiology.

1. Wilkinson MD, Dumontier M, Aalbersberg IJ*, et al.* The FAIR Guiding Principles for scientific data management and stewardship. *Sci Data* 2016; **3:** 160018.

RIMLS portfolio

Institute for Molecular Life Sciences
Radboudumc

Name PhD candidate:	Andreas Kompatscher	*PhD period:*	01-03-2014 – 28-02-2018
Department:	Physiology	*Promotors:*	Prof. dr. R.J.M. Bindels
Research School:	Radboud Institute for Molecular Life Sciences		Prof. dr. J.G.J. Hoenderop
		Co-promotors:	Dr. J.H.F. de Baaij

TRAINING ACTIVITIES	**Year(s)**	**ECTS**
a) **Courses & Workshops**		
- RIMLS Graduate Course	2014	2
- Winterschool Nierstichting	2014	1
- DevCom Computational Workshop for chIP-seq and RNA-seq	2014	2
- Academic Writing	2015	1
- Scientific Integrity course	2015	1
b) **Seminars & lectures**		
- RIMLS Radboud Research Rounds / Lecture Series	2014-2018	1
- RIMLS Seminars	2014-2018	1
- RIMLS Spotlights / Kidney Theme Meetings	2014-2017	1
- RIMLS Technical Forums	2014-2018	0.5
c) **(Inter)national Symposia & Congresses**		
- RIMLS Radboud New Frontiers	2014	0.5
- RIMLS PhD retreat *#	2014-2017	3
- RIMLS Radboud New Frontiers #	2015-2017	2.5
- NfN Najaarssymposium *	2016	1
- Dutch Nephrology Days *	2016	1.5
- Radboud Science Day *	2016	0.5
- Experimental Biology Meeting * #	2017	1
TEACHING ACTIVITIES		
e) **Lecturing**		
- Teaching Medical course: Practicum Water en Zouthuishouding Q3	2016, 2017	0.4
- Teaching Medical course: Vrije Keuzeruimte	2016, 2017	0.4
f) **Students**		
- Supervision Bas Olde Dubbelink	2014	1.3
- Supervision Enna Offerman	2014, 2015	1.5
- Supervision Kelly Warmink	2015	1.3
- Supervision Aline de Nooijer	2015, 2016	1.5
- Supervision Tom van Haaren, Steffi Bressers, Henrieke van Elst & Babette de Geest	2015	1
- Supervision Eline Visser	2016	2.6
- Supervision Lex van Son	2016, 2017	2
- Supervision Markus Bösch	2017	1.5
TOTAL		**34**

Oral and poster presentation are indicated with a * and # after the name of the activity, respectively

9 Dankwoord
Acknowledgements
Danksagung

Wel het is volbracht. Met wat gepaste trots ben ik ontzettend blij met mijn proefschrift. In mijn tijd bij fysiologie heb ik enorm veel geleerd en ben ik menig persoon grote dank verschuldigd. In dit hoofdstuk wil ik dan ook graag mijn promotoren, collaborateurs, collega's, vrienden en familie bedanken, die mij gemotiveerd, geholpen en gesteund hebben en zo, op hun eigen manier, een bijdrage hebben geleverd aan dit proefschrift.

Uiteraard wil ik eerst graag mijn promoteren Prof. dr. Joost Hoenderop, Prof dr. René Bindels en mijn co-promoter Dr. Jeroen de Baaij bedanken voor hun begeleiding, steun en vertrouwen gedurende mijn 5 jaar bij fysiologie. **Joost**, jouw aanstekelijke enthousiasme en drive werkten altijd zeer motiverend. Ik ben verder ook heel blij en dankbaar voor het vertrouwen die je gedurende al die jaren in mij gestoken hebt. De enorm gezellige bbqs bij jouw thuis zal ik me altijd herinneren al was het maar om die ene keer dat ik een nat pak haalde in je vijver. Ik hoop niet dat je nu eerst een rol afzetlint gaat kopen voor je aan de volgende lab bbq begint. **René**, jouw scherpe blik en oog voor detail hielden mij op het goede spoor. Ik heb veel geleerd van je gedisciplineerde manier van werken en veel respect voor de manier waarop je de afdeling en het RIMLS richting geeft. Jij ook bedankt voor al je vertrouwen in mij.

Tja, **Jeroen**, jij bent de originele aanstichter van mijn hele traject bij fysiologie. Ik zal (je) nooit ~~vergeven~~ vergeten dat je tijdens mijn sollicitatiegesprek vroeg waarom ik een 6 voor celbiologie had en ook nooit begrepen waarom je me daarna hebt aangenomen. Ik zal er wel goed omheen gezwetst hebben. Ik ben begonnen bij fysiologie als je persoonlijke technician. In die rol heb je direct veel vertrouwen in mij gestoken en kreeg ik al vrij snel een student en project om mee aan de slag te gaan. Dat project is mede dankzij jouw begeleiding uitgegroeid tot alles wat erin dit proefschrift staat. Jouw passie voor wetenschap, tomeloze energie (behalve in de ochtend) en wilde maar toch ook soms briljante ideeën waren een enorme inspiratie voor mij en ik heb dan ook veel van je kunnen leren. Ik ben ook erg blij dat ik je ook persoonlijk goed heb leren kennen. Van het broodnodige 'bullshitten' in het lab tot aan onze lange en vooral late drank- en discussie sessies in de Kluizenaar. Ik heb het bovenal toch erg gezellig gehad en ik hoop dat we elkaar nog geregeld blijven zien.

None of the research in this thesis would have been possible without the great collaborations I have had with various laboratories around the world. I am incredibly grateful to them for all their contributions to this thesis.

De bereidwillige samenwerking met Prof. Dr. Gertjan Veenstra maakte het mogelijk om de verschillende NGS technieken die in dit proefschrift gebruikt zijn op te zetten en uit te voeren. **Gertjan**, ik ben dan ook ontzettend dankbaar voor alle tijd en hulp die je in mijn project hebt gestoken. Wat me altijd is bijgebleven is dat je het ook geen probleem vond om meerder uren van de dag met mij achter de computer te gaan

zitten om met mij de data door te nemen. Dat werkte ontzettend motiverend en heeft heel veel geholpen bij de data interpretatie. I also want to thank **George Georgiou**, Dr. **Saartje Hontelez** and **Matteo Perino** from the Veenstra lab that helped with the data analysis and prep work in chapter 2 and 4. I want to give special commendations to Matteo, since despite being up to your eyeballs in work finishing your own PhD, you still managed to help met out big time with the RNA-seq work in chapter 4.

I would like to sincerely thank Prof. dr. **Peter Igarashi** for our collaborations in chapter 2 and 3. The results from the HNF1B KO mouse was essential for both papers to elevate my findings and further substantiate my conclusions. To this end, extensive qPCR and staining work has also been performed by Dr. **Karam Aboudehen**, Dr. **Svetlana Avdulov** and Dr. **Shayan Farahani**. Thank you all so much for your valuable contributions!

Dankzij de samenwerking met Prof. Dr. **Michiel Vermeulen** was het mogelijk om het proteomics gedeelte in hoofdstuk 4 uit te voeren. Heel erg bedankt voor de suggesties en hulp om deze experimenten tot een succesvol resultaat te brengen. **Pascal Janssen** en **Marijke Baltissen** hebben hier eveneens veel aan bijgedragen. Door jullie hulp verliepen deze experimenten vrijwel vlekkeloos! Iets wat ik zelf zelden meemaak en wat een zeer welkome ervaring was.

Ich möchte Prof. Dr. **Markus Bleich** danken für seine Zusammenarbeit an Kapitel 4. Vielleicht waren die Ergebnisse nicht wie wir sie gewünscht haben, aber unsere Diskussionen waren für mich von großen Wert und ich habe daraus viel gelernt. Mein Dank gilt auch Dr. **Susanne Milatz** und Dr. **Nina Himmerkus** die substanziell an den Ergebnissen beigetragen haben. Danke Nina für das gemütliche Dinner und dass du dich so rührend um Lex gekümmert hast. Es war eine gute Zeit in Kiel!

Verder heb ik gedurende deze jaren het geluk gehad om te mogen samenwerken met een grote groep zeer fijne collega's, die mijn onderzoek en leven op hun eigen manier verrijkt hebben.

Mark Hess, het was geweldig om met jouw een unit te delen. Je aanstekelijke lach en gevoel voor humor zorgden ervoor dat ik slechte resultaten vergat en menigmaal krom lag van het lachen. Vooral jouw discussies met Robert over Mg^{2+}-standaarden hebben inmiddels mythische vormen aangenomen op het lab en mij vooral ontzettend veel plezier opgeleverd. Jij hebt enorm bijgedragen aan mijn leuke tijd bij fysiologie en ik was dan ook zeer vereerd om jouw paranimf te zijn. ik hoop dat we elkaar snel weer eens zien. **Robert**, you were one of the original gangsters in my unit. We had some real fun times together and you always managed to make me laugh either intentionally or not. I still cherish the 1L Mg^{2+}-standard you made. It should become

a physiology museum piece to preserve it for posterity. **Maxime**, you were the level-headed bald guy in our unit/insane asylum and a welcome breath of sanity. Luckiley you survived the literal shitstorm in 2014, which hopefully did not result in any longterm averse effects. Despite all the silliness we had fun together and I very much appreciated your sensible and intelligent contributions to the lab and especially our unit. **Marla** en **Femke L.**, jullie waren van af het begin af mijn mede-technicians. Ik herinner me nog goed hoe wij drieën 1 bureau en 1 laptop moesten delen. Heel erg bedankt voor alle hulp door de jaren heen en Femke L. nog extra bedankt voor die enorme berg HEK293 kweek die je voor me hebt doorgezet gedurende de jaren.

Sjoerd, jij had altijd een neus voor goede ideeën en je was ook altijd bereid om dat talent te delen met je collega's. Ik heb in ieder geval enorm genoten van onze wetenschappelijke discussies en ook veel gehad aan je welkome bijdragen. Verder kon ik ook altijd goed een biertje met je drinken en die gezelligheid was me eigenlijk nog dierbaarder. Bedankt voor al je hulp en hopelijk zien we mekaar snel weer eens. **Paco,** eeh Spanish guy!, We had a lot of fun together, whether it was playing football after work or you introducing this dutch barbarian to the glories of Spanish culture in the Spanish cultural centre. Although, we had to burn our clothes afterwards, it was great fun. I also feel especifically privileged to be one of the few that actually witnessed the existence of your thesis in book form. I am putting it here in writing; it does exist! Thanks for all the good times and your friendship. **Jenny,** jouw nuchtere houding en intelligente bijdragen aan het Mg^{2+}-team en mijn onderzoek werden door mij zeer gewaardeerd. Gelukkig heb je ook een goed gevoel voor humor en ben je niet snel op je tenen getrapt…of toch wel ;-). **Ellen,** Hee Ellie! Of het nu spelletjesavonden of BBQs waren, jij was altijd in voor gezelligheid. Ik mis onze zang sessies in de celkweek. Misschien moeten we toch maar eens die dubbel cd 'songs for in the cell culture' gaan opnemen.

Steef, STOOF! Het lot plaatste je samen met mij in een unit en de rest is geschiedenis. Onze voorliefde voor zwaar metaal en slechte grappen maakte jouw praktisch voorbestemd als mijn goede vriend en dus ook paranimf. Buiten al het grappen en grollen heb ik veel respect voor je diepe nierkennis en vlijmscherpe kritische blik. Ik ga je gelukkig nog vaak zien aangezien we al een hoop concertjes op de planning hebben staan en ik hoop ook zeker dat we dat in de toekomst gewoon blijven doen. Veel succes in ieder geval met het afronden van de laatste loodjes nog een paar maanden en dan ben jij er ook Dokter Steefe!

Anique, PE-- ! Aah laat ik maar niet beginnen met al je bijnamen opnoemen. Bedankt Anique dat je altijd zo een gewillige slachtoffer was voor mijn grappen. Dat was altijd bijzonder therapeutisch voor mij en een welkome afleiding. Gelukkig heb je niet een

te grote hekel aan mij gekregen en kon je er zelf ook altijd wel om lachen, waarvoor hulde!

Caro, Jij hebt zo vaak je heksenhoed voor mij op moeten zetten om mijn antilichamen aan de praat te krijgen. Daarom Bossie bedankt! Voor al je hulp met de kleuringen, FAM muizen en natuurlijk alle gezelligheid.

Lisanne, Buurman bedankt! Het was ontzettend fijn om gedurende mijn laatste jaar jouw buurman te zijn. Zet em nog maar eens op standje 5 als je me begint te missen. We moeten ook snel weer eens aan de whisky met de Huubster en JdeB.

Omar, Mijn andere buurman! Ook jij bedankt voor alle gezelligheid zo in mijn laatste jaar. Je karakteristieke lach en goede humeur werkten aanstekelijk op mij wat zorgde voor een goede sfeer aan onze kant. **Sami,** your dry sense of humor made it a joy to work with you. Thanks as well for your help with the RNA-seq stuff. It was very much appreciated. **Eric,** Boxmé-r! Jij bedankt voor alle goede lunchgesprekken. Het was fijn om eens een politieke medestander te hebben. **Frans,** Ik heb zeer genoten van de regelmatige bordspelavondjes bij jouw thuis en ook op het lab was je altijd wel in voor een goede flauwe grap. Ik hoop dan ook dat je snel weer terugkomt van Frakantie ;-). **Marjolein,** jij ook bedankt voor alle supergezellige spelletjesavonden bij jouw thuis. Ik hoop dat we die traditie blijven voortzetten. **Jojanneke,** Bedankt voor de gezellige tijd zowel in het lab als in de concertzaal ;-p.

Irene, jouw wil ik toch speciaal bedanken voor al je inzet om het lab draaiend te houden en al die irritante bestellingen van mij in goede banen te leiden. Het is eigenlijk jammer dat we elkaar pas aan het eind van mijn PhD eens een keer uitgebreid hebben gesproken. Ik vond ons fijne gesprek tijdens de 'science day' namelijk ontzettend leuk!

Verder wil ik ook alle collega's bedanken die tijdens mijn PhD hebben bijgedragen aan mijn fantastische tijd op het lab: **Anke L., Liz, Laurianne, Silvia, Ramon, Jitske, Theun, Annemiete, Eline van der H., Wilco, Sabina, Marco, Luke, Mohammed, Claudia, Dennis, Peter, Sjoeli, Rachael, Femke van der H., Lotte, Gijs, Chao, Hacene, Mark van G., Juan, Sara, Nikki, Niky, Valentina, Margo, Kim, Anke van M.** en alle collega's van integratieve fysiologie.

Tijdens mijn promotie heb ik ook goede hulp gehad van veel studenten. Zij hebben allemaal een flinke bijdrage geleverd aan mijn onderzoek en daar ben ik ze zeer dankbaar voor.

Anke H., jij hebt zoveel hard werk gestoken in het uitvoeren en optimaliseren van de chIP-seq wat de basis was voor een groot deel van de mooiste verhalen in dit proefschrift. Super bedankt voor al je hulp en inzet! **Bas,** Het was erg gezellig met jouw in het team. Heel veel succes met je opleiding tot leraar Biologie! **Kelly,** Ik ken

maar weinig studenten die zo moeiteloos hun experimenten opzetten en uitvoeren. Heel erg bedankt voor al je bijdragen aan hoofdstuk 2. **Enna en Aline,** Al waren jullie niet voltijd in het lab. Toch hebben jullie je vol ingezet!, zowel bij mij in Nijmegen als op jullie succesvolle stages in de USA. Heel erg bedankt! **Eline,** jij hebt ook hard werk verzet waarvoor heel veel dank! Ik zal ook nooit je fantastische zelfgemaakte afscheidscadeau vergeten. Al weet ik niet helemaal precies waarom je het spel 'Secret Hitler' bij mij vond passen. Ik was hopelijk toch niet zo streng ;-p. **Lex,** Sommigen op het lab vonden je misschien een blaaskaak maar jij was toch mijn favoriete toeteraar. Jij ook bedankt voor al je inzet en je bijdragen aan hoofdstuk 3 en 4. **Markus,** Na het vertrek van Mark H. kon ik mijn hart niet op met het verschijnen van een nieuwe Duitser op het lab. Je hebt het fantastisch gedaan en het was bovenal ook weer erg gezellig.

Cas, Julia en **Daan,** Jullie waren dan wel niet officieel mijn studenten, maar we hebben samen wel een hoop lol gehad. En Daan jij hebt nog bergen qPCRs gedraaid voor hoofdstuk 5 waarvoor heel veel dank. Ik hoop dat we mekaar blijven zien voor een biertje in de Kluizenaar!

Dan wil ik ook graag mijn vrienden en familie bedanken voor alle steun en afleiding de afgelopen jaren. **Marco, Gerhard, Robert, David, Maarten** en **Sebastiaan**, ik ben heel blij dat we elkaar door de jaren toch regelmatig zien. Ondanks het feit dat we inmiddels door heel Nederland wonen. Gelukkig delen we een aantal passies waaronder goed bier, slechte muziek en harde humor. Onze proefavondjes zijn dan ook altijd combinaties van die drie ingrediënten en een welkome afleiding van het werk. Bedankt voor alle goede tijden en dat we dit nog lang mogen voortzetten!

Liebe **Oma** und Verwandten aus Südtirol, leider habe ich wenig Zeit in Südtirol verbringen können, aber die wenige Zeit in Südtirol bei euch war mir lieb und teuer. Danke dafür und hoffentlich sehn wir uns bald wieder.

Reini, auch Dir möchte ich danken dass du Zeit gefunden hast und mit mir so manche Bergwanderung gemacht hast. Ich hoffe dass du jetzt eine Idee hast über welchen Transport ich gesprochen habe. Danke für die gute Zeit beim Bergwandern.

Karin, mijn lieve zus, Het was altijd fijn om elkaar zo nu en dan eens te zien. Al was het maar zodat ik een beetje bij kon praten en dat jij weer eens vis kon eten ;-). Het is ook altijd fijn dat ik jaarlijks in december bij jouw en **Joris** terecht kan om te slapen en uit te brakken. En dat ik nog steeds welkom ben, ondanks het feit dat ik midden in de nacht bijna je kat heb laten ontsnappen ;-). Bedankt voor al je steun. Nog even en dan ben jij ook aan de beurt!

Pa en **Ma**, jullie ben ik natuurlijk ook veel dank verschuldigd voor al jullie steun en hulp door de jaren. Het is altijd fijn om even in Almere Hout te kunnen toeven in jullie fijne tuin en door te spreken welke verbouwingen jullie nu weer gestart zijn. Jullie rust en kalmte stel ik altijd erg op prijs. Bedankt ook voor de fijne tijd in Süd-Tirol en dat ik zo nu en dan met jullie kon meeliften om Oma te bezoeken.

Lieve **Elja**, we hebben elkaar natuurlijk twee jaar geleden leren kennen op het lab. Geen idee of het zo cheesy was als liefde op het eerste gezicht, maar ik ben zo blij dat ik de tweede helft van mijn PhD samen met jouw heb mogen doorbrengen. Je bent een immense steun voor mij, zeker de laatste maand van mijn PhD waar de laatste loodjes me erg zwaar vielen, heb ik het mede door jouw liefde en zorg toch goed kunnen afronden. Wat de toekomst ook mag brengen ik ben blij dat ik die met jouw mag delen. Ik hou van je.

Institute for Molecular Life Sciences
Radboudumc